UNIVERSITY OF SOUTHAMPTON

FACULTY OF ENGINEERING AND PHYSICAL SCIENCES

National Centre for Advanced Tribology at Southampton (nCATS)

A study of the influence of sulfonate containing lubricants on White Etching Crack (WEC) formations in 100Cr6 bearing steel

By

Alexander David Richardson

Thesis for the degree of Doctor of Philosophy

August 2018

UNIVERSITY OF SOUTHAMPTON

ABSTRACT

FACULTY OF ENGINEERING AND PHYSICAL SCIENCES

National Centre for Advanced Tribology at Southampton (nCATS)

Thesis for the degree of Doctor of Philosophy

A study of the influence of sulfonate containing lubricants on White Etching Crack (WEC) formations in 100Cr6 bearing steel

Alexander David Richardson

Wind turbine gearbox bearing (WTGB) failure is dominated by the premature failure mode known as White Structure Flaking (WSF), where WSF is caused by White Etching Cracks (WECs) formed beneath the contact surface under rolling contact fatigue (RCF), WECs being associated with a microstructural alteration known as White Etching Area (WEA). WSF failure is unconventional and has been of great interest to the Wind industry for a number of years. This failure mode is not well understood, it involving a number of complex factors due to its unpredictability. Formation drivers and initiation mechanisms continue to be highly debated and are suggested to be driven by combinations of mechanical, tribochemical, and electrical/electrothermal effects. Two key cited drivers are transient operating conditions and hydrogen diffusion into the steel during operation. By replicating and using combinations of these drivers, studies have been able to re-create WECs so that their formation mechanisms can be investigated.

An array of RCF tests have been conducted using FAG-FE8 and PCS Micro-pitting (MPR) test rigs to create WECs under *non*-hydrogen charged conditions using 100Cr6 steel lubricated with oils containing sulfonate additives. Over-based calcium sulfonates (OBCaSul) are specifically focused upon; these additives being considered critical in driving WEC formations and their 'driving' effect remaining unclear. Serial sectioning techniques have enabled this study to capture and investigate the WEC evolution mechanisms from initiation to final flaking failure. Clear evidence for subsurface initiation of WECs at non-metallic inclusions has been observed at the early infant stages of WEC formation, WECs propagating from the subsurface to the contact surface eventually causing flaking with increase in RCF test duration. The effect of differing concentrations

of OBCaSul in the oil on WECs have also been examined, serial sectioning being used to quantify WEC damage formations. An increase in WEC formations with increase in OBCaSul concentration from 1.4% (no WECs found), to 2.8% and 5.6% (WECs found) is shown. However, no WECs were found to have formed in the MPR tested rollers under the lubrication of oils containing 2.8% and 5.6% OBCaSul while a number of WECs had formed in those lubricated by the 1.4% OBCaSul oil. This is thought to be due to the different contact dynamics and potentially different tribofilm formations on the two test rigs.

Thermal desorption analysis (TDA) was used to measure the concentration of diffusible hydrogen in FE8 RCF tested bearings so that hydrogen diffusion effects on WEC formations could be assessed. By coupling TDA with serial sectioning, relationships between hydrogen diffusion and WEC formations were examined. A positive correlation between the increase in diffusible hydrogen concentration and the formation of WECs over the increased RCF test duration was found in the FE8 rollers, while negligible hydrogen concentrations corresponding to no WECs were measured in the raceways.

Detailed analysis of the tribofilms formed during RCF operation using SEM/EDX was conducted so that the influence of OBCaSul additives on tribofilm formation, and thus WEC formations via hydrogen diffusion could be explored. Overall, OBCaSul containing oils have been found to form thick Ca dominated tribofilms, which may have promoted hydrogen diffusion and WEC formations in the FE8 rollers. The thinner Zn-S tribofilms formed on the FE8 raceways on the other hand may have demoted hydrogen diffusion and WEC formations.

Table of Contents

Table of Tables

Table of Figures

Table of Figures

Table of Figures

Table of Figures

List of Accompanying Materials

To view the videos please use this link: https://doi.org/10.5258/SOTON/D0620

Chapter 2

Video 2.1 - Orthoslice sweep of WEC-10 R2 showing the crack at each slice interval demonstrating the morphology of the WEC in 3D.

Video 2.2 – Total WEC damage recorded in 18 hour Roller 1 modelled in 3D. The video shown a 2D segmentation and 3D orthoslice sweep through the entire volume of the roller representing each individual WEC recorded across the roller from the outer to inner edge.

Appendix C

Video C.1 – Orthoslice sweep of WEC 1 showing the crack at each slice interval demonstrating the morphology of the WEC in 3D.

Video C.2 – Orthoslice sweep of WEC 2-S showing the crack at each slice interval demonstrating the morphology of the WEC in 3D.

Video C.3 - Orthoslice sweep of WEC 3 showing the crack at each slice interval demonstrating the morphology of the WEC in 3D.

Declaration of Authorship

I, Alexander David Richardson, declare that this thesis and the work presented in it are my own and has been generated by me as the result of my own original research.

A study of the influence of sulfonate containing lubricants on white etching crack (WEC) formations in 100Cr6 bearing steel

I confirm that:

1. This work was done wholly or mainly while in candidature for a research degree at this University;
2. Where any part of this thesis has previously been submitted for a degree or any other qualification at this University or any other institution, this has been clearly stated;
3. Where I have consulted the published work of others, this is always clearly attributed;
4. Where I have quoted from the work of others, the source is always given. With the exception of such quotations, this thesis is entirely my own work;
5. I have acknowledged all main sources of help;
6. Where the thesis is based on work done by myself jointly with others, I have made clear exactly what was done by others and what I have contributed myself;
7. Parts of this work have been published and these are listed on the following page;

Signed: .....

Date: .....

Publications and Award

Journal publications

- Richardson, A. D., M-H. Evans, L. Wang, R. J. K. Wood, and M. Ingram. "Thermal desorption analysis of hydrogen in non-hydrogen-charged rolling contact fatigue-tested 100Cr6 steel." *Tribology Letters* 66, no. 1 (2018): 4.
- Richardson, A. D., M-H. Evans, L. Wang, R. J. K. Wood, M. Ingram, and B. Meuth. "The evolution of white etching cracks (WECs) in rolling contact fatigue-tested 100Cr6 steel." *Tribology Letters* 66, no. 1 (2018): 6.
- Evans, M-H., A. D. Richardson, L. Wang, R. J. K. Wood, and W. B. Anderson. "Confirming subsurface initiation at non-metallic inclusions as one mechanism for white etching crack (WEC) formation." *Tribology International* 75 (2014): 87-97.

Awards

2014 **Thomas Andrew Common Award Grant, Institute of Mechanical Engineers (IMechE)**

Award travel grant for overseas international conference

2014 **Silver poster prize, Society of Tribologists and Lubrication Engineers (STLE)**

3rd place poster prize, STLE 69th annual conference, Florida, USA

2015 **Best presentation prize, TriboUK conference**

1st place oral presentation prize, TriboUK conference, Loughborough University, UK

2015 **Institute of Physics (IOP) research student conference fund award**

Award travel grant for overseas conference

2015 **Platinum poster prize, Society of Tribologists and Lubrication Engineers (STLE)**

1st place poster prize, STLE 70th annual conference, Dallas, USA

Acknowledgements

This PhD project has been partially funded by Afton Chemical. I would like to thank the past and present supervisory team at Afton that have supported and guided me throughout this PhD, you have all been invaluable and I hope to stay in contact with you in the future. Many thanks to Kuba Rydel, Marc Ingram and William Anderson. Special thanks also to Kevin Munday, your help running the numeral tests at Afton has been vital to the success of this project, I truly enjoyed my time popping up to Afton and chatting with you and your team down at the rigs! Thanks also to Grant Pollard for your assistance running the SEM/EDX tribofilm analysis. For your quick response and help, I am very grateful.

I would also like to thank my supervisors here at Southampton University, Ling Wang, Martin Evans and Robert Wood, your guidance and knowledge has been vital to this project, I cannot thank you all enough! Ling, you have been such a huge aid to me in this project, your kindness and encouragement throughout this PhD and in my recent tough times has helped me a great deal. Martin, over the last years you have been a good friend and I sincerely thank and owe you a lot for your support throughout this PhD. The last 6 years I have worked with you, we have had many a great time, and may the 'Bruker boys' long continue.

Thanks also go to Sally Day for facilitating the TDA at TWI Cambridge and Steve Ooi for TDA at Cambridge University, your assistance has been instrumental to this PhD project.

Ben Meuth, Zach Rowland and Gabriel Llanos, I sincerely thank you all for your hard work and dedication in the face of sectioning, I wish you all the greatest of success in your future.

Pawee Kucita, Victorija Smelova and Michael Evans, many thanks for your assistance with transportation of samples and LiN to/from Afton and TWI Cambridge. Pawee, special thanks to you for lending me a hand throughout my PhD and with the SEM, you have been a great friend!

Thank you to the whole host of academics, PhD students, technicians and staff at Southampton University who have helped in numeral ways throughout this project and my time at Southampton.

I would like to make a special mention to the whole team at Southampton General Hospital and Hampshire Constabulary. You are all truly amazing people and do a fantastic job. If it was not for you then I would not be here alive today and finishing this PhD. I sincerely cannot thank you all enough. Keep up the good work!

I would also like to thank all my friends at Southampton University past and present, you have all been great and made this a time of my life that I will never forget!

To my partner Danai, your support, care, patience, and friendship over the last years has helped me through the lows and highs of this PhD and got me over the finish line, to you I truly cannot thank you enough! Again, I say congrats on completing your own PhD this year too and I look forward to joining you as a fellow Doc soon!

Mum and dad, your care and moral support throughout my time at Southampton from undergraduate to now PhD has been invaluable, and I owe a big part of where I am now to you both, thanks for always believing in me! My brother, Jake, you have been a top bro and always been there for me, cheers to you! Nan Wendy and Grandad Dave, thanks for all the visits and days out during my PhD, they all counted to getting me to the finish line! To all my family, for being there and coming to visit me in Southampton, you have all been amazing, thanks!

My time as a PhD student has ended, but the memories and times I have had will always be remembered. Cheers!

Chapter 1 Introduction

Wind turbine gearbox bearing (WTGB) failure is putting a significant strain on the economy of the wind energy sector, wind turbine life being reduced from the predicted 20 years to less than 5 years. Gearbox failure is dominated by the premature failure of rolling element bearings by the phenomena known as White Structure Flaking (WSF) caused by White Etching Cracks (WECs) below the contact surface that are associated with a microstructural change called White Etching Area (WEA). Formation drivers as well as initiation and propagation mechanisms continue to be highly debated and are thought to be driven by combinations of mechanical, tribo-chemical and electrical effects.

Through this PhD study, a number of critical questions regarding the failure of WTGBs have been addressed via experimental testing and analytical techniques including: (i) The mechanisms of WTGB failure, (ii) hydrogen's role in these failure mechanisms and (iii) the influence of specific lubricant additives in the oil.

This introduction chapter has four parts. Part 1.1 provides a background to the wind turbine industry. Part 1.2 covers the background of WTGB failure. Part 1.3 covers the background to White Structure Flaking failures and Part 1.4 sets out the aims, objectives and structure of the thesis.

1.1 Background to the wind turbine industry

1.1.1 The expansion of wind energy

Modern wind turbines harvest energy from wind and convert kinetic energy into rotational energy through the movement of air on the turbines blades, subsequently the rotational energy is converted into electricity via an electric generator. A wind turbine system comprises a number of major elements, including its foundation, tower, nacelle and the rotor blades [1]. The majority of wind turbines used on and offshore have horizontal-axis of rotation and are composed of three blades (sometimes two) with the blades up-wind connected through a hub to the main shaft and nacelle at the top of the turbine tower. Vertical-axis turbines and other innovative designs are less common but are seen across the globe. The electricity generated by a wind turbine is determined by its nameplate capacity (kW or MW), turbine tower height, rotor diameter, quality of the wind and the operation and maintenance (O&M) strategy [2].

Chapter 1

Wind power has become a front-runner in the efforts to meet global energy targets and filter out the need for fossil fuels. The wind energy market has grown significantly since about 1980, with a rapid expansion being seen over the last 10 years due to wind turbine technologies allowing for increased turbine capacity [1, 2]. In 2017, 85% of all new power capacity in the EU came from renewables, 65.3% of that being wind [3]. In 2016, wind overtook coal to become the 2nd largest form of power generation capacity in the EU [3]. Over the last years, record numbers of wind turbines have been installed around the world, with 2017 being the third largest since a peak in 2015, when the overall global cumulative wind turbine capacity reached 539, 581 MW (Figure 1-1).

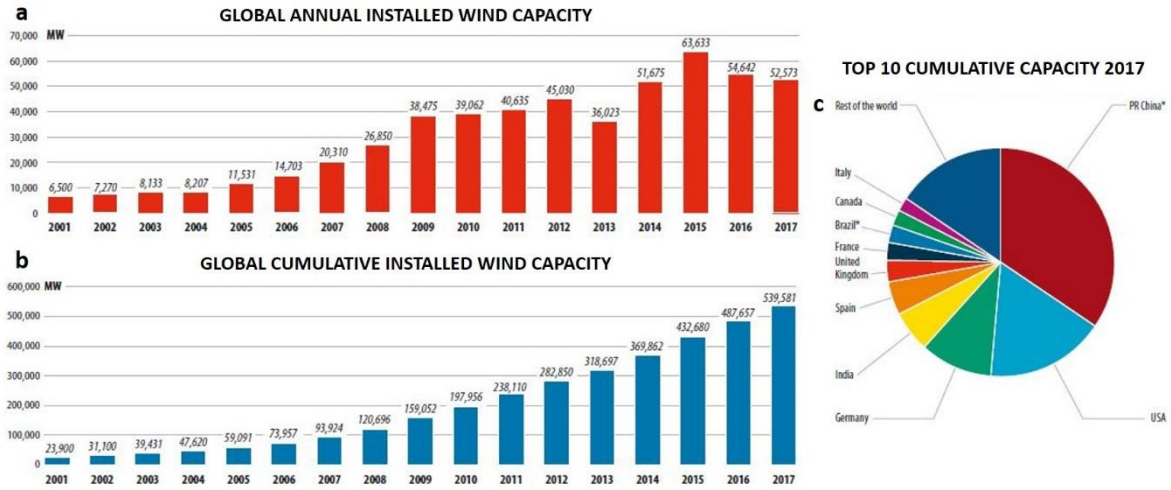

Figure 1-1: (a) Global annual installed wind capacity as of 2017, (b) global cumulative installed wind capacity as of 2017 and (c) top 10 cumulative wind capacity countries as of 2017 [4].

Wind turbines can be located onshore or offshore, however, onshore is dominating global installations. Asia continues to be top in annual installed capacity and the UK leads the way in cumulative offshore wind capacity [4]. In 2017 the electricity generated through wind energy accounted for 11.6% of the EU-28's total electricity demand, where the majority came from onshore turbines with Denmark leading the way covering 44.4% of its annual electricity demand [3]. In terms of installed power generating capacity wind energy accounts for 18% of the EU total [3].

Wind turbines are typically installed in groups (wind farms) with numbers reaching the hundreds of turbines. A recent example of this is the Rampion wind farm just off the South coast of the UK (116 turbines reaching a capacity of 400 MW). Presently, the onshore Gansu wind farm in China is the largest with a planned capacity of 20 GW by 2020, China being by far the greatest wind turbine market with a cumulative capacity of 188 GW compared to the UKs 18 GW (Figure 1-1).

As the demand of wind power increases, larger and more powerful wind turbines have become a trend. In 1979 wind turbine manufacturer Vestas paved the way for a modern era of wind turbine technology, producing what was then large turbines (10 – 30 KW) to generate electricity [2]. Since then, wind turbines have grown in size tremendously. In a 2017 report by REN21 [5], the average onshore wind turbine size in the EU was 2.7 MW, with offshore being 4.8 MW and the largest commercially available turbines being rated at 8 MW. As part of the EU Strategic Energy Technology Plan (SET plan), the wind energy road map forecasts that wind turbines with rotor circle the size of 4 football pitches will be seen by the end of 2020 (Figure 1-2). As the size of the wind turbines goes up, their weight increases significantly too. For a 5 MW wind turbine the total weight can be in the range of 150 – 200 tonnes [1].

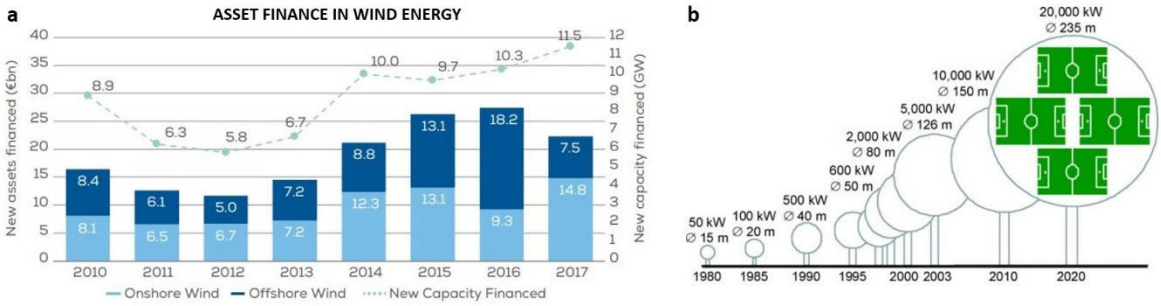

Figure 1-2: (a) Asset finance in wind energy 2010 – 2017 [3] and (b) projected wind turbine size by SET plan [6].

On the other hand, the investments in wind energy in the EU have seen a rise to its peak value of over €25 bn in 2016 (mainly on offshore turbines) however, has fallen in 2017 due to cuts on offshore investments while onshore hit a record high (Figure 1-2). In total, wind energy investments accounted for 52% of all new clean energy finance in the EU in 2017 [3]. Wind turbine prices and installation costs have fallen since a peak between 2007 - 2010 and the costs of wind energy technologies will continue to change with supply and demand [2]. Wind turbines manufacturing costs account for a significant portion of the overall capital costs (64% - 84% onshore and 30 - 50% offshore, prices as of end 2017 being below 1000$/kW) fluctuating with material commodity prices, government policies and technological advancement [2]. The economic impacts on the industry when a turbine experiences failure can have a heavy financial consequence.

As the wind energy sector continues to grow at such rapid rates, so the wind turbine industry has had to face significant challenges in reducing the overall costs and compete with other available renewables and non-renewable sources. Wind turbines have to adapt to unpredictable wind conditions and wind loads and so wind turbines often require frequent maintenance. Because of this, a major concern to the wind energy industry is that of O&M and reliability costs due to

unexpected wind turbine failures. The market for wind energy O&M is predicted to increase to $27 bn by 2026, EU O&M costs in 2017 being between $109-140/kW/year [2].

More recently, O&M has moved from expensive strategies to correct issues toward preventative and predictive strategies. To ensure wind turbines are cost effective, it is important to know component failure rates, downtimes, repair costs etc. Electronic and electrical systems represent the highest percentage of failure rates in the wind turbine system; however, the respective O&M costs are far lower due to the much shorter downtimes and inexpensive parts (difference in downtime being days vs. weeks) in comparison to those associated with rotor blades, gearbox, pitch drives and pitch and main bearings failures (Figure 1-3).

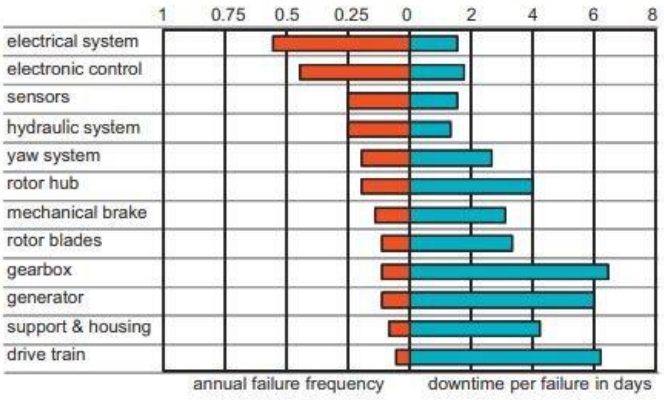

Figure 1-3: Wind turbine failure distribution 2009.

Under the international standard IEC 61400 [7] the desired lifetime of a wind turbine is 20 years, however, only a small percentage of wind turbines will reach this time without a major failure. With the continual growth in wind turbine capacity and the harsh operating conditions turbines are subjected to, gearbox failures are one of the biggest concerns to the industry. The replacement of an unpredicted gearbox failure results in significant O&M cost and downtime, especially when dealing with an offshore turbine where stringent logistics and special equipment including cranes are needed. Despite being designed to operate for the 20 year desired lifetime, it is well established that gearboxes are failing prematurely within the first five years of operation. The replacement of a gearbox and lubrication represent 38% of the turbines part costs and for a 1.5 MW turbine this can be upward of $250,000 [8]. As will be discussed later on, gearbox failure is most commonly associated with bearing failures, bearing failures accounting for about 70% [9], an up-tower bearing exchange costing up to €15,000 [10].

1.2 Wind turbine gearbox failure

1.2.1 The wind turbine gearbox

To facilitate the conversion of wind energy to electricity, a gearbox located inside the nacelle is used. The gearbox is one of the heaviest components of the wind turbine weighing around 10 tonne/MW [1]. Wind turbine gearboxes convert high torques and low speed to low torque and high speed, this being the opposite to conventional industrial gearboxes [8]. The gearbox ramps up the rotational speed from the low-speed rotor input (~13 – 20 rpm depending on rotor diameter) to the high-speed electric generator output (~1500 - 1800 rpm depending on the nominal rotational speed of the generator) for AC generation (50 Hz, Europe and 60 Hz, USA) [1]. To facilitate this, multi-stage gearboxes consisting of planetary and parallel gear stages are required [11]. This planetary gear system (also known as an epicyclic gearing system) consists of outer spur or helical gears (planets) that revolve around a single central gear (sun), ramping in speed (rpm) being achieved by the use of an outer ring (annulus). Figure 1-4 shows the typical wind turbine gearbox configuration.

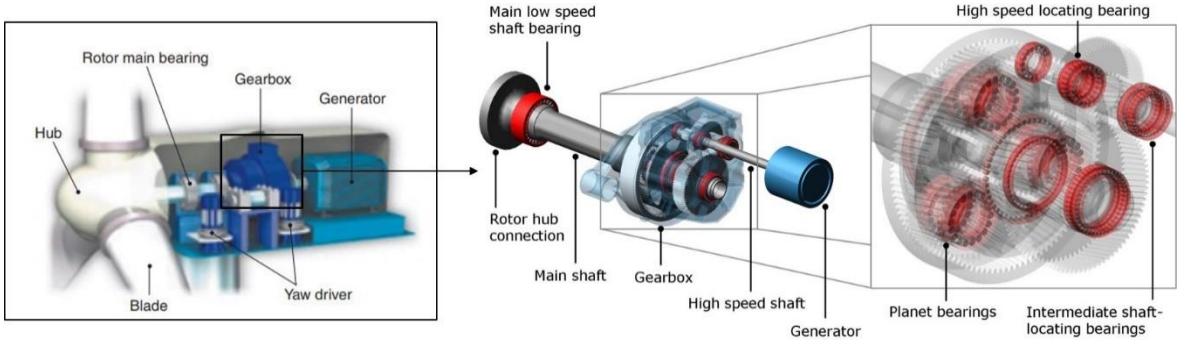

Figure 1-4: Wind turbine gearbox configuration. Taken and adapted from [12, 13].

1.2.2 Gearbox failure modes

As previously mentioned, in spite that manufacturers designing wind turbine gearboxes with the highest quality and resources available, the majority of gearbox failures come from bearings [9]. Bearing failure is not limited to the gearbox, the pitch and yaw systems and generator also being affected [1, 14, 15]. Wind turbine gearboxes typically use rolling element bearings and contain ~12 or more rolling elements [16]. Rolling element bearing failures are reported to be universal having no preference when it comes to any one bearing design, gearbox model, and manufacturer [8, 14, 17]. The critical locations for gearbox bearing failure is dominated by high-speed locating shaft (HSS) bearings, Intermediate shaft (IMS) bearings, and planet bearings (see Figure 1-4 for locations inside the gearbox and Figure 1-5 for damage statistics).

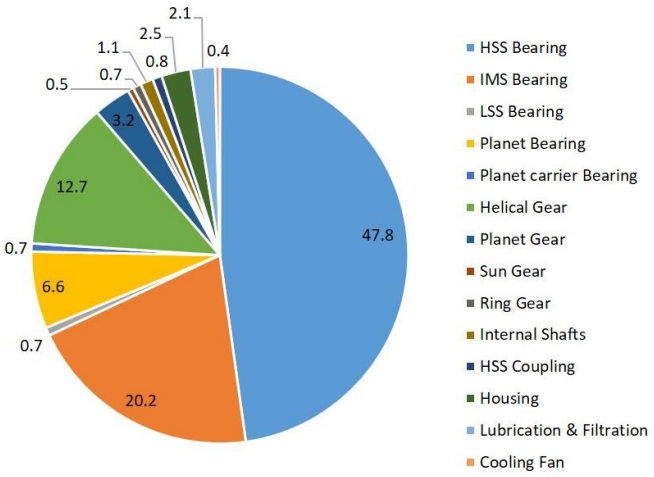

Figure 1-5: Wind turbine gearbox damage distribution based upon the damage records of 750 wind turbine gearbox by U.S Department of Energy and National Renewable Energy Laboratory (NREL) [18].

The main failure modes for wind turbine gearboxes are smearing, micro pitting, scuffing, electric discharge damage and White Structure Flaking (WSF) (Figure 1-6). WSF failure is an unconventional RCF failure and has been of hot topic to the industry for a number of years as it is the least understood failure mode and a critical and complicated issue due to its unpredictable nature. Major wind turbine original equipment manufacturers (OEMs) suggest that ~70% - 90% of WTGB bearing failures are associated with WSF [11, 12, 19, 20].

1.2.3 Conditions experienced by wind turbine gearboxes

The unique operating conditions that wind turbines have to operate in means that a wide range of challenging environments and tribological obstacles present themselves. With rapid development rate in wind turbine size, the conditions in which wind turbine gearbox bearings are subjected to are becoming more aggressive.

Wind turbine gearboxes experience a number of dynamic transient load/torque conditions and vibration/motion changes due to the unpredictable nature and uneven distribution of wind, premature generator connections to the electrical grid and emergency stops. Gearbox components need to be large in order to support the heavy fluctuating loads/torques, however, these heavy components can cause the gearbox casing and shafts to flex resulting in misalignments. For example, the planet bearing can be misaligned several times during a single revolution [21]. Deformations within the bedplate can cause dynamic misalignments of the gearbox with the generator shafts, this results in a negative effect on bearing load and damage to

the high speed bearings and gears [22, 23]. Gearboxes also come under braking loads when the over speed brakes connected to the high-speed shaft are engaged [24].

Another factor is the connection/disconnection of the generator to/from the electrical grid, if too quick this can result in rapid acceleration and decelerations with resultant release of potential energy producing high instantaneous torque reversals [14] and high overloads [25]. Loading zones on bearings can be relocated due to torque reversals causing stress peaks [14]. Condition monitoring on a 1.3 MW input shaft revealed that the intermediate shaft can typically experience ~3000 start-ups per year resulting in ~5 torque oscillations at each start-up (an acceleration from 375 to 422 rpm in 2 seconds and a torque change of -800 kNm to + 430 kNm in less than 100 ms) totalling ~15000 overloads per year [25]. The measured intermediate shaft displacement consequently is significant (200 µm laterally and 550 µm vertically) the maximum radial clearance specified for the particular bearing class being well-surpassed (120 µm) [25].

Wind turbines are exposed to a variety of severe environmental conditions due to the diverse geographical areas in which they planted, including high/cold temperatures, humidity, dust from desert conditions and sea-salt environments and moisture offshore. Wind turbines are therefore complicated when it comes to lubrication. Wind turbine gearboxes will typically use a single oil to lubricate both gears and bearings across a wide range of load conditions and speeds, bearings will therefore often run under mixed and boundary lubricating regimes [26]. Therefore, lubricant film thicknesses can vary significantly between locations inside the gearbox [14]. Gearbox oils often endure long standstills waiting for connection to the grid, where in this time small vibrations and oscillatory movements can push out lubricant from the contact [27]. To help combat the harsh lubrication regimes, gearbox oils and greases for wind turbines are typically high in additive PAG and PAO synthetic or semi-synthetic base oils [27]. Wind turbine gearbox oils will often have additive packages that have been developed and applied in the automotive industry, however issues may arise as the lubricant chemistry is not necessarily optimised for wind turbine gearbox operation [26, 27]. If oil temperature is too high scuffing wear in the gears can occur, therefore oil coolers and filters are used [28]. In conditions where humidity and moisture can be high, wind turbine gearbox oils are designed to contain additives that will aim to ingress more/less water and avoid the formation of micro-bubbles that can damage the oil film [27]. Wind turbine gearboxes can also be exposed to multiple electrical currents/potentials [29, 30] and electro-static charging due to friction at the rotor [31, 32].

With such an array of conditions acting on wind turbines during service, it is no wonder why this has led to inadequate conclusions on how to combat any one of these obstacles, this putting significant strain on manufacturers to achieve large meter scale bearings with 20-year lifetimes.

1.3 White Structure Flaking (WSF)

The bearing 'L_{10} life' or 'minimum expected life' characterises the RCF life of a bearing under given operating conditions where statistically 90% of bearings will survive [33]. Conventional RCF failures usually exceed the L_{10} life while WSF typically occurs at 5% - 20% of L_{10} with one report specifying as quickly as 1% of L_{10} [34].

WSF is a premature failure mode that is due to the formation of White Etching Cracks (WECs), which are networks of micro-cracks that are associated with a microstructural alteration called White Etching Area (WEA) (see Figure 1-6 for examples). WECs typically form ~1 mm below the contact surface. The 'white' in WEA/WECs refers to the white appearance of the altered microstructure when cross sections of bearing steel samples are polished and etched with nital solution (~2% Nitric acid in ethanol) or picral and observed under reflected light using an optical microscope (Figure 1-6). WSF has also discussed in relation to butterflies (Figure 1-6), which are also associated with WEA microstructural change and are formed around stress raisers such as non-metallic inclusions under highly localised subsurface shear stresses. This gives the butterfly shape, the butterfly wings comprising of the WEA. WEAs are not a new phenomenon, with literature dating as far back as the 1960s, however, more recently in the last decade WECs have become increasingly more reported. White etching cracks are not unique to wind turbine bearings and have been reported to occur in a number of other applications, nor it is restricted to any one bearing type, steel type or heat treatment, where a comprehensive list of these can be found in [27].

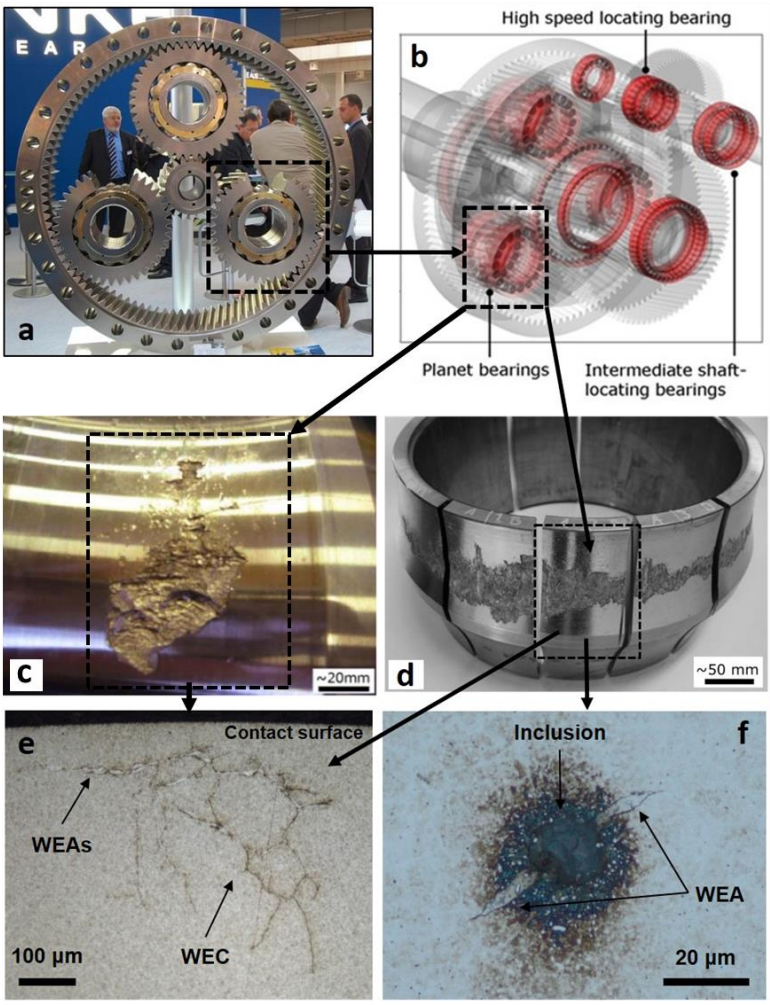

Figure 1-6: (a) Model of a one stage planetary bearing supports for a 1.5 MW wind turbine gearbox (image source [35]). (b) Inside the gearbox, adapted from [26]. (c - d) WSF damage on double row spherical bearing inner rings, (c) from [12] and (d) from [26, 36]. (e) Branching network WECs and respective WEAs. (f) Typical butterfly showing inclusion and branching butterfly wings and associated WEAs.

1.3.1 White Etching Cracks (WECs)

WEC failure modes have come under significant interest parallel to the expansion of the wind turbine industry over the last decade. Despite WEC failures being reported in a number of industrial applications, formation mechanisms are either lacking or not fully explored.

Under light optical microscopy (LOM), WECs appear to be sporadic, branching networks with WEAs bordering the cracks (Figure 1-7). The cracks are typically very thin (width < 1 µm). WEC morphologies are shown to differ significantly depending on the orientation (axial or circumferential cross-sections) they are viewed when observing WECs under LOM. This has been confirmed in a number of studies, a pioneer being Evans et al with the use of high resolution

manual serial sectioning (fine grinding, polishing and imaging of cross-sections at ~ 3 - 5 µm material removal intervals) and full 3D modelling of WECs [36-39]. WECs appearing vertically radially branched when viewed in the circumferential direction and parallel w.r.t the contact surface with less vertical branching when viewed in the axial direction [26, 27, 36-39].

WEAs have mainly been observed at borders of cracks, while cracks have been often observed without WEAs, and conversely WEAs without cracks. This has led to many questions, such as '*do cracks occur prior to WEA microstructural changes or vice versa?*' or '*Does WEA form cooperatively with the crack?*'; '*Does WEA form suddenly or gradually?*' and '*Does WEA form preferentially on one side of the crack?*' In the meantime, many features in the formation of WEA have been proposed. WEAs are a nanocrystalline ferrite structure of grain sizes ~ 5 - 30 nm, ~ 10 - 50% harder than the surrounding matrix and consisting of wholly/partially dissolved spherical carbides that have been suggested to occur as part of the WEA formation process [11, 12, 26, 36, 37, 40-45]. WEAs have also been shown to have amorphous-like phases that form first before WEA is generated [41, 46, 47], amorphisation being noted as a feature of the WEA formation process [41, 46-49]. Two forms of WEA have been proposed, where both forms can exist under RCF and are dependent on the extent of plastic deformation accumulation; (i) deformed WEA predominantly consisting of nanocrystallites, these have sheared microstructures and elongated carbides, the structure being unchanged despite nanoscale grain refinement; (ii) transformed WEA involving shear-driven amorphisation, the WEA being compact and having a well-developed morphology, WEA comprising a co-existence of nanocrystallites and amorphous phase (no spherical carbides being present due to refinement and dissolution). [49] Other features of the WEA formation process include, low temperature recrystallisation [42, 50], energy release by secondary recrystallisation driven by internal friction and plastic deformation near the crack in the formation of needle/plate like structures which are a precursor to nanocrystalline WEA formation [51, 52], and electrothermal effects [53-55]. Elongated and globular ferritic grains have been seen in altered regions around WECs in addition to high/low carbon distributions, where differences in nano hardness between the steel matrix and these features was observed [56]. Similarly, this study also showed the same features in dark etching regions (DERs) and white etching bands (WEBs), where these grains form at the earliest stages of microstructural alteration in DERs [57]. At later stages of WEC formation, elongated grains have been observed in zones of localised nanocrystalline WEA or undeveloped WEAs [58]. In the same study, at earlier stages, it was also found that primary spheroidised carbide dissolution transformed to WEAs when microcracks cut through carbides.

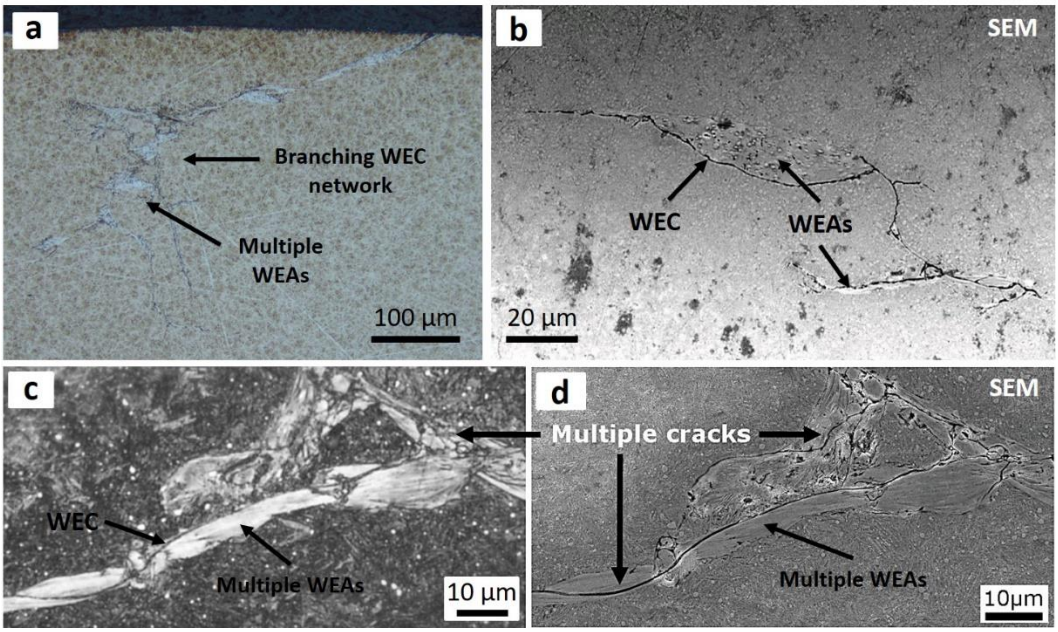

Figure 1-7: (a) Optical image of WEC and associated WEAs from an FAG-FE8 tested cylindrical roller thrust bearing in etched condition. (b) SEM image of WEC and adjacent WEAs in an FAG-FE8 tested cylindrical roller thrust bearing. (c - d) Optical and corresponding SEM of WECs and adjacent WEAs in a wind turbine gearbox planet bearing, taken and adapted from [12, 26].

One of the most popular theories for WEA generation is due to crack face rubbing causing localised mechanical deformation during RCF (this being enhanced in the presence of hydrogen [59], higher concentrations potentially existing at these sites [60]), during the crack face rubbing/beating process, material is transferred and deposited from one side of the crack face to the other [45, 50, 60]. Similarly it was suggested that WEA forms due to frictional energy at the rubbing crack faces [48]. The model quantifies the energy dissipated and suggests that part of this energy is converted to heat and microstructural decay and WEA forms due to amorphisation because of high-density dislocation accumulation [48]. By artificially inducing microcracks into steel prior to RCF, it has been shown that hard WEAs formed in the near vicinity to the microcracks, thus validating that cracks can be a precursor to WEAs, progressive ferrite deformation due to crack rubbing following recrystallisation to nano-ferrite [44]. The volume of WEA found adjacent to cracks is said to be dependent upon factors such as crack width, orientation of the crack w.r.t the rolling direction, and the depth relative to subsurface shear stresses, these factors affecting the extent of crack rubbing [44]. Negative and positive sliding zones are also suggested to affect crack face rubbing in WEA generation [61, 62]. In negative slide zones, traction forces are in the same direction as rolling, as a result crack faces come together and rub generating WEA; in positive slide zones, traction forces are opposite to rolling direction and cracks move away reducing the chance for rubbing, thus less WEA. A schematic illustrating this can be seen in [62]. Serial sectioning has also shown that through mapping of WECs in 3D,

little or no WEAs were present at the crack tips (i.e. the ends of WEC network propagation) [36-38]. Arguments against crack face rubbing come through subsurface inspection using Barkhousen noise measurements, subsurface changes being examined without the presence of cracks [63]. One study observed small (< 4 μm) microcracks without WEAs in the subsurface at the early stages of FAG-F11 RCF testing (10 hrs) [58]. In the same study, early forms of nanocrystalline WEAs were found at later RCF stages (20 hrs), WEAs being found predominantly on one side of the crack face. The study suggests that the crack face rubbing mechanism is unlikely (however, noted that crack face rubbing cannot be dismissed in the case where WEAs where found on both sides of the crack) to have generated these WEAs, generation proposed to be due to local plastic deformation after a transition process of groups of equiaxed grain formations. Local transformations in the microstructure have been observed as 'crack free' irregular dark etching regions (DER) and are suggested to be the precursor to WEA formations, where, similarities between microstructural alterations in WECs and those found in DER have been shown [40, 56, 61, 63, 64].

1.3.1.1 Initiation and propagation of WECs

WECs are extensive 3D networks, and as mentioned in the previous section, the introduction of serial sectioning to map WECs fully in 3D has shown the importance of considering multiple cross-sections to reveal substantial information regards crack morphology. At the early part of this decade, WEC initiation and propagation mechanisms were highly disputed, with hydrogen embrittlement commonly being pinned as the main culprit. Questions regarding whether WECs could initiate at the contact surface or subsurface via defects such as non-metallic inclusions, butterflies or independently were discussed, however theories lacked physical evidence to back proposed mechanisms. [12] The fine serial sectioning and 3D mapping of WECs has enabled the investigation and confirmation of WEC structures and initiation processes, especially confirming surface and subsurface initiation mechanisms [36-39]. Other techniques, such as the use of X-ray microtomography, have recently been used to map WECs fully in 3D from high-speed wind turbine gearbox bearings returned from the field [65-67]. Although strides have been made in the understanding of how WECs are initiated, identifying and locating WECs at their early stages of initiation have been difficult, this being mainly because of studies concentrating on running tests to failure in order to examine WECs. More recently, a study using electric current applied across 52100 steel bearings was conducted at a series of time durations on an FAG-F11 test rig to capture and observe the initiation and development of microstructural changes under optical microscopy and SEM [58].

Hypothesis for WECs initiation can be split up into either contact surface or subsurface mechanisms, where each of these hypotheses having a number of potential mechanisms.

Contact surface initiation

This hypothesis suggests that it is essential to have microcracks on the contacting surface prior to the formation of WECs. Three mechanisms for surface initiated WECs have been proposed,

1. Shear stress-induced fatigue microcracks that form independently under reduced frictional tensile stress with an initial shallow crack inclination to the contact surface in the over-rolling direction [64].

2. Localised high circumferential tensile stress (maximum at the contact surface) leading to spontaneously induced cleavage-like axial cracks that are typically 0.1 - 0.2 mm in length. These cracks are suggested to initiate at the near surface either independently [64, 68, 69] or at inclusions [27, 64, 68, 70, 71], or defects at the near surface for example at sites of contamination, dents, corrosion pits, machining defects or electrical erosion pits [27]. The assistance of hydrogen is suggested to be a driving force for this type of crack propagation, lubricant penetration inside the crack allowing for a release of hydrogen at the crack tip driving growth. [27, 64, 72, 73]
3. High surface shear forces due to the tribofilm formed (heterogeneous tribofilms composed of anti-wear and extreme pressure, and detergent/corrosion and rust inhibiting additives, tribofilms being discussed in more detail later on in 1.3.2.3) in sliding areas. Initially line cracks propagate vertically downwards (10 – 20 μm), cracks then propagating at an incline, the direction of propagation being dependent upon sliding zone. In negative sliding, the cracks propagate in the opposite direction of rolling; in positive cracks propagate in the rolling direction. WEAs develop only on cracks propagating in the negative sliding zones due to crack face rubbing (see previous section 1.3.1). [62]

Detailed schematic representations and examples of these mechanisms can be seen in an updated review by Evans in [74], with the exception of (3).

The assistance of hydrogen is suggested to be a driving force for this type of crack propagation, lubricant penetration inside the crack allowing for a release of hydrogen at the crack tip driving growth. [27, 64, 72, 73]

Subsurface initiation

It is now widely considered that WECs are predominantly initiated in the subsurface; however, the mechanisms of subsurface initiation are still debated. A significant contributor to this has been Evans and the author of this thesis in a number of studies on hydrogen charged (hydrogen charging being applied to drive crack growth, see section 1.3.2) two-roller and FAG-FE8 non-hydrogen charged tests [26, 36-39, 75]. Using extensive serial sectioning, these studies have proven for the first time that WECs have no contact to the surface, or such minimal contact length and crack volume connection that initiation of these cracks at surface is infeasible. X-ray microtomography has also supported subsurface initiation through 3D mapping of entire WECs in high-speed wind turbine gearbox bearing returned from the field [65-67] and an inner ring section from a large spherical roller bearing used in an industrial application [66]. FAG-F11 testing using electrical current applied to the test bearing observed very small (< 4 μm) randomly orientated microcracks at early RCF stages in the subsurface (~ 100 μm depth) under SEM examination, the electrical loading effects suggested to drive micro cracking [58].

There are a number of proposed mechanisms for subsurface initiated WECs and they are,

1. Subsurface initiation by non-metallic inclusions (see '*Non-metallic inclusions*' below) [26, 36-39, 66, 75, 76].

2. Adiabatic shear banding including or independent of defects through impact events, the crack forming after WEA microstructural changes occur [77, 78].

3. It has been proposed that cleavage-like axial cracks can be initiated subsurface [19, 79]. Subsurface cracking in hydrogen charged tests are suggested to lead to crack branching to the surface and subsequent axial cracks [80].

4. Lubricant self-charging that trigger localised transient current flow causing a local electromagnetic induction that crosses the contact surface leading to electrothermal mechanisms that trigger WEA microstructural changes [54, 55].

5. Multistage initiation of WECs due to the migration of carbon under shear stress and high-localised energy [81].

6. Lubricant controlled WEC failure – WEC initiation occurring in zones where the overlapping of high subsurface shear stresses and high concentrations of hydrogen occur. Metal containing additives in the lubricant forming films that allow hydrogen to diffuse where high frictional energy at the contact is present. [82]

7. Tribofilm induced water dissociation model – Patchy/rough tribofilms and nascent surfaces formed by metal containing additives in the lubricating oil cause high friction at the contact

during an incubation period. This results in disassociation of water and generation of hydrogen that diffuses into the steel, crack initiation forming dark etching regions and crack propagation forming WECs occurs. [83]

Examples and detailed schematic representations of these subsurface mechanisms can be viewed in an updated review by Evans in [74] with the exception of mechanism (5), (6) and (7) for which illustrations can be viewed in [81], [82] and [83] respectively.

Non-metallic inclusions

Subsurface WECs are commonly believed to be revolved around stress raising non-metallic inclusions that are located in the steel bearing matrix introduced during the steel manufacturing process. Typical non-metallic inclusions include sulfides nitrides, silicates and oxides. A wide range of studies have shown evidence for WEC-inclusion initiated cracks from different test specimens and bearings including; test specimens/bearings from laboratory studies under hydrogen charged [37, 39] and non-hydrogen charged conditions [26, 38], including under increased surface traction and in pre-damaged specimens through impact loading [84], and wind turbine gearbox bearings tested on large-scale test rigs [36] and returned from the field [76, 85]. These studies have shown extensively that sulphide inclusions including manganese or aluminates embedded in manganese sulphide, globular manganese sulphide + oxide inclusions and globular oxide inclusions are predominantly associated with WEC-inclusion interactions, inclusions being typically small and short in size ranging between ~ 1 – 30 µm diameter/length. [26, 36-39, 75, 76, 84, 85] WEAs have also been observed to form adjacent to inclusions, where high surface traction accelerates this and may be essential for their initiation [84]. Oxide encapsulations within the inclusion are responsible for inducing tensile residual stresses, poor coherence/debonding and mismatch in hardness between oxide part and tempered martensite matrix [42, 86, 87]. Debonding between inclusion and steel matrix for inclusion initiated cracks, micro-cracks or butterflies in the subsurface has been shown, where tensile/shear stresses are experienced in the debonding gap [85]. RCF testing has shown that a range of contact pressures and the amount of surface traction affects the level of debonding, in addition to being accelerated by impact loading [84]. Non-metallic inclusions are proposed to function as propagators or crack deflectors of WECs, this being due to the hydrogen trapping nature of the stress fields produced around these inclusions [27, 88]. It is proposed that small NMI-initiated WECs coalesce to form larger networks that eventually branch to the contact surface causing WSF or axial cracking [12, 26, 36-39, 41, 74, 75], where a detailed schematic of this is illustrated in [74] and [26].

Steel cleanliness analysis takes into account the type, number and size of inclusions to assess how ‘clean’ a steel is under the ISO 4967-B standard [89]. Fatigue life has been shown to be inversely

proportional to the square root of inclusion size (√area parameter model), super clean steels greatly improving RCF life [90]. Larger inclusion sizes are proposed to have a 'reinforcing' effect reducing peak stresses in the surrounding matrix, thus improving bearing life [91]. Analysis of inclusions from bearings returned from the field noted larger inclusions to be more damaging to bearing life, where relationships between inclusion length and the length of inclusion+micro-crack or butterfly wing were found [85]. Tests on differing steel cleanliness levels have observed no differences in time-to-spall thus it is reasoned that inclusions do not participate in the WEC formation [27, 53]. This argument is however contested, where if the standards used in the analysis of steel cleanliness levels do not take into account small sized inclusions typically found to be associated with WEC-inclusion interactions, then the comparative difference of small inclusions between steels cannot be validated and the conclusions are void [36, 37, 39, 74]. Cleanliness standards are said to be limited, as the relatively small inclusions found to interact with WECs are outside of the set thresholds, it has therefore been proposed that standards should focus on the density of small inclusions opposed to maximum inclusion lengths [36, 37, 39]. It is suggested that standards should record these small inclusions and be able to differentiate between pure sulfides and sulfides in combination with oxide parts [36]. It should also be noted that WEC networks [27], small microcracks (< 4 μm) at early RCF durations without the presence of WEA [58], and very small near surface WECs [37, 38] can been found without interaction with inclusions, thus suggesting they are not necessarily needed for WEC initiation/propagation.

1.3.2 White etching crack drivers

The formation drivers for WSF/WECs are highly debated but are thought to be driven by combinations of mechanical, tribochemical, and electrical/electrothermal effects. The two key cited drivers are *transient operating conditions* e.g. wind gusts, grid engagement, load reversals, braking, generating high impact loads, vibrations and slip and the *effect of hydrogen diffusion* in the steel during RCF operation (sourced from the lubricating oil and additives or water contamination). Other cited drivers include electrical and electrothermal effects, tensile hoop stresses, water/corrosion and lubricant/additives. Combinations of these drivers have been used to re-create WECs and appear crucial to their formation. The driving effects of hydrogen diffusion and lubricant additive chemistry on WEC formations are a focus of this thesis, where slip is also an important factor in testing in this study. These specific drivers are explained in more detail below.

1.3.2.1 Slip

Slip experienced by WTGBs due to for example, roller misalignment, torque reversals, rapid acceleration-decelerations etc. is frequently suggested to be a contributing factor to WSF/WECs. It is shown that slip can influence WEC formation in both FAG-FE8 and three ring roller Micro-Pitting rig (MPR) tests using an oil known to promote WECs [54, 61, 92], evidence for negative slip being more dominant in WSF over positive slip [61]. Slip has also been demonstrated to be influential on two-disc test rig set-up, negative slip again showing dominance in WEC/WEA formation over positive [93, 94]. This is attributed to lowered fracture mechanic properties under alternating load, higher material stressing and preferential surface crack propagation due to surface motion vectors pointing in the same direction in negative slip and traction forces [93]. Compressive closure of cracks due to negative slip is also proposed to enhance the crack face rubbing mechanism in the creation of WEAs [61]. In negative sliding, it is reported that crack propagation in FAG-FE8 raceways was on an incline and in the opposite direction to rolling; conversely, in positive sliding, crack propagation was in the same direction as rolling [62]. Negative and positive slide zones are also suggested to affect hydrogen penetration into surface cracks, positive slide zones causing crack mouths to open due to traction and rolling directions being opposite to each other, thus allowing increased hydrogen penetration [61]. 'Slip energy criteria' has been linked to WSF, where WSF occurs in zones of greatest slip energy (PVmax). Slip energy criteria has also been extended to take into account asperity contact (P_cV value which takes into account the asperity contact pressure P_c), and also asperity friction accumulation $e_{a,c\ max}$, this relating the specific frictional energy inputted to the surface during a contact load cycle and the regeneration time span between consecutive contact load cycles on tested WEC lives [95]. Further extension of the concept has been developed using information taken from different test rigs, using normal load and representing slip energy criteria per film thickness sheared ($N.V/\lambda$) in order to determine WEC formation thresholds in a variety of roller bearing configurations [27, 88]. There are limitations to the criteria however, for example, lubricant formulations are not taken into account. Tests under full fluid lubrication ($\lambda > 3$) and boundary conditions ($\lambda < 1$) showed WECs only formed in boundary regimes [94], where the degree of boundary lubrication (λ range) is also shown to control the propensity for WEC formations, higher severity boundary conditions ($\lambda = 0.06 - 0.7$) resulting in more WECs formed [61].

Increasing the degree of boundary lubrication while maintaining constant SRR has shown to increase RCF running time on a two-disc test rig set-up, conversely maintaining λ and reducing SRR lowered run time [94]. Areas of greatest slip energy have also been found to coincide with zones of highest concentrations of detected hydrogen [96-98]. It has also been shown in FAG-FE8

tests and tests using angular contact ball bearings that WECs first appeared at zones of high frictional energy [54, 95].

1.3.2.2 Hydrogen

As Evans points out in his updated review of the field [74], at the beginning of the decade hydrogen diffusion into the steel during operation was considered the root cause of WSF by the majority of researchers. Hydrogen being sourced from either lubricant or water contamination that is released during operation, diffusion leading to an 'embrittlement' of the steel and promoting WEC formations [12, 14, 40, 42, 99-101]. Since then research has focused on trying to quantify and investigate the mechanisms of hydrogen diffusion and continues to be a highly debated aspect of WSF. One of the governing factors in this has been the difficulty in measuring diffusible hydrogen in-situ and immediately post operation, diffusible hydrogen measurements in WTGBs never being recorded. Lab RCF tests have therefore used dry ice or liquid nitrogen to freeze tested samples as soon as possible after a test has finished in order to trap any diffusible hydrogen and stop it from effusing out, this being practically and logistically near impossible for a WTGB in the field.

To simulate the hydrogen diffusion process into the bearing steel during operation, a number of investigations have used hydrogen charging of test samples pre-RCF testing [37, 60, 88, 98, 99, 101-107]. In general, it is noted that pre-hydrogen charging samples decreases the RCF life of bearing steels that fail from WSF. It must be noted that pre-charging may not be a realistic interpretation of what happens in WTGBs and different WEC initiation and propagation mechanisms may result. For example, the location of WECs in angular contact ball bearings tests that were pre-hydrogen charged changed when comparing to non-hydrogen charged tests [27, 88]. More recently a new 'real-time hydrogenation method' (mixing water, poly ethylene glycol and ammonium thiocyanate (NH_4SCN) in 2:2:1 ratio to form a homogeneous solution) has been used to lubricate samples on a pin-on-disc set-up in order to re-create WEAs more quickly [108]. Non-hydrogen charged conditions are used to better simulate the environments experienced by actual WTGBs. As mentioned above, difficulties in measuring hydrogen in-situ RCF have meant that gathering information on hydrogen diffusion concentrations during operation has been limited or non-existent.

Theories for the detrimental effect of hydrogen on steel

There are a number of theories to explain the detrimental effect of hydrogen diffusion on steel, however there is no consensus as to which theory prevails in bearing steels. These theories include,

1. Hydrogen enhanced localised plasticity (HELP) [109], mobile hydrogen enhances dislocation plasticity, increasing dislocation mobility and reducing the barriers to dislocation movement. Dislocations thus pile-up and microscopic areas of high deformation surround these pile-up areas. As a result, application of stress in these areas is concentrated.
2. Hydrogen enhanced decohesion (HEDE) [110], solute hydrogen increases the lattice strength by reducing the cohesive forces required to separate crystals along crystallographic planes, thus the binding energy required for cleavage is reduced.
3. Hydrogen enhanced strain induces vacancy (HESIV), the formation of nanovoids and vacancies induced by strain in the company of hydrogen leading ductile crack growth by localised slip [111].

Typically, in the event of hydrogen diffusion, hydrogens role in steel increases slip deformation and induces localised plasticity at the fatigue crack tip [112, 113], as well as decreasing the mode I/II stress limits for crack propagation and growth [112, 114].

Hydrogen formation and diffusion mechanisms

There are a number of mechanisms to explain how hydrogen formation and diffusion into the steel could occur during RCF and these are,

1. Through wear induced nascent surfaces in mixed/boundary lubricating regimes and areas of high slippage or impaired/heterogeneous tribofilm, hydrogen is generated by the decomposition of lubricants through catalytic reactions [115, 116] and tribochemical reactions of water. See Figure 1-8.
    a. One mechanism of water disassociation being due to high friction in the initial incubation period (~20 hrs for FE8 tests) as a result of patchy and rough tribofilms formed due to nascent surface generation and tribochemical reactions, hydrogen is generated and diffusion into the steel results [83] (see Figure 13 in [83] for an illustration of this mechanism).
    b. Decomposition is proposed to occur in three stages [115] (i) Decomposition of lubricant by catalytic reaction at fresh nascent surface, (ii) Molecular chains in the lubricant break by shearing on the contact surfaces during sliding operation, (iii) Thermal decomposition of the lubricant is caused by heat generation due to the induced shearing on sliding. Hydrogen then diffuses through the steel contact surface to depths consistent with subsurface rolling contact stress fields (few hundred microns).

2. Lubricant and/or water penetration through surface cracks allowing a local release of hydrogen ions by tribochemical reactions at nascent crack tips, hydrogen then diffuses into steel, WEA microstructural change induced by the HELP mechanism [64]. See Figure 1-8
3. Two alternative proposed methods based on 'cathodic' and 'energetic' mechanisms, (1) Cathodic –Chemical reactions caused by strong electrical fields or continued boundary layer replacement/wear resulting in the formation of hydrogen, adsorption of hydrogen onto the cathodic steel surface results before diffusing into the steel. The deposition rate of hydrogen being enhanced in the case of high electric field strength and thus high ion mobility or high frictional energy accumulation. (2) Energetic - Atomic hydrogen formation through thermal dissociation due to high flash temperatures which may be caused due to electric discharge in the lubricant gap or rolling element acceleration upon entry to radial bearing load zones. [100] See Figure 1-8.

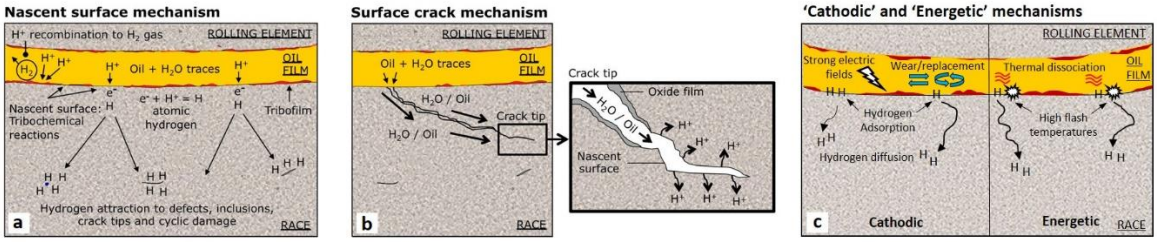

Figure 1-8: Hydrogen formation and entry mechanisms. (a) Hydrogen entry through wear induced nascent surfaces, taken from [74]. (b) Surface crack mechanism, taken from [74]. (c) Cathodic and Energetic mechanisms.

In all cases, it is the highly mobile mono-atomic form of hydrogen (H) that diffuses through the steel matrix potentially becoming trapped at inclusions/voids etc. The atomic hydrogen can potentially recombine to form molecular hydrogen (H_2), pockets of trapped H_2 existing unable to 're-diffuse' through the steel. When water is present, it is noted that hydrogen mainly derives from the oil and not the water [117]. Studies on WEC failed FE8 rollers using oils saturated with heavy water showed through thermal desorption spectroscopy that water was the prominent source of hydrogen [83]. Hydrogen diffusion through the nascent surface mechanism is supported by researchers who have found that hydrogen has diffused into steel during RCF testing [14, 111, 115, 118, 119], hydrogen measurements being proportional to wear on the steel during sliding tests [115] concentrations being between 0.1 and 4.2 ppm [14, 115, 118]. It is noted frequently that regions of the tested samples where concentrations were highest failed first. It is suggested that shallow (10 - 20 µm) hydrogen diffusion through wear induced nascent surfaces can increase the chance for contact surface tensile stress induced cleavage-like axial cracks [27]. It has been

proposed that a possible reason why WEC features/butterflies have not been found at the near surface (< 50 µm) is due to insufficient hydrogen penetration into the depth of the steel to enhance crack initiation and propagation [37, 103]. A 'real-time hydrogenation method', as mentioned previously, has been used to mimic hydrogen diffusion, the breakdown of water, poly ethylene glycol and NH_4SCN at nascent steel surfaces generating hydrogen, where hydrogen diffusion is said to aid in WEA formation process [108]. Studies have also suggested that hydrogen can be generated indirectly by static electrical discharge from stray currents across bearing faces, which in turn produce nascent surface zones for hydrogen generation [120] or hydrogen generation through static electricity where water becomes the source of hydrogen through the process of electrolysis [121].

Computational modelling of hydrogen diffusion into steel during RCF has indicated that subsurface stresses due to rolling motion have little effect on hydrogen diffusion [122], where further modelling shows small elevated hydrogen concentrations in the fatigue process zone, hydrogen concentration increase being due to trapping at deformation induced defects [123]. Studies have shown increased hydrogen permeation in zones of high PV_{max} (slip energy criteria, the product of contact pressure, P, and slip velocity, V) [96-98], where high-dissipated energy, slippage and boundary regimes exist, this potentially effecting nascent surface generation and the tribofilm. An extension of this is in studies that have linked asperity frictional energy accumulation $e_{a,c\ max}$ (a characteristic parameter linking PV_{max}, specific film thickness for calculating asperity contact pressure P_c and time between subsequent contact load cycles – regeneration time) with the absorption of hydrogen to explain the low susceptibility of rollers to form WECs in FE8 tests and why failure locations move after extended test times [95]. Experimental results coupled with simulations have shown that the initiation of WECs is governed by the overlap of high subsurface shear stresses and hydrogen concentrations, where contact width across the rolling direction is proposed to influence hydrogen diffusion [82]. Simulations also showed that concentrations of hydrogen were higher in regions of maximum slip across FAG-FE8 raceways (over a 40-hour test), the inner edge of the raceway having higher diffusion penetration depth and concentration of hydrogen than the outer [82, 100]. In addition, simulations showed hydrogen penetration concentrations to be greater at the near surface (<0.8 mm deep) after 40 hours with gradual decrease in % concentration further into the depth of the steel where comparison between MPR and FAG-FE8 tested samples also showed that the concentration and penetration of hydrogen was much lower on the MPR samples [82].

Hydrogen transport and diffusion of hydrogen through the steel in ideal cases (without the presence of traps/voids) is described by Fick's Laws. For given materials the diffusion coefficient *D* i.e. rate of diffusion m^2/second is different, for steel typical reported values are around $10^{-11} m^2/s$

[124]. Through electrical permeation tests conducted by Solano-Alvarez [125] the effective hydrogen diffusivity for cracked and un-cracked samples were found to be 1.57 x 10^{-11} m^2/s and 5.235 x 10^{-11} m^2/s respectively, showing that the hydrogen permeation in un-cracked sample is much stronger providing evidence for their ability to strongly trap hydrogen. Simulations of hydrogen diffusion in a steel cylindrical roller thrust bearing (FE8 raceway) have used diffusion coefficient of 0.765 mm^2/h at 100 °C [100]. Through Fick's laws an estimate for the depth of hydrogen diffusion penetration 'x' can be calculated by $x = \sqrt{Dt}$ where, 'D' is the diffusion coefficient (m^2/s) and 't' is time (s), however, this is limited since diffusion in reality is not ideal, hydrogen becoming trapped at defects.

Tests on 52100 steel in a vacuum pump using a PFPE fluorine based oil (virtually no hydrogen radicals present) still showed WECs to develop [52], thus indicating that hydrogen is not necessary for WSF.

Techniques for measuring diffusible hydrogen

There are a number of techniques that can be used to measure the bulk concentration of diffusible hydrogen in bearing steels and these are discussed in more detail in Chapter 3 of this thesis. The primary method for measuring hydrogen in weld steels under BS ISO 3690 [126] has been the mercury method, however due to health hazards of using mercury and long analysis times other methods have been exploited. One of the most popular methods is Thermal Desorption Analysis (TDA), TDA being recognised under the BS ISO 3690 standard [126]. Consequently, TDA has been used to measure diffusible hydrogen in bearing steels in a number of studies [37, 59, 60, 102, 104, 112, 116, 127, 128]. There are a number of potential caveats and pitfalls when it comes to TDA, and these are discussed in Chapter 3.

Trapping sites

Hydrogen can remain in mono-atomic (H) form as an interstitial solute retaining its mobility in high strength steels [118]. After diffusion, hydrogen can exist as either (i) 'Non-mobile', non-diffusible hydrogen that is strongly trapped or residual at irreversible sites or (ii) 'Mobile' or 'diffusible' hydrogen that is weakly trapped at reversible sites. [111, 119, 129, 130] As mentioned above, methods for measuring hydrogen including Thermal desorption techniques can be used to gain information on potential trapping sites of hydrogen. Trapping sites proposed include cracks, inclusions, grain boundaries, dislocations, strain fields, carbides, microvoids, retained austenite and areas of local plastic deformation where the density of crystal defects (dislocations) is large and hydrogen binding occurs [125, 127, 129, 131-139].

Traps can be split up in terms of their respective binding energies and desorption temperatures. Traps with low binding energies and desorption temperatures are referred to as weak reversible traps and strong binding energies and desorption temperatures referred to as strong irreversible traps. Reversible traps have desorption temperatures (TE) and Binding energy (EA) that are relatively low, a trap being considered reversible if its activation energy is lower than ~ 50 KJ/mol [140]. Traps can also be sub-categorised as being either physical or attractive (or a combination of the two). Physical traps are those that hydrogen is trapped by the way of mobile hydrogen's random walk and attractive traps are those such as electrical fields (e.g. electronegative impurity atoms) and temperature/stress gradients [141]. Thermal effects caused by circuit currents leading to sinks in the microstructure are also described as acting as attractive traps for hydrogen [54].

Strongly trapped hydrogen or hydrogen in its molecular form (H_2) is considered not harmful regarding WSF, it being the diffusible atomic hydrogen that 'embrittles' the steel. It has also been demonstrated that through artificially impregnating 52100 steel with small micro-cracks within the steel matrix and subsequent hydrogen charging, cracks can act as strong hydrogen traps rendering the hydrogen non-threatening and unable to assist in hydrogen embrittlement mechanisms [125]. However, it is noted that trapping and saturation of cracks with hydrogen could eventually lead to an internal pressure build up stimulating crack growth. Counter arguments to this are that the saturation of the crack could alleviate the ability for crack face rubbing/beating to occur during RCF [59], where crack rubbing/beating is proposed to generate WEAs [59, 60]. Thermal desorption and Secondary Ion Mass Spectroscopy (SIMS) showed that hydrogen trapped in Cr-Mo martensitic steel at inclusions is 'non-diffusive', hydrogen trapped in the microstructure being 'diffusive', where it is suggested that hydrogen trapped at inclusions can drive crack initiation, hydrogen trapped in the microstructure lowering fatigue crack growth thresholds [129]. In ultrasonic loaded tests on 52100 steel, in the presence of hydrogen (after pre-charging), the fatigue strength was found to be reduced and when the hydrogen was allowed to escape prior to testing (aged for 24hr to allow as much hydrogen to escape) the fatigue strength was recovered [118]. Tritium autoradiography (TAR) experiments on AISI 440C steel have shown that hydrogen trapping predominantly occurs at locations with tensile stress fields (Al_2O_3 inclusion and Cr carbide matrix interfaces) [135]. During the 'clumping' or clustering of cementite, hydrogen may get trapped at the clustered hydrogen interfaces resulting in the formation of 'sub-micron level porosity' [108]. However, hydrogen was also found to be trapped at locations with compressive stress fields (MnS inclusion), tensile and compressive stress fields created due to the differing CTE compared with the steel matrix. Hydrogen microprint technique (HMT) experiments have also shown that the interface between Al_2O_3 and the steel matrix acts as a diffusion path for hydrogen, low diffusivity being shown directly on the Al_2O_3 inclusion. Decreasing large MnS

inclusions (a weak reversible trap), is reported to improve resistance to WSF [142], however restricting the number of irreversible traps may increase the propensity for WSF [139]. This could be because irreversible traps can have the effect of rendering hydrogen non-harmful as in the case mentioned above in [125], more irreversible traps being beneficial. It is postulated that as steels become cleaner and thus less trapping sites are available, instead of hydrogen becoming trapped at less critical defects, hydrogen will remain in its mobile mono-atomic form moving towards more critical defects and locations enhancing hydrogen embrittlement [74]. It is also proposed that hydrogen may permit crack initiation at small inclusions that would be otherwise deemed not serious in the Mode I stages of WEC formation [26].

1.3.2.3 Tribofilm chemistry and lubrication

During rolling and sliding, tribofilms form on contact surfaces with varying degrees of composition, depending upon the lubricants, its additives, and the type of material involved. Tribofilms act as a third interface within the system providing significant impact on friction, wear performance, corrosion resistive properties and impediment of hydrogen into the steel. Flash temperatures at asperities govern the formation of tribofilms over nascent surfaces [143].

Extreme pressure (EP) and anti-wear (AW) additives consisting of sulphur and phosphorus compounds chemically react at flash temperatures and high pressure to form tribofilms to prevent metal-to-metal contact [144]. Additives found in lubricants that have been shown to reduce RCF life and promote WSF/WECs include greases and lubricants containing EP and AW additives such as zinc dithiophosphates (ZDDP/ZnDTP/ZnDDP) and detergent/rust preventatives such as calcium sulfonates [38, 53, 61, 62, 81, 83, 92, 94, 101, 145-147]. EP/AW additives, for example ZDDPs, are proposed to generate hydrogen via decomposition at catalytic nascent surfaces [115, 116]. Brittle flaking of bearings has been shown to be significantly affected depending on the type of grease used, synthetic ether base oil being shown to provide the best resistance [101]. Hydrogen poisoning sulphur can inhibit atomic hydrogen recombining to form molecular hydrogen (H2) leaving more available atomic hydrogen to diffuse into the steel [148]. An In-situ hydrogen detection technique using an adapted conventional Devanathan H-permeation cell and relying on a semi-quantitative approach, revealed that hydrogen ‘up-take’ (or permeation) was increased when EP/AW additives such as ZDDP were blended into a PAO base oil with water [149]. AW additives can increase friction and reduce oil film thickness [150], thus lead to breakdown of oil film and subsequent fresh nascent surfaces exposure. Other hydrogen poisoners including Poly-urea (CON_2H_4) grease lubricated rolling element bearings have shown to suffer from WEC associated failures [101, 120]. AW ZDDP tribofilms during run-in are shown to inhibit surface roughness reduction stimulating crack initiation [151]. ZDDP and Na, Ca and Mg

alkyl sulfonates are commonly associated with being hygroscopic, where these additives may carry water molecules to rubbing contact surfaces [83]. Mini-traction-machine Space Layer Interferometry Imaging (MTM-Slim) investigations have shown these additives form thick films, where it is proposed that these thick films cause high friction (and high heat) in an incubation period aiding in water disassociation and subsequent hydrogen generation that can diffuse into the steel promoting WEC formations [83].

Effect of oil chemistries containing Over-based Calcium Sulfonate

Detergents/dispersants and rust preventing additives to help keep contact surfaces clean, prevent deposits from adhering to the surface and avoid additive fall-out. Typical detergent additives are calcium-based alkysulfonates, these often being used with an over-based component (OBCaSul) formulation. A number of studies, including this thesis, have used an automotive gear oil known to be 'bad' or 'WEC critical' to promote WSF in order to investigate WEC formation mechanisms from bench top testing [38, 53, 58, 61, 62, 69, 95, 152]. This oil contains polyalphaolefin synthetic oil (PAO) base in combination with OBCaSul and AW short chain ZDDP. This oil causes bearing failure on an FAG-FE8 test rig between 16 – 40 hours [38, 54, 153]; this is in contrast to testing under the same conditions used in [54] where by using pure base oils tests run to 1000 hours without WSF. FAG-FE8 testing has showed that oils containing ZDDP, without the introduction of metal or non-metal additives formed WECs, addition of Ca/Na sulfonates also formed WECs as well as Ca/Na in the absence of ZDDP [83]. It was also noted that blends containing Ca/Na/Mg sulfonates, but not in combination, formed WECs but dependent upon concentration.

If OBCaSul does help to promote WSF, then this could be due to what authors believe to be a competition between ZDDP and OBCaSul. Calcium detergents and specifically OBCaSul are routinely used in automotive gear oils, they prevent deposits on the surface by forming a protective layer, have good AW/EP performance, anti-scuffing properties and reduce friction. OBCaSul are non-temperature dependent, when OBCaSul interacts with iron, the colloidal carbonate forms a film that can act as a barrier between metal surfaces [154]. ZDDP and OBCaSul having an antagonistic effect on the tribofilm AW properties [155], OBCaSul having an antagonistic effect toward sulphur containing species film formation [156], OBCaSul inhibiting ZDDP tribofilm formation [68, 157, 158], creating 'patchy/weakened' heterogeneous ZDDP tribofilms [158-162] and CaSul potentially aiding in hydrogen diffusion processes by promoting and prolonging nascent surface exposure [163]. Ball-on-disc tests coupled with electrical contact resistance (ECR) techniques have shown that ZDDP in combination with over-based detergents (Ca and Mg) slow down the rate of boundary film formation on 52100 steel (this in comparison to

ZDDPs alone) [162]. This potentially increasing wear rates, suggested to be due to competition to adsorb to the surface or calcium carbonate effect on the phosphate glass formation [162].

A number of suggestions using an array of experimental techniques to explain the role of OBCaSul effect when in mix with ZDDP are as follows; OBCaSul inhibits the formation of a ZDDP film due to the formation of a colloid dispersion with ZDDP [164]. OBCaSul competition with ZDDP at the contact surface in the formation of a tribofilm, the OBCaSul breaks down to form carbonate, which is deposited on the metal surface [165]. It has been shown from multiple surface techniques (AES, XPS, SIMS, SEM/TOF-SIMS, XANES) that the Ca displaces the Zn polyphosphates in the AW film [166, 167], OBCaSul may inhibit polyphosphate chain formation by formation of Ca phosphate [156]. X-ray absorption near-edge structure spectroscopy (XANES) has shown that mix of ZDDP and OBCaSul resulted in the formation of considerable Ca phosphate in the film [168]. The over-basing component is suggested to retard the rate-determining step of AW action (decomposition stage) of ZDDP [169], however others suggest that it can improve AW performance by forming a 'paste-like' structure in the contact [170, 171]. OBCaSul *alone* are proposed to provide good AW performance [172-174], forming thick (~100+ nm) calcium carbonate boundary films in the contact [173, 174] consisting of calcium oxide film in the subsurface with an upper surface consisting of $CaCO_3$ and SO_3 [174].

FAG-FE8 tests using a pure base oil with no additives and an oil containing OBCaSul and ZDDP revealed that the latter had formed WECs, the pure base oil showing no WECs [54]. This is explained by a 'self-charging' of the lubricant in the WEC formation process, promoting a current flow that leads to thermal effects and potential hydrogen trapping sites. Through X-ray photoelectron spectroscopy (XPS), Focused Ion Beam (FIB), and Secondary Neutral Mass Spectrometry (SNMS) of FAG-FE8 tested bearings, an oil containing OBCaSul and resulting in WECs being detected (using ultrasound) in the raceway, showed a trend for increased tribofilm thickness, with thick (100 nm) Ca-P tribofilms developing in zones of high slip [92]. In contrast removing OBCaSul from the oil resulted in no WECs being detected and showed a thinner (20 nm) Zn-S film in the same zones. It must be noted that these tests used ceramic roller to induce WEC failures in the raceways. WECs have been created using oils that do not contain calcium sulphonates, thus they are not required for WEC formation [27], however, that isn't to say that they cannot accelerate or aid in WEC formations. Hydrogen concentrations in zones where WEC formations occur are shown to be reliant upon the presence of metal containing additives in the lubricant and frictional energy accumulation [82]. Studies on an FAG-FE8 test rig using an 'WEC critical' oil containing Ca, S, Zn and P (as well as Na and B) additives, revealed through FIB and Scanning Transmission electron microscopy (STEM) that a heterogeneous tribofilm of varying thickness (5 – 100 nm) developed (see Figure 1-9) [62]. The oil tribofilm being found only in sliding

areas, confirming surface shear forces are responsible for the tribofilm formation. FIB/STEM analysis on a ball-on-disk rig using 52100 steel indicated a homogeneous film consisting of Mg, P, S, Zn and Mo, however at higher magnifications the film appeared heterogeneous varying between thin (~ 10 nm) and thick (~ 100 nm) regions, some areas showing no tribofilm, shallow cracking and penetration of the film into the surface [175] (see Figure 1-9). Results also indicated that steel type (AISI 52100 and 3310 being analysed) can play a significant role in defining the near surface material structure and tribofilm developed, the AISI 3310 steel showing a much more uniform film with no cracking and penetration into the steel, however, further work was recommended to confirm the reasoning behind this [175]. In rolling sliding conditions, heterogeneous ZDDP tribofilms have been stated to increase surface traction forces [176]. MTM-SLIM results using an oil containing metal based additives revealed that patchy ZDDP tribofilms of thickness ~120 nm formed on 52100 steel samples associated with WEC failures, on the other hand 'metal free' oils showed no or slight visible tribofilm [83]. RCF testing on an NTN-SNR Machine S bench top rig using angular contact ball bearings (ACBB) lubricated by an ISOVG46 mineral gearbox oil reported that WECs were only found to form at the contact edges, where SEM/EDX of the tested ACBBs showed little or no tribofilm formed at the contact edges [27]. A study on the structure of films on automotive cam followers by XPS depth profiling showed that high detergent levels were present in the AW film associated with high wear rates, conversely little or no Zn or P were found on the high wear surfaces [177]. The thickness of the film was shown to be approximately double that of ZDDP alone under similar test conditions. It has been identified through the use of electrical contact resistance and Auger electron spectroscopy (AES) that by using neutral detergents opposed to over-basing, neutral detergents only had a minor effect on the AW properties of the film compared to the over-based [164]. AES showed that by using neutral calcium sulfonate with ZDDP, the film contained Ca but the film was otherwise similar to ZDDP, the OBCaSul showing Ca and O in the film with no trace of ZDDP elements. XANES showed neutral calcium sulfonates only react with ZDDPs at concentrations above ≥2 wt%, Ca not affecting polyphosphate formation and being found in the topmost surface of the film [178].

Interpreted models for a developed ZDDP AW film and a ZDDP in the presence of calcium salicylate detergent additive tribofilms are shown in Figure 1-9 (c) and (d) [166]. These models are constructed upon experimental data and are noted to be 'gross simplifications', it is also noted that these are interpreted based upon automotive lubricants and conditions. The model shown in Figure 1-9 (c) is of a ZDDP + mineral oil, the sulphide film is said to form as a result of high temperature and pressure at asperity contact, this is followed by a rapid coating of a protective phosphate film (some sulphide remaining), with increasing depth, the composition of the sulphide varies to incorporate Fe and oxide by ionic exchange and diffusion. RAIRS, XPS and AES have also

shown that ZDDP without the presence of detergents form films of amorphous short chain ortho and pyro-phosphates with Zn [179, 180]. The model shown in Figure 1-9 (d) is of a ZDDP + detergent/dispersant (calcium salicylate). This time there is a defined separation between the Fe substrate and phosphate film with no sulphide layer suggested to be due to the competition for surface sites, where separate islands of ZnS and ZnO are shown; Fe is not found in the film and instead high levels of Ca and Zn are in the phosphate film, Ca displacing Zn to some degree. As mentioned above multiple techniques have shown Ca displacement of Zn. It is noted that the dispersant (Carbon-Nitrogen) does not form a part of the structure of the film. In addition it is noted that the XPS showed ZDDP + detergent/dispersant oil to be much thicker [166].

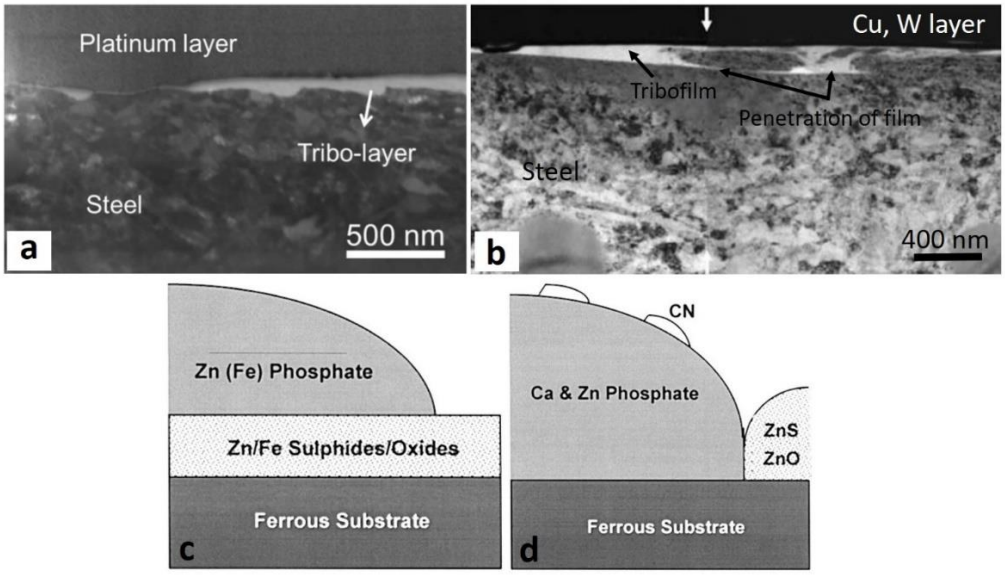

Figure 1-9: (a) Cross-sectional STEM image of the developed tribofilm on 52100 steel from FAG-FE8 test [62], see permission [1.1]. (b) Cross-sectional TEM image of tribofilm developed on 52100 steel during ball-on-disk test (white arrow indicates two spliced images) [175], Reprinted and adapted by permission from Springer Nature: Springer, Tribology Letters, Influence of Steel Type on the Propensity for Tribochemical Wear in Boundary Lubrication with a Wind Turbine Gear Oil, R. D. Evans, G. L. Doll, C. H. Hager et al, Copyright (2010), https://link.springer.com/journal/11249 (permission [1.2]). (c) Interpreted model of a ZDDP AW tribofilm [166]. (d) Interpreted model of a ZDDP AW tribofilm in the presence of calcium salicylate detergent additive [166]. For (c) and (d) see permission [1.3].

Additive preventative measures to hydrogen and WSF

Rust preventatives and Zn naphthenate metal deactivators, organic metal salts (cetylpyridinium salt [181]) and succinic acid can form films that inhibit hydrogen diffusion and WSF during testing [182]. Isopropylaminoethanol additives condense into surface microcracks alongside water and

help to trap hydrogen ions that are formed [183]. Zincdialkyldithiocarbamate (ZnDTC), ashless phosphate AW additive and/or non-metallic additive packages have been shown to suppress WEC failures when tested on an FAG-FE8 rig [83]. VG68 oil with copper powder and oxidised iron powder additives is reported to create WSF due to decomposition of the lubricant forming hydrogen at wear induced nascent surfaces [101]. Rust preventatives have been shown to prevent WSF by forming a passivating layer, on the other hand rust preventatives keeping surfaces clean accelerated WEC failures [101]. In steel weldments, studies in the arc chemistry reveal fluoride and calcite to prevent hydrogen diffusion [184]. Sliding tests under vacuum revealed that fluorine based PFPE oils (no hydrogen radicals present) did not generate hydrogen when exposed to fresh metal surfaces [115]. Tests also revealed that water-glycol oils containing corrosion inhibiting $NaNO_2$ and K_2MoO_4 are effective preventers of hydrogen generation/penetration; the deactivation of the catalytic reactive nascent steel surfaces by the formation of a passivating oxide film/compound film is suggested to be responsible for this. TEM/XPS has shown that lubricant additives containing sulphur are found to lead to the formation of iron sulfide films at crack tips, where these films are suggested to 'block' the pathway for decomposition of lubricants at catalytic reactive nascent surfaces, or provide a barrier to hydrogen diffusion [145]. WS_2 nanoparticles are proposed to be effective additives, forming films that can reduce water content in steel, inhibit hydrogen generation by limiting catalytic nascent surface formation and reduce hydrogen permeation into bearing steel by acting as a physical barrier to diffusion [185]. Thermal desorption spectroscopy has shown that trioctylphosphate (TOP) and ZDDPs reduced hydrogen permeation into steel specimens run on a ball-on-disc setup, where it is suggested these additives can form protective film preventing hydrogen permeation [186]. Phosphate films are reported to be effective in reducing hydrogen generation/penetration by forming a protective film [187]. Testing of higher viscosity base-stocks have been shown to delay the formations of WECs [83].

1.4 Aims and structure

1.4.1 Aims and objectives

The overall aim of this thesis is to study the effect that oils containing over-based calcium sulfonate detergent additives have on hydrogen diffusion and WEC formations in bearing steel, where WEC bearing failures are of major concern to the wind industry. This is accomplished by investigating three key question areas recognised in the fields' literature including, 1) '*What is the evolution of WEC formation?*' 2) '*What is the role of hydrogen diffusion in the WEC formation and propagation process?* ', and 3) '*How do critical additive components such as over-based calcium sulphonates in the lubricating oil affect WEC formations?*'

The main objectives based upon these questions were recognised as follows,

- This study firstly aimed to create and study the evolution of WECs under *non*-hydrogen charged conditions on a FAG-FE8 test rig by testing at several durations to capture the initiation of WECs.
- Analysis of hydrogen diffused into the FAG-FE8 tested bearings to investigate and reveal any correlations between diffusible hydrogen measured in the test bearings and the number of WECs formed in them.
- Finally, investigation of the influence of critical additive components such as over-based calcium sulfonate detergent additives in the oil have on hydrogen diffusion and WEC formations.

To achieve the objectives of this study, two RCF test set-ups (FE8 and MPR) have been used to create WECs. Advanced metallographic techniques have been used to quantify the WECs formed in the tested specimens. The content of diffusible hydrogen has been analysed using two different TDAs to gather more details on the hydrogen contents. The tribofilms formed on the tested specimens have been analysed using SEM/EDX to investigate the influence of oils containing over-based calcium sulfonates.

Structure of the thesis

This thesis comprises five chapters, including an introduction chapter, three chapters of journal papers (2 published and 1 submitted) and a final chapter summarising the conclusions of this study and future work suggestions. The published papers in Chapters 2 and 3 have been re-formatted for the thesis, contributions to the work are detailed on the following page.

Chapter 2 presents the paper entitled 'The evolution of white etching cracks (WECs) in rolling contact fatigue-tested 100Cr6 steel' [153], where the results from the study of WECs under non-hydrogen charged conditions and their evolution are presented. This study for the first time uses the technique of serial sectioning metallography under non-hydrogen charged test conditions over a range of test durations to capture the evolution of WEC formation from initiation to final flaking. It has been shown that WECs initiate subsurface at non-metallic inclusions, with increasing test duration these cracks propagate eventually leading to flaking of the contact surface. The amount of WEA microstructural change adjacent to cracks is found to increase with test duration, this being indicative of the crack being a prerequisite to microstructural alteration. This paper was written by the author and edited by the co-authors.

Chapter 3 presents the paper entitled 'Thermal desorption analysis of hydrogen in non-hydrogen-charged rolling contact fatigue-tested 100Cr6 steel' [188]. The results from detailed thermal

desorption analysis using two experimental approaches are presented in this paper and the correlations between WECs and diffusible hydrogen are discussed. The hydrogen concentration in non-hydrogen charged steel bearings over increasing RCF test durations were measured for the first time. Results revealed that hydrogen diffused into the rolling elements, increasing concentrations being measured for longer test durations, with numerous WEC formations being recorded. On the other hand, negligible concentrations of hydrogen were measured in the raceways, no WECs being recorded. Evidence for a relationship between diffusible hydrogen concentration and the propensity for WEC formations is shown in the rolling elements. Through combined metallographic results and thermal desorption analysis, it is assumed that hydrogen diffusion occurred at wear induced nascent surfaces or areas of heterogeneous/patchy tribofilm. This paper was written by the author and edited by the co-authors.

Chapter 4 presents the paper entitled '*The effect of over-based calcium sulfonate detergent additives on white etching crack formation in rolling contact fatigue tested 100Cr6 steel'* (submitted) will be described. This work presents RCF testing of 100Cr6 steel using two different test rigs lubricated with oils consisting of varying concentrations of OBCaSul additive. Serial sectioning techniques, TDA, and SEM/EDX have been used to explore the effects that oils containing OBCaSul additives have on the tribofilm formed, diffusion of hydrogen into the steel during operation and WEC formations. Results show that oil chemistries containing OBCaSul detergents can affect the number of WECs formed. Evidence for oils containing OBCaSul forming thick Ca dominated tribofilms have been found, and these films may have promoted hydrogen diffusion and WEC formations in the FE8 rollers. Thinner Zn-S tribofilms formed on the FE8 raceways however, may demote hydrogen diffusion and WEC formations. This paper was written by the author and edited by the co-authors.

Chapter 5 presents the overall conclusions of this study and suggestions for future work.

Contributions to the work

The following contributions to the papers detailed in Chapters 2 – 4, and Appendix C of this thesis as described above are as follows:

- FAG-FE8 is a standardized test (DIN 51819-3), test conditions co-designed by myself, co-authors, and Afton Chemical. FAG-FE8 testing was directed by myself and operated by personnel at Afton Chemical Bracknell.
- MPR test conditions co-designed by myself, co-authors and Afton Chemical. MPR tests were directed by myself and operated by personnel at Afton Chemical Bracknell.

- The formulated OBCaSul oils tested in Chapter 4 on the FAG-FE8 and MPR test rigs were co-designed by myself, co-authors and Afton Chemical.
- Serial sectioning analysis was designed and facilitated by myself. A significant part of the serial sectioning was conducted by myself and summer internship students, Mr. Ben Meuth, Mr. Zach Rowland, and Mr. Gabriel Llanos under the management and direction of myself to support the PhD study. Interpretation of serial sectioning data conducted by myself. SEM/EDX analysis of inclusions facilitated and directed by myself and SEM operated with the support of Pawee Kucita and Nan Zhou (nCATS), interpretation and analysis of data conducted by myself.
- The SEM/EDX tribofilm analysis experiment was designed by myself, co-authors and Afton chemical, SEM/EDX was executed by Grant Pollard at Afton Chemical Richmond USA. All interpretation and analysis of data was carried out by myself.
- 3D crack imaging was designed by myself, image processing partly conducted by myself and with the support of Dan Mckay (University of Southampton), interpretation and analysis of data conducted by myself.
- Thermal desorption analysis (TDA) analysis designed and executed by myself and co-authors, the TDA analysis conducted using ‘set-up 1’ and ‘set-up 2’ as defined in the thesis, was operated by Sally Day at The Welding Institute (TWI) and Steve Ooi (Cambridge University) respectively under the direction of myself. All interpretation and analysis of the data was done by myself.
- Steel cleanliness analysis was conducted at the Dr. Sommer Werkstofftechnik GmbH lab.
- For the publication in Appendix C, FAG-FE8 testing co-designed by Afton Chemical and Martin Evans (nCATS). Serial sectioning analysis was conducted by myself. Interpretation and analysis of data conducted by Martin Evans. The publication was written by Martin Evans and edited by the co-authors. This paper has been re-formatted for the thesis.

Chapter 2 WEC Evolution in RCF tested steel

The Evolution of White Etching Cracks (WECs) in Rolling Contact Fatigue-Tested 100Cr6 steel

A.D. Richardson[a*], M.-H. Evans[a], L. Wang[a], R.J.K. Wood[a], M. Ingram[b], B. Meuth[a]

[a]nCATS, Faculty of Engineering and the Environment, University of Southampton, UK

[b]Afton Chemical Ltd, Bracknell, UK

Notation list for Chapter 2

α	Pressure viscosity coefficient [GPa^{-1}]
C_i	Global cleanliness index
η_o	Dynamic viscosity [Pas]
θ	WEC angle w.r.t axis of direction of compression
h_{min}	Minimum oil film thickness [m]
HV	Vickers pyramid number
L_{10} life	RCF life of a bearing for given operating condition where statistically 90% of bearings will survive
λ	Lambda ratio
N	Normal contact load [N]
P	Contact pressure [Pa]
P_{max}	Maximum contact pressure (Hertzian stress) [Pa]
R_q	Root mean squared roughness [m]
σ	Yield stress
$\tau_{o,\,max}$	Maximum orthogonal shear stress [Pa]
$\tau_{uni,\,max}$	Maximum unidirectional shear stress [Pa]
V	Absolute sliding velocity [ms^{-1}]

2.1 Abstract

The formation of white etching cracks (WECs) in steel rolling element bearings can lead to the premature rolling contact fatigue (RCF) failure mode called white structure flaking (WSF). Driving mechanisms are still debated but are proposed to be combinations of mechanical, tribochemical and electrical effects. A number of studies have been conducted to record and map WECs in RCF tested samples and bearings failed from the field. For the first time, this study uses serial sectioning metallography techniques on non-hydrogen charged test samples over a range of test durations to capture the evolution of WEC formation from their initiation to final flaking. Clear evidence for subsurface initiation at non-metallic inclusions was observed at the early stages

WEC formation, and with increasing test duration the propagation of these cracks from the subsurface region to the contact surface eventually causing flaking. In addition, an increase of the amount of associated microstructural changes adjacent to the cracks is observed, this being indicative of the crack being a prerequisite of the microstructural alteration.

2.2 Introduction

Rolling element bearings used in wind turbine gearboxes suffer from a premature failure mode called white structure flaking (WSF). This typically occurs in 1 – 20% of the bearing's L_{10} life, where the wind turbine lifetime is reduced from the predicted 20 years to < 2 years [74, 77]. WSF is due to the formation of white etching cracks (WECs) typically ~ 1 mm below the contact surface. WECs are networks of micro-cracks with an associated microstructural alteration called white etching area (WEA) which borders, or is intermixed with the WEC. The appearance of WEA is revealed when etched in nital solution (2% nitric acid in ethanol). WEA is a nano-crystalline ferrite structure of grain sizes ~ 5 - 300 nm, ~ 10 - 50% harder than the surrounding matrix and comprised of wholly or partially dissolved spherical carbides found to be part of the WEA formation process [11, 12, 26, 36, 37, 40-45]. Amorphous like phases have also been shown to be present in WEA, these amorphous like structures forming first before WEA is generated [41, 46, 47]. WEA has been proposed to exist in two ways, deformed WEA consisting predominantly of nanocrystallites and transformed WEA consisting of coexistence between nanocrystallites and amorphous phase [49].

The formation drivers as well as the initiation and propagation mechanisms for WSF and WEC in rolling bearings are still highly debated but are thought be driven by combinations of mechanical, tribochemical and electrical effects including,

(i) transient operating conditions such as wind gusts, load reversals, grid engagement, braking etc. generating high impact loads, vibrations and slip,
(ii) electrothermal and electrical effects,
(iii) tensile hoop stresses,
(iv) hydrogen release and diffusion into the bearing steel (sourced from the lubricating oil and additives or water contamination).

The proposed initiation and propagation mechanisms for WSF/WECs are,

1. Surface initiation through two opposing mechanisms, (i) shear stress induced fatigue microcracks [74] and (ii) Localised high circumferential tensile stress spontaneously induced cleavage-like axial cracks that initiate independently [26, 64, 189], at defects

such as inclusions [27, 64, 70, 71, 189] or due to corrosion, machining defects or electrical erosion pits [27].

2. Subsurface initiation by non-metallic inclusions (NMIs) [26, 36-39, 66, 75, 76], perhaps in some cases due to tensile stresses [190].
3. Adiabatic shear banding independent or including defects through impact events, cracks forming after microstructural changes occur [77, 78].
4. Self-charging of lubricants triggering localised transient current flow causing local electromagnetic induction that crosses the contact surface leading to electrothermal mechanisms triggering subsequent WEA microstructural change [54, 55].
5. A multistage initiation of WECs as a result of migration of carbon under shear stress and high localised energy [81].

Subsurface initiated cracks are difficult to identify and quantify. When a 'young' crack is found, the mechanism of formation is easier to understand, and is frequently believed to be revolved around NMIs. One technique used for recording WECs is the application of serial sectioning to map entire WECs in 3D. This technique has been perfected by the authors [36-39] where it is confirmed that at least one mechanism of WEC formation is initiation and propagation in the subsurface, with strong evidence for subsurface initiation being at NMIs. Supporting evidence for subsurface initiation has been provided from 3D-mapping of entire WECs by X-ray microtomography conducted on high-speed wind turbine gearbox bearings (WTGBs) returned from the field [66, 67, 191] and an inner ring section of a large spherical roller bearing used in an industrial application [66]. X-ray tomography of this spherical roller bearing revealed large (> 26 µm in axial and circumferential length) multiphase inclusion combinations of Al, Mn and S elongated in the direction of over-rolling to have initiated subsurface WECs. Through metallographic analysis of field returned WTGBs, it has also been found that small/short sized 8 - 24 µm MnS inclusions were mainly associated with butterfly/small-WEC crack initiation [76]. Analysis of failed low speed shaft WTGBs, however, have found that oxide and dual phase inclusions are more detrimental than MnS inclusions [192]. Subsurface WECs and inclusion interactions have also been found through testing and metallographic analysis of WTGBs with induced tensile stresses from bearing seat deviation [190]. This supports evidence from previous studies conducted on WTGBs by authors of this manuscript [36] where predominantly small/short sized (3 - 20 µm) sulphides, globular oxides and globular MnS-oxide inclusions were recorded and judged likely initiators of WECs. It is proposed that small NMI initiated WECs coalesce to form larger networks that eventually branch to the contact surface causing WSF or axial cracking [12, 26, 36-39, 41, 74, 75].

There is also debate on whether the crack or WEA microstructural change occurs first, whether WEAs form cooperatively with the crack and whether WEA forms gradually or suddenly, where proposed formation mechanisms include amorphisation [41, 46-49], adiabatic shear, severe localised plastic deformation, low temperature recrystallisation, carbide break-up and dissolution and electrothermal effects, these being extensively reviewed in [74]. One popular hypothesis is due to crack face rubbing causing a localised mechanical deformation during RCF (this being enhanced in the presence of diffusible hydrogen [59], higher concentrations could exist at these sites [60]), an associated material transfer from one side of the crack to the other occurs, and recrystallisation results [45, 50, 60]. A more recent hypothesis developed through modelling is energy dissipation at rubbing crack faces [48]. The developed crack model quantifies the amount of energy dissipated as a result of friction at crack faces; part of this energy is converted to heat and microstructural decay, WEA formation being a result of amorphisation due to high-density dislocation accumulation. The energy generated during crack rubbing leading to amorphisation is also proposed to be sufficient enough to dissolve large amounts of carbides in the WEA [49]. A counter argument to crack rubbing comes through subsurface inspection using Barkhousen noise measurements, where subsurface changes are investigated without the presence of cracks [63]. A local transformation in the microstructure is observed as 'crack free' irregular dark etching regions and is suggested to lead to the formation of WEAs. Similarities have been shown between microstructural alterations in WECs, and those alterations found in dark etch regions [56]. An experimental approach by artificially inducing microcracks into the steel prior to RCF has also shown that hard WEAs formed in close proximity to the microcracks, providing an experimental validation that cracks can be a precursor to WEA formations [44]. In an investigation to study the effect of brittleness on the generation of WEA, modified AISI 8620 steel was intentionally heat treated to produce intergranular embrittlement [193]. During RCF, cracks formed preferentially along the grain boundaries due to lowered toughness where WEA was found to form along these intergranular cracks. It is suggested that the movement of the crack faces under subsurface shear promoted the formation of WEAs along the crack faces. Finally subsurface crack rubbing has been shown to produce wear debris with an identical composition to the steel matrix, the wear debris being a result of the disintegration of lamellar structure formed during crack rubbing [49].

This study uses extensive metallographic analysis including standard and serial sectioning techniques to record and map individual WECs in 3D and associated damage features in RCF-tested 100Cr6 steel cylindrical roller thrust bearings (CRTBs) on an FAG-FE8 test rig, this being a continuation of the works conducted previously by the authors [194, 195]. Many previous studies have applied different techniques to record and map WECs in failed bearings from the field and RCF-tested samples; however, little attempt has been made to record the evolution of WECs from

their initiation to final flaking. This study aims to provide evidence for the stages of subsurface inclusion initiated WEC evolution for the first time to give valuable insight into this bearing degradation mechanism.

There is an accompanying piece of work [153] to this investigation that explores the role of hydrogen diffusion in the RCF tests conducted in this study (see Chapter 2).

2.3 Materials, techniques and experimental methods

2.3.1 Rolling contact fatigue testing

Testing was conducted on a standard FAG-FE8 rig (see Figure 2-1). Two 100Cr6 steel CRTBs are tested simultaneously, usually used in the standardised test (DIN 51819-3). Two plate springs apply load. Each bearing has 15 individual rollers mounted in a brass cage sandwiched between two washer raceways (see Figure 2-1 (c)). The raceways are pre-roughened before testing to R_q values of 0.25 µm and 0.5 µm for the two bearings respectively, the 0.5 µm bearing being focused upon, this is to induce boundary regime conditions. On the raceway at the centre of the bearing contact zone exists a pure rolling condition with rising slip to the edges of up to ± 12.5% slide-roll-ratio (SRR) along the contact major axis (see Figure 2-1 (c), [196]). On the rollers, the slip zones experience both – ve and + ve directional slip, due to the roller being sandwiched between two raceways. Eight tests were conducted from 0 to 18 hours, two of the tests (at 16.5 and 18 hours) were shut down due to a vibration threshold limit being reached; other tests were shut down manually at pre-determined running durations (0hr control, 2hr, 4hr, 6hr, 6hr repeat and 12hr). The calculated maximum Hertzian contact pressure Pmax is in the range of ~ 1.5 – 1.9 GPa, this being in accordance to the contact length used for a range of lengths between 7 – 9 mm (this dependence taking into account the profile of the rolling element geometry and where roller/raceway contact is assumed to start based upon bearing drawings and software). The test conditions are shown in Table 2-1.

Initial minimum oil film thickness (h_{min}) between rollers and washer raceways is calculated using the Hamrock and Dowson equation [197, 198]; see equation (A.1.1) in A.1. Lambda ratio (λ) has been calculated based upon h_{min} and the roughness (R_q) values given in Table 2-1; see equation (A.1.2) in A.1. Fully formulated semi-synthetic gear oil was used as the lubricant for all tests (detailed in Table 2-1). The oil temperature in the contact is controlled at 100 ˚C during operation.

It should be noted that no method to artificially induce WECs was used, such as pressure transients, hydrogen charging or applying electrical currents. The pressure, speed and temperature are in steady state. Although the lubricant used is known to readily induce WSF.

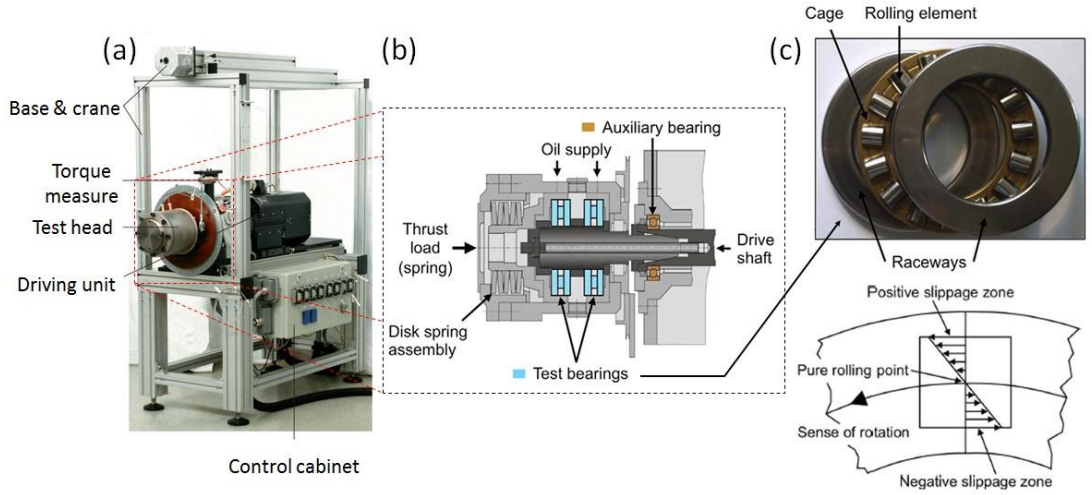

Figure 2-1: (a) FAG-FE8 test rig, (b) schematic of test chamber (side on view), and (c) CRTB used in the RCF testing and slippage condition experienced. Adapted from [38].

Table 2-1: FAG-FE8 RCF test conditions.

Test system	
Test rig	FAG-FE8
Test sample	Cylindrical roller thrust bearings
Bearing type	F-562831-01 / 81212
Oil properties	
Oil type	Automotive gear oil, fully formulated semi-synthetic (ISO VG64)
Viscosity	64 cSt (40 °C), 9.5 cSt (100 °C)
Pressure viscosity coefficient (α)	6.6 GPa^{-1}
Dynamic viscosity η_o (100ºC)	0.0046 Pas
Oil additives	Sodium and calcium sulfonates, ZDDP antiwear additives, VI improvers and FMs
Bearing material properties	
Washer / roller / cage material	Martensitic 100Cr6 steel / Martensitic 100Cr6 steel / Brass
Hardness roller / washer	765 HV / 590 HV
Surface roughness (R_q) roller / washer	0.09 µm / 0.50 µm
Test conditions	
Rotational shaft speed	750 rpm
Axial load	60 kN
Max contact pressure	~ 1.5 – 1.9 GPa (depending on contact length used 7-9 mm, 9 mm used in this study)
Bearing / oil temperature	100 °C
Minimum film thickness (h_{min})	0.053 µm
Lambda ratio (λ)	0.1
Test durations	
Test number (duration) 1/2/3/4/5/6/7/8	0/2/4/6/6-repeat/12/16.5/18 (hours)
Subsurface shear stresses	
Max orthogonal shear stress ($\tau_{o,\,max}$)	~375 - 475 MPa (acting @ ~92 µm below the contact surface)
Max unidirectional shear stress ($\tau_{uni,\,max}$)	~456 - 578 MPa (acting @ ~145 µm below the contact surface)

2.3.2 Metallographic analysis and contact surface inspection

Metallographic analysis including fine and coarse serial sectioning techniques were conducted on the RCF tested bearing rollers and raceway washers to record and fully map individual WECs in 3D and associated damage features. Optical macroscopy was used to inspect the contact surface of the bearing parts before metallographic analysis.

Before sectioning, the raceway washers were cut into ~ 20 x 20 mm sections, the rollers kept whole. Rollers and raceway sections were subsequently hot mounted in Bakelite. Rollers were mounted in groups of three for each test duration (excluding the 16.5 hr test) to make sure analyses were statistically representative of each test duration. Raceway sections for the 18 hour test only were mounted singularly, four individual sections being analysed covering ~ 1/3rd of the washer to inspect a representative area of steel. Notches were cut into the rollers to act as a marker for identifying individual WECs at each sectioning slice interval around the circumference, individual WECs, when recorded, being numbered in regards to the numbers around a clock face, the notch representing 12 o'clock. Rollers were mounted such that they were sectioned in the axial direction from the outer roller edge through to the inner. Raceway washers were mounted such that the contact surface was sectioned, material removal being performed in the radial z-direction. See Figure 2-2 for sample preparation.

Figure 2-2: Stages of sample preparation for rollers and raceway sections.

Sectioning was performed on automatic grinding/polishing machines (Struers TegraPol-15 with a TegraForce-1 and a Struers LaboPol-21 with a LaboForce-3) using 800, 1200 and 4000 SiC papers followed by 9 and 3 µm diamond suspension lubricants for the final polishing stages. The polished sample cross sections were then chemically etched in nital (2%) before imaging. Images were taken by optical microscopy (Olympus BX41M-LED and BX51) at 50 – 200x magnification to map and record WECs, with 500x and 1000x magnifications accompanied with SEM/EDX (JEOL JSM-6500F SEM and Oxford Inca 300) to image and analyse inclusion-WEC interactions. Open source image processing software (ImageJ) was used to measure the dimensions of WECs and damage features. To create a controlled sectioning process, macro-Vickers indents were used to track the grinding/polishing removal rate as well as being used to track individual WECs.

2.3.3 Contact surface inspection

Optical macroscopy was conducted on the same rollers and raceway sections that were subsequently sectioned. Images were taken at 60˚ intervals around the circumference of the rollers. The four individual raceway sections were imaged to give an overview of the contact surface.

2.3.4 Sectioning analysis

Fine serial sectioning was conducted on the 2, 6 and 18 hour RCF tests with removal intervals of ~ 3.4 – 3.9 µm per slice.

Coarse serial sectioning was conducted on the 4 and 12 hour tests, and post fine serial sectioning on the same 6 and 18 hour test rollers to continue recording WECs across the length of the rollers. Coarse serial sectioning was not conducted on the 2 hour test due to no WECs being found through fine serial sectioning. Removal intervals were conducted at ~ 15, 30 or 50 µm per slice. Coarse serial sectioning was conducted from the outer roller edge through to the inner on the 6, 12 and 18 hour tests, the 4 hour test being cut short due to lack of WECs recorded. Coarse serial sectioning was conducted up to ~ 9.6 – 10.41 mm across the 6, 12 and 18 hour tests, this being due to time considerations and that through initial macro-sectioning WECs were first found at ~ 1.7 – 2.6 mm from the outer edge. Inclusions were recorded during coarse serial sectioning; only inclusions recorded in the outer roller half being displayed. Coarse serial was conducted on the 18 hour raceway sections at intervals of ~ 50 µm, starting at the contact surface (0.00 mm) up to a total depth of ~ 500 µm. The individual fine and coarse serial sectioning interval ranges for rollers and raceway sections are listed in Table 2-2 and Figure 2-3 explains the serial sectioning steps**.**

Table 2-2: Sectioning intervals and removal rates conducted during the metallographic analysis.

Test duration	Analysis type	Nº samples analysed	Sectioning interval (~mm)			Slice removal rate (~µm/slice)	
			Macro sectioning	Fine serial	Coarse serial	Fine serial	Coarse serial
2 hr	Fine serial	3x Rollers	R1: 0.00 – 1.65 R2: 0.00 – 1.76 R3: 0.00 – 1.51	R1: 1.65 – 2.22 R2: 1.76 – 2.37 R3: 1.51 – 2.17	- - -	R1: 3.4 R2: 3.6 R3: 3.9	- - -
4 hr	Coarse serial	3x Rollers	R1: 0.00 R2: 0.00 R3: 0.00	- - -	R1: 1.7 –2.84 R2: 1.86 – 2.8 R3: 1.7 – 2.82	- - -	R1: 15 R2: 15 R3: 15
6 hr	Fine + coarse serial	3x Rollers*	R1: 0.00 – 1.92 R2: 0.00 – 1.73 R3: 0.00 – 1.51	R1: 1.92 – 2.68 R2: 1.73 – 2.57 R3: 1.51 – 2.28	R1+: 2.68 – 10.3 R2+: 2.57 – 9.6 R3+: 2.28 – 9.67	R1: 3.4 R2: 3.7 R3: 3.4	R1†: 15/30/50 R2†: 15/30/50 R3†: 15/30/50
12 hr	Coarse serial	3x Rollers	R1: 0.00 R2: 0.00 R3: 0.00	- - -	R1: 1.8 – 10.26 R2: 2.03 – 10.41 R3: 1.86 – 9.7	- - -	R1†: 15/30/50 R2†: 15/30/50 R3†: 15/30/50
18 hr	Fine + coarse serial	3x Rollers* 4x Raceways	R1: 0.00 – 2.01 R2: 0.00 – 1.77 R3: 0.00 – 1.77	R1: 2.01 – 2.59 R2: 1.77 – 2.41 R3: 1.77 – 2.36	R1+: 2.59 – 10.27 R2+: 2.41 – 9.8 R3+: 2.36 – 9.64 RW1: 0.00 – 0.047 RW2: 0.00 – 0.051 RW3: 0.00 – 0.048 RW4: 0.00 – 0.047	R1: 3.4 R2: 3.8 R3: 3.5	R1†: 15/30/50 R2†: 15/30/50 R3†: 15/30/50 RW1: 50 RW2: 50 RW3: 50 RW4: 50

KEY

*: Same samples used for fine and coarse serial sectioning analysis, samples mounted as a group of three.

+: Coarse serial sectioning conducted post fine serial sectioning analysis.

†: Slice intervals of ~15 µm conducted initially, with intervals of ~30 and 50 µm being conducted subsequently due to time considerations.

NOTE: All samples are macro sectioned at ~50 µm slice intervals at the start outer rolling element edge (0.00 mm) until the first visible sign of WECs are found in any one-test roller. R: Denotes rolling element and RW: Denotes raceway washer.

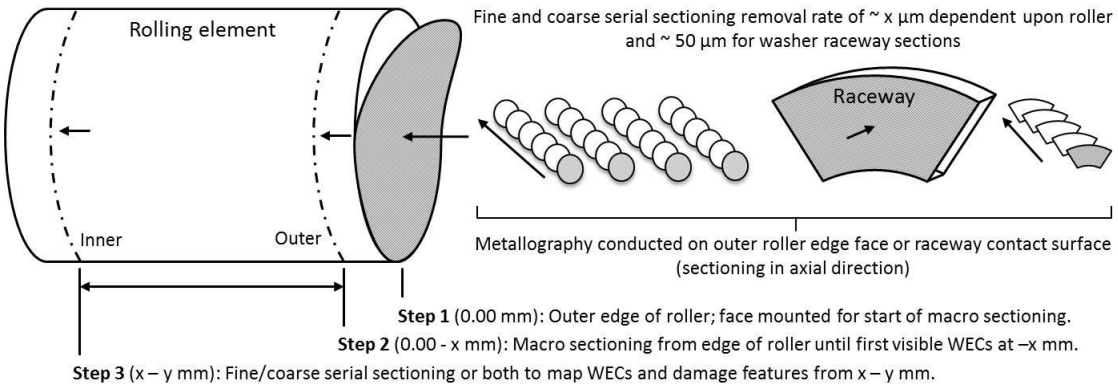

Figure 2-3: Schematic showing serial sectioning steps.

2.3.5 WEC tomography and 3D crack modelling

One of the individual WECs recorded in the 6 hour test (WEC-10 R2) had each fine serial sectioning slice interval image at 200x magnification aligned using layering tools using Photoshop CS3 and subsequently stacked. The image stacks are then used to make a video using Fiji software showing an orthoslice sweep through the volume of steel showing the WECs morphology in 3D from start to finish.

The total WEC damage recorded in one individual roller (Roller 1) from the 18 hour test was modelled in 3D. Optical microscope images at 200x of every individually recorded WEC in the roller were segmented at 0.25 mm intervals across the roller from outer to inner edge (0 – 11 mm). These images were then aligned and stacked before being imported into Fiji software where interpolation between individually segmented WECs was conducted. 3D models were subsequently constructed using Aviso and VGStudio MAX software. Animations of the 3D model were constructed using VGStudio MAX and Fiji.

2.3.6 WEA volume analysis

ImageJ has been used to quantitatively analyse the average total volume (μm^3) and area (μm^2) of white etching microstructural alteration associated with individual WECs across the RCF test durations. Five individual slices taken from start to finish across four individual WECs from the 4–18 hour tests were analysed (see Figure 2-4). At each slice (1 - 5), the WEA associated with the WEC are segmented in 2D to give the total WEA (μm^2) for that particular slice. Multiplication of the individual total WEAs at the 2nd, 3rd (middle) and 4th slices with the axial length between slices

plus the total WEA at the 1st and 5th slices gives the total WEA volume (μm³) for that particular WEC i.e. 1st WEA + 2nd WEA (Axial distance between 1st – 2nd) + 3rd WEA (Axial distance between 2nd - 3rd) + 3rd WEA (Axial distance between 3rd - 4th) + 4th WEA (Axial distance between 4th - 5th) + 5th WEA. The average WEA volume for each RCF test duration is then calculated for comparison based upon the four WECs analysed. It is important to note that this approximates the WEA volume found associated with the crack and therefore measurements can be over/under estimated and not fully representative of the actual amount of WEA present.

In addition, ImageJ has also been used to quantify the area (μm²) vs. WEC angle w.r.t the axis of compression (θ) (see Figure 2-18 (d)) for five individual WECs from the 18 hour test. For each WEC, one plane from the sectioning analysis has been taken (approximately the middle slice, see Figure 2-4 below). Individual WEAs have then been segmented out in the same way as described above and in Figure 2-4. However, in addition the angle of the WEC w.r.t the axis of compression associated with the segmented WEA region is recorded. Cracks are recorded between 0˚ (a crack that is perpendicular to the compression) and ± 90˚ (a vertical crack in the same direction as the compression).

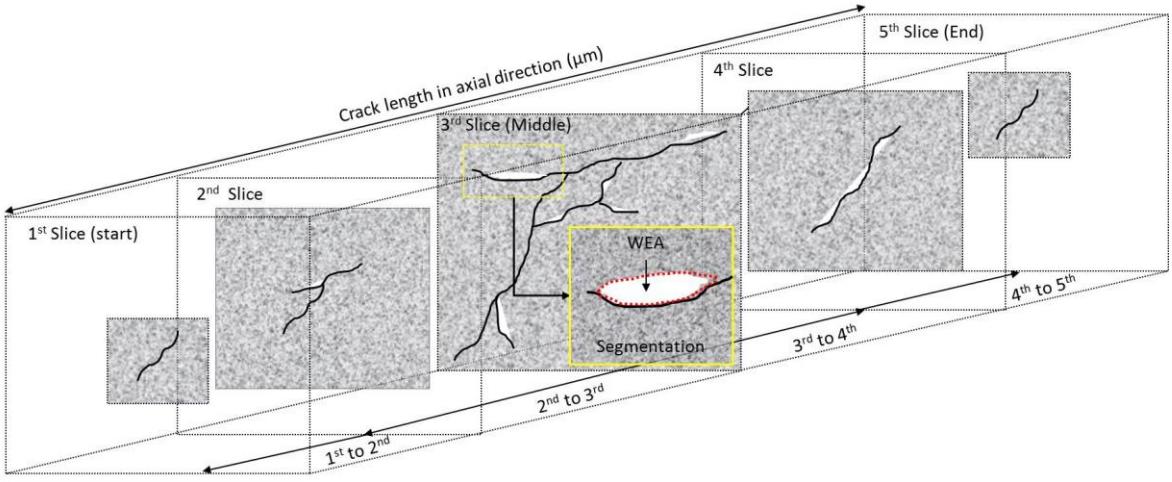

Figure 2-4: Schematic illustrating the methodology of WEA volume measurements.

2.4 Materials characterisation

2.4.1 Steel cleanliness

Steel cleanliness analysis was performed under ISO 4967-B standard [89] to measure the density of NMIs in the rollers and raceway washers. Analysis was conducted at the Dr. Sommer Werkstofftechnik GmbH lab. An Olympus BX51M optical microscope and software (analysis auto version 5.2 + Inclusion Inspector) was used for automatic detection of the inclusion size, type and

count. A global severity index (C_i) was given to the inclusions recorded during the analysis. Under the thresholds set by the ISO 4967-B standard, the global cleanliness index C_i was found to be 0.2 and 1.5 for the raceway and roller, respectively. Analysis of the raw cleanliness data (this data including the addition of NMIs recorded outside of the thresholds set by the ISO 4967-B standard) gave global cleanliness index C_i of 35.6 and 344.1 for the raceway and roller, respectively.

2.5 Results

2.5.1 Contact surface inspection

Wear across the rollers for increasing RCF test durations has been observed on both sides of the central pure rolling region corresponding to the outer and inner zones (see Figure 2-6). RCF test durations of 2 – 12 hours showed very little surface damage. The 18 hour test showed visible signs of damage on the outer half in the form of dents/impressions, but conversely little surface damage on the inner (see Figure 2-5 (a) and Figure 2-6). Surface analysis of a typical indent using SEM (JEOL JSM-6500F) and optical profilometry (Alicona InfiniteFocusSL) revealed the indent to have a width of ~ 800 µm and maximum depth of ~ 2 µm (see Figure 2-5). No signs of spalling were found on the rollers that were subsequently sectioned; however, spalling was observed on other rollers from the same bearing. Figure 2-6 shows the wear and damage across the 2 – 18 hours rollers. Inspection of the raceway washer sections at 18 hours revealed little surface damage. Again wear zones can be seen on either side of the central pure rolling region, see Figure 2-6.

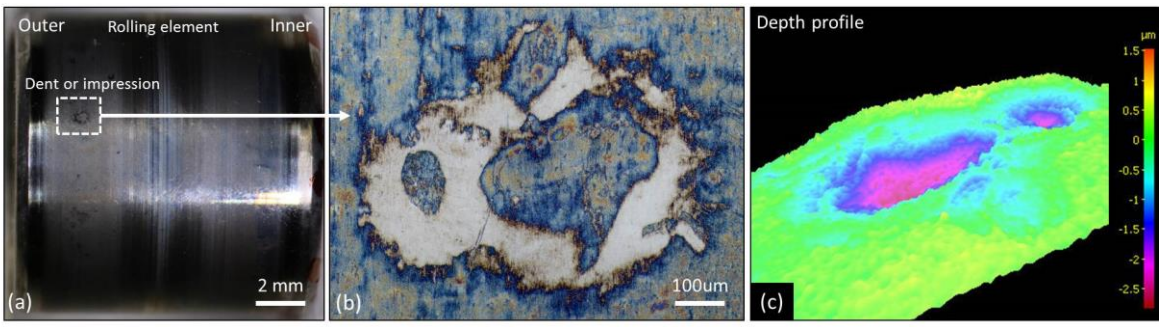

Figure 2-5: Surface analysis of a typical indent found on the 18 hour rollers. (a) Optical macro image of roller indicating location of indent on the contact surface. (b) Magnified optical image of the indent. (c) Depth profile analysis of the indent.

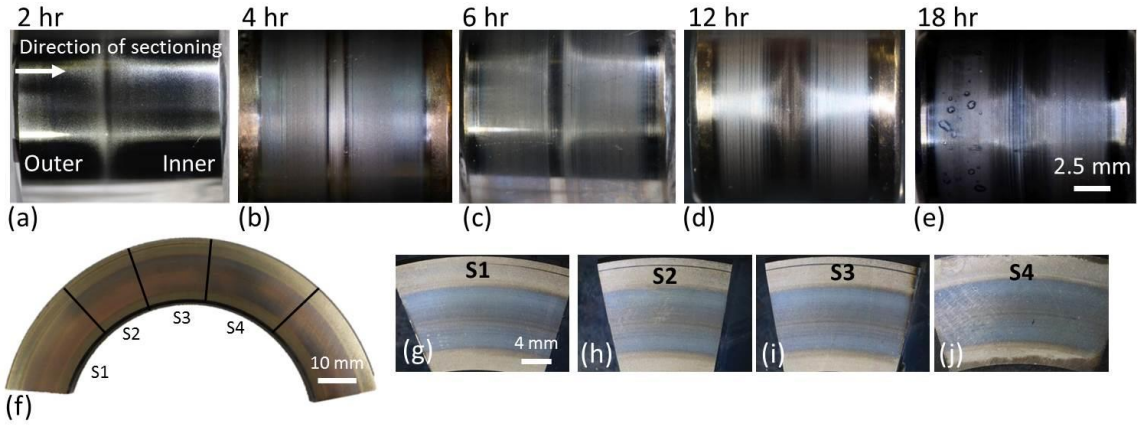

Figure 2-6: Optical macroscope images of a single roller from each RCF test duration (2 - 18 hours) and 18 hour raceway sections chosen for subsequent sectioning. Images (a - e) show one of the 60˚ interval zones around the circumference of the roller. (f) Overview image of raceway sections (S1 – S4). Images (g - j) are optical macro images of the corresponding sections (S1 – S4) shown in (f). S denotes sample number.

2.5.2 Metallographic analysis

2.5.2.1 Fine serial sectioning

The results from the fine serial sectioning analysis are described below and are detailed in Table 2-3.

2 hour: No WECs or butterflies were recorded.

6 hour: Ten individual WECs were recorded. Eight of these were mapped from start to finish (imaging at every slice), no surface connections being recorded. Through WEC tomography, the 3D morphology of one of the fully mapped WECs (WEC-10 R2) can be seen in Video 2.1. Five out of the eight WECs had their respective images at 500x magnification aligned in strips from start to finish, an example is shown in Figure 2-9. Twenty-four butterflies were recorded. Twelve inclusion interactions were recorded (see Figure 2-9 and Figure 2-10 for examples), nine inclusions interacting with the eight fully mapped WECs, with multiple inclusion-WEC interactions being recorded for single WECs. Every WEC had at least one inclusion-WEC interaction. Small sized (~ 2 - 15 µm) globular sulfide-oxides (D_{Dup}) and globular oxide (D) were the most common inclusions found. All twelve inclusions were evaluated as having either a rank of 1 or 2 (see details about the ranking system in A.2 and Figure 2-9). Spatial distributions and depth of inclusion-WEC interactions are shown in Figure 2-11.

18 hour: Seventy-eight individual WECs were recorded; no WECs were mapped (see [38] for 3D mapping and orthoslice sweep videos of 18.5 hr WECs in their entirety). Sixteen out of seventy-eight WECs made a surface connection or near surface interaction (< 1 µm below the contact surface); the near surface interactions showing no apparent connection with the contact surface when viewed under optical microscope at 1000x magnification (Figure 2-7 (c)). Most surface connections at 18 hours have small surface connection/interaction crack volumes (< 1 µm) with short connection lengths with respect to sectioning in the axial direction (a few slice intervals) (see Figure 2-7 (a)). This being opposed to some surface connections that had connection lengths over multiple slices ranging over hundreds of microns (see Figure 2-7 (b)). A significant number of small individual WEA/WECs were also found in the near surface zone (< 25 µm), 8700 of these features being recorded (see Figure 2-8 for examples) where evidence for the propagation or coalescence of these features was not seen. Fifty inclusion-WEC interactions were recorded, multiple inclusion interactions being found for single WECs. Small sized (~ 2 - 15 µm) globular sulfide-oxides (D_{Dup}) and globular oxides (D) were the most frequent inclusions found to interact, 30/50 inclusions being ranked as either 1 or 2 regarding initiation of WECs; examples are shown in Figure 2-10. Spatial distributions and depths of a number of these inclusion-interactions are presented in Figure 2-11. Further inclusion-WEC interaction examples from an 18.5 hour RCF test can been found in [38]. Sixteen butterflies were recorded.

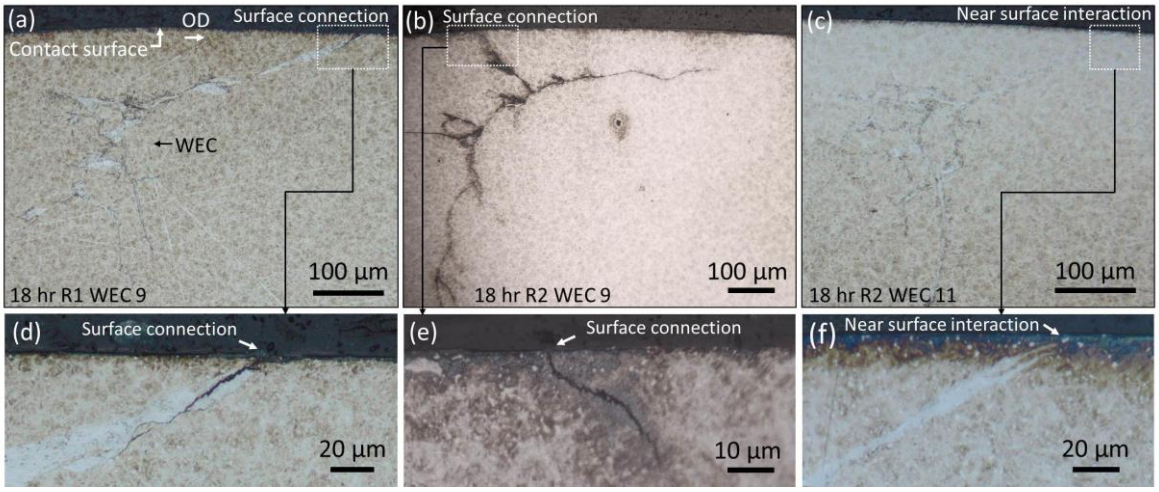

Figure 2-7: Optical images of 18 hour surface connections and near surface interactions. (a) WEC-9 R1 surface connection, surface connection length in axial sectioning direction <30 µm. (b) WEC-9 R2 surface connection, surface connection length ~ 500 µm. (c) WEC-11 R2 near surface interaction. (d - f) 500x optical images of the surface connections and near surface interactions shown in (a - c). Over-rolling direction (OD) left to right.

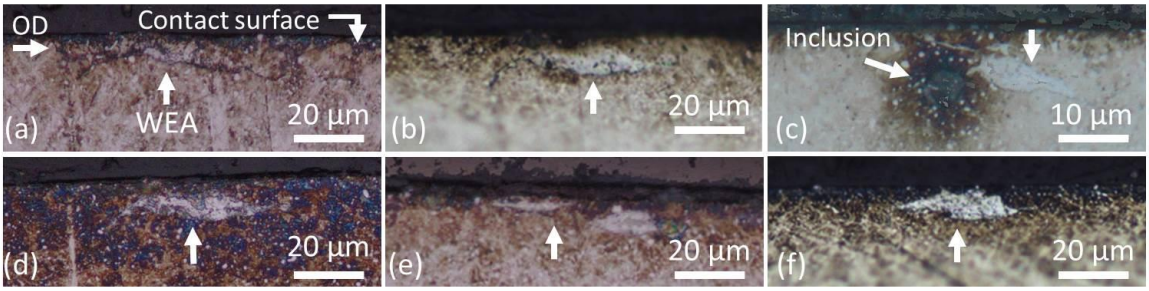

Figure 2-8: Optical images of typical 18 hour near surface WEA/WEC features (a - f). Over-rolling direction (OD) left to right.

2.5.2.2 Coarse serial sectioning

The results from the coarse serial sectioning analysis are described below and are detailed in Table 2-3.

4 hour: Through analysis of 3x rollers only, one WEC (WEC-9 R1) was found, this WEC being comparable (but smaller in size) to the smallest WECs recorded at 6 hours. It should also be noted that this WEC could be judged as a butterfly; however, due to the forking nature of the crack tip it is of the authors' opinion that this is an extended butterfly or WEC. WEC-9 R1 was subsequently mapped (serial sectioned). No connection to the surface was made. After mapping, standard sectioning resumed. Individual slice images of WEC-9 R1 were aligned in a strip and are shown in Figure 2-9. One inclusion-WEC interaction was recorded (see Figure 2-9), a small (~ 6 µm) globular Al_2O_3 (D_{Dup}) rank 1 inclusion. Spatial distribution and depth of this inclusion interaction can be seen in Figure 2-11. Eleven butterflies were recorded.

6 hour: Coarse serial sectioning was conducted on the same rolling elements post serial sectioning; WECs that had not finished during fine serial sectioning, cracks continuing to be recorded. The total number of WECs equals the sum of WECs not finished during fine serial sectioning plus the coarse serial sectioning. Fourteen individual WECs were recorded. No surface connections were recorded. One inclusion-WEC interactions were recorded; this is likely due to the larger sectioning intervals where inclusions may have been missed or removed during sectioning due to their typical small size (~ 2 - 15 µm). Six butterflies were recorded.

12 hour: Twenty-seven individual WECs were recorded with no surface connections. Eleven inclusion-WEC interactions were recorded, and twelve butterflies, inclusion-WEC interaction spatial distributions are shown in Figure 2-11.

18 hour: Coarse serial sectioning was conducted post serial sectioning on the same rolling elements, WECs being recorded as in the case of the 6 hour test described above. One-hundred-

forty-five individual WECs were recorded. Nineteen surface connections were found. Nine inclusion-WEC interactions were recorded; their respective spatial distributions shown in Figure 2-11. Likewise, inclusion-WEC interactions may have been lost due to larger sectioning intervals. Two butterflies were recorded. Also, note that the number of near surface WEA/WECs features recorded through fine serial sectioning significantly decreased in number when going from the outer to the inner roller halves.

No signs of 'conventional' WEC/WEAs were recorded in the raceway washers. However, some fine 'WEC-like lines' have been observed in 18.5 hour raceway segments [38], but no extensive WECs were found.

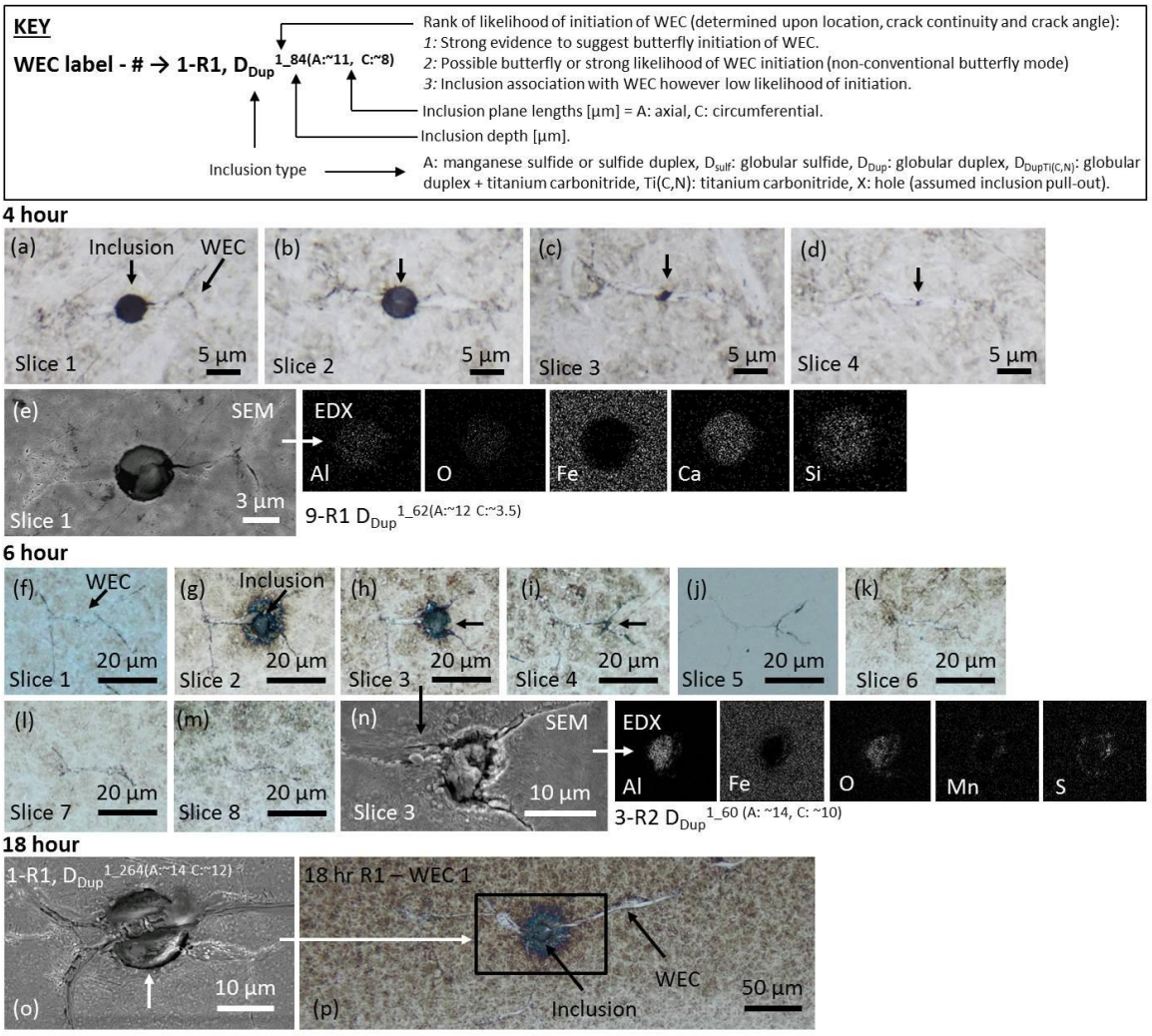

Figure 2-9: Optical images of mapped WECs and inclusion-WEC interactions at 4, 6 and 18 hours. (a - d) represent the individual slices from start (slice 1) to finish (slice 4) of mapped 4 hour WEC-9 R1. SEM image (e) shows inclusion-WEC interaction from (a) slice 1 with corresponding EDX chemical maps. (f - m) Mapped 6 hour WEC-3 R2, images (f - m) represent the individual slice images from start (slice 1) to near finish (slice 8). Images (g - i) show the location of the inclusion-WEC interaction. (n) Is an SEM image of the inclusion-WEC interaction from (h) (slice 3) with

corresponding EDX chemical maps. (o) SEM image of inclusion-WEC interaction recorded in 18 hour WEC-1 R1 with corresponding location of the inclusion-WEC interaction shown in optical image (p). A key above the images details how to interpret the inclusion-WEC interaction information in each case. See A.2 regards the inclusion ranking system.

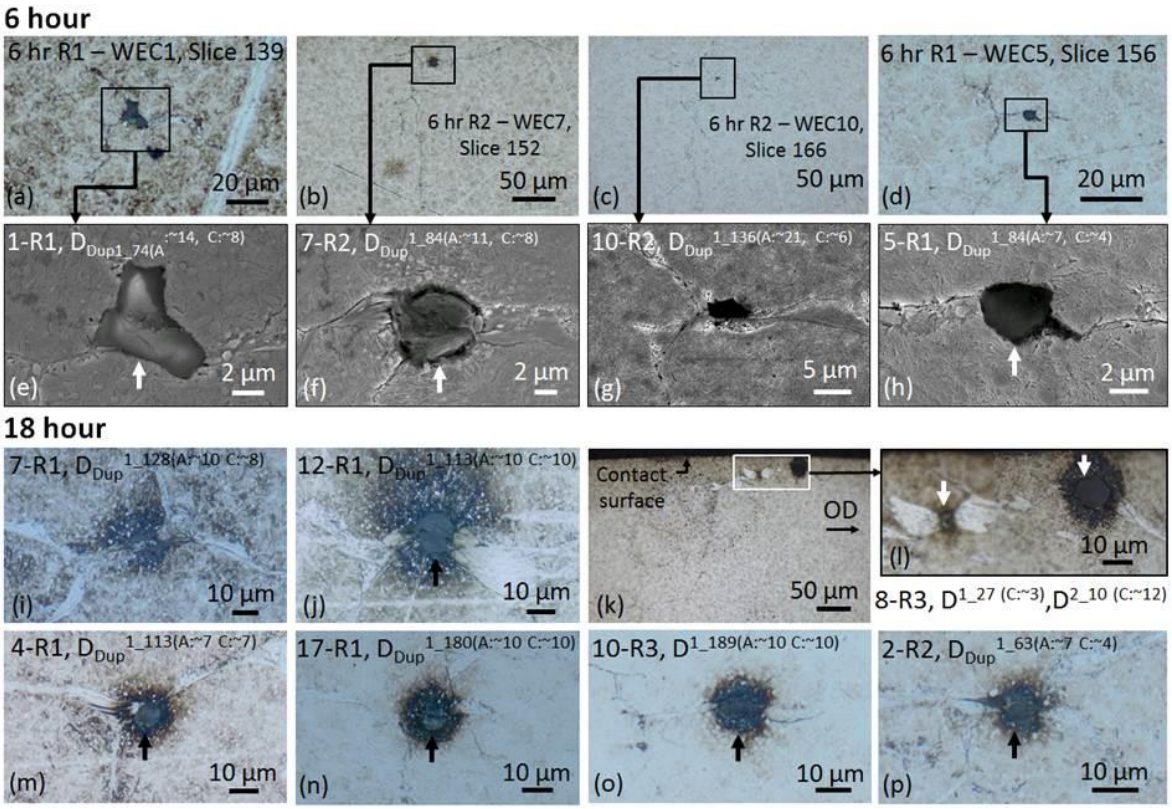

Figure 2-10: Images of typical inclusion-WEC interactions recorded at 6 and 18 hours. Images (a - d) show the location of the inclusion-WEC interactions from SEM images (e - h) respectively at 6 hours. Images (I - p) are optical images of typical inclusion-WEC interactions recorded at 18 hours. (k) and (l) show an example of a butterfly WEC with corresponding inclusion linking to another inclusion in the WEC network, (l) showing a magnified image of the highlighted region. Arrows highlight the inclusion in each case. See Figure 2-9 and A.2 for more information on the inclusion ranking system.

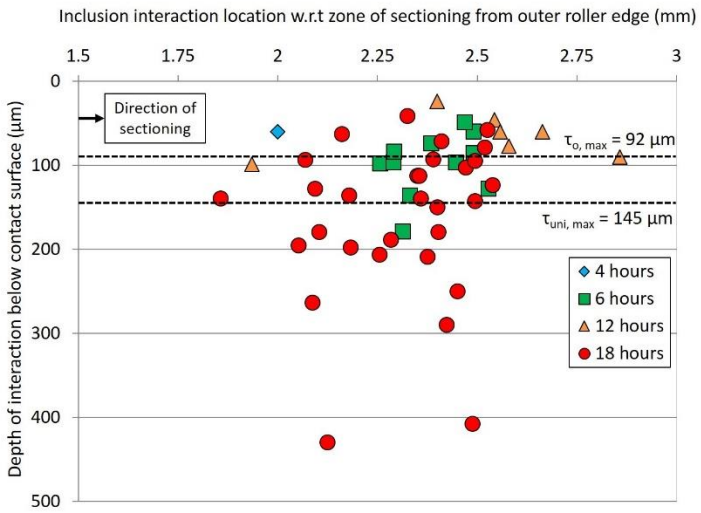

Figure 2-11: (a) Spatial distribution and depth of inclusion-WEC interactions w.r.t the depth of maximum subsurface sheer stresses judged to have a high likelihood of crack initiation (rank 1 or 2). See Figure 2-9 and A.2 for more information on the inclusion ranking system.

2.5.2.3 Summary of sectioning analysis

Table 2-3 and Figure 2-13 to Figure 2-14 summarise the combined fine and coarse serial sectioning results. Figure 2-14 provides the average WEC dimensions for the 2 - 18 hour tests.

A WEC severity index has been calculated based upon the WEC length in the axial sectioning direction, the radial length of the WEC (maximum depth minus minimum depth) and the maximum WEC span, see Figure 2-14. The average severity of WEC formations across 2 - 18 hours (averaged across 3 x rolling elements) has been calculated as well as the average severity in individual rollers and the outer and inner halves at 18 hours.

The total WEC damage recorded across roller 1 from the 18 hour test has been modelled in 3D. This is to visualise the extent, density and distribution of damage seen typically at the late stages of RCF before failure, see Figure 2-12 (see Video 2.2 for a 2D segmentation, 3D orthoslice sweep through the entire volume of the roller representing each individual WEC recorded across the roller from outer to inner edge). Figure 2-12 (a) shows an example of an axial slice cross-sectional image of one of the WECs recorded in 18 hour R1 that was subsequently segmented in 2D and placed in its relative position in the roller (see Figure 2-12 (b) and (c)). Figure 2-12 (d), (e) and (f) show three views of the 3D model.

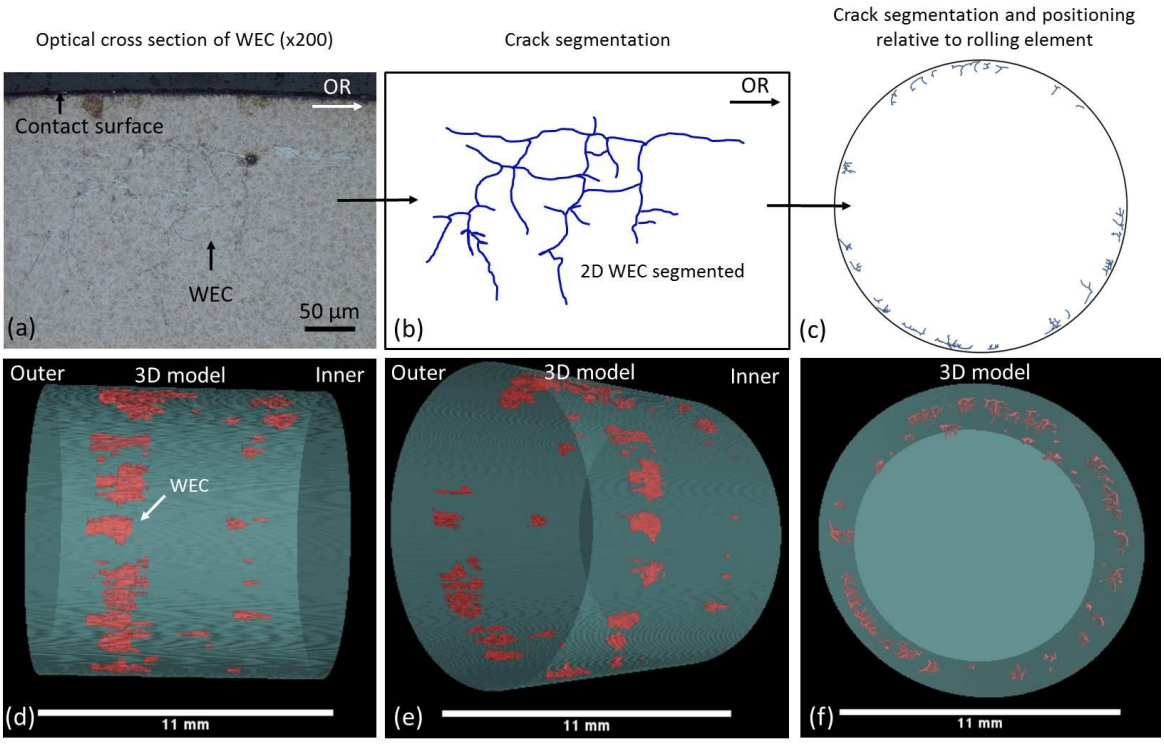

Figure 2-12: 3D model of total WEC damage recorded across 18 hour R1. (a) Optical cross-sectional image of a WEC. (b) 2D segmentation of WEC from optical image in (a). (c) Placement of 2D segmented WEC into its relative position across the roller. (d - f) 3D model with all WECs highlighted in red across the roller from outer to inner edge. See Video 2.2.

Table 2-3: Summary of WECs and inclusion interactions recorded from combined fine and coarse serial sectioning analysis.

Test duration	WECs recorded	Surface connections	Near surface WEC/WEAs	Inclusion interactions	Butterflies	WECs recorded in roller halves	
						Outer	Inner
2 hr	**Total: 0**	**Total: 0**	**Total: 0**	**Total: 0**	**Total: 0**	**Total: 0**	**Total: 0**
4 hr	R1: 1	R1: 0	R1: 0	R1: 0	R1: 7	R1: 1	R1: 0
	R2: 0	R2: 0	R2: 0	R2: 0	R2: 2	R2: 0	R2: 0
	R3: 0	R3: 0	R3: 0	R3: 1	R3: 2	R3: 0	R3: 0
	Total: 1	**Total: 0**	**Total: 0**	**Total: 1, Total: 1***	**Total: 11**	**Total: 1**	**Total: 0**
6 hr	R1: 6	R1: 0	R1: 0	R1: 5	R1: 14	R1: 5	R1: 1
	R2: 10	R2: 0	R2: 0	R2: 8	R2: 12	R2: 7	R2: 3
	R3: 6	R3: 0	R3: 0	R3: 0	R3: 4	R3: 6	R3: 0
	Total: 22	**Total: 0**	**Total: 0**	**Total: 13, Total: 13***	**Total: 28**	**Total: 18**	**Total: 4**
12 hr	R1: 13	R1: 0	R1: 0	R1: 4	R1: 4	R1: 8	R1: 5
	R2: 9	R2: 0	R2: 0	R2: 4	R2: 4	R2: 9	R2: 0
	R3: 5	R3: 0	R3: 0	R3: 3	R3: 4	R3: 2	R3: 3
	Total: 27	**Total: 0**	**Total: 0**	**Total: 11, Total: 11***	**Total: 12**	**Total: 19**	**Total: 8**
18 hr	R1: 59	R1: 9	R1: 3730	R1: 44	R1: 8	R1: 43	R1: 16
	R2: 52	R2: 9	R2: 3653	R2: 7	R2: 5	R2: 44	R2: 8
	R3: 53	R3: 1	R3: 1316	R3: 9	R3: 5	R3: 30	R3: 23
	Total: 164	**Total: 19**	**Total: 8699**	**Total: 60, Total: 40***	**Total: 18**	**Total: 117**	**Total: 49**

Key: *: Total number of inclusions ranked 1 or 2.

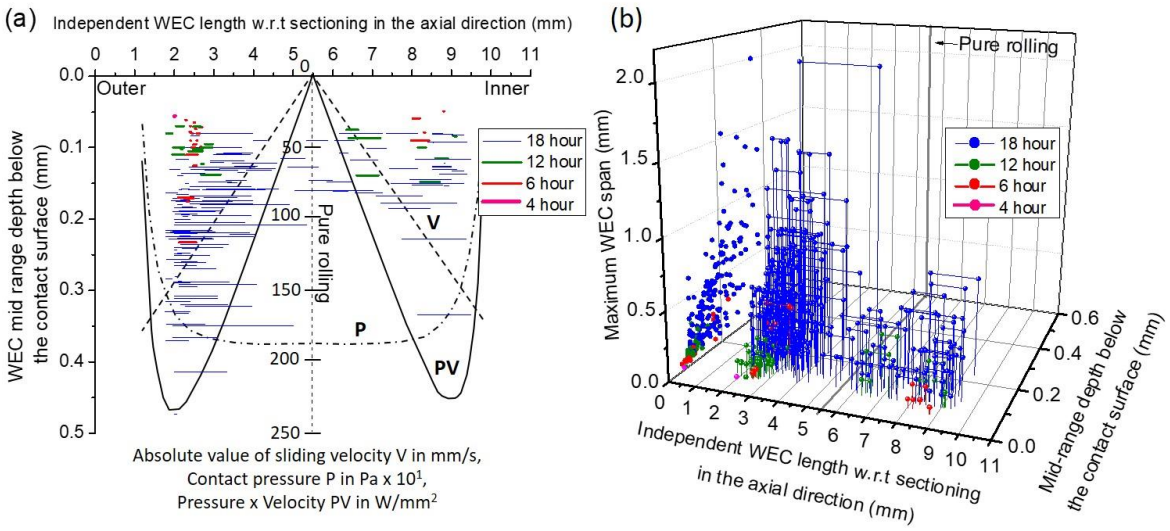

Figure 2-13: (a) Distribution of individual WECs recorded in 4 - 18 hour rollers across the entire axial length (x-axis) of rollers from outer to inner edge and corresponding mid-range depth below the contact surface (0.00 mm) (y-axis). Pressure P, absolute sliding velocity V and slip energy PV are also superimposed onto the plot (adapted from [100] (b) 3D plot of all independently recorded WECs across 4-18 hours. X-axis represents the entire axial length of the roller from outer to inner edge. Y-axis represents the WEC mid-range depth below the contact surface (0.00 mm) (this is the (max depth – min depth)/2, see Figure 2-14). Z-axis represents the maximum WEC span (see Figure 2-14 for more details). The dots on the YZ-projection represent the position of each independent WEC in the Y-axis and Z-axis. The distances between spheres for each WEC represent the total length in the X-axis.

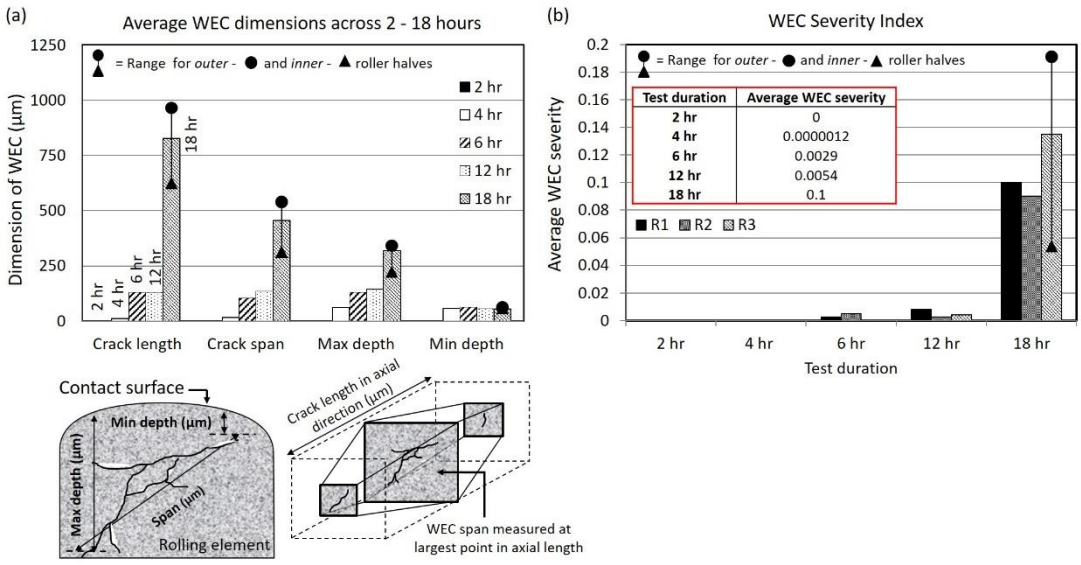

Figure 2-14: (a) Average WEC dimensions in the rollers across 2 – 18 hour tests including schematic on how respective WEC dimensions are measured. (b) WEC severity index in the rollers for the 2-18 hour tests.

2.5.2.4 WEA volume analysis

Results show the average amount of WEA volume increases with test duration (see Figure 2-15 (a)). The total 'white etching area' (µm^2) when quantifying the WEA at five individual positions within the WEC (see Figure 2-4) shows that the 3rd slice (middle zone) of the WEC network has on average the greatest amount of WEA associated (see Figure 2-15 (a)). Total WEA volume versus respective WEC axial length for the WECs analysed shows that for an axial crack length over 500 µm a significant increase in total WEA volume exists (see Figure 2-15 (b)). Analysis of five individual WECs from the 18 hour test, WEA vs. crack angle w.r.t the axis of compression has shown that a greater amount of WEA is associated with a crack the nearer a crack gets to 0˚ (perpendicular to the axis of compression). Vertically propagating cracks (± 90˚ in the direction of compression) showing far less WEA (see Figure 2-15 (c)).

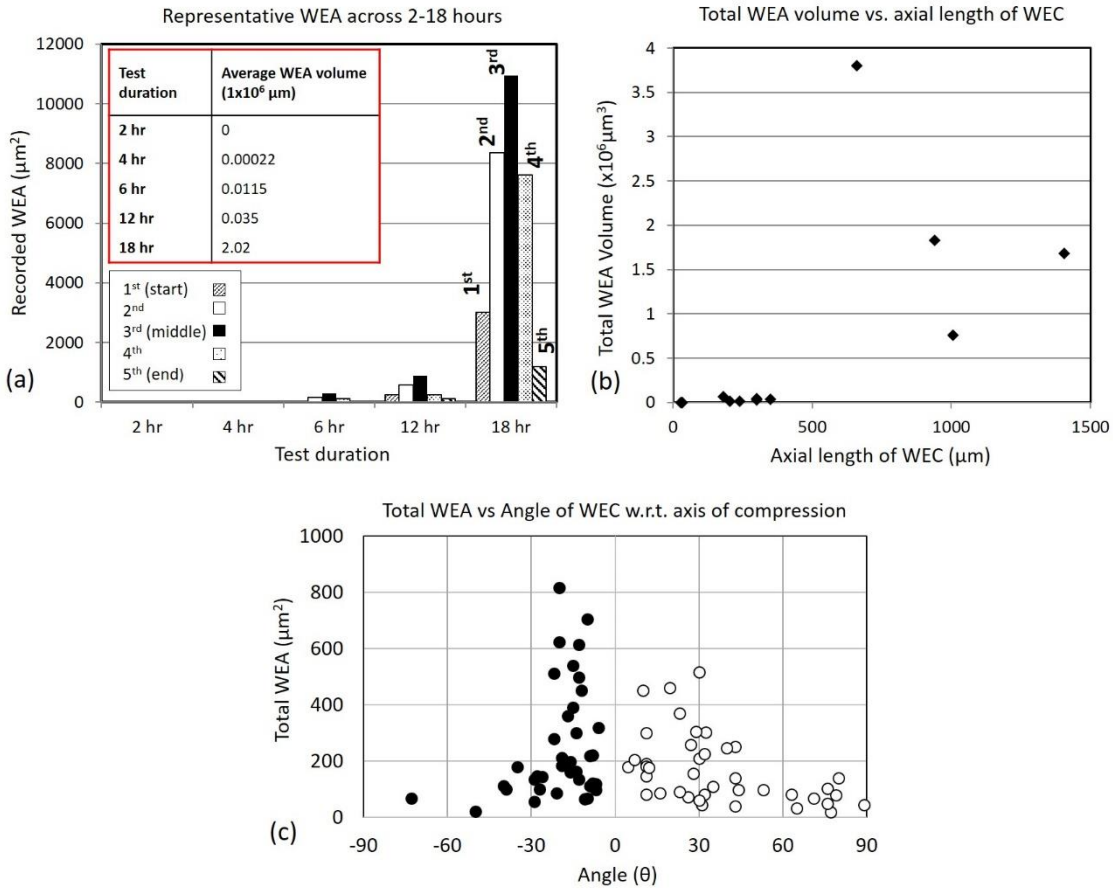

Figure 2-15: WEA volume and area analysis. (a) Representative average WEA across 2 - 18 hours. (b) Total WEA volume vs. axial length of WEC. (c) Total WEA measured vs the respective angle of the WEC for five different randomly chosen WECs at 18 hours.

2.6 Discussion

2.6.1 RCF testing

This study has used contact pressure P_{max} at 1.56 GPa to re-create WECs in CRTBs on a FAG-FE8 test rig lubricated with a 'special' oil known to promote WSF. It must be taken into account that the FAG-FE8 test rig has differing dynamics to those experienced by WTGBs during service, e.g. the relatively high slip experienced in the CRTBs. However, large slippage can occur during rapid acceleration/deceleration of the shaft in wind turbine gearboxes [98] and transient events causing ~ 20 - 110% SRR in WTGBs [199]. Simulations have revealed that moderate sliding occurs (3 - 10% SRR) continuously for spherical roller bearings in intermediate shaft locations of the gearbox at roller-raceway interface in the unloaded zone [199].

2.6.2 Features of WECs

2.6.2.1 Near surface WEAs/WECs

Serial sectioning analysis of 18 hour rollers revealed a large number of small near surface (< 25 µm zone) WEC/WEAs (see Figure 2-8). These were rarely seen with connection to the contact surface, limited interaction with inclusions, and it was also found in cases that there was no apparent presence of a crack; thus, evidence shows that a crack is unnecessary for WEAs to form in this case. These near-surface features were predominantly found in the outer half of the rollers with a decrease in their respective numbers being found across the inner half. The occurrence of these near surface features has been documented previously by the authors in FAG-FE8 tests [38], hydrogen charged TE-74 two-roller specimens during RCF testing [37] and actual WTGBs from service [74], where rare connection to the contact surface has been found with limited cases of inclusion interaction [37].

It is hypothesised that the occurrence of these features is a result of either, or a or combination of,

(i) increase in traction between contacts at later stages of RCF operation, resulting in a rise of the maximum subsurface shear stress zone towards the surface. This would be significantly increased in the case of insufficient lubrication and higher surface roughness,
(ii) micro-indentations at the contact surface causing local regions of mixed/boundary lubrication regimes increasing the traction coefficient,
(iii) areas of localised increase in contact pressure,
(iv) increase in the concentration of mobile diffusible hydrogen over longer RCF operation [153], where locally at the near surface, higher localised penetration and concentrations may exist and aid in the acceleration of these features.

Figure 2-16 illustrates the hypothesised mechanisms for the formation of these features.

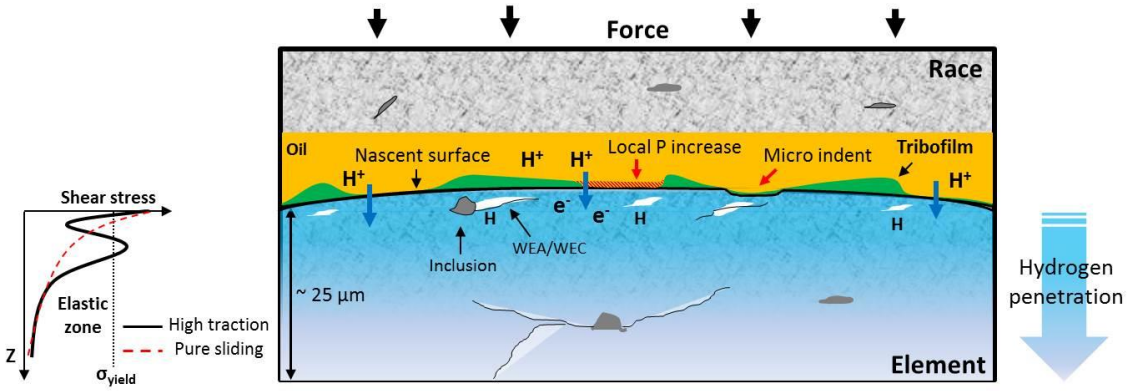

Figure 2-16: Hypothesised mechanisms of near surface (<25 µm) WEA/WECs formation. H^+ denotes molecular hydrogen, H denoting mono atomic hydrogen diffused into the bearing steel. e^- denotes free electrons at the fresh nascent surface. 'P' and 'σ' denote pressure and yield stress respectively.

2.6.2.2 WEC initiation and evolution

Analysis has shown that the propensity and average size (see Figure 2-14) of WECs recorded in the rollers increases with RCF test duration (see Table 2-3, and Figure 2-13 to Figure 2-14) no WECs being found in the raceway. Two factors to explain this could be,

(i) steel cleanliness has shown that the raceway is 'cleaner' than the roller (see 2.4.1),

(ii) lack of hydrogen being available to accelerate WEC formations [153],

(iii) raceway is ~ 23% softer (590 HV) than the rollers (765 HV), therefore the raceway is less prone to cracking due to an increased toughness.

The importance of high toughness steel has been highlighted in the reduction of intergranular subsurface cracking and the subsequent movement of crack faces in generating WEA [193]. It is well recognised that hydrogen effects higher strength steels, hydrogen embrittlement occurring when hydrogen is in its atomic mobile form, hydrogen able to retain its mobility in high strength steels [118]. Hydrogen has, however, been shown to have little influence on toughness and no effect on the hardness of 100Cr6 bearings steel [106]. To confirm the non-existence of WECs in the raceway washer, later nine randomly selected individual sliver sections of raceway were mounted such that the sections were examined in the opposite axial direction (side on instead of top down contact surface direction). Two sections at 100 um intervals were taken and examined through optical microscopy. No evidence of WECs was found.

No WECs were recorded at 2 hours; this could be thought logical due to the short RCF test time. Results show that the number, size and severity of WECs do not increase linearly (see Figure 2-13 to Figure 2-14), a ramped increase seen at the later stages of RCF operation (12 - 18 hours). This

could be due to WECs coalescing to form larger crack networks resulting in a 'weakening' of the surrounding steel accelerating WEC growth, this being heightened in the event of a sufficient threshold concentration of diffusible hydrogen being reached [153]. Variance in severity is also observed between rollers. This highlights the importance of analysing a representative volume of steel. Differences in the severity between outer and inner roller halves at 18 hours are also shown, the outer half having a greater severity than the inner.

Condition monitoring on FAG-FE8 tests [54] have suggested a rapid release of subsurface WECs occurring at ~ 20% outstanding RCF test time before WSF failure. This is proposed to be due to the steel experiencing a failure-free period (no WECs detected), energy is absorbed in this period (explained by Barkhousen noise (BN) measurements [200]), a limit being reached with a sudden release of WECs. This failure-free period could be local subsurface transformations that have been observed as 'crack free' dark etching regions suggested to lead to the formation of WEA and subsequently WEC [63]. This investigation shows that WECs do exist during this period before a sudden rupture occurs, ~ 20% outstanding RCF time corresponding to 14.4 hours, WECs being recorded between 4 and 12 hours.

When comparing the inclusion-WEC interactions recorded at 4 - 18 hours inclusions are,

(i) consistent in type and size, typically small/short ~ 2 - 15 µm D_{Dup} or D type inclusions,

(ii) inclusion-WEC interaction depths are within/close to the zones of maximum subsurface shear stress ($\tau_{0,\,max}$ = 92 µm, $\tau_{uni,\,max}$ = 145 µm), specifically at the early stages of RCF (4 and 6 hours) where initiation is suggested to occur (see Figure 2-11),

(iii) visually comparing the inclusion-WEC interactions recorded across 4 – 18 hours, a number of similarities in regards to crack shape/angle and continuity, inclusion type and size, direction of crack propagation and location of inclusion within the WEC network can be observed (see Figure 2-10, Figure 2-11 and Figure 2-17).

It is therefore proposed that the WECs recorded in this study were formed because of WECs that initiated at NMIs in the subsurface, individual WECs propagating and coalescing at later stages of RCF (12 - 18 hrs) to form larger WEC networks. It can also be said that the nineteen WECs that did make a connection to the contact surface at 18 hours are likely formed because of subsurface initiation at inclusions. A number of these surface connections/interactions had very small contact crack volumes and connection to the surface over short axial lengths (see Figure 2-7 (a) and (c)); it is proposed that these connections are not sufficient enough to drive such extensive WEC networks in the subsurface. Note that a number of these surface connections were in fact very near (< 1 µm) surface 'interactions' (see Figure 2-7 (c) and (f)), where under optical microscopy no apparent connection to the contact surface was observed. Further evidence for subsurface

initiation comes from the fact that for the nine fully mapped subsurface WECs at 4 and 6 hours, each WEC had at least one or multiple inclusion-WEC interactions. Additional evidence to support subsurface initiation of WECs by NMIs is shown through the visual comparison of typical recorded WECs across the 4 – 18 hour tests (see Figure 2-17). As it can be seen the initial shape and propagation route of WECs at 4 and 6 hours follow a close link to those WECs recorded at 12 and 18 hours, this is in conjunction with the fact that the inclusion-WEC interactions are also closely linked by the similarities discussed above. At 4 and 6 hours, WECs are found to initially resemble butterfly cracks, which propagate into 'star-like' cracks with forking of the butterfly crack tips. This 'star-like' crack shape can be seen to fit a number of the WECs found at 12 and 18 hours as shown in Figure 2-17. It is thus proposed that the WECs recorded at 4 and 6 hours are the early initiation stages of WECs that subsequently propagate and evolve into the large WEC networks recorded at 18 hours. The proposed evolutionary stages of WEC initiation are shown in Figure 2-17 (g).

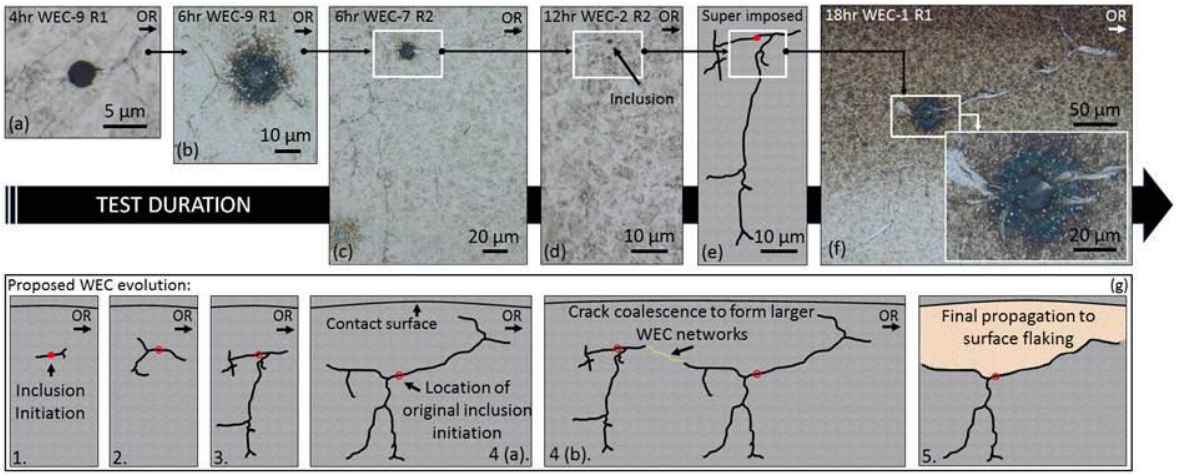

Figure 2-17: Optical images of WECs recorded at 4-18 hours. (a - f) Show examples of typical WECs recorded between 4-18 hours. (e) Super imposed image of the 12 hour WEC shown in (d), the inclusion highlighted in red. (g) Proposed stages of WEC evolution; (1) Initiation via inclusion in the subsurface, (2) propagation into 'star-like' WEC (see b), (3) further propagation in radial and over-rolling direction, (4a) continued propagation (4b) coalescing of independent WECs to form larger WEC networks and (5) final propagation to the surface resulting in flaking. Over rolling direction (OR) is from left to right.

The outer and inner roller halves have shown to significantly influence the propensity and size of WEC formations, the outer half being dominant over the inner (see Table 2-3, Figure 2-12 to Figure 2-14 and Video 2.2). Slip has been shown to influence the formation of WECs in both FAG-FE8 and three ring roller Micro-Pitting Rig (MPR) tests using the same 'special' oil known used in this study [54, 61, 92], where evidence for the influence of negative slip being more dominant in WSF over positive slip is provided [61]. More recently the influence of slip on WEC formations has

also been shown in a two-disc test rig set-up, where again negative slip showed dominance in WEC production in contrast to positive [93]. This dominance has been 3attributed to higher material stressing, lowered fracture mechanic properties under alternating load and preferential surface crack propagation due to the traction force and surface motion vectors pointing in the same direction in negative slip as opposed to positive [93]. It is proposed that negative slip results in the compressive closure of cracks enhancing the crack rubbing mechanism for WEA formation [61]. The localisation of the WECs recorded across 4 - 18 hours are more densely populated in the 2 - 3 mm (outer) and 8 - 9 mm (inner) zones across the roller (see Figure 2-13 and Video 2.2). These zones correspond to areas of high slip energy, (PVmax, the product of contact pressure P and slip velocity V, W/m^2, see Figure 2-13), slip energy taking into account asperity contact (P_cV value which takes into account the asperity contact pressure P_c) and asperity friction accumulation $e_{a,c\ max}$ which relates the regeneration time span between consecutive contact load cycles on tested WEC lives and the specific frictional energy input into the a surface during the contact load cycle [95]. Slip energy criteria has been linked to WSF, WSF occurring at areas of greatest PVmax. These areas have also been found to coincide with zones of highest concentrations of hydrogen [96-98]. Supporting evidence for the slip energy criterion has been shown on FAG-FE8 tests where WECs appeared firstly at areas of high frictional energy, this also being demonstrated in tests using angular contact ball bearings [54, 95]. A number of inclusion-WEC interactions were also recorded during fine serial sectioning corresponding to the 2 - 3 mm zone of high slip energy dissipation and asperity accumulation (see Figure 2-11). Further progression of the slip energy criteria concept has been developed based upon information from different test rigs, using normal contact load and representing the slip energy criteria per film thickness sheared ($N.V/\lambda$, $N\ ms^{-1}$) to determine a threshold for WEC formation in most roller bearing configurations [27, 88]. It is postulated that this threshold could exist due to the fact that sliding energy generates local flash temperatures influencing the tribochemical reactions taking place at nascent surfaces [27]. Limitations, however, do exist, as this criterion does not take into account the lubricant formulation. Evidence for the degree of boundary lubrication (the range of λ) controlling the propensity for WEC formation is also suggested, more WECs forming for more severe boundary regimes (λ in the range of 0.06 - 0.7) [61]. No WECs were found in the raceway washers, with no evidence of WEC formations being observed in the zones corresponding to high slip energy dissipation or asperity friction accumulation. It is noted that the asperity friction energy accumulation is greater in the washers than the rollers, where energy dissipation is greater in the inner raceway than the outer (see Fig. 6, [95]). This is contradictory to the result seen in this study, this discrepancy not being understood.

2.6.2.3 WEA volume

Metallographic analysis has shown that the volume of WEA associated with cracks increases for longer RCF test operation. Through quantitative WEA analysis, the average WEA volume (μm^3) and area (μm^2) associated with cracks increased between 4 and 18 hours, a ramped increase found between 12 and 18 hours (see Figure 2-15 (a)). Analysis also reveals that for greater axial WEC lengths a significant increase in the associated WEA volume is found (Figure 2-15 (b)). It is proposed that the evidence found in this study supports the theory of crack rubbing/beating in the formation of WEAs [59]. As WECs grow and propagate during RCF operation, further crack rubbing/beating occurs at the newly formed crack faces, larger cracks having a greater amount of 'free' crack faces available for extended crack rubbing/beating to occur. This can also be exhibited in Figure 2-17 where it can be seen that the amount of WEA associated with the cracks increases across 4-18 hours, an increase being observed between 12 and 18 hours. Further to this, by visually observing the mapped WECs at 4 and 6 hours (see Figure 2-9) a decrease in WEA volume is seen at the start and ends of the WEC, i.e. the extreme tips when visualised as a 3D network. Taking for example the 6 hour WEC in Figure 2-9. It is proposed that the inclusion is the site of initiation; it can be seen that the volume of WEA is greater around the inclusion site (see Figure 2-9 (g)) than at the end 'tips' where branching/forking has occurred (final stages of propagation) where it is proposed that less time has been available for crack rubbing/beating. This is exhibited in two videos through serial sectioning of an 18.5 hour FAG-FE8 test previously conducted by the authors [38]. This point is strengthened through WEA analysis where it has shown that the average amount of WEA (μm^2) is less at the tips (1^{st} (start) and 5^{th} (end) measurements) than at the centre (3^{rd} (middle) measurement) (see Figure 2-15 (a)). As discussed, a large number of near surface WEA/WECs were recorded at 18 hours (see Table 2-3 and Figure 2-8). A number of these features were found not associated with a crack, leading to the conclusion that near surface WEAs do not seem to require a crack to form WEA. However, note that in this study only optical microscopy has been used in the classification of WEAs associated with cracks, further analysis using SEM to confirm the non-existence of small cracks that may be present inside the WEA regions should be conducted.

Through metallographic analysis, it is indicated that the angle of crack propagation, crack width and zone of maximum subsurface shear stresses, can influence the degree of WEA generated. WEA analysis has shown that the amount of WEA associated with a crack increases the nearer to 0˚ or perpendicular to the axis of compression a crack propagates (see Figure 2-15 (c)). A vertical crack ± 90˚ parallel to the axis of compression is found to have very little WEA associated (see Figure 2-15 (c)). This is also exhibited clearly in the 18 hour crack shown in Figure 2-18. As suggested by others [59], it is proposed that a vertically branching crack will be subjected to a

much lesser amount of crack rubbing. The localisation of strain has been found to be strongly reliant on crack orientation in relation to stress [201]. High strain rate compressive tests have shown regions of WEA [202], this being in comparison to equivalent tensile tests; as a result it is proposed that crack rubbing/beating under RCF shear stresses or compressive loading result in WEA formations and thus adiabatic shearing is an unlikely cause [203]. The crack width also appears to influence WEA formations. For example, in Figure 2-19 it is seen that very little or no WEAs are associated with sections (Area 1) of the WEC that have large crack width when compared to crack faces that are close together (Area 2). It is proposed that for adjacent crack faces that are further apart, less action is available for crack rubbing/beating. This is not to say, however, that these particular areas of the WEC network would have not been associated with WEAs at some point during operation. The proposed mechanism (see Figure 2-19) to explain this is as follows,

1. Inclusion initiation of butterfly and 'star-like' WECs with subsequent generation of WEAs due to crack rubbing/beating.
2. WECs propagate and WEAs continue to develop.
3. Short crack growth from inclusions/butterflies by Mode I loading [114] stops and further growth is governed by Mode II/III shear loading if the Mode II/III stress intensity factor threshold is surpassed [114], WECs may propagate and coalesce to form larger networks. Until a critical length is reached, crack growth rate may be slow, where once exceeded rapid propagation results under applied stress.
4. Due to the rapid growth of the crack and crack volume, the time and action available for WEA development is alleviated and thus a reduction or non-existent presence of WEA is seen. In the event of hydrogen diffusion, hydrogen acts to decrease the Mode I/II stress limits for crack growth and propagation [112, 114], it may be reasoned that this step increase in WEC formations is due to a threshold concentration of hydrogen being reached for a decrease in Mode II crack growth [153].

Analysis also indicates that the zone of maximum subsurface shear stresses influences WEA generation. This is most clearly exhibited in WECs recorded at 18 hours. For example WEC-2 R1 in Figure 2-18 show that a greater amount of WEA exists within and in the regions around the zone of maximum subsurface shear stresses ($\tau_{0,\,max}$ = 92 μm, $\tau_{uni,\,max}$ = 145 μm).

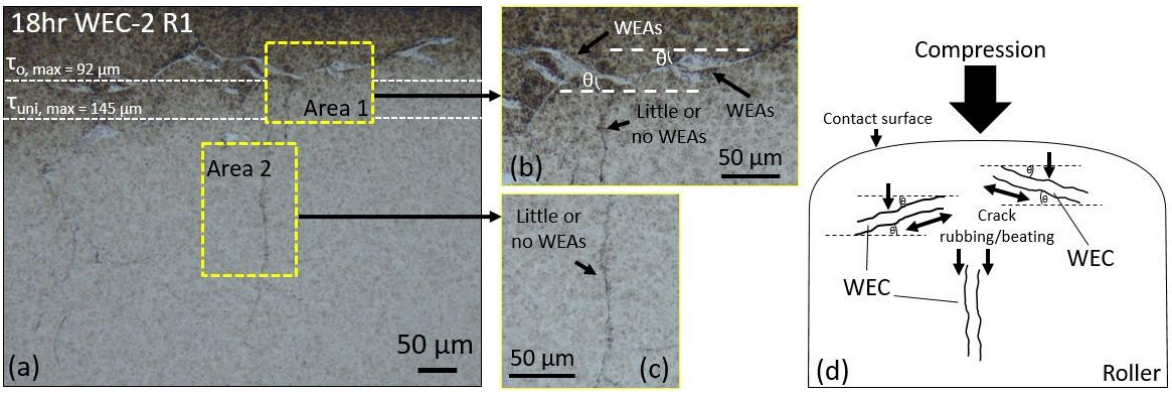

Figure 2-18: Optical image of a WEC demonstrating the influence of crack angle w.r.t the axis of compression and depth of maximum subsurface shear stresses ($\tau_{0,\,max}$ = 92 µm, $\tau_{uni,\,max}$ = 145 µm) on the formation of WEAs. (a) Area 1 and 2 show two different orientations of crack propagation, Area 1 shows cracks at an angle θ to the axis of compression along with a vertical crack parallel to the compression axis, and the zones of maximum subsurface shear stresses are shown. Area 2 shows a vertical crack parallel to the compression axis. (b) and (c) show magnified x500 images of the two areas respectively. (d) Is a schematic demonstrating the influence of crack orientation angle w.r.t the direction of compression and the associated action of crack rubbing/beating.

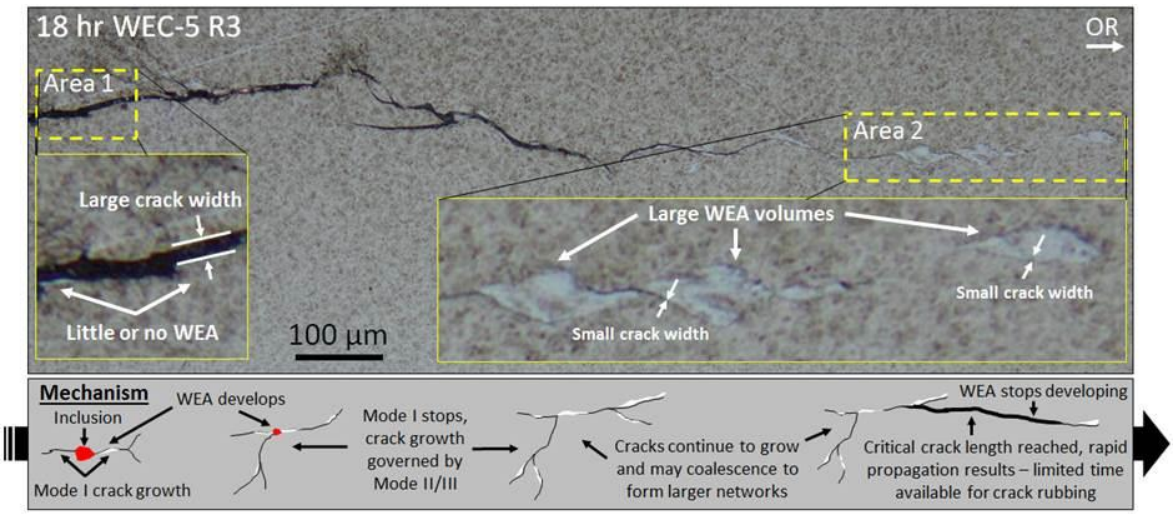

Figure 2-19: Optical image of a WEC demonstrating the influence of crack width on the generation of WEAs. Area 1 shows a large crack width and Area 2 shows a small crack width, with respective magnified optical images. The proposed mechanism for the development of WEA w.r.t crack width is shown. Over rolling (OR) direction left to right.

2.6.2.4 Inclusion-WEC interactions and steel cleanliness

Eighty-two NMIs were recorded during the metallographic analysis; sixty-two were ranked with a high likelihood of WEC initiation (rank 1 or 2). Most inclusions were found to be small sized (~ 2 - 15 µm (diameter) and ~ 4 - 21 µm in axial length) globular duplex inclusions (globular manganese

and/or calcium sulfide surrounding aluminate) (D_{Dup}) and globular oxide inclusions (D). At the early infant stages of WEC formation (4 and 6 hrs), D_{Dup} and D type inclusions were found to interact with the WECs, EDX analysis of inclusions at these stages being either Al_2O_3 or MnS surrounding Al_2O_3. Inclusion types found to interact with the large WEC networks found at the later stages of RCF duration (18 hrs) are consistent with those found at the early infant stages. This agrees with the findings found from the 18.5 hr RCF test in [38], that found forty-nine NMIs and forty-one rank 1 or 2 NMIs in five fully mapped WECs, these predominantly being small sized (~2-15 µm) D_{Dup}, $D_{DupTi(C,N)}$ and D type inclusions. The oxide encapsulations are responsible for hardness discrepancy with the martensite matrix, induced tensile residual stresses due to differing coefficients of thermal expansion and weak coherence/de-bonding of the oxide and matrix [42, 86, 87]. The majority of the inclusion-WEC interactions were recorded at a depth of ~ 50 - 200 µm, this being consistent with the depth of high subsurface shear stresses ($\tau_{0,\,max}$ = 92 µm, $\tau_{uni,\,max}$ = 145 µm) (see Figure 2-11).

Steel cleanliness analysis indicates that the raceway is 'cleaner' than the rollers (C_i = 1.5 (standard) and C_i = 344.1 (non-standard) for the rollers and (C_i = 0.2 (standard) and C_i = 35.6 (non-standard) for the raceway). The 'cleaner' raceway would therefore have fewer inclusions available to initiate cracks, which could explain why no WECs were recorded. The lower cleanliness and therefore greater density of inclusions in the rollers, would also lead to an increased propensity for WECs to initiate and coalesce forming networks that are more extensive. This is elevated if inclusions lie in critical locations. It is important to note the significant increase in C_i when only counting inclusions recorded under the thresholds set by the ISO 4967-B standard [89] and when counting inclusions recorded outside of these domains; however, the ratio difference in cleanliness between the roller and raceway remains similar. Small/short inclusions have been found to be dominant in initiating and interacting with WECs. Thresholds set by the standard do not factor in these small/short inclusions, comparisons of the C_i highlighting the potential limitations of the standard when considering steels used in WTGBs. These limitations are currently being investigated and will be presented in a future study by the authors.

2.7 Conclusions

1. Metallographic analysis has been used to map White Etching Crack (WEC) damage in RCF tested bearings in standard 100Cr6 steel. For the first time, this study has captured the evolution of WEC formation, using serial sectioning methods to investigate the formation mechanisms of WECs in FAG-FE8 tested bearings under non-hydrogen charged conditions.

2. From the characteristics, location and apparent evolution of WECs over the increasing test durations, macro and serial sectioning has enabled further verification of the author's original revelations that,
    a. WECs can initiate and propagate entirely within the subsurface.
    b. The frequent interaction with small/short inclusions strongly indicates that WECs can often be initiated by non-metallic inclusions. The inclusion interactions are ~ 2 - 15 µm in the circumferential direction, and ~ 4 - 21 µm in axial length, being globular sulfides (D_{sulf}), globular duplex inclusions (globular manganese and/or calcium sulfide surrounding aluminate) (D_{Dup}) and globular oxide inclusions (D). D_{Dup} and D type inclusions are found to interact with the WECs at the early infant stages of WEC formation, inclusions being either Al_2O_3 or MnS surrounding Al_2O_3. Inclusion types found to interact with large WEC networks found at the later stages of RCF duration are consistent with those found at the early infant stages. The cleanliness of the roller and raceway were found to be significantly different, the rollers having a much lower cleanliness than the raceway, which may help explain why no WECs were found in the raceway sections.
3. Detailed analysis of WEC characteristics across the test durations, such as quantification of the amount of WEA microstructural change associated with the WECs over the test durations, and also within certain planes of the WEC, has provided supporting evidence for the crack being a prerequisite to WEA, where a possible mechanism for this is crack face rubbing. Conversely to this mechanism, in the samples exposed to most test duration, numerous small very near-surface WEAs were also found without any visible crack; thus, evidently the formation of the microstructural change to WEA does not require the presence of a crack. Further analysis including SEM should be carried out, however, to also confirm the non-existence of small cracks associated with WEA as only light optical microscopy has been used in this study.
4. An interesting finding is a heterogeneous distribution of WEC formation occurred in the bearing rollers, most WECs forming in a relatively limited zone corresponding to where the largest energy dissipation occurs, this agreeing with recent literature observations.

Chapter 3 Influence of hydrogen diffusion on WEC formation during RCF testing

Thermal Desorption Analysis of Hydrogen in Non-hydrogen-Charged Rolling Contact Fatigue-Tested 100Cr6 steel

A.D. Richardson[a*], M.-H. Evans[a], L. Wang[a], R.J.K. Wood[a], M. Ingram[b]

[a]nCATS, Faculty of Engineering and the Environment, University of Southampton, UK

[b]Afton Chemical Corporation, Bracknell, UK

Notation list for Chapter 3

α	Pressure viscosity coefficient [GPa^{-1}]
η_o	Dynamic viscosity [Pas]
h_{min}	Minimum oil film thickness [m]
HV	Vickers pyramid number
λ	Lambda ratio
N	Normal contact load [N]
P	Contact pressure [Pa]
P_{max}	Maximum contact pressure (Hertzian stress) [Pa]
R_q	Root mean squared roughness [m]
$\tau_{o,\,max}$	Maximum orthogonal shear stress [Pa]
$\tau_{uni,\,max}$	Maximum unidirectional shear stress [Pa]
V	Absolute sliding velocity [ms^{-1}]

3.1 Abstract

Hydrogen diffusion during rolling contact fatigue (RCF) is considered a potential root cause or accelerator of white etching cracks (WECs) in wind turbine gearbox bearing steels. Hydrogen entry into the bearing steel during operation is thought to occur either through the contact surface itself, or through cracks that breach the contact surface, in both cases by the decomposition of lubricant through catalytic reactions and/or tribo-chemical reactions of water. Thermal desorption analysis (TDA) using two experimental set-ups has been used to measure the hydrogen concentration in non-hydrogen charged bearings over increasing RCF test durations for the first time. TDA on both instruments revealed that hydrogen diffused into the rolling elements, increasing concentrations being measured for longer test durations, with numerous WECs having formed. On the other hand, across all test durations, negligible concentrations of hydrogen were

measured in the raceways, and correspondingly no WECs formed. Evidence for a relationship between hydrogen concentration and either the formation or the acceleration of WECs is shown in the rollers, as WECs increased in number and severity with increasing test duration. It is assumed that hydrogen diffusion occurred at wear induced nascent surfaces or areas of heterogeneous/patchy tribofilm, due to most WECs did not breach the contact surface, and those that did only had very small crack volumes for entry of lubricant to have occurred.

3.2 Introduction

Driving mechanisms for white structure flaking (WSF) and white etching cracks (WEC) in wind turbine gearbox bearings are highly contested. One of these suggested drivers is hydrogen, where hydrogen that is either sourced from the lubricant or water contamination is released during operation and diffuses into the bearing steel, diffusion of hydrogen leading to an 'embrittlement' of the steel and promoting WEC formations [12, 14, 40, 42, 99-101].

During rolling contact, hydrogen formation and diffusion into the steel could occur by a number of mechanisms,

1. Through surface cracks where water or lubricant entry allows for a local release of hydrogen ions by tribo-chemical reactions at nascent crack tips [64].
2. Through wear-induced nascent surfaces in areas of high slippage or heterogeneous tribofilm, hydrogen being generated by the decomposition of lubricants through catalytic reactions [115, 116] and tribo-chemical reactions of water.
3. (i) Chemical reaction causing formation of hydrogen cations, which are adsorbed on the cathodic steel surface before diffusing into the steel. The deposition rate of hydrogen being enhanced in the case of high electric field strength and thus high ion mobility or due to increased wear; (ii) atomic hydrogen formation through thermal dissociation as a result of discharge in the lubrication gap [100].

In all cases, it is the highly mobile mono-atomic form of hydrogen (H) that diffuses through the material matrix becoming potentially trapped within the steel. The mechanism of hydrogen diffusion through wear-induced nascent surfaces is supported by researchers who have found hydrogen to have diffused during RCF testing [14, 111, 115, 118, 119] with measured concentrations of between 0.1 – 4.2 ppm [14, 115, 118], the concentration of hydrogen measured also being proportional to the wear on the steel during sliding tests [115].

Hydrogen can remain in mono-atomic (H) form as an interstitial solute retaining its mobility in high strength steels [118]. After diffusion, hydrogen can exist as either

1. ‘Non-mobile’, non-diffusible hydrogen that is strongly trapped or residual at irreversible sites.
2. ‘Mobile’ or ‘diffusible’ hydrogen that is weakly trapped at reversible sites [111, 119, 129, 130].

Traps can include inclusions, cracks, grain boundaries, carbides, microvoids, retained austenite and areas of local plastic deformation where the density of crystal defects (dislocations) is large and hydrogen binding with these crystal defects occurs [125, 127, 129, 131-139]. Traps can be split in terms of their desorption temperature and binding energies. Traps with low binding energies and desorption temperatures are referred to as weak reversible traps, strong binding energies and higher desorption temperatures referred to as strong irreversible traps. Traps can also be sub categorised as either physical or attractive (or a combination of the two). Physical traps are those where hydrogen is trapped by the way of mobile hydrogen’s random walk and attractive traps are those such as electrical fields (e.g. electronegative impurity atoms) and temperature/stress gradients [204].

It is considered that strongly trapped hydrogen or hydrogen in its molecular form is not harmful regarding WSF, it being the diffusible hydrogen that ‘embrittles’ the steel; however, recombination of hydrogen to molecular gas can cause hydrogen-induced cracking in steels. It has also been demonstrated that small cracks within the steel matrix can act as strong hydrogen traps rendering the hydrogen non-threatening and unable to assist in the mechanisms of hydrogen embrittlement [125]. It is, however, noted that trapping and saturation of cracks with hydrogen could eventually lead to an internal pressure build up stimulating crack growth. A counter-argument to this is that saturation of the crack could alleviate the ability for crack face rubbing/beating to occur during RCF [59], where crack rubbing/beating is proposed to generate WEAs [59, 60]. It is suggested that in the formation process of WEAs, hydrogen serves only to enhance brittle cracking, forcing cracks open and inducing additional crack rubbing/beating [59].

There are a number of theories explaining the detrimental effect of hydrogen on steel however there is no agreement as to which theory explains the effect of hydrogen on bearing steels. Popular mechanisms include; (i) hydrogen enhanced localised plasticity (HELP), hydrogen enhancing the mobility of dislocations ahead of the crack tip resulting in localised plasticity, (ii) hydrogen enhanced decohesion (HEDE), hydrogen increasing lattice strength by a reduction in cohesive binding energy lowering the stress required for cleavage, and (iii) hydrogen enhanced strain induces vacancy (HESIV), hydrogen diffusion towards vacancies and nanovoids, their formation being assisted under strain leading to ductile crack growth by localised slip [109, 111].

To measure the concentration of diffusible hydrogen in bearing steels, a number of techniques are typically used, including; mercury method [126], thermal desorption analysis (TDA) using thermal conductivity detection (TCD) (e.g. gas chromatography (GC) or hot carrier gas extraction [126]), TDA coupled with a mass spectrometer (TDMS) [60, 104, 116, 129, 205], and secondary ion mass spectrometry (SIMS), this being used to measure the local concentration of hydrogen in specimens and at defects such as inclusions [206, 207]. The primary method for measuring hydrogen in weld steels under the BS ISO 3690 [126] has been the mercury method; however, due to the health hazards when using mercury and the long analysis times involved other methods for measuring hydrogen have been exploited. TDA is one of the more popular methods, where negligible differences in measurable hydrogen concentrations between TDA methods and the primary mercury methods have been found [208, 209], and thus TDA methods are consequently recognised in the BS ISO 3690 [126] for measuring hydrogen in steel welds. Consequently, TDA has been used to measure the concentration of diffusible hydrogen in bearing steels in a number of studies [37, 59, 60, 102, 104, 112, 116, 127, 128].

TDA using a TCD can be classified into two methods,

1. Hot carrier gas extraction where the sample is heated at high temperature (up to 400 °C), the diffusible hydrogen desorbed out being measured continuously, where TDA can also be carried out by ramping the temperature gradually at a pre-defined rate (°C/min).
2. Where a sample is placed into a chamber that is heated at relatively low temperature (typically between 45 °C and 150 °C), hydrogen being measured separately after collection [126].

Potential downfalls to elevated temperature analysis using the hot extraction method lie in the reduction in analysis time and thus a potential increase in the rate of hydrogen desorption from the specimen, resulting in a greater release of hydrogen than that which might desorb out under ambient conditions [208]. The measured concentrations obtained at higher temperatures are a true representative concentration of the hydrogen measured. Other factors that may influence the TDA result include the effect of oxide layers at the surface. It has been observed that hydrogen trapped in the steel reacts with oxygen at the surface during desorption to form water molecules, this producing additional unwanted peaks in the TDA spectra [208, 210].

There is debate between standards and studies employing TDA as to what is defined as diffusible or non-diffusible hydrogen. At ≤ 400 °C, desorbed hydrogen is defined by BS ISO 3690 standards [126] as diffusible hydrogen, elevated temperatures > 400 °C being used to measure strongly trapped residual hydrogen, and this is in contrast to the Australian standard for example that defines significant amounts of residual hydrogen are released > 150 °C [211]. TDA conducted on

bearing steels, as discussed above, however, does show deposition peak ≤ 400 °C corresponding to diffusible hydrogen, the desorption peak occurring at elevated temperatures > 400 °C corresponding to non-diffusible strongly/residually trapped hydrogen. Since a large number of parameters can affect TDA results, strict measures must be taken. The important parameters to consider are,

1. Heating method (rate, duration, upper temperature).
2. Weight of samples (affects lower detection limit of hydrogen).
3. Geometry of specimens (surface area of samples during TDA).
4. Time to start of TDA (length of time samples are at temperature before TDA or before freezing), where freezing of the sample is used to ensure that as much diffused hydrogen remains trapped before conducting TDA).
5. Freezing method (Liquid Nitrogen (LiqN)) or dry ice; the colder the temperature the more hydrogen's mobility and thus effusion is inhibited).
6. Specimen surface preparation (removal of contaminants such as moisture, oxide layers and lubricant residue).
7. Precision of TDA instruments (resolution, calibration and minimum hydrogen detection limits).

To investigate the role of hydrogen diffusion in WTGBs, this study uses TDA to measure the diffusible hydrogen concentration in FAG-FE8 tested cylindrical roller thrust bearings, this being a continuation of the works conducted previously by the authors [194, 195]. Many previous investigations have concentrated on the analysis of pre-hydrogen charged RCF test specimens [37, 60, 88, 98, 99, 101-107], where it is generally noted that pre-charging decreases RCF life in bearing steels that fail from WSF. This study uses TDA to measure the concentration of diffusible hydrogen in non-hydrogen charged specimens to better simulate the environments experienced in service. Finally, the link between the role of hydrogen and the propensity for WEC formations has been explored through the combination of TDA and extensive metallographic analysis conducted in a parallel paper by the authors of this manuscript [153] (Chapter 2).

3.3 Materials, techniques and experimental methods

3.3.1 Rolling contact fatigue testing

RCF testing was conducted on two 100Cr6 steel cylindrical roller thrust bearings (CRTBs) on an FAG-FE8 test rig under non-hydrogen-charged test conditions. Each bearing has fifteen individual rollers mounted in a brass cage sandwiched between two washer raceways. The test rig, set-up

and conditions are more extensively detailed (Chapter 2), [153] where metallographic analysis has been conducted on the same test bearing rollers and raceways analysed in this study. The test conditions are shown in Table 3-1.

Minimum oil film thickness (h_{min}) between rollers and washer raceways is calculated using the Hamrock and Dowson equation [197, 198]; see equation (A.1.1) in A.1. Lambda ratio (λ) has been calculated based upon h_{min} and the roughness (R_q) values given in Table 3-1; see equation (A.1.2) in A.1.

Table 3-1: FAG-FE8 RCF test conditions.

Test system	
Test rig	FAG-FE8
Test sample	Cylindrical roller thrust bearings
Bearing type	F-562831-01 / 81212
Bearing dimensions roller/raceway	15 x rollers, Diameter = 11 mm, Length = 11 mm / 2x raceway, Outer diameter = 95 mm, Inner diameter = 60 mm, thickness of each raceway = 7.5 mm. Thickness of compiled bearing rollers + brass cage and raceways = 26 mm
Oil properties	
Oil type	Automotive gear oil, fully formulated semi-synthetic (ISO VG64)
Viscosity	64 cSt (40 °C), 9.5 cSt (100 °C)
Pressure viscosity coefficient (α)	6.6 GPa^{-1}
Dynamic viscosity η_o (100ºC)	0.0046 Pas
Oil additives	Sodium/calcium anti-corrosion sulfonates, ZDDP antiwear, VI improvers and FMs
Bearing material properties	
Washer / roller / cage material	Martensitic 100Cr6 steel / Martensitic 100Cr6 steel / Brass
Hardness roller / washer	765 HV / 590 HV
Surface roughness (R_q) roller / washer	0.09 µm / 0.50 µm
Test conditions	
Rotational shaft speed	750 rpm
Axial load	60 kN
Max contact pressure	~1.5 – 1.9 GPa (depending on contact length used 7-9 mm, 9 mm used in this study)
Bearing / oil temperature	100 °C
Minimum film thickness (h_{min})	0.053 µm
Lambda ratio (λ)	0.1
Slide to roll ratio (SRR)	± 12.5% rising to the edges, pure rolling exists at the centre of bearing contact
Test durations	
Test number 1/2/3/4/5/6/7/8	0/2/4/6/6-repeat/12/16.5/18 (hours duration)
Subsurface shear stresses	
Max orthogonal shear stress ($\tau_{o,\,max}$)	~375 - 475 MPa (acting @ ~92 µm below the contact surface)
Max unidirectional shear stress ($\tau_{uni,\,max}$)	~456 - 578 MPa (acting @ ~145 µm below the contact surface)

3.3.2 Thermal desorption analysis (TDA)

To detect any hydrogen that may have diffused and become trapped in the steel during RCF testing, TDA was performed using two different experimental set-ups under BS ISO 3690 standards [126] as detailed below. See Figure 3-1 for the respective TDA equipment set-ups.

1. TDA at ≤ 400 °C (diffusible hydrogen) and 1100 °C (strongly trapped/residual hydrogen) was performed on a Bruker G4 Phoenix DH utilizing the carrier gas (nitrogen) hot extraction method with TCD of the desorbed hydrogen. A rapid infrared-heated clamshell furnace with a 30 mm-diameter quartz specimen chamber heats up the sample material. For TDA at 1100 °C, a 20 mm-diameter wire-heated tube is equipped. The system uses the

hot extraction method, and the system is heated up to 400 °C or 1100 °C before the sample is placed into the chamber, the sample only being placed once temperature is reached. It is expected that the sample temperature rapidly increase until 400 °C is reached throughout, including the sample core. The carrier gas transports the desorbed gases through molecular sieve and Schuetze reagent, and the Schuetze reagent converts CO, CO_2, H_2O together with other interfering substances and is removed from the carrier gas by the molecular sieve before the TCD so that only hydrogen is measured. The G4 phoenix is an open system, and thus at the inlet of the analysing tube more carrier gas is being supplied than is being released from the outlet preventing the entry of ambient air into the system. The minimum concentration of hydrogen measurable by the analyser is 0.05 ppm (depending upon sample weight) and the precision is ± 0.05 ppm. Hydrogen detection levels during measurement indicated that all hydrogen was removed within the sensitivity of the instrument within 20 min, and therefore the measurement time was set specifically to 20 min for all tests.

2. Ramped TDA was conducted using GC method at a rate of 25 °C/hour up from room temperature to a final temperature of 300 °C (diffusible hydrogen) using an in-house TDA system. TDA using this set-up was only conducted on the 0 hour control, 6 hour and 18 hour RCF-tested bearings. The sample is heated at a linear rate using a resistance tube furnace, a thermocouple being used in close proximity to the sample to measure the temperature. The GC is calibrated with a helium gas containing 60.7 ppmv (part per million per volume) hydrogen before measurement. Helium is used as the carrier gas and flows at a constant rate of 10 ml/min. The carrier gas transports the desorbed gases from the sample through the GC system. The mix of gases is injected into the GC column every 3 min, where the mix of gases is separated and detected by a pulsed discharge ionization detector. The hydrogen desorption rate (ppm/min) is then measured. Analysis time was conducted over 1250 minutes, the final temperature of 300 °C being reached after 615 min.

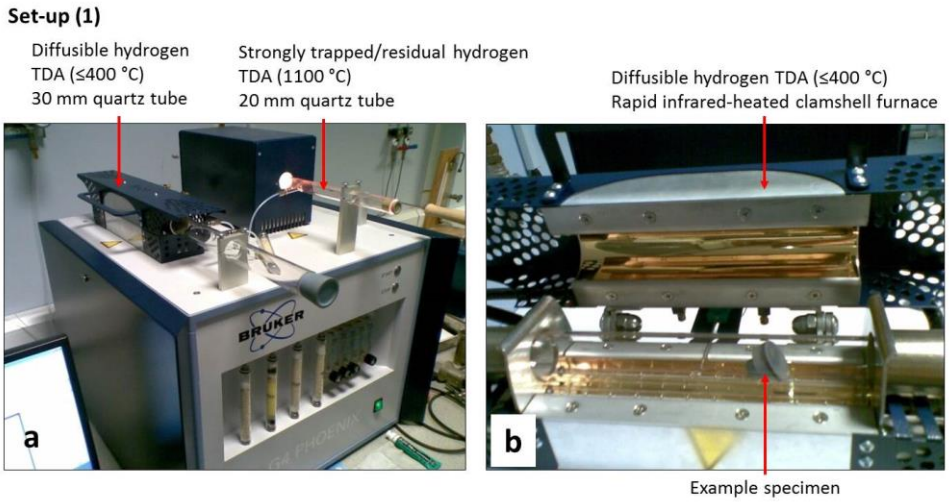

Figure 3-1: TDA equipment set-up (1). (a) Diffusible and strongly trapped/residual hydrogen analysis tubes and (b) infrared-heated clamshell furnace. Adapted from [212].

3.3.2.1 Sample preparation

Prior to TDA, necessary sample preparations post-RCF-testing are required to minimise losses and control contamination in the hydrogen detection process.

Once testing had finished, the bearing was removed, cleaned of residual oil and immersed in LiqN under BS ISO 3690 standards [126] prior to TDA. The downtime between the end of RCF tests and immersion in LiqN was kept to a minimum where possible to mitigate any potential losses of hydrogen. The immersion in LiqN ensures that as much mobile diffusible hydrogen remains trapped in the steel bearing before TDA. LiqN at -196 ˚C inhibits hydrogen from effusing out of the steel bearing; however, some hydrogen will still desorb out of the steel overtime.

Prior to TDA, the bearing was prepared into the relevant samples to be analysed. The raceway washers were cut into ~ 20 x 20 mm square sections and the rollers kept whole or cut into halves to investigate the influence of outer and inner roller zones. Cutting time was kept to a minimum to limit the desorption of hydrogen (< 1 min). In set-up 1, single and multiple rollers and raceway sections were analysed, only single roller and raceway sections being analysed in set-up 2. The rollers analysed were either non-spalled or spalled to investigate the influence of spall sites as exposed surfaces/cracks for additional hydrogen entry into the bearing steel during operation. The samples were kept continuously immersed in LiqN for a period of 2 – 15 days under BS ISO 3690 standards [126] until TDA was conducted. Before TDA samples were lightly blasted with alumina grit for < 60 s to remove contaminants, residues and the oxide layer, this is with the exception of the 0 hour (control) roller and raceway analysed by set-up 2 which were lightly ground using 800 grit SiC paper. The samples were then ultrasonically cleaned in acetone for 60 s

to remove surface contaminants, air-dried and then weighed on a mass balance before being placed in the TDA analyser tube. A flow diagram of the sample preparation process prior to TDA analysis is illustrated in Figure 3-2.

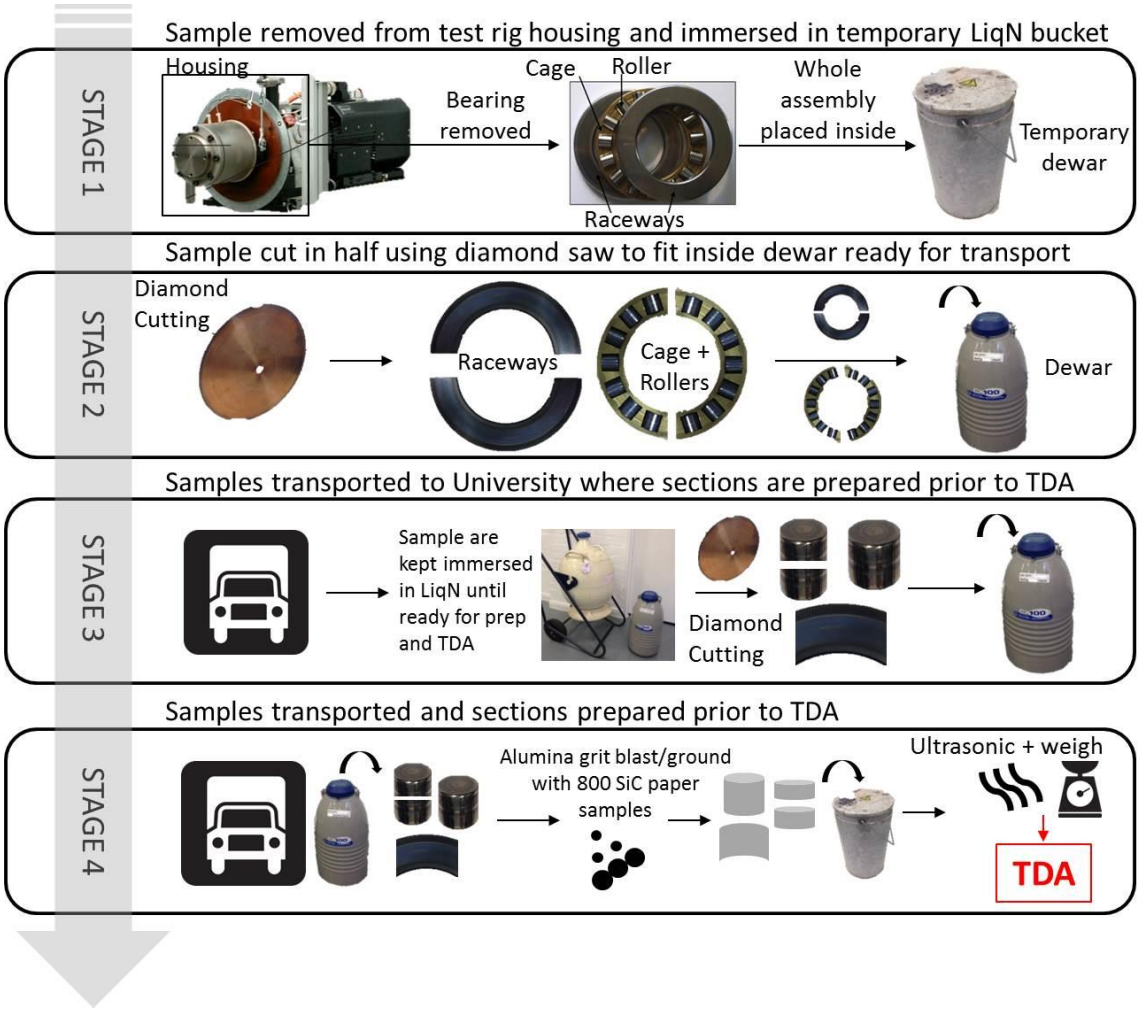

Figure 3-2: Flow diagram demonstrating the stages of sample preparation post RCF testing and before conducting TDA.

3.4 Results

3.4.1 Thermal desorption analysis

The results from the TDA are detailed below and displayed in Table 3-2, Figure 3-3 and Figure 3-4. Results have shown,

- Negligible (close to the detection limit of the instrument) concentrations of diffusible hydrogen were measured in the raceway sections across 0-18 hours (0.01 - 0.15 ppm) using TDA set-up 1 at 400 °C, these being similar to the 0 hour sample (0.02 - 0.12 ppm).

- Elevated concentrations of 0.29, 0.16 and 0.32 ppm were measured in the raceway sections at 18, 6 and 0 hours respectively, using TDA set-up 2.
- For TDA of a 2 hour raceway section at 1100 °C using set-up 1, the evolved hydrogen curve showed a double hump. The first hump, relating to diffusible hydrogen (≤ 400 °C) measured a negligible concentration of ~ 0.01 ppm, and the second hump relating to strongly trapped/residual hydrogen also measuring a negligible concentration of 0.10 ppm.
- Elevated concentrations of diffusible hydrogen were measured in the rollers. Increased concentrations have been measured for longer test duration across 0-18 hours using TDA set-up 1. TDA using set-up 2 showed elevated diffusible hydrogen concentrations of 0.78, 0.71 and 0.40 ppm for the 18, 6 and 0 hour rollers respectively.
- TDA at 1100 °C using set-up 1 was conducted post 1st round TDA at 400 °C on the same 3x 16.5 hour rollers. A concentration of 0.30 ppm was measured, representing the strongly trapped/residual hydrogen.
- Through TDA of outer and inner roller halves at 18 hours, no significant differences between hydrogen concentrations were found.
- No considerable differences were found between spalled and non-spalled rollers.

From the TDA curve in Figure 3-4 (a), it can be seen that the 18 hour roller shows a shallow desorption hump between 0 and ~ 50-75 °C, with steady desorption between ~ 50 and 200 °C. Another more pronounced desorption peak is observed just beyond at ~ 200-300 °C. For the 18, 6 and 0 hour raceway sections, a single desorption peak is observed just beyond 175 °C. A single desorption peak is observed just beyond ~ 150 °C for the 0 hour (control) roller. The 6 hour roller shows a steady desorption between ~ 0 and 150 °C; beyond this a desorption peak is observed at ~ 200-300 °C. The desorption curves presented in Figure 3-4 show that hydrogen started to desorb out right away for the 18 and 6 hour rollers and at just after ~ 250-375 min for the 18, 6, and 0 hour raceway sections and the 0 hour roller after TDA had started. TDA indicates that all diffusible hydrogen was fully desorbed by the time the analysis had finished at 1750 minutes.

Table 3-2: Concentration of diffusible hydrogen (ppm) measured by TDA using set-up 1 and 2.

Bearing section	**0 hr (ctrl)**		**2 hr**	**4 hr**	**6 hr**		**12 hr**	**16.5 hr**	**18 hr**	
Set-up 1 (TDA @ 400 °C), Set-up 2 (TDA to 300 °C @ 25 °C/hr)										
Rolling element	**SU 1**	**SU 2**	**SU1**	**SU1**	**SU 1**	**SU 2**	**SU1**	**SU1**	**SU 1**	**SU 2**
1x element		0.40		0.04, 0.10, 0.10, 0.12	0.11, 0.13	0.71	0.24, 0.27,		0.46, 0.45, 0.35‡	0.78
2x elements	0.12		0.10		0.32, 0.21, 0.18,		0.28, 0.35			
3x elements					0.37*			0.57†		
2x inner halves									0.57, 0.44	
2x outer halves									0.63, 0.58	
Raceway										
1x section	0.07	0.32		0.07	0.02	0.16	0.014	0.01	0.12	0.29
2x sections									0.15	
TDA @ 1100 °C										
Rolling element										
3x element								0.30†#		
Raceway										
1x section			0.10							

KEY

All samples with non-spalled contact surfaces unless otherwise stated.

SU 1 or SU 2 denotes set-up 1 or set up 2.

*: TDA results from 6 hr repeat RCF test.

†: 1x spalled roller, 1x non-spalled roller, 2x non-spalled roller "halves" analysed simultaneously.

‡: The rolling element analysed was spalled on the contact surface.

#: Analysed post 1st round of TDA at 400 °C. Oxide layer was removed with a file and wire brush prior to TDA and were re-weighed.

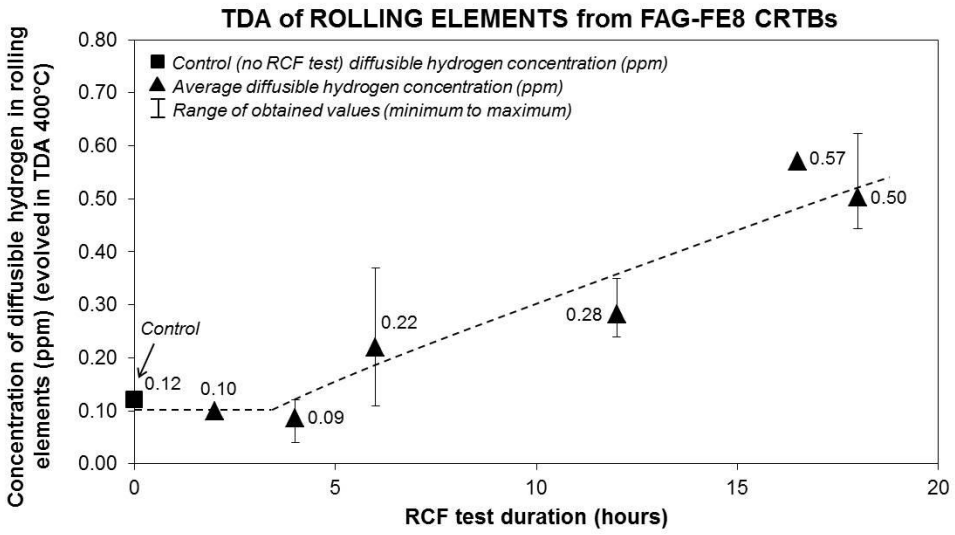

Figure 3-3: Average concentrations of diffusible hydrogen measured by TDA at ≤ 400 °C using set-up 1 in the rolling elements post RCF testing. See Table 3-2 for individual hydrogen TDA measurements.

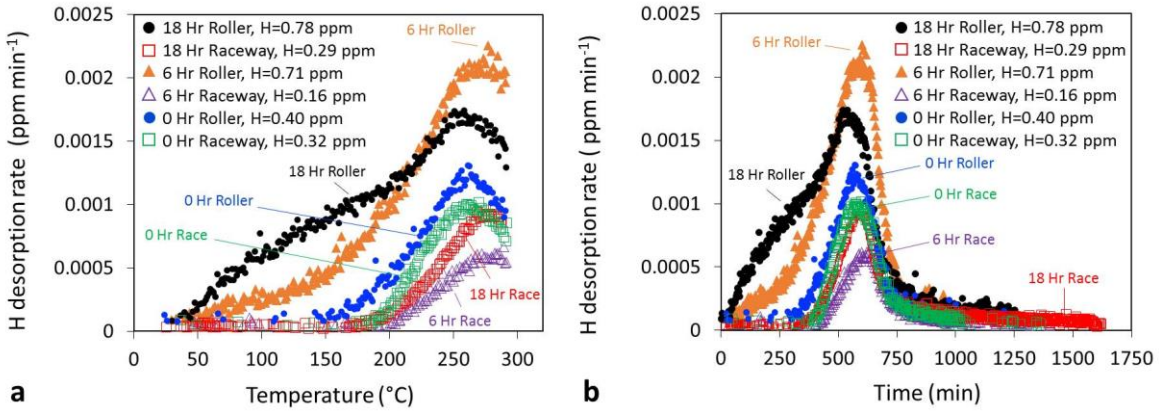

Figure 3-4: Hydrogen desorption curves for 0, 6 and 18 hour RCF tested roller and raceway washer section analysed by ramped TDA to 300 °C using set-up 2 including the total diffusible hydrogen concentration measured. (a) Hydrogen desorption rate (ppm/minute) vs. desorption temperature (°C). (b) Hydrogen desorption rate (ppm/min) vs. analysis time (min). See Table 3-2 for individual TDA measurements.

3.5 Discussion

3.5.1 RCF testing

This study has used non-hydrogen charged testing to better simulate the conditions experienced in service by WTGBs, where many previous investigations have used pre-charging to accelerate WEC formations. The FAG-FE8 test rig, however, does have differing dynamics to those experienced by WTGBs during service. On the other hand, one similarity between the FAG-FE8 and those experienced in service is slip, this being discussed in further detail in [153] (Chapter 2) Slip between roller and raceway can cause metal-to-metal contact resulting in the exposure of wear induced nascent surfaces [115, 116]. It has been demonstrated that hydrogen diffusion is increased in the presence of slip, where hydrogen is generated as a result of decomposition of lubricants through catalytic reactions and/or tribochemical reactions of water at these nascent sites, the amount of hydrogen diffusion being proportional to wear on the steel [115, 116].

It is important to note that the FAG-FE8 set-up does not use any additional external contributors that can influence hydrogen concentration i.e. hydrogen charging, adding water, and thus it is proposed that the lubricant is the source of hydrogen. However, it is unknown how much water may be in the oil, where small amounts may be sufficient to create hydrogen, thus hydrocarbons may not be the only source of hydrogen in the oil. One argument for diffusible hydrogen being unnecessary in the formation of WECs is through a study conducted using fluorinated oil (free of hydrogen molecules) where WECs were created [52], however, again water contents were not

measured, and thus it is unknown whether small amounts in the oil could have generated sufficient amounts of hydrogen to drive WEC growth.

Studies have shown that at certain thresholds for slip energy criteria (PVmax, the product of contact pressure P and slip velocity V, MPa ms^{-1}), WSF prevails, where locally higher permeation of hydrogen was found in these zones. The concept of slip energy criteria has been further developed, represented by the slip energy criteria per film thickness sheared (N.V/λ, λ = lambda ratio, N = normal load, N ms^{-}1) and is based upon data obtained from different test rigs [27] to determine a threshold for WEC formation in most roller bearing configurations. It is postulated that this threshold could exist due to the fact that sliding energy generates local flash temperatures influencing the tribochemical reactions taking place at nascent surfaces [27]. Limitations however do exist, as this criterion does not take into account the lubricant formulation. For example, in this study the 'special' oil used is known to promote WSF.

Through serial sectioning analysis conducted by the authors it has been shown that the localisation of WEC formations coincide with areas supported by thresholds for slip energy criteria and asperity energy friction accumulation, these results being shown briefly in Figure 3-6, where more details are available in [153] (Chapter 2). This suggests that the combination of slip/frictional energy input into the system and diffusion of hydrogen during operation may influence the propensity for WEC formations. Hydrogen diffusion analysis through finite element simulations attempts to link asperity friction energy with the absorption of hydrogen to explain the vulnerability of bearings to WEC formations in FE8 tested cylindrical roller thrust bearings [95]. Simulations show higher hydrogen concentrations in areas of high slip energy and asperity friction accumulation. Simulations, however, do reveal that the rollers hydrogen concentration, in all cases except for long running times under the assumption that no hydrogen flux crosses the surface, is below that of the washer. This is explained by shorter hydrogen absorption and emission location at the roller and free surface compared to the raceway. In addition, after a certain time is reached hydrogen concentrations in the roller exceed the washer due to the smaller relative volume of the rollers. The regeneration time, or time span between contact load cycles, could also be thought to effect the steel-to-steel contact duration. Regeneration times in rollers are lower than the raceway, this would in turn effect the time ('wear time') for oxide film to regenerate, hydrogen diffusion being inhibited by the protective passivating reaction layer at the surface where a nascent surface is needed for electrochemical desorption and chemisorption to occur [213, 214]. This conflicts with the results found in this study where negligible hydrogen concentrations are measured in the raceway relative to the rollers, and this discrepancy is, however, not fully understood given that similar test conditions and material were used. This discrepancy could be explained through steel cleanliness analysis conducted by the authors [153]

(Chapter 2), where the cleanliness of the raceway was found to be significantly 'cleaner' than the rollers. Therefore, this inconsistency could be due to differences in the cleanliness of the materials used between studies, where there is a lack of inclusion sites readily available to trap hydrogen. Evidence for the degree of boundary lubrication (the range of λ) controlling the propensity for WEC formation is also suggested, more WECs forming for more severe boundary regimes (λ in the range of 0.06-0.7) [61]. It could be reasoned that a more severe contact condition results in additional asperity contact and thus wear induced nascent surface exposure for hydrogen generation and diffusion to take place.

3.5.2 Thermal desorption analysis (TDA)

TDA has shown that hydrogen has diffused into the bearing steel rollers during RCF (see Figure 3-3 and Figure 3-4), higher concentrations of diffusible hydrogen being measured for longer test durations. TDA using set-ups 1 and 2 have also shown that negligible amounts of hydrogen have diffused into the raceways during RCF operation, concentrations being similar to the 0 hour test. TDA of outer and inner roller halves at 18 hours showed no significant differences, suggesting that the effect of these two zones has not influenced the generation and diffusion of hydrogen.

For the 0 hour test, negligible concentrations are expected since the tempering stage at ~ 200 °C would allow any weakly trapped hydrogen in the steel from manufacture to escape, in addition to any hydrogen that could have entered into the steel from final manufacturing processes would have desorbed out at room temperature over time.

For the rolling elements at 2-4 hours, hydrogen concentrations were similar to the 0 hour sample with no significant increases. This is logical, as 2-4 hours is short test duration, thus there is only a short time frame in which hydrogen can be generated and diffuse into the steel. Through contact surface inspection of rollers from the same test bearing, very little surface damage and no evidence of surface micro-cracking was also found at these early stages of RCF operation (see [153] (Chapter 2) for further details), where surface micro-cracks and spall sites can act as sumps and zones for lubricant penetration and subsequent hydrogen generation.

At 6 hours, elevated concentrations were measured when compared to 0-4 hours. It is proposed that at 6 hours, a significant time had been reached for sufficient tribo-chemical reactions at wear induced nascent surfaces or areas of heterogeneous tribofilm to occur generating hydrogen.

TDA at 12 hours showed comparable hydrogen concentrations to the 6 hour test. It could be thought that at 12 hours, hydrogen concentrations would be higher than at 6 hours; however, this may partly be driven by variability in rollers and RCF tests (see Figure 3-3). It could be argued that

the increased concentrations are due to lubricant penetration into surface micro-cracks. However, again through contact surface analysis of rollers from the same test bearing conducted in [153] (Chapter 2), SEM showed no evidence of surface micro-cracks; a more comprehensive analysis, however, should be conducted. In addition, serial sectioning analysis from the same study showed a minimal amount of cracks connecting to the contact surface, and all rollers analysed between 0-12 hours were non-spalled. Therefore, lubricant penetration into surface micro-cracks is infeasible, and elevated hydrogen concentrations are proposed to be the result of wear induced nascent surfaces and heterogeneous tribofilm forming.

TDA was also conducted on non-spalled and spalled rollers at 16.5 and 18 hours with no significant differences being found between them. Serial sectioning analysis of rollers from the same test bearing at 18 hours revealed a number of very small crack connections relative to the extent of the WEC network, see [153] (Chapter 2) for further details. It is proposed that these surface connections would be insufficient to allow adequate lubricant penetration for hydrogen generation to occur. To investigate the nature of nascent surface and heterogeneous tribofilm formation during operation and to further develop the mechanism hypothesis, analysis is being conducted by the authors and will be presented in a future paper.

As hydrogen concentrations for 0-4 hour are comparable, it is proposed that the hydrogen measured is trapped hydrogen from short RCF times (where if the amount of diffusible hydrogen is too small, it would not be measurable by TDA), manufacturing processes or minor contaminants. The increase in hydrogen concentration from 4–18 hours being a reflection of the trend for increased hydrogen diffusion during RCF operation.

Figure 3-5 discusses the key features found from the results obtained by TDA set-up 2 and detailed in Figure 3-4.

During RCF, hydrogen generated at the time of operation was at that point in its diffusible state. This hydrogen can then diffuse and become attracted to the various trapping sites within the steel matrix, some of this hydrogen becoming strongly trapped. Therefore, if it is to be contested as to what is considered ‘diffusible’ or ‘non-diffusible’ hydrogen at temperatures ≤ 400 °C, then one could consider that hydrogen that has become strongly trapped or ‘non-diffusible’ (that was once ‘diffusible’ during RCF operation) is still a measure of the hydrogen that has ‘diffused’ into the steel at some point during operation. It is also important to note that at higher TDA temperatures (1100 °C) conducted post 1st round TDA at ≤ 400 °C on the 16.5 hour rollers (see Table 3-2), additional hydrogen was measured (0.30 ppm). This is classed as ‘non-diffusible’ strongly/residually trapped hydrogen (sourced during operation or from manufacturing processes). Therefore, not all (or any) of the ‘non-diffusible’ strongly trapped/residual hydrogen

was released when conducting TDA at ≤ 400 °C and so the hydrogen measured is considered to be weakly trapped 'diffusible' hydrogen.

It can be seen in one case (6hr rollers) that an increased concentration of diffusible hydrogen was measured when analysing 2x rollers simultaneously as opposed to a single rolling element (0.18 – 0.37 ppm). This could be due to a lack of total hydrogen evolved by the single roller to be detectable by the TDA, variability between different rolling elements, an increase in the surface area analysed, increased chance of surface contaminants, residue and oxide layer, though strict measures were taken to reduce the possibility of this effect.

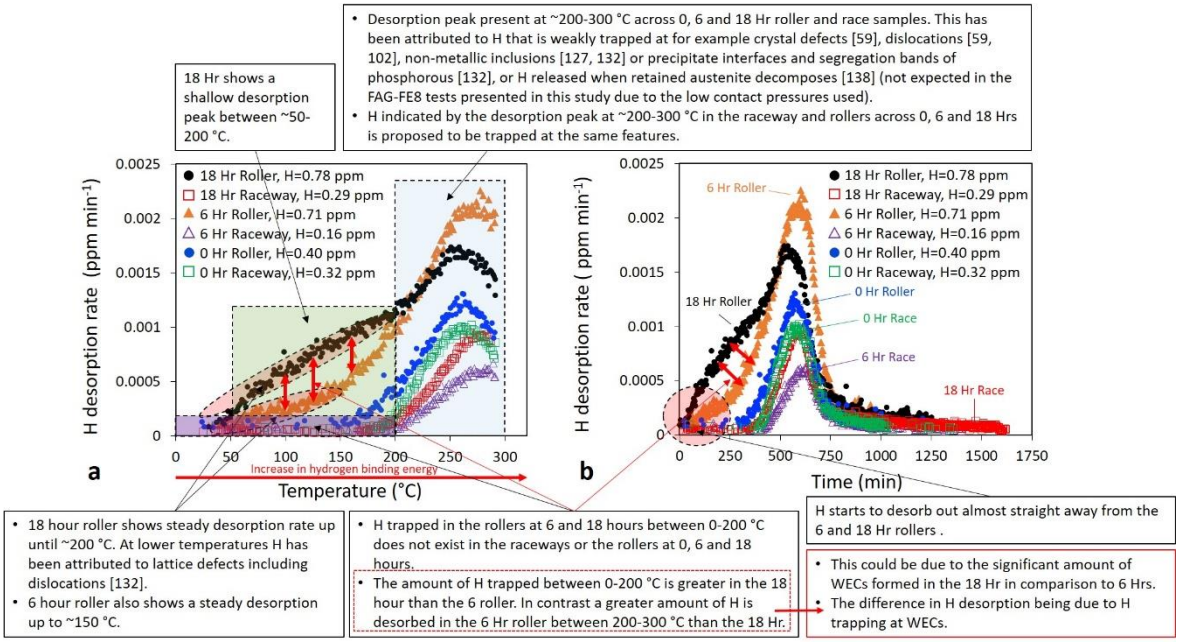

Figure 3-5: Annotated discussion points of key features from TDA set-up 2 results shown in Figure 3-4.

Raceway washers and rollers in some cases were cut into relevant sections before TDA. The heat generated due to cutting would lead to hydrogen losses; however, as it can be seen from the TDA results no significant differences in hydrogen concentrations were measured when analysing rolling element halves and whole rolling elements and so the cutting has not significantly influenced the TDA measurement.

The values measured by TDA between the two test set-ups are comparable. The results measured by test set-up 2 are higher than those measured using set-up 1 by ~ 0.20 - 0.30 ppm; however, this can be regarded as an offset between set-ups. Therefore, the trend for elevated hydrogen concentrations being measured over increasing test duration in the rollers and negligible concentrations measured in the raceways still holds. In terms of absolute bulk concentrations, these results are not readily comparable between other studies that have used different

preparation techniques and test machines due to uncertainties and experimental factors when performing hydrogen measurements. They are, however, comparable between the multiple trips and analyses conducted by the authors using these set-ups. Note also that these bulk values reported are not representative of concentrations found within certain zones of the steel (e.g. near surface), nor locally where hydrogen is attracted at traps such as crack tips [59, 214], areas of plastic deformation and inclusions [129]. It is likely the concentration at these locations will be higher due to hydrogen being attracted and trapped at these sites [59, 60, 214].

In summary the major findings are as follows,

- In comparison to the baseline 0 hour hydrogen concentration measurement, for longer test durations the trend for increased hydrogen concentration measured in the rollers has been shown through TDA. Therefore, TDA on two independent instrument setups has revealed that hydrogen *has* diffused into the bearing rollers during RCF operation, higher concentrations being measured for longer test durations.
- TDA has shown negligible amounts of hydrogen has diffused into the raceways during RCF operation. The authors are unable to confirm the weight of each factor at this point; however, it is likely that the difference in dynamics experienced on the raceway and how this affects the tribofilm and wear are responsible. In addition, factors including hardness difference between the raceway and roller and steel cleanliness could also be influential.
- It is the authors' opinion that the hydrogen measured ≤ 400 °C is a valid measure of the mobile 'diffusible' hydrogen, hydrogen measured above this being 'non-diffusible'. It is considered that during RCF operation, strongly trapped 'non-diffusible' hydrogen is still a measure of hydrogen that was at one point during operation 'diffusible'. Additional hydrogen was also measured at higher temperatures (1100 °C) post TDA at ≤ 400 °C on selected samples.
- TDA using set-up 2 has revealed a number of factors in regards to the diffusion of hydrogen during RCF operation. The authors cannot explicitly explain each factor through the results obtained in this study; however, it is considered that the introduction of WECs affects the trapping of hydrogen.

3.5.3 TDA relation to WEC formations

Metallographic analysis has been conducted on rollers from the same bearing under the same test conditions used in this study to record and map WECs through serial sectioning, comprehensive details being described in [153] (Chapter 2). The following section combines these

results along with the TDA conducted in this study to discuss the relationships between WEC formations and diffusion of hydrogen.

Progressive wear, very little surface damage and no cracks making contact surface connections were observed between 2-12 hours, with only a small number of very small/short surface crack volume connections being found at 18 hours [153] (Chapter 2). It is reasoned that such small/short interactions recorded at 18 hours would not drive extensive WEC networks in the subsurface or allow sufficient lubricant penetration into the crack to aid in WEC growth. Therefore through the combined TDA and metallographic analysis, evidence shows that the mechanism of hydrogen entry is diffusion through wear induced nascent surfaces or areas of heterogeneous tribofilm, hydrogen being generated through the decomposition of lubricant through catalytic reactions [115, 116]. However, as discussed in section 3.5.1, it should be noted that small amounts of water in the oil could generate sufficient amounts of hydrogen. Therefore, without measuring the water content in the oil it is unknown whether small amounts of water are present and that significant amounts of hydrogen were also generated through tribo-chemical reactions with water [42]. It is however also reported that when water is present hydrogen predominantly derives from the oil opposed to the water [117]. Analysis is currently being conducted by the authors to understand chemical/tribofilm heterogeneity effects and mechanisms.

It has been shown by the authors [153] (Chapter 2) that the propensity and average size of WEC formations increases with test duration from 0-18 hours, a ramped increase being seen at the later stages of RCF operation (12-18 hours), and this result is shown in Figure 3-6. Figure 3-7 (a) shows the relationship between measured diffusible hydrogen concentration for set-ups 1 and 2 and the total number of independent WECs recorded from 0-18 hours during metallographic analysis that are displayed in Figure 3-6. In addition, the relationship between diffusible hydrogen concentration and severity index for WEC formation (Figure 3-7 (b)) and the diffusible hydrogen concentration vs. average WEA volume measured (Figure 3-7 (c)) are also shown. The WEC severity index is calculated and weighted upon the combined WEC length in the axial roller direction, WEC radial size (maximum depth minus the minimum depth the WEC propagates into the subsurface) and WEC span, see Figure 3-6. The average WEA volume is a measure of the total amount of WEA found in association with a crack, this being calculated through examination of a number of WECs for each test duration and individually measuring the total WEA found at varying slice intervals through a whole 3D WEC network. The average WEC severity and WEA volume for each test duration are shown in Figure 3-6, further details of which can be found in [153] (Chapter 2). The combined results in Figure 3-7 indicate that a link exists between diffusible hydrogen concentration and the formation of WECs. An increase in WEC formations accompanying elevated hydrogen concentrations. Through the combined results discussed above, it is proposed that

hydrogen that has diffused into the steel matrix during RCF operation can aid in the formation and propagation of WECs in the subsurface.

Evidence for WECs recorded at short RCF test times have been found through serial sectioning analysis of 4 hour rollers [153] (Chapter 2) (see Figure 3-6). TDA for the 4 hour rollers measured negligible concentrations of diffusible hydrogen, comparable to the 0 hour and 2 hour tests (see Figure 3-3). This, however, may have been due to the lack of a sufficient volume of hydrogen being effused for the detection limit of the TDA analyser. Considering the case if there was indeed no increase in hydrogen concentration at the 4 hour roller. Since evidence for WEC initiation was consequently found at 4 hours; either, i) the local concentration of hydrogen was relatively high at the inclusion or crack to aid in crack initiation as opposed to the bulk average of the steel, or ii) hydrogen has not aided in the initiation stage of this WEC, rather hydrogen accelerated crack propagation. This only occurring once additional hydrogen has diffused into the steel above some threshold. This is supported as for longer RCF test durations (6 - 18 hours) an increase in WEC formation and size accompanies an increase in diffusible hydrogen concentration. It may be that a sufficient threshold concentration of diffusible hydrogen is reached accelerating WEC formations where hydrogen acts to decrease the Mode I/II stress limits for crack growth and propagation [112, 114]. Hydrogen acceleration of WECs is also supported by the fact that under the test conditions used in this study (P_{max} 1.5 – 1.9 GPa (depending on contact length used between 7 - 9 mm) and low RCF test times) flaking is not known to normally occur with other lubricants.

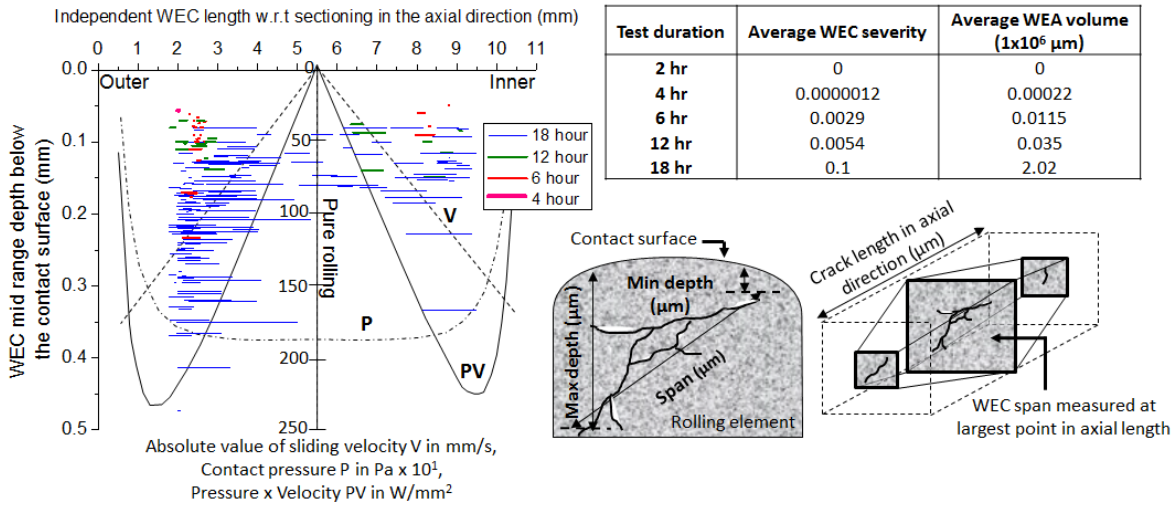

Test duration	Average WEC severity	Average WEA volume (1x10⁶ µm)
2 hr	0	0
4 hr	0.0000012	0.00022
6 hr	0.0029	0.0115
12 hr	0.0054	0.035
18 hr	0.1	2.02

Figure 3-6: Distribution of the individual WECs recorded in 4 - 18 hour rollers through metallographic analysis conducted in. The table shows the average WEC severity and WEA volume recorded for each test duration. Schematic illustrates relevant dimensions recorded for individual WECs. Adapted from [153] (Chapter 2).

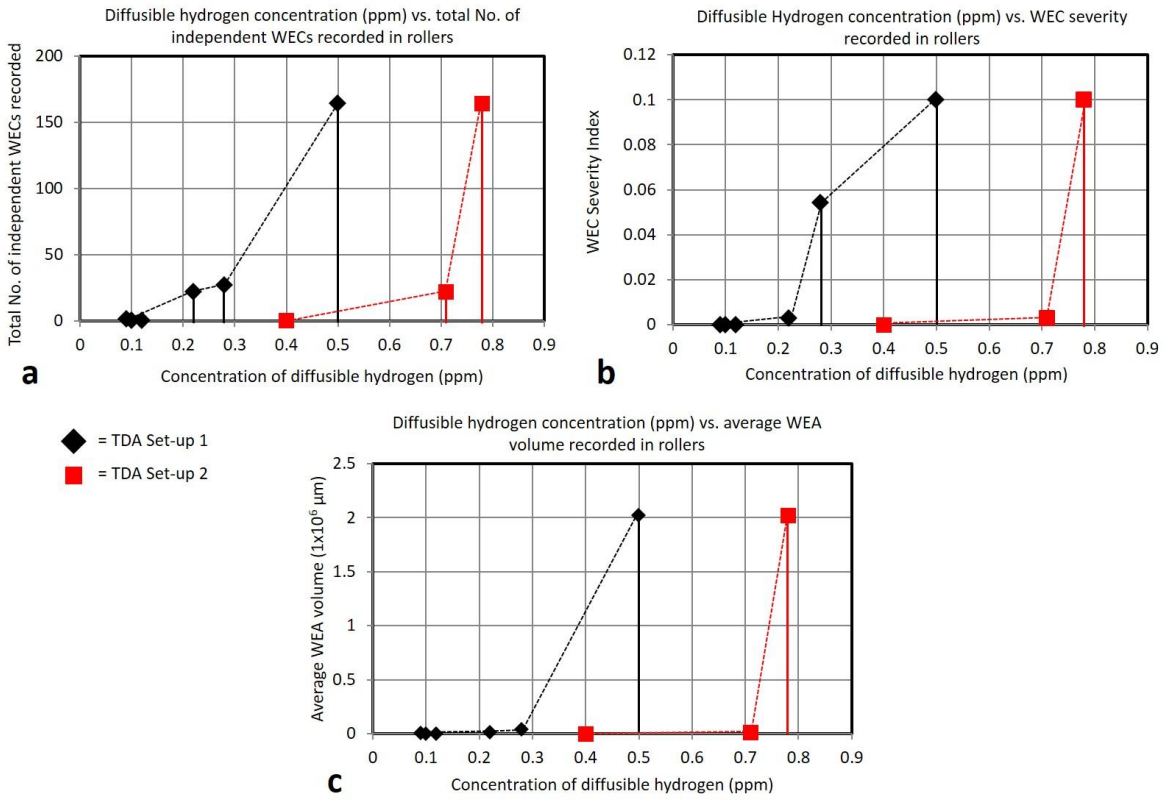

Figure 3-7: Relationship between the concentration of diffusible hydrogen measured for set-up 1 and 2 and WEC formations recorded through metallographic analysis in [153] (Chapter 2). (a) Diffusible hydrogen concentration vs. the total number of independent WECs recorded in the rolling elements. (b) Diffusible hydrogen concentration vs. average severity for WEC formations in the rolling elements. (c) Diffusible hydrogen concentration vs. average WEA volume recorded in the rolling elements.

It has been shown through serial sectioning [153] (Chapter 2) that the total WEA volume found associated with the crack increases with RCF test duration with a step increase in the total WEA volume being recorded at the later stages of RCF operation between 12 - 18 hours (see Figure 3-6). From Figure 3-7 (c) it can be seen that the average WEA volume increases for an increase in hydrogen concentration, a significant step increase occurring for hydrogen concentrations beyond ~ 0.3 ppm. Therefore, it is hypothesised that the diffusion of hydrogen can aid in the formation of WEAs. This appears to be at a greater extent at the later stages of RCF duration, the diffusion of hydrogen promoting WEC growth. Supporting evidence for the crack being a prerequisite to the WEA is shown in [153] (Chapter 2), a possible mechanism for this being crack face rubbing/beating [59, 60], it is thus proposed that the addition of hydrogen aids in crack growth thus enhancing the ability for crack face rubbing/beating to occur in the formation of WEAs.

Metallographic analysis has also revealed that a large number of small near surface (< 25 µm) WEA/WECs formed in 18 hour rollers, examples of which can be seen in [153] (Chapter 2). One influencing factor in the formation of these features is considered to be due to the increased diffusible hydrogen concentration between 12 - 18 hours, where locally at the near surface region, higher localised penetration and concentrations of diffusible hydrogen may exist than in the depth of the steel.

It has also been revealed that the outer and inner roller halve zones significantly influence the propensity for WECs to form, the outer half being considerably more dominant in the formation of WECs [153] (Chapter 2), see Figure 3-6. However, TDA of outer and inner roller halves showed no significant differences in measured hydrogen concentration; therefore, it was not a difference in concentration that contributed to the WEC formations. Studies have shown increased hydrogen permeation in zones of high PVmax (slip energy criteria) [96-98], these zones coinciding with WSF where proposed thresholds for slip energy criteria correspond to a ~ 2 mm zone from either the outer or inner roller edge (see Figure 3-6) for the FAG-FE8 set-up [27]. Metallographic analysis [153] has revealed that a higher density of WEC formations is found in this ~ 2 mm zone (see Figure 3-6); therefore, analysis to measure the concentration of hydrogen in this specific zone may be more applicable.

TDA of raceway washer sections revealed on average lower concentrations of diffusible hydrogen than those measured in the rollers, see Table 3-2. Metallographic analysis of raceway washer sections at 18 hours [153] (Chapter 2) and at 18.5 hours [41] showed no signs of 'conventional' WEC/WEAs, this being in contrast to the extensive number of WECs found in the rollers. It is proposed that one possible reason as to why no WECs were found in the raceways is due to the lack of diffusible hydrogen available to accelerate crack growth. The raceway is also ~ 23% softer (590 HV) than the rollers (765 HV); therefore, the raceway is less prone to cracking due to an increased toughness. It is well recognised that hydrogen effects higher strength steels, hydrogen embrittlement occurring when hydrogen is in its atomic mobile form, hydrogen able to retain its mobility in high strength steels [118]. Hydrogen has, however, been shown to have little influence on toughness and no effect on the hardness of 100Cr6 bearings steel [106]. There are a number of theories that try to explain the effect of hydrogen on high strength bearing steels (see Introduction) however, no agreement yet has been made. Steel cleanliness analysis has shown that the raceway is significantly cleaner than the rollers [153] (Chapter 2). The reduced cleanliness and thus density of inclusions indicates that there are less available inclusion sites for hydrogen to become trapped, this perhaps providing supporting evidence for the lack of diffusible hydrogen measured in the raceways. Differences in solubility between steels may also have an effect on the diffusion of hydrogen. While the solubility has not been checked by the authors, both roller and

raceway are the same steel type from the same bearing, the only difference being hardness, and therefore solubility differences are suggested to be negligible. At this point, the authors are unable to confirm the significance of each of these factors on influencing hydrogen permeation. However, it is likely that a combination of these factors alongside differences in the dynamics experienced by the raceway, and how this affects the tribofilm and wear could be the answer.

3.5.4 Influence of oil

A number of additives found in lubricants have been shown to promote WSF occurrence. These include; extreme pressure (EP) and anti-wear (AW) additives consisting of sulphur and phosphorus compounds [150, 215], where sulphur aids in hydrogen diffusion by preventing atomic hydrogen recombination [148], and formulations of AW zinc dithiophosphates (ZDDP/ZnDTP/ZnDDP) with detergent/rust preventative calcium sulfonate additives [38, 53, 54, 61, 81, 92, 101, 146].

A link between oil additives and the formation of WSF/WECs clearly exists; however further investigation is needed to understand the effects and relationships of the additives. The 'special' oil used in this study has shown that a relationship exists between the propensity for WEC formations and the diffusion of hydrogen into the bearing steel during RCF operation. This 'special' oil contains mixes of calcium sulfonate and ZDDP additives (as well as other potentially influential additives such as sodium sulfonates, EP additives and friction modifiers); therefore, the relationship between calcium sulfonate and ZDDP mixes, diffusion of hydrogen and the propensity for WEC formations is currently being investigated and will be presented in a future study by the authors.

3.6 Conclusions

TDA through two set-ups has been used to measure the concentration of diffusible hydrogen in standard 100Cr6 bearing steel. This has been conducted for the first time under non-hydrogen charged conditions and over increasing RCF test durations, the aim being to investigate the mechanism of hydrogen diffusion and the relationship between measured diffusible hydrogen concentration and operation time. In addition, the link between hydrogen diffusion and the propensity for WEC formations recorded through metallographic analysis conducted in [153] (Chapter 2) has been explored.

1. TDA on two independent setup instruments revealed that hydrogen diffused into the rolling elements during RCF operation, higher concentrations being measured for longer

test durations. Negligible concentrations were measured in the raceway washers over all test durations.

2. There is debate as to what state hydrogen is when measured at ≤ 400 °C, whether it is mobile 'diffusible' or whether an amount of non-mobile, 'non-diffusible' hydrogen is also measured. TDA using two experimental set-ups has shown correlation between results, where it is of the author's opinion that the state of hydrogen recorded at ≤ 400 °C is an applicable measure of the mobile 'diffusible' hydrogen that has entered the steel during RCF operation. Above this temperature, it is considered 'non-diffusible'.
3. TDA coupled with extensive metallographic analysis conducted in a separate study by the author's has shown that,
    a. A relationship exists between the diffusion of hydrogen and the propensity for WEC formations, this also correlating directly with the volume of WEA and WEC severity index.
    b. Metallographic analysis has shown no evidence for conventional WEA/WECs in the raceway washers, it is suggested that this may be due to the lack of hydrogen readily available to accelerate WEC formations and the raceways higher toughness retarding crack initiation/propagation. Steel cleanliness analysis has also shown the raceway washer to be far 'cleaner' than the rollers, and thus less crack initiation sites may have been available for WECs. It is also suggested that an absence of WEC formations and negligible hydrogen concentrations measured may be due to the lack of inclusion sites available to trap hydrogen.
    c. Hydrogen diffusion into the steel during operation is thus proposed to act as an accelerator in WEC formations and propagation in the subsurface. The mechanism of hydrogen entry into the steel is suggested to be diffusion at wear induced nascent surface or areas of heterogeneous/patchy tribofilm, since most WECs did not breach the contact surface, and those that did only had very small crack volumes for lubricant entry to occur. Hydrogen would be generated by decomposition of lubricant through catalytic reactions and/or tribo-chemical reactions of water, where measurements for small amounts of water in the oil should be taken.

Chapter 4 The influence of over-based calcium sulfonate (OBCaSul) additive

The effect of over-based calcium sulfonate detergent additives on white etching crack formation in rolling contact fatigue tested 100Cr6 steel

A.D. Richardson[a*], M.-H. Evans[a], L. Wang[a], M. Ingram[b], Z. Rowland[a], G. Llanos[a], R.J.K. Wood[a]

[a]nCATS, Faculty of Engineering and the Environment, University of Southampton, UK

[b]Afton Chemical Ltd, Bracknell, UK

Notation list for Chapter 4

α	Pressure viscosity coefficient [GPa^{-1}]
C_i	Global cleanliness index
η_o	Dynamic viscosity [Pas]
θ	WEC angle w.r.t axis of direction of compression
h_{min}	Minimum oil film thickness [m]
HV	Vickers pyramid number
L_{10} life	RCF life of a bearing for given operating condition where statistically 90% of bearings will survive
λ	Lambda ratio
N	Normal contact load [N]
P	Contact pressure [Pa]
P_{max}	Maximum contact pressure (Hertzian stress) [Pa]
R_q	Root mean squared roughness [m]
σ	Yield stress
$\tau_{o,\,max}$	Maximum orthogonal shear stress [Pa]
$\tau_{uni,\,max}$	Maximum unidirectional shear stress [Pa]
V	Absolute sliding velocity [ms^{-1}]

4.1 Abstract

Additive chemistry is considered a potential major influencing factor driving White Structure Flaking (WSF) and White Etching Cracks (WECs) in wind turbine gearbox bearing steels. In addition, specific additives in the oil are proposed to aid in the generation and diffusion of hydrogen into the steel during rolling contact fatigue (RCF), promoting WEC formation. One of the critical additives in question driving WEC formations is over-based calcium sulfonate detergents

(OBCaSul), where this 'driving' effect is unclear. RCF testing of 100Cr6 steel using FAG-FE8 cylindrical roller thrust bearing rig and PCS Micro-Pitting-Rig (MPR) lubricated with oils containing varying concentrations of OBCaSul have been conducted in this study, the tested samples being analysed using serial sectioning techniques, Thermal desorption analysis (TDA), and SEM/EDX of the tribofilms formed. Serial sectioning appears to show that WEC formations increase with increase in OBCaSul concentration from 1.4% where no WECs were found, to 2.8% and 5.6% where WECs were recorded. Conversely, for the MPR tested rollers, the higher OBCaSul concentrations (2.8% and 5.6%) showed no WECs, the lower concentration (1.4%) revealing WECs to have formed. Evidence for oils containing OBCaSul forming thick Ca dominated tribofilms promoting hydrogen diffusion and WEC formations in the FE8 rollers is found, where thinner Zn tribofilms on the FE8 raceways demote hydrogen diffusion and WEC formations. The results from the tests with the purposely-formulated OBCaSul containing oils are also compared with the results from a fully formulated oil known to promote WECs to evaluate the influence of OBCaSul on hydrogen diffusion and WEC formations.

4.2 Introduction

Premature failures of wind turbine gearbox bearings (WTGBs) cause significant downtime and high repair costs causing substantial impact to the wind energy industry. One of the most noted failure modes of WTGBs is that of White Structure Flaking (WSF) due to the formation of White Etching Cracks (WECs) typically ~ 1 mm below the contact surface.

Driving mechanisms for WSF and WECs have been debated for a number of years and a consensus into what the major influencing factor is has yet to be decided. One specific factor is the effect of additive chemistry and in addition, the effect additive chemistry has on the generation and diffusion of hydrogen, as a prominent driver for WSF and WECs. Additives found in lubricants that have been shown to reduce RCF life and promote WSF include; greases and lubricants containing sulphur-phosphorous extreme-pressure/anti-wear (EP/AW) additives, such as zinc dithiophosphates (ZDDP/ZnDTP/ZnDDP) and detergent/rust preventatives such as calcium sulfonates [38, 53, 61, 81, 83, 92, 101, 145-147]. Hydrogen poisoning sulphur can aid in hydrogen diffusion by inhibiting molecular hydrogen recombination [148], where decomposition of EP/AW additives such as ZDDPs at nascent catalytic surfaces can generate hydrogen [115, 116].

A number of studies conducted by the authors of this manuscript and others have used an automotive gear oil known to be 'bad' and rapidly promote WECs, this oil containing OBCaSul and AW ZDDP additives. This oil causes bearing failure on the FAG-FE8 test rig between 16 – 40 hours in contrast to the 1000 hours test under the same conditions without WSF, where a pure base oil

was used [54]. FAG-FE8 testing conducted by the authors using this oil has shown that the diffusible hydrogen measured in the test rollers increased with RCF test duration, where this was coupled with an increase in WEC formations [188]. FAG-FE8 testing has showed that oils containing ZDDP, without the introduction of metal or non-metal additives formed WECs, addition of Ca/Na sulfonates also formed WECs as well as Ca/Na in the absence of ZDDP [83].

Calcium sulfonate detergents and more specifically OBCaSul are typically used in automotive gear oils, therefore the majority of literature focuses on their impact on AW performance on engine components for the automotive industry. Calcium sulfonate detergents are used to keep metal surfaces clean by forming a protective layer as well possessing good AW/EP, friction reducing and anti-scuffing properties. ZDDP decomposition rates have been found to be retarded by the OBCaSul detergents since the reaction between ZDDP and OBCaSul is proposed to be antagonistic to the performance of the AW tribofilm [155]. OBCaSul are suggested to have an antagonistic effect toward sulphur containing species in film formation, OBCaSul inhibiting ZDDP tribofilm formation [68, 157, 158], creating 'patchy/weakened' heterogeneous ZDDP tribofilms [158-162] and potentially aiding in hydrogen diffusion processes by promoting and prolonging nascent surface exposure [163].

A number of suggestions explaining the antagonistic effect of OBCaSul are as follows; OBCaSul inhibits the formation of a ZDDP film due to the formation of a colloid dispersion with ZDDP [164]. OBCaSul competition with ZDDP at the contact surface in the formation of a tribofilm, the OBCaSul breaks down to form carbonate, which is deposited on the metal surface [165]. It has been shown from multiple surface techniques that Ca displaces the Zn polyphosphates in the AW film [166, 167], OBCaSul may inhibit polyphosphate chain formation by formation of Ca phosphate [156]. X-ray absorption near-edge structure spectroscopy (XANES) has shown that mix of ZDDP and OBCaSul resulted in the formation of considerable Ca phosphate in the film [168]. The over-basing component is suggested to retard the rate-determining step of AW action (decomposition stage) of ZDDP [169], however, others suggest that it can improve AW performance by forming a 'paste-like' structure in the contact [170, 171].

Based on past literature, it is considered that the OBCaSul in the 'bad' oil mentioned above is the critical additive driving WEC formations, where this 'driving' effect is unclear, this study aiming to investigate this. To accomplish this, rolling contact fatigue (RCF) testing of 100Cr6 steel using FAG-FE8 and PCS-MPR test rigs and lubricated with the 'bad' oil and oils containing varying wt% of OBCaSul additive have been conducted. The tested samples have been examined and analysed using serial sectioning techniques, Thermal desorption analysis (TDA), and SEM/EDX of the tribofilms formed (RCF testing, serial sectioning and TDA for the FE8 tests lubricated with the

'bad' oil are from previous studies conducted by the authors and are used for comparison in this study, for which more details can be found in [153, 188]). By using these techniques, the effect that oils containing OBCaSul additive have on WEC formations, and based upon how they influence tribofilm formation in the contact, and diffusion of hydrogen into the steel have been explored.

4.3 Materials, techniques and experimental methods

4.3.1 FAG-FE8 testing

Testing was conducted on a standard FAG-FE8 rig, comprehensive details of which can be seen in [153] (Chapter 2). The test conditions (with the exception of the oils used) can be found in [153] (Chapter 2). The tested and examined bearing raceway are pre-roughened before testing to R_q value of 0.5 µm. As illustrated in [153] (Chapter 2), the centre of the raceway track and rollers experiences pure rolling with rising slip of up to ± 12.5% slide-roll-ratio (SRR) along the contact major axis towards the edges. The rollers experience both – ve and + ve directional slip due to being sandwiched between two raceways.

Four tests were conducted in total using an oil specifically formulated for this study containing Group III ISO VG 68 with ZDDP AW additive, where the OBCaSul detergent wt% in the oil for each of the four tests was altered (ZDDP only (0% OBCaSul), 1.4%, 2.8% and 5.6%), base and ZDDP staying constant. Tests were shut down manually at 18 hrs to keep duration constant between tests. The calculated maximum Hertzian contact pressure Pmax is in the range of ~1.5 – 1.9 GPa.

Initial minimum oil film thickness (h_{min}) between rollers and raceways is calculated using the Hamrock and Dowson equation [197, 198] (see Eqn A.1.1 in A.1). Lambda ratio (λ) is calculated based upon h_{min} and the roughness (R_q) values given in [153] (Chapter 2) (see Eqn A.2.2 in A.1), the bearing has been run under boundary lubrication. Oil temperature in the contact is controlled at 100 ˚C.

4.3.2 Micro-Pitting Rig (MPR)

Testing was also conducted on a Micro-Pitting Rig (MPR) (Figure 4-1) so that a comparative assessment between the MPR and FAG-FE8 rigs on the WEC formations could be made. The MPR is a computer controlled RCF rig in which three equal diameter counterface rings are in contact with a smaller diameter roller positioned in the middle of the rings. The three rings have a diameter of 54 mm and the test roller is 12 mm with a 1 mm wide wear track (Figure 4-1). Rings and rollers are AISI 52100 martensitically through hardened steel. Chemical composition of the

roller and rings can be found in [61]. Rollers and rings have a Rockwell C hardness of 60 (746 HV) and 63 (867 HV) respectively [61]. Servo controlled motors control the rings and roller separately to allow for testing at different SRR. Lubricant is supplied to the contact through a dip lubrication system. A motorised ball screw applies load, which acts through an arm. A piezoelectric accelerometer is used to measure vibration in the contact during operation, once a threshold is reached the test is stopped automatically.

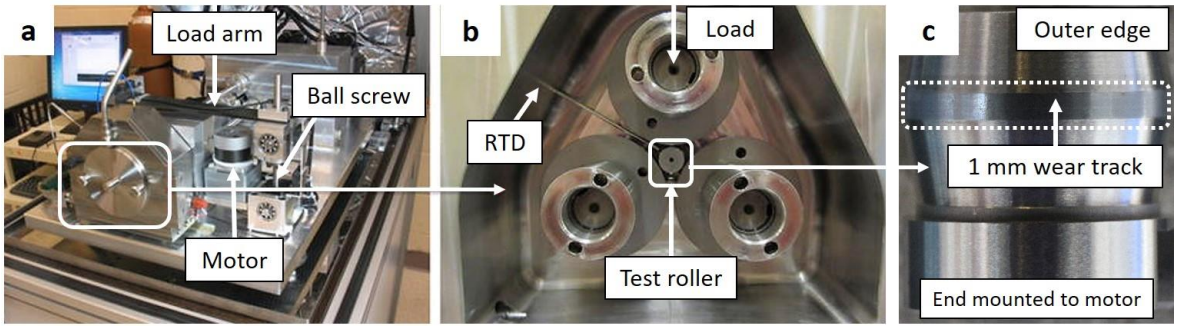

Figure 4-1: MPR set-up. (a) Overview of MPR test rig. (b) Inside the test cell. RTD denotes Resistance temperature detector. (c) Test roller. Adapted from [61]. (a) and (b) Reprinted and adapted by permission from Springer Nature: Springer, Tribology Letters, The Influence of sliding and contact severity on the generation of white etching cracks, Gould, B. and A. Greco, Copyright (2015), https://link.springer.com/journal/11249 (permission [4.1]).

Five tests were conducted using the same four OBCaSul oils tested on the FAG-FE8 as detailed above, and a fully formulated semi-synthetic gear oil (Oil X) that contains ZDDP and OBCaSul 2.8% which is known to be 'bad' and promote WEC formations (full details can be found in [153] (Chapter 2)). The water content of these oils was also measured pre-RCF testing using Karl Fischer titration (see Table 4-1). All tests were run to 18 hrs before being shutdown manually. The calculated Hertzian contact pressure P_{max} is 1.9 GPa. Subsurface shear stresses have been calculated using Hertzian contact theory. The SRR during operation is set at - 30%. The test conditions of the five tests are given in Table 4-2.

Table 4-1: Water content (ppm) for the tested oils pre-RCF test.

Test Oil	Water content (ppm)
ZDDP only (OBCaSul 0%)	40
OBCaSul 1.4%	83
OBCaSul 2.8%	87
OBCaSul 5.6%	175
Oil X (OBCaSul 2.8%)	209

Initial minimum oil film thickness (h_{min}) between the rings and roller has been calculated using the Hamrock and Dowson equation [197, 198]. Lambda ratio (λ) has been calculated based upon h_{min}

and the roughness (R_q) values given in Table 4-2. Oil temperature is kept at 100 ˚C during operation as is measured by a probe inserted into the test chamber.

Table 4-2: MPR test conditions.

Test specimen dimension	
Test Roller	Diameter 12 mm
Test Rings	Diameter 54 mm
Oil properties	
Oil type	Group III ISO VG 68 with ZDDP anti-wear and OBCaSul detergent (varied between 0 – 5.6%) additives
Viscosity	62 cSt (40 °C), 10.23 cSt (100 °C)
Pressure viscosity coefficient (α)	1.6E-08 Pa^{-1}
Dynamic viscosity η_o (100 °C)	8.7E-03 Pa*S
Bearing material properties	
Rings / roller	Martensitic AISI 52100 steel / Martensitic AISI 52100 steel
Hardness roller / roller	746 HV / 867 HV
Surface roughness (R_a) rings / roller	0.1 - 0.15 µm / 0.1 - 0.2 µm
Test conditions	
Rolling speed (m/s)	3.4 m/s
Load (N)	500 N
SRR (%)	-30%
Max contact pressure (P_{max})	~1.9 GPa
Bearing / oil temperature (°C)	100 °C
Minimum film thickness (h_{min})	0.125 µm
Lambda ratio (λ)	λ = 0.5 – 0.8 (depending on Ra used)
Test durations	
Test number (all 18 hrs) 1/2/3/4/5	ZDDP only (0% OBCaSul), 1.4% OBCaSul, 2.8% OBCaSul, 5.6% OBCaSul and Oil X
Subsurface shear stresses	
Max orthogonal shear stress ($\tau_{o,\,max}$)	~495MPa (acting @ a depth below the contact surface of ~80µm)
Max unidirectional shear stress ($\tau_{uni,\,max}$)	~602MPa (acting @ a depth below the contact surface of ~126µm)

4.3.3 Contact surface inspection & subsurface examination using metallographic analysis

All tested sample surfaces were initially inspected using optical macroscopy. For the FAG-FE8 test samples, images were taken at 60 ˚ intervals around the circumference of the rollers. For the MPR samples, images were taken at 120 ˚ intervals around the circumference of the rollers. Example images of the contact surface for each test can be seen in Figure 4-3.

Metallographic analysis was then conducted to record individual WECs and associated damage features in all the RCF tested samples from both FAG-FE8 and MPR testing using the same procedures as detailed in [153] (Chapter 2). For the FAG-FE8 tests, rollers were prepared in the same way as in [153] (Chapter 2). The MPR test roller were prepared in a similar way, the single test roller being analysed. Rollers were mounted such that they were sectioned in the axial direction from the outer roller edge (see Figure 4-1(c)). Details of the sectioning analysis for FAG-FE8 and MPR samples are given below.

FAG-FE8: Macro sectioning (at 50 µm per slice material removal rate) was first conducted on rollers from all the tests from the outer edge of the rollers until the point where WECs were first found. This was then followed by coarse serial sectioning (at average material removal rate of ~30, 35 and 38 µm per slice depending on the test). This is deemed a suitable sectioning removal rate to catch the majority of WECs including smaller networks; however, very small WECs may

have been missed due to the slice removal rates. Imaging of WECs was taken at every five slices. Inclusions were recorded during sectioning. Inclusions may have been missed due to the sectioning removal rates conducted, where inclusions observed in the FAG-FE8 rollers are typically small in size (typically ~ 2 - 15 µm) [153] (Chapter 2). The individual sectioning ranges (sectioning start and stop range) and removal rates (µm/sectioning slice) for each test are listed in Table 4-3. Oil X data is from [153] (Chapter 2), data for Oil X rollers given in Table 4-3 is for an 18 hour test for comparison. Figure 4-2 details the sectioning analysis procedure**.**

MPR: Careful material removal was first conducted on all tests from the outer edge of the roller up until the edge of the wear scar at ~ 3.5 mm (no contact between roller and rings before this point). Once completed, fine serial sectioning was started (~ 4.3 - 7.4 µm per slice depending on the test). Imaging of WECs was taken at every five slices. Inclusion-WEC interactions were recorded during sectioning. The individual sectioning interval ranges and removal rates for each test are listed in Table 4-3. Figure 4-2 details the sectioning analysis procedure**.**

Table 4-3: Sectioning intervals and removal rates conducted during the metallographic analysis.

Test Oil	Nº samples analysed		Sectioning range (start and stop positions) (~ mm)				Removal rate (~ µm/slice)	
			Macro sectioning/material removal		Serial sectioning		Serial sectioning	
	FAG-FE8	MPR	FAG-FE8	MPR	FAG-FE8	MPR	FAG-FE8	MPR
ZDDP only (OBCaSul 0%)	3x Rollers	1x Roller	Avg: 0 – 1.52	0 – 3.5	Avg: 1.52 – 3.0	3.5 – 3.8	Avg: 35	4.3
OBCaSul 1.4%	3x Rollers	1x Roller	Avg: 0 – 2.01	0 – 3.5	Avg: 2.01 – 3.0	3.5 – 3.8	Avg: 30	4.3
OBCaSul 2.8%	3x Rollers	1x Roller	Avg: 0 – 2.04	0 – 3.5	Avg: 2.04 – 3.0	3.5 – 3.8	Avg: 30	4.3
OBCaSul 5.6%	3x Rollers	1x Roller	Avg: 0 – 1.52	0 – 3.5	Avg: 1.52 – 3.0	3.5 – 3.8	Avg: 38	7.4
Oil X [153]	3x Rollers	1x Roller	Avg: 0 – 1.85	0 – 3.5	Avg: 1.85 – 3.0	3.5 – 3.8	Avg: 3.6 or 15	7.4

KEY

For the FAG-FE8 rollers, macro sectioning at ~ 50 µm slice intervals is conducted at the start from the outer roller edge (0.00 mm) until the first visible sign of WECs are found in any one test roller. For the MPR roller, careful material removal from the outer roller edge (0.00 mm) until the edge of the wear track is reached (at ~3.5 mm) was conducted. Note for the FAG-FE8 rollers, sectioning ranges and removal rates are given as an average across the 3x analysed rollers. Note data for Oil X FAG-FE8 is from [153] (Chapter 2), this data is from an 18 hr FE8 test for comparison.

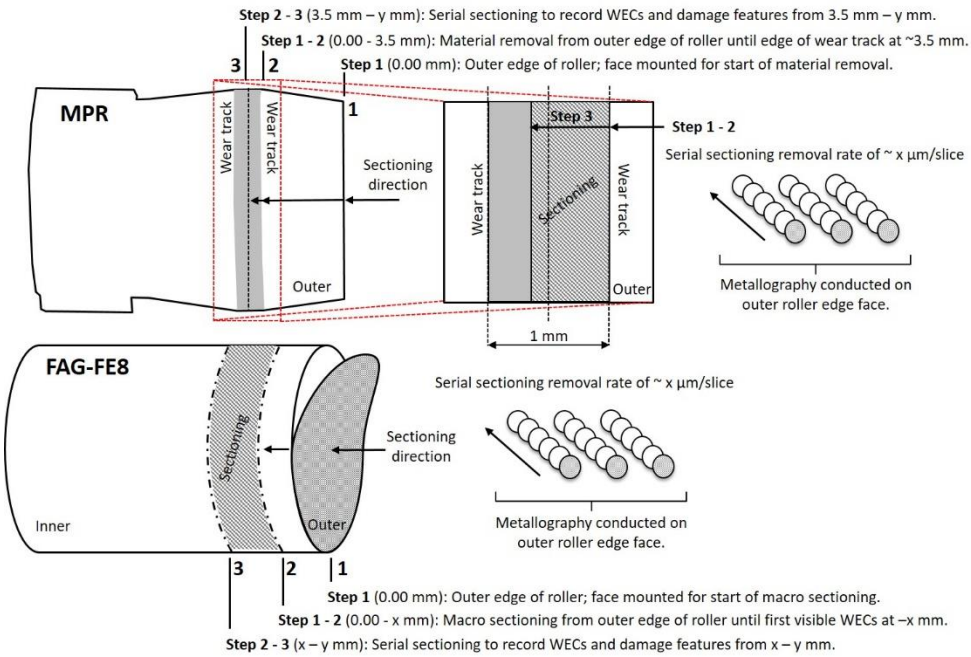

Figure 4-2: Details of the sectioning procedure for the FAG-FE8 and MPR tests.

4.3.4 Thermal desorption analysis (TDA)

To measure the hydrogen content in the tested samples, that may have diffused into and been trapped in the steel during RCF testing, TDA was performed for the samples from the FAG-FE8 tests using two different experimental set-ups under BS ISO 3690 standards [126] as detailed in [188] (Chapter 3).

4.3.5 Tribofilm analysis

The rollers and raceways from FAG-FE8 testing have been analysed using SEM/EDX to check the tribofilms formed on the contact surface during operation. The MPR samples were not analysed in this study. Tribofilms formed by ZDDP only (0%), OBCaSul (1.4% - 5.6%) and Oil X have been examined, where for Oil X the tribofilms formed at 2, 6 and 18 hr RCF test durations have been examined (Oil X RCF testing is from [153] (Chapter 2)). Prior to the analysis, samples are rinsed in heptane, isopropyl alcohol and blow-dried. 5 kV accelerating voltage is used for the analysis. The estimated tribofilm thickness is calculated based upon an empirical power fit of 100+ MTM-slim analyses spanning ashless and ZDDP AW tribofilms. The fit is developed between a normalisation factor for the 100+ tests and the tribofilm thickness when measured by the MTM-SLIM. For the FAG-FE8 analysed tribofilms, no corresponding MTM-SLIM data was available; therefore, the normalisation factor is used to get an estimate.

4.4 Results

4.4.1 Contact surface inspection

FAG-FE8: Wear across the rollers is observed on both sides of the central pure rolling region corresponding to outer and inner zones (Figure 4-3). No visible signs of spalling were seen on any of the rollers except that from Oil X test. Mild wear is observed on the ZDDP only (OBCaSul 0%) and OBCaSul 1.4% tests with a slight increase seen for OBCaSul 2.8% and 5.6%. Oil X [153] (Chapter 2) in comparison showed visible signs of damage on the surface in the form of dents/impressions, no signs of spalling were found on the rollers sectioned, however spalling was observed on other rollers from the same bearing.

MPR: Only Oil X showed spalling damage (Figure 4-3 (j)). Wear and micro-pitting are observed on all rollers from the OBCaSul oil tests.

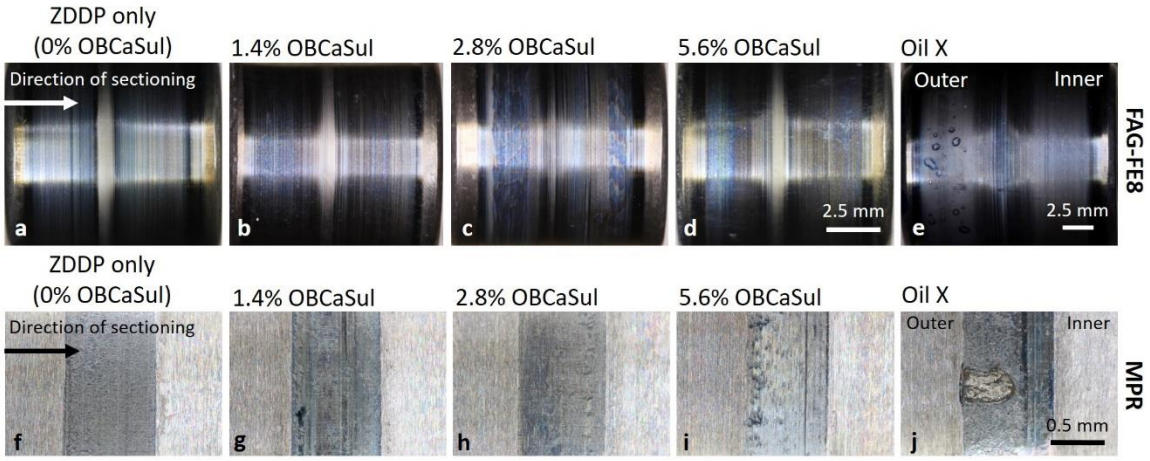

Figure 4-3: Optical macroscope images of rollers from each test for the FE8-FAG and MPR test rigs. Images (a) – (e) show one of the 60˚ interval zones around the circumference of the roller for the FE8-FAG tests, for Oil X see [153] (Chapter 2). Images (f) – (j) show one of the 120˚ interval zones around the circumference of the roller for the MPR tests.

4.4.2 Metallographic analysis

An overview of the FAG-FE8 and MPR tests results, including numbers of WECs, NMIs interacted with WECs and whether the WECs have surface connections, is summarised in Table 4-4. Inclusions were evaluated using a ranking system described in A.2.

Table 4-4: Summary of serial sectioning results.

Test oil	WECs recorded		Surface connections		Inclusion interactions	
	FAG-FE8	MPR	FAG-FE8	MPR	FAG-FE8	MPR
ZDDP only (OBCaSul 0%)	Total: 0	Total: 49 Total SF: 21	Total: 0	Total: 1	Total: 0	Total: 12, Total: 11*
OBCaSul 1.4%	Total: 0	Total: 27 Total SF: 9	Total: 0	Total: 2	Total: 0	Total: 7, Total: 6*
OBCaSul 2.8%	Total: 17 Total SF: 15	Total: 0	Total: 5	Total: 0	Total: 2, Total: 2*	Total: 0
OBCaSul 5.6%	Total: 12 Total SF: 8	Total: 0	Total: 0	Total: 0	Total: 10, Total: 10*	Total: 0
Oil X [153] (Chapter 2)	Total : 119 Total SF: 63	Total: 27 Total SF: 18	Total : 16	Total: 2	Total : 50, Total: 30*	Total: 7, Total: 7*

Key: *Total number of inclusion-WEC interactions ranked high likelihood (1 or 2) of initiation (see A.2 for details on ranking system). Note 1: data for Oil X FAG-FE8 is from [153] (Chapter 2), this data is from an 18 hr test for comparison. Note 2: for the FAG-FE8 tests, the 'Total' number of WECs recorded is the total across all 3x analysed rollers, for the MPR this is across the 1x analysed roller. **Total SF** denotes the total number of WECs recorded that started and finished within the sectioning range i.e. recorded in the entirety.

Examples of NMIs found to have interactions with WECs are shown in Figure 4-4, where the corresponding information of the inclusion type, size, location and test oil type is provided. As it can be seen, from the MPR testing, inclusions observed in the OBCaSul 0%, 1.4% and Oil X are small (average size at ~3 – 11 µm, ~2 - 8 µm and ~3 – 13 µm respectively) and are either globular sulfide-oxides (D_{Dup}), globular oxide (D) of manganese sulphide or manganese duplex (A). For the FAG-FE8 tests, the inclusions have been previously observed in the rollers as either globular sulfide-oxides (D_{Dup}) and globular oxide (D) based upon extensive collection of inclusion results [153]. Due to the size of the serial sectioning rates (15 - 38 µm) conducted on the rollers from the ZDDP only (OBCaSul 0%) and OBCaSul (1.4% - 5.6%) oils tests in this study, it was not possible to gather clear data on the length of inclusions. However since same type of bearings are used, it is assumed similar type and size of inclusions present in the rollers from the ZDDP only (OBCaSul 0%) and OBCaSul (1.4% - 5.6%) oil tests.

The spatial distributions and depth of inclusion-WEC interactions for the FAG-FE8 and MPR tests are shown in Figure 4-5.

During the serial sectioning processes, where possible, the dimension and location of individual WECs was observed and have been recorded, the results from the FAG-FE8 and MPR tests are summarised in Figure 4-6 to Figure 4-8.

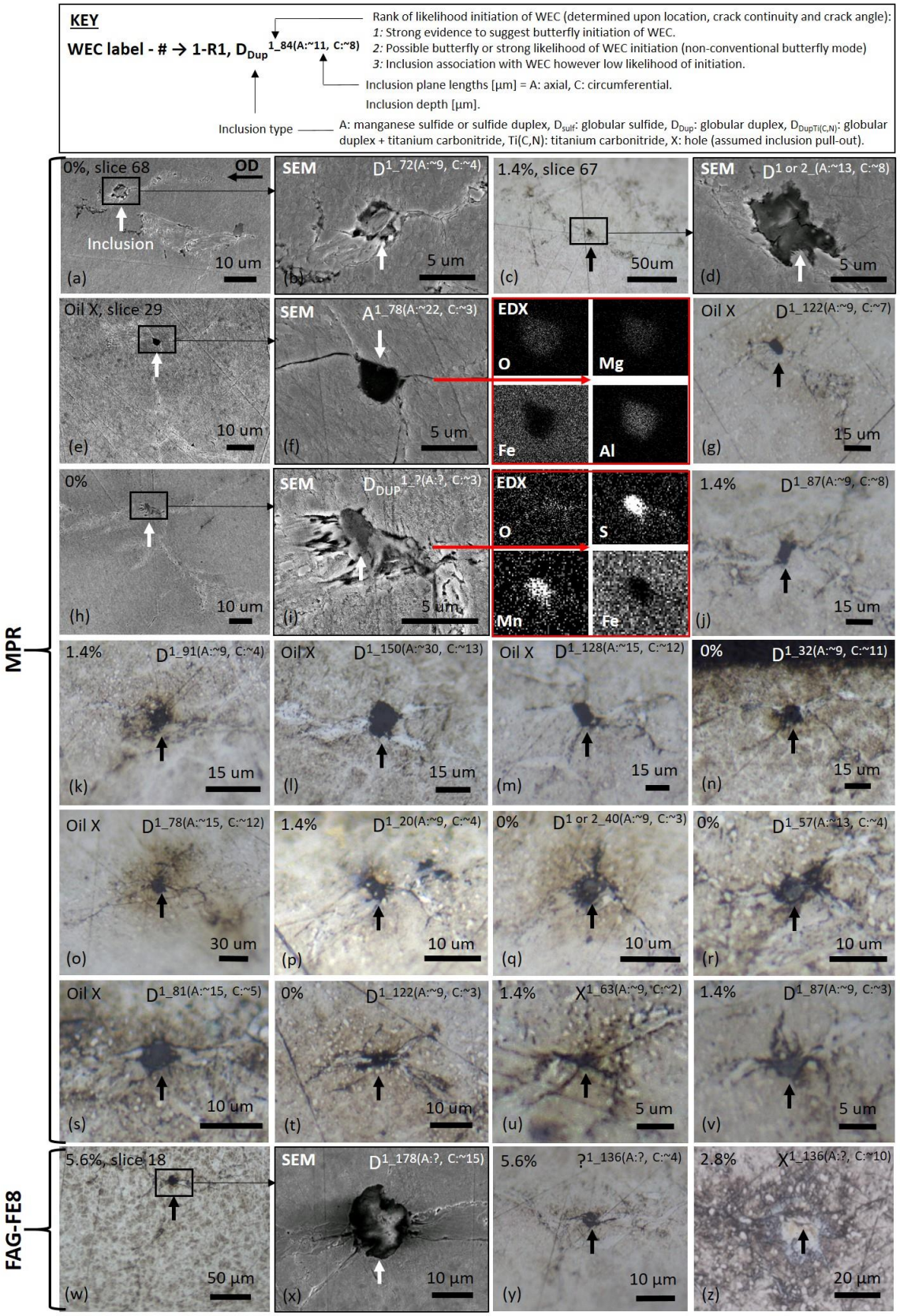

Figure 4-4: Images of typical inclusion-WEC interactions recorded in the MPR and FAG-FE8 analysed rollers. The white and black arrows indicate the inclusion in each case. A key above the images details how to interpret the inclusion-WEC interaction information in each case. See A.2 for more details on the ranking system.

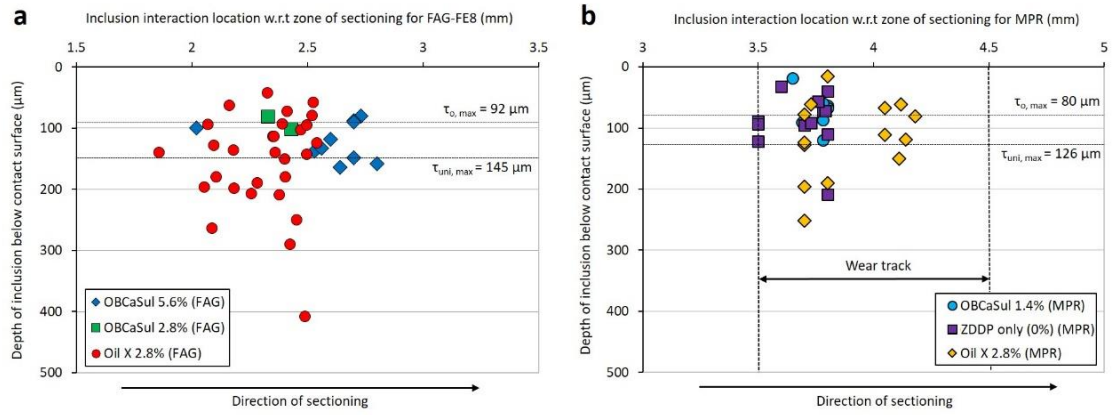

Figure 4-5: Spatial distribution of inclusion-WEC interactions. (a) FAG-FE8 with respective zone of maximum subsurface shear stress, Oil X data from [153] (Chapter 2). (b) MPR with respective zones of maximum subsurface shear stress.

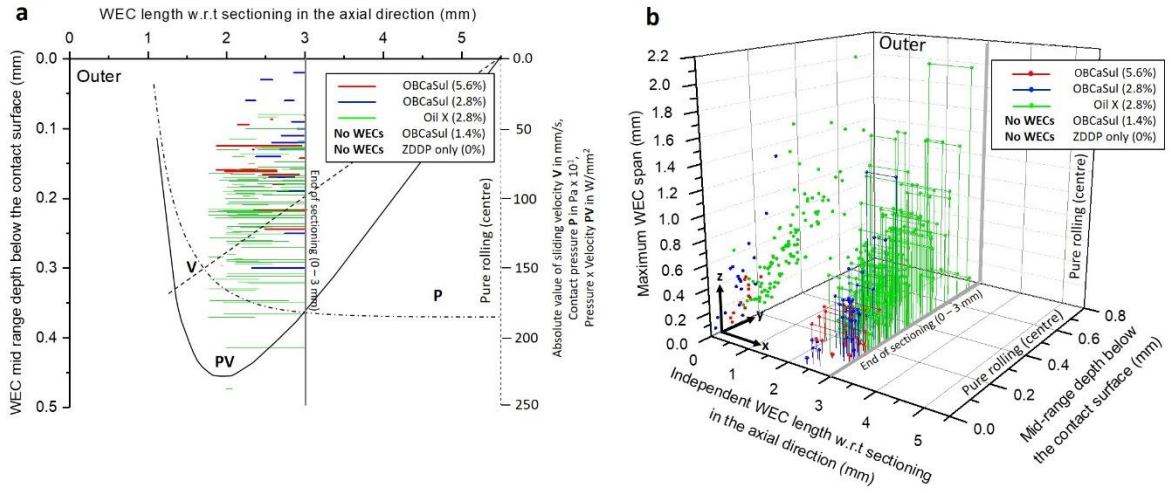

Figure 4-6: (a) Distribution of individual WECs recorded in the FAG-FE8 tested rollers across the area of sectioning with respective corresponding crack mid-range depth below the contact surface (0.00 mm) (y-axis). Pressure P, absolute sliding velocity V and slip energy PV are also superimposed onto the plot (adapted from). (b) 3D plot of recorded WECs in the FAG-FE8 tested rollers. X-axis represents the axial length of the roller (0 – 5.5 mm). Y-axis represents the mid-range depth below the contact surface (0.00 mm). Z-axis represents the maximum span of individual WECs (see Figure 4-8 for details). The dots on the YZ-projection represent the position of each independent WEC in the Y-axis and Z-axis. Note: no WECs were recorded in the OBCaSul 1.4% and ZDDP only (OBCaSul 0%) oils. Oil X data is taken from [153] (Chapter 2) and presented here for comparison reasons.

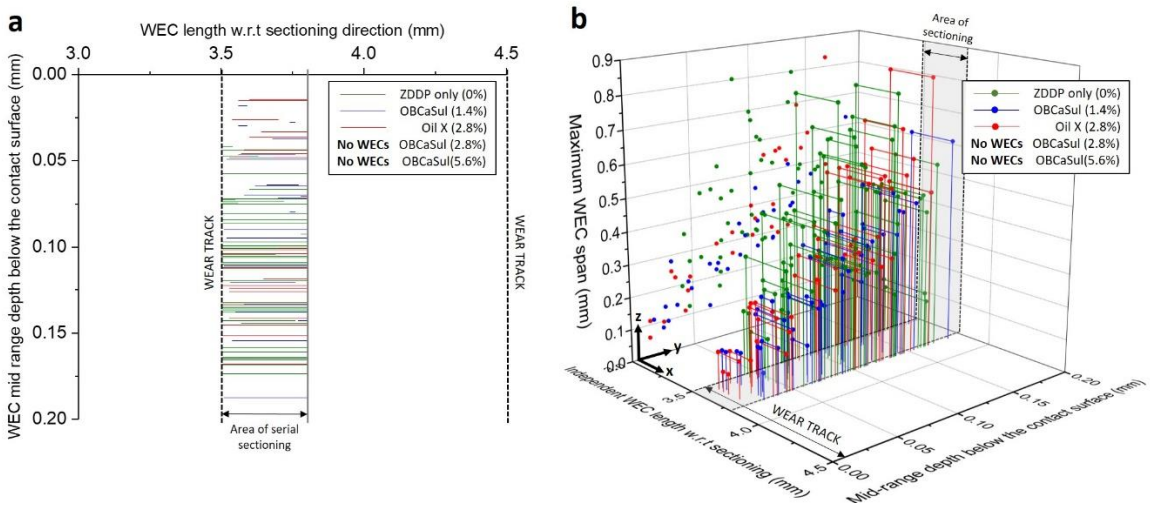

Figure 4-7: (a) Distribution of individual WECs recorded in the MPR tested rollers across the area of sectioning with respective corresponding crack mid-range depth below the contact surface (0.00 mm) (y-axis). (b) 3D plot of individual WECs recorded in the MPR tested rollers. X-axis represents length along the roller in the axial direction. Y-axis represents the mid-range depth below the contact surface (0.00 mm). Z-axis represents the maximum span (see Figure 4-8 for details). The dots on the YZ-projection represent the position of each independent WEC in the Y-axis and Z-axis. Note: no WECs were recorded in the OBCaSul 2.8% and 5.6% oils.

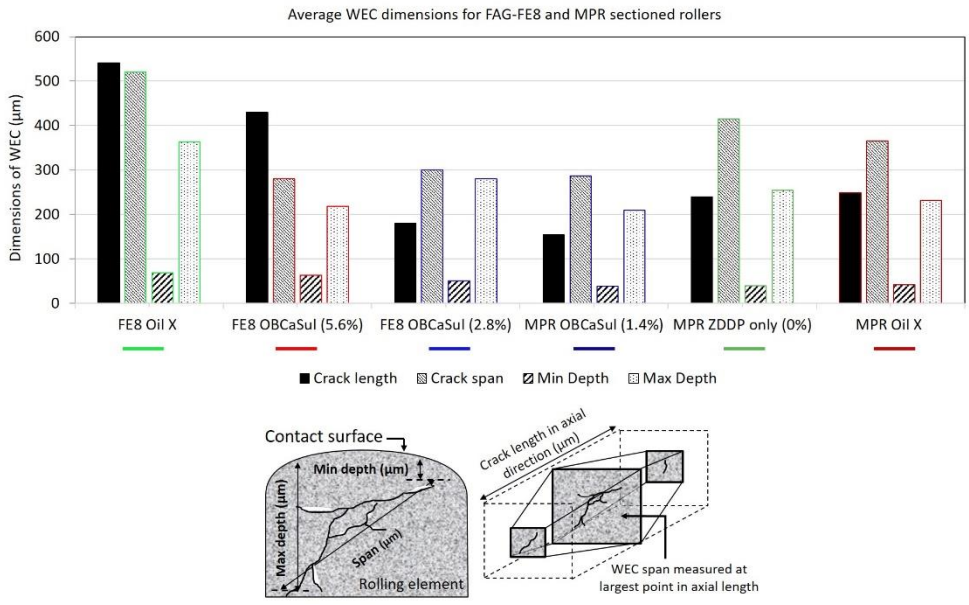

Figure 4-8: Average dimensions for the FAG-FE8 and MPR recorded WECs. Note no WECs were recorded in rollers from the FE8 OBCaSul (1.4%), FE8 ZDDP only (0%), MPR OBCaSul (2.8%), and MPR OBCaSul (5.6%) tests. FAG-FE8 Oil X data is from [153] (Chapter 2).

4.4.3 Thermal desorption analysis

Both rollers and the raceways from the FAG-FE8 tests have been analysed to measure their content of diffusible hydrogen and the TDA results are summarised below and in Figure 4-9 and Figure 4-10 (TDA results for Oil X are from [188] (Chapter 3). TDA results from set-up 1 (Figure 4-9) have shown that,

- Elevated concentrations of diffusible hydrogen were measured in the rollers.
- An increase in diffusible hydrogen is measured for increase in OBCaSul (1.4% - 5.6%).
- ZDDP only oil (OBCaSul 0%) showed average hydrogen concentration of 0.37 ppm.
- For both TDA setups, diffusible hydrogen contents in raceway sections are found to be negligible across all oils (close to the detection limit of the instrument) and are similar to that of the untested (0 hour) control rollers.
- Higher water content (ppm) coupled with higher concentrations of diffusible hydrogen measured.

TDA set-up 2 (Figure 4-10) has shown that,

- Elevated concentrations of diffusible hydrogen measured for ZDDP only oil (OBCaSul 0%) and OBCaSul 5.6% w.r.t untested (0-hour) control rollers.
- For Oil X rollers and raceways, hydrogen desorbs out from the start of the analysis, this being later (250-300 mins) for the OBCaSul 0% and 5.6% oils at a temperature range of ~125 – 150 ˚C.
- A single desorption peak is seen at ~250 – 300 ˚C for the ZDDP only oil (OBCaSul 0%) and OBCaSul 5.6% oil roller and raceways, this being much shallower for the raceways.

Table 4-5: Concentration of diffusible hydrogen (ppm) measured by TDA using set-up 1 and 2.

Bearing section	0 hr (ctrl)		ZDDP only (OBCaSul 0%)		1.4% OBCaSul		2.8% OBCaSul		5.6% OBCaSul		*Oil X @ 18 hrs [188] (Chapter 3)	
Set-up 1 (TDA @ 400 °C), Set-up 2 (TDA to 300 °C @ 25 °C/hr) concentrations in ppm												
Rolling element	**SU 1**	**SU 2**	**SU 1**	**SU 2**	**SU 1**	**SU 2**	**SU 1**	**SU 2**	**SU 1**	**SU 2**	**SU 1**	**SU 2**
1x Roller		0.40	0.39, 0.31, 0.40	0.36, 0.58	0.25, 0.24, 0.37	-	0.35, 0.43, 0.45	-	0.60, 0.40, 0.45, 0.50	0.46, 0.63		0.78
#Multiple roller combinations	0.12										#Avg: 0.50	
Raceway section												
1x Section	0.07	0.32	0.02	0.12	0.16	-	0.13	-	0.09	0.23		0.29
†Multiple raceway section combinations											†Avg: 0.09	

KEY

All samples with non-spalled contact surfaces unless otherwise stated. **SU 1 or SU 2** denotes setup 1 or setup 2.

* TDA results for Oil X at 2, 4, 6, 12 and 16.5 hrs are detailed in [188] (Chapter 3).

Average concentration from multiple Oil X 18 hr rollers (combinations of 1, 2, 3x rollers and 2x inner and outer roller halves).

† Average concentration from multiple Oil X 18 hr raceway sections (combinations of 1 and 2x sections).

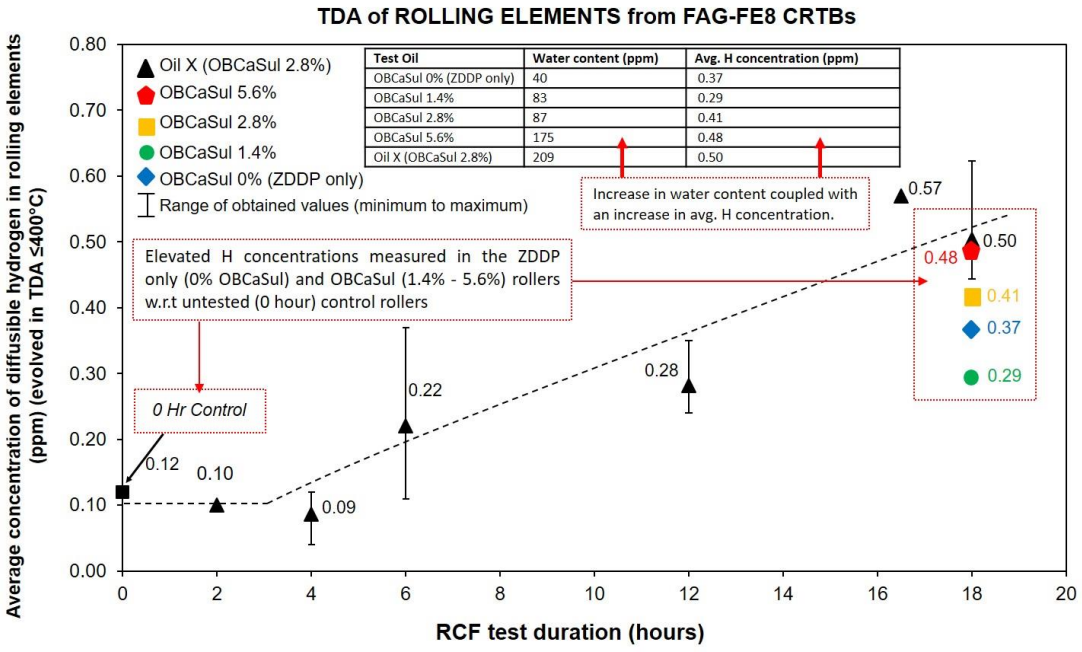

Figure 4-9: Thermal desorption analysis (set-up 1 TDA @ 400 °C) of rollers from FAG-FE8 ZDDP only (OBCaSul 0%) and OBCaSul (1.4% - 5.6%) tested oils and Oil X. Oil X TDA data is from [188] (Chapter 3). Diffusible hydrogen concentrations in ZDDP only (OBCaSul 0%) and OBCaSul (1.4% - 5.6%) oil tested rollers (all run to 18 hours), superimposed onto the measured concentrations for Oil X tested rollers on the FAG-FE8 rig.

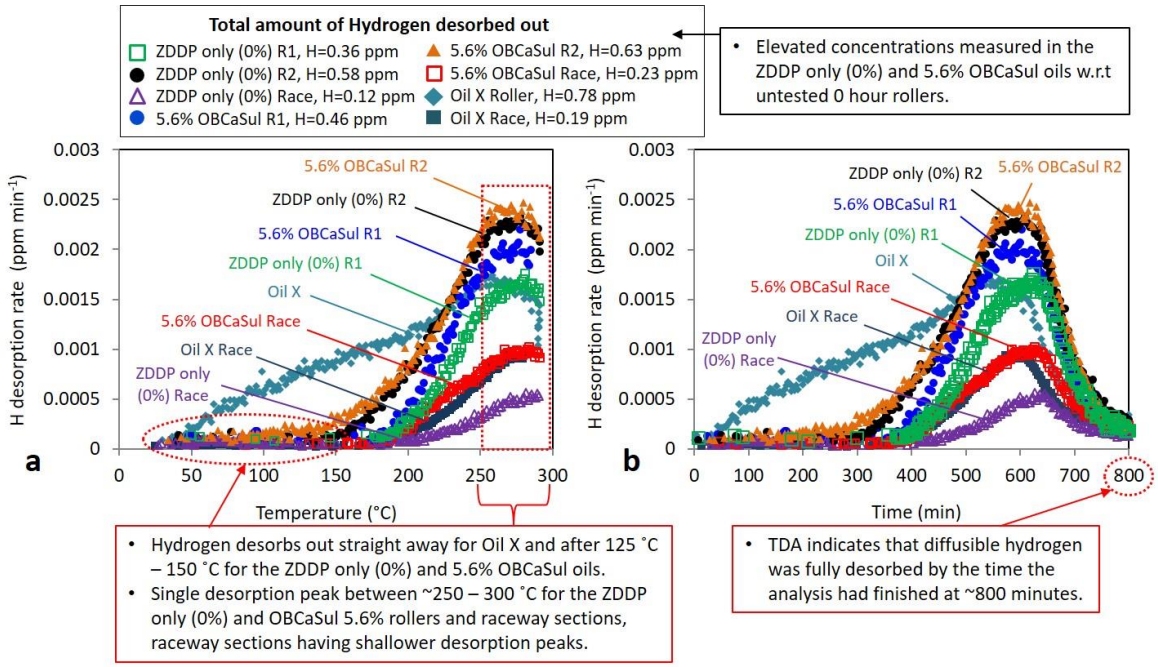

Figure 4-10: Hydrogen desorption curves for FAG-FE8 ZDDP only (0%), 5.6% OBCaSul and Oil X (18 hours only) RCF tested bearings using TDA set-up 2 (ramped TDA to 300 °C including the total diffusible hydrogen concentration measured. (a) Hydrogen desorption rate (ppm/minute) vs. desorption temperature (°C). (b) Hydrogen desorption rate (ppm/minute) vs. analysis time (minutes). See Table 4-5 for individual TDA measurements. Note: Data for Oil X is from [188] (Chapter 3).

4.4.4 Tribofilm analysis

Tribofilm analysis results using SEM/EDX on rollers and raceways from FAG-FE8 testing are summarised in Figure 4-11 to Figure 4-15 and Table B-1 to Table B-3 in Appendix B (raw elemental tribofilm results can be found in Appendix B). EDX results of the film formed across the axial contact length of rollers and width of the wear track on the raceways for Oil X (2, 6 and 18 hrs) are shown in Figure 4-11, and the corresponding results for the ZDDP only (0%) and OBCaSul (1.4% - 5.6%) oils are shown in Figure 4-12. Estimated tribofilm thicknesses are presented in Figure 4-13. Figure 4-14 and Figure 4-15 present EDX phase maps for Oil X (2, 6 and 18 hr) rollers and raceways.

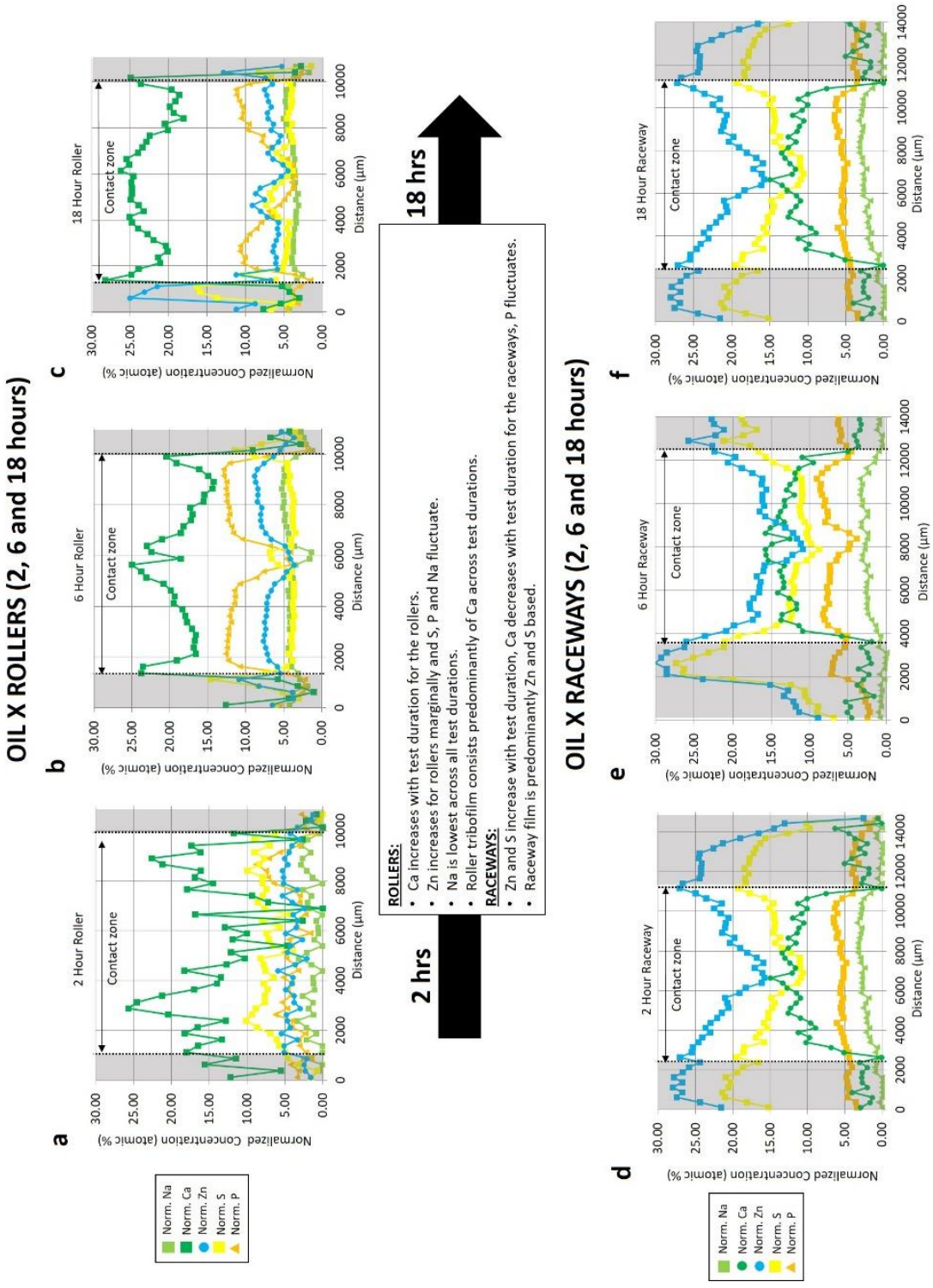

Figure 4-11: EDX analysis of the RCF tested Oil X normalised tribofilms in the approximate roller/raceway contact zone formed across 2, 6 and 18-hours. (a-c) rollers and (d-f) raceways.

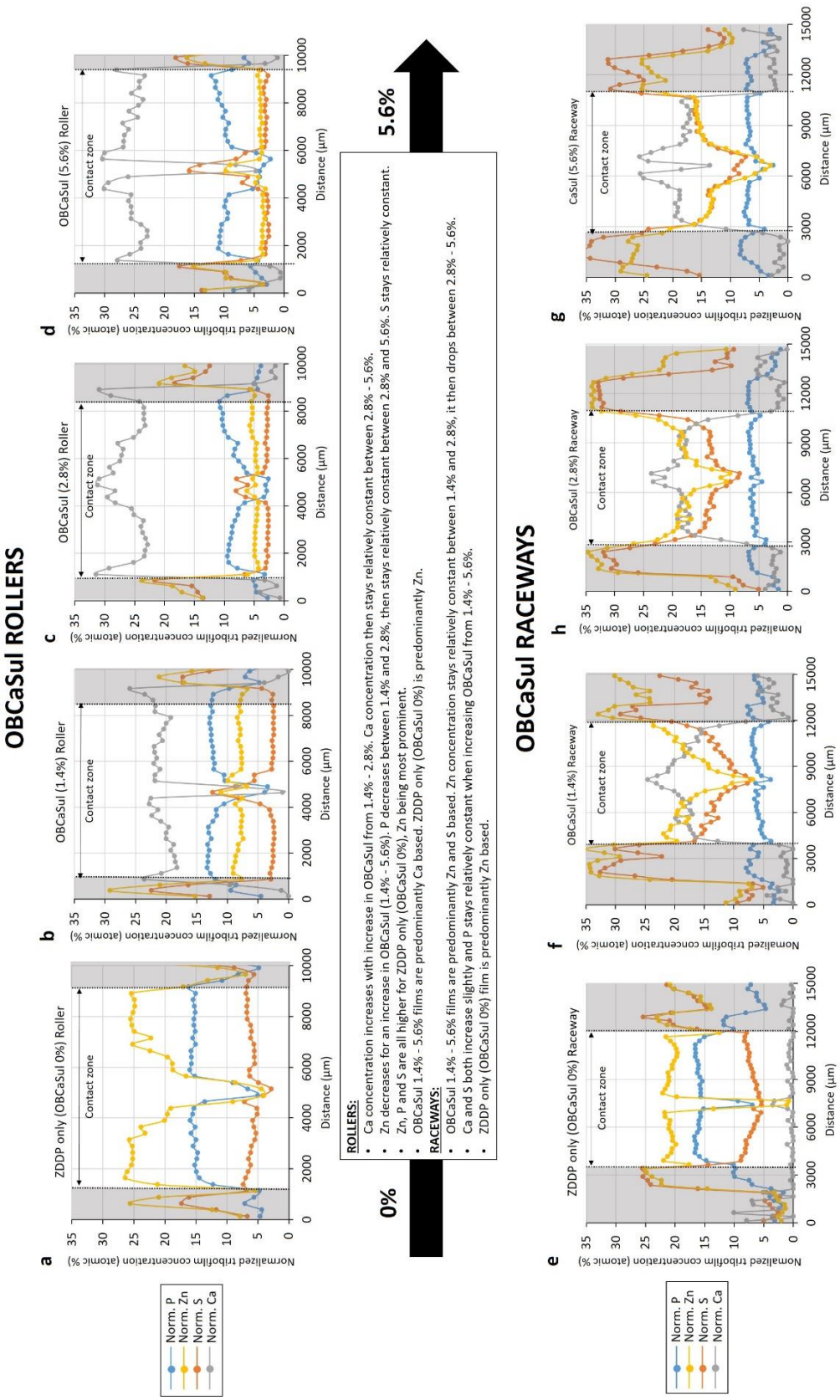

Figure 4-12: EDX analysis of normalised tribofilms formed in the approximate roller/raceway contact zone for RCF tested ZDDP only (OBCaSul 0%) and OBCaSul (1.4% - 5.6%) oils. (a) ZDDP only (OBCaSul 0%) roller. (b - d) OBCaSul 1.4% - 5.6% rollers. (e) ZDDP only (OBCaSul 0%) raceways. (f – g) OBCaSul 1.4% - 5.6% raceways.

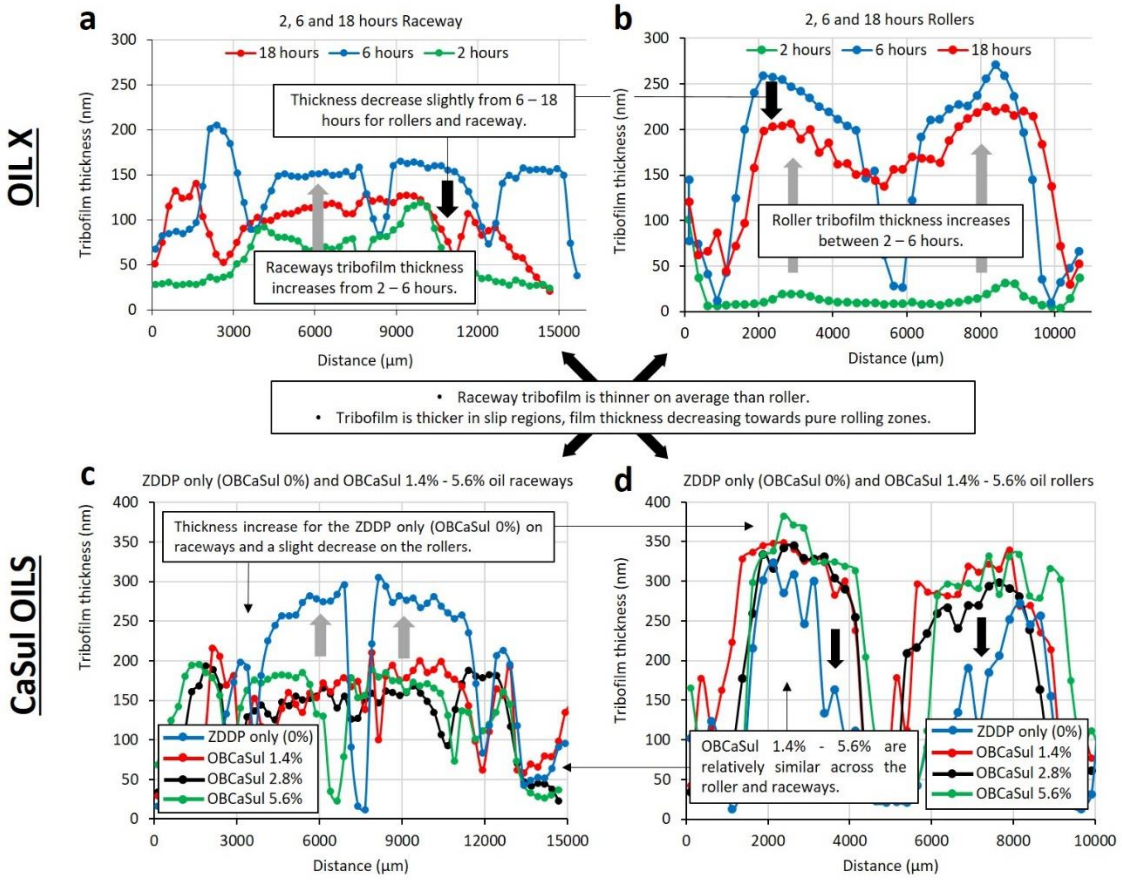

Figure 4-13: Estimated tribofilm thickness from SEM/EDX analysis. (a - b) Oil X 2, 6 and 18 hrs and (c - d) OBCaSul 0% - 5.6%.

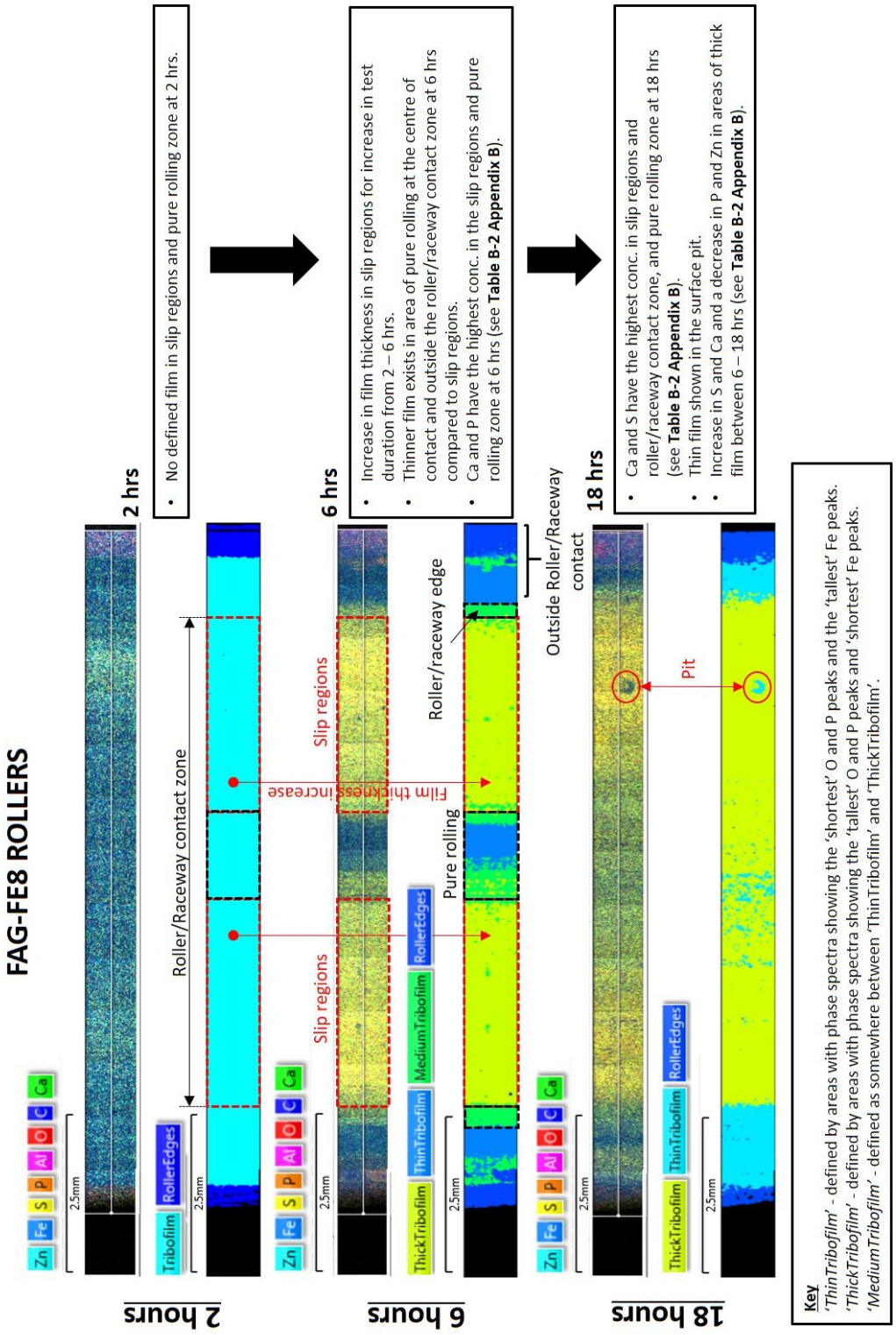

Figure 4-14: EDX phase maps for Oil X rollers across 2, 6 and 18 hours. Key explains difference between thickness terms.

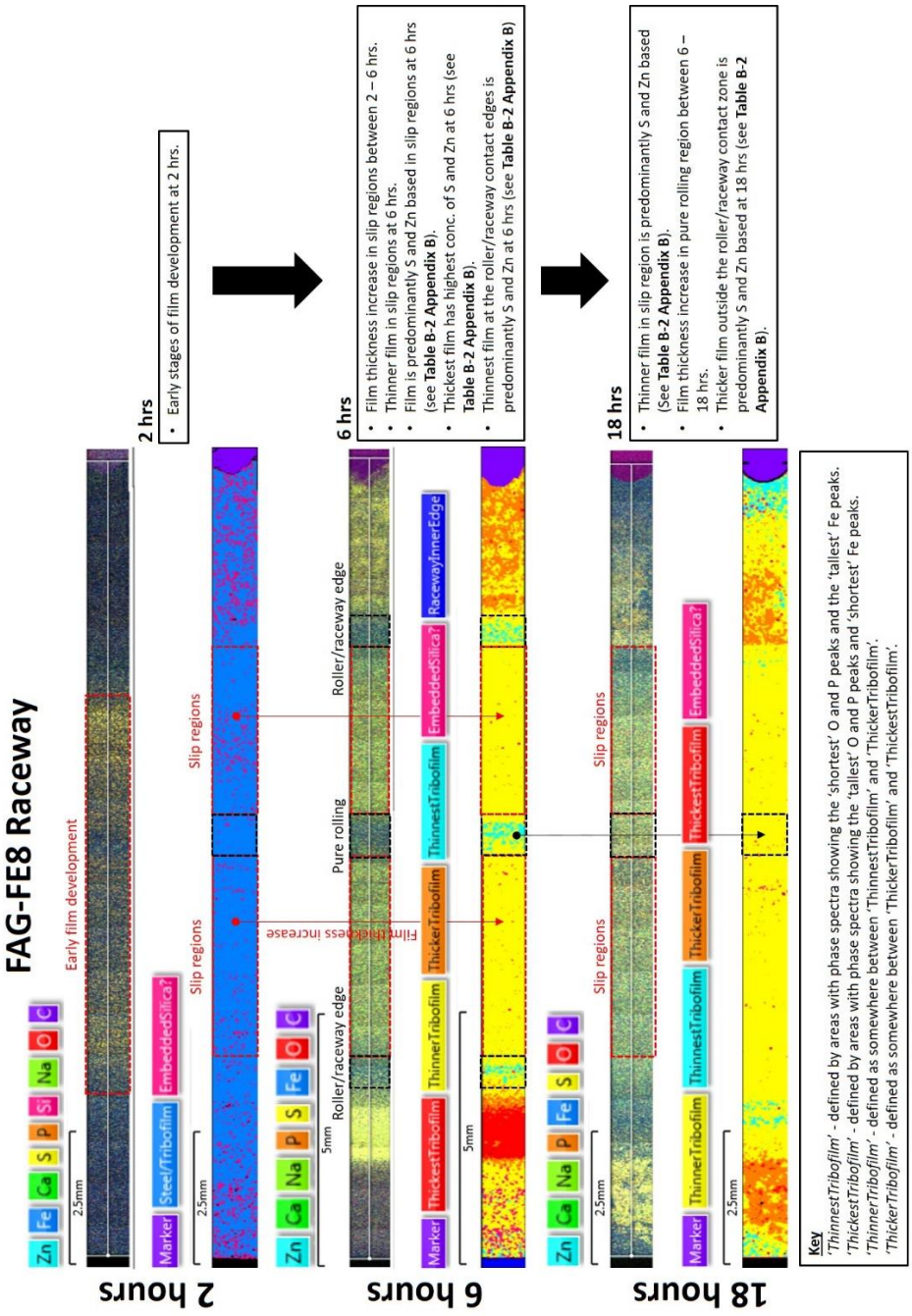

Figure 4-15: EDX phase maps for Oil X raceways across 2, 6 and 18 hours. Key explains difference between thickness terms.

4.5 Discussion

4.5.1 Oil chemistry influence on WEC formations

4.5.1.1 WEC formation propensity

A significant difference in propensity and size of WEC formations is found for Oil X compared to the ZDDP only (OBCaSul 0%) and OBCaSul (1.4% - 5.6%) oils (see Table 4-4 and Figure 4-6 to Figure

4-8), thus the different oil chemistry of Oil X promotes WEC formations more so than OBCaSul oils. ZDDP only oil (OBCaSul 0%) when tested on the FE8 showed no WECs (see Table 4-4 and Figure 4-6), conversely, when tested on the MPR rig, this is the most detrimental oil to WEC size and propensity (see Table 4-4 and Figure 4-7 and Figure 4-8).

For the FE8 rollers, an increase in OBCaSul wt% from 1.4% to 2.8% and 5.6% resulted in a jump from zero WECs recorded to a number of WECs being recorded (17 and 12 WECs recorded for the 2.8% and 5.6% oils respectively) (see Table 4-4 and Figure 4-6). Further testing with different wt% of OBCaSul between 1.4% and 2.8% should be conducted to examine if any trend in WEC propensity exists between these wt%. For an increase in OBCaSul wt% from 2.8% to 5.6%, although no great difference in number of WECs recorded, WECs were found to be on average longer for the 5.6% oil (see Figure 4-6 and Figure 4-8).

The opposite is seen in OBCaSul wt% versus number of WEC for the MPR tests, a decrease in OBCaSul from 2.8% to 1.4% resulted in a jump from no WECs recorded to a number of WECs being recorded (see Table 4-4 and Figure 4-7), the 5.6% oil also showing no WECs. Testing of OBCaSul wt% below 1.4% but more than 0 wt% should be conducted to see if there is any trend for decrease in WEC propensity. It is suggested that the opposite behaviour between the FAG-FE8 and MPR tests may be due to differences in the rigs respective contact dynamics influencing the behaviour of OBCaSul, where differences may include,

(i) Slip – On the FAG-FE8 at the centre of bearing contact exists a pure rolling region, with rising slip of up to ±12.5% SRR along the contact major axis, corresponding to slip regions on the roller/raceway. The MPR tests on the other hand run at -30% SRR, calculated ‘frictional energy accumulation’ [95] is thus far greater for the MPR (300%) compared to the FAG-FE8 (100%) [82]. It is noted, however, that lubricant factors are not accounted for in the energy accumulation model [82]. Frictional energy accumulation in areas of high slip [95] and resultant higher hydrogen adsorption are proposed to lead to higher concentrations below the surface resulting in WEC failures.

(ii) Contact conditions - smaller area of contact for the MPR in comparison to the FAG-FE8, where for the MPR case it is proposed through modelling that the smaller contact area allows for less hydrogen diffusion/penetration and a faster escape rate due to the surrounding ‘out of contact’ area [82].

(iii) Contact cycles and ‘regeneration time’ - (the time between subsequent contact cycles, rollers being slightly longer than the raceways in the FE8 case), where longer regeneration times lead to longer WEC lives [95]. This is considered to be due to lower frictional energy

accumulation and influence on surface film formation, which in turn may affect hydrogen diffusion.

It was also suspected that the differences in lubrication chemistry between the tested oils could affect the tribofilm formed during RCF operation (this is discussed in 4.5.2 of this paper), where contact dynamics/conditions could effect this, in turn potentially playing a role in hydrogen diffusion, and WEC formations.

WECs recorded in the FAG-FE8 rollers across all oils fall within the zones (around ~ 2 mm zone) of high slip energy (PVmax, see Figure 4-6). It has been identified previously by the authors on serial sectioning analysis of the Oil X rollers [153] (Chapter 2), that this zone is where the highest propensity for WEC initiations exists (as shown in Figure 4-6).

4.5.1.2 Subsurface or surface initiation of WECs

The vast majority of WECs recorded in the FAG-FE8 rollers across all oils were contained entirely within the subsurface and without connection to the contact surface, therefore surface initiation of these WECs is infeasible (Table 4-4). Any interaction/connections to the surface made were predominantly small/short in size relative to the size of the WEC network. Only five cases of interaction/connection to the contact surface were recorded for WECs across all oils tested on the MPR rig (Table 4-4), connections again being small/short in size. It must be noted that for any WECs that had not started and finished within the sectioning range, interactions/connections still may exist, and further sectioning would be needed to confirm this.

A number of inclusion-WEC interactions have been recorded in the OBCaSul oil rollers (see Table 4-4 and see Figure 4-4 for examples). Inclusions recorded are small/short in size (FE8: ~ 2 – 20 μm, and MPR: ~ 2 – 13 μm) and being predominantly globular sulfide-oxides (D_{Dup}), globular oxide (D) or manganese sulfide/sulfide duplex (A) (A type only recorded in MPR rollers) in type. For the FAG-FE8, inclusion-WEC interactions recorded in the OBCaSul oil rollers are within a similar size range and type to the inclusion-WEC interactions recorded in the Oil X rollers [153] (Chapter 2). It is considered that a number of inclusions may have been missed in the OBCaSul oils due to size of the sectioning removal rates (~ 15 – 38 μm) conducted relative to the small size of the inclusions. A far greater number of inclusion-WEC interactions have been recorded in the FAG-FE8 Oil X rollers in comparison to the OBCaSul (1.4% - 5.6%) oils (see Table 4-4), this is proposed to be due to (i) smaller removal rates (~ 3 – 5 μm); therefore, more chance to 'catch' WEC-inclusion interactions; (ii) higher number of WECs recorded in the Oil X rollers, thus more inclusion interactions; (iii) specific lubricant chemistry of Oil X allowing inclusion initiation to occur more

easily. More details and examples of inclusion-WEC interactions recorded for Oil X can be seen in [153] (Chapter 2).

Given the evidence, one mechanism for WEC initiation and propagation for the FAG-FE8 and MPR tested oils is in the subsurface, where differences in lubrication chemistries between the tested oils has not affected this. This further verifies the author's previous findings on FAG-FE8 testing using Oil X [38, 153] and other works by the authors [36, 37, 39] that WECs can initiate and propagate entirely within the subsurface. WECs have been created and recorded previously through MPR testing [61, 81] however, the authors of this manuscript point out that conclusive evidence on whether WECs initiated at the surface/subsurface or interacted with inclusions cannot be made, since 3D mapping of WECs in their entirety was not conducted. This study showing conclusively that subsurface initiation and propagation can be one mechanism in the MPR tests. In addition, evidence from this study further verifies the author's previous revelations that subsurface initiation is highly likely at small/short non-metallic inclusions [36-39, 153]. Again, differences in in lubrication chemistries between the tested oils has not affected this. For the FAG-FE8 case this is strongly supported, since inclusion-WEC interactions have been recorded at the infant stages of their evolution [153]; however, for the MPR case, this would require further sectioning analysis to catch inclusion-WEC at the early stages.

4.5.2 Influence of oil chemistry on hydrogen diffusion

Discussions are focused on FE8 testing only. Due to time considerations, TDA was not conducted on the MPR rollers.

TDA for set-up 1 has shown that oils containing OBCaSul with ZDDP, and ZDDP only oils have allowed the diffusion of hydrogen into the FE8 steel rollers during RCF operation and not the raceways (negligible concentrations measured similar to untested '0 hour control' samples) (Table 4-5 and Figure 4-9). Differences in oil chemistry between oils therefore having no effect on the diffusion of hydrogen into the raceway, this potentially being due to the tribofilm formed on the raceway (discussed in 4.5.2). For the OBCaSul (1.4% - 5.6%) oils, there is a positive correlation between increase in OBCaSul wt% and increase in diffusible hydrogen concentration. Again, this could be due to the tribofilms formed (see 4.5.2 for further discussion), where it is considered that differences between oil chemistries (and respective tribofilms formed) could affect the flux/rate of hydrogen diffusion into the steel during operation. TDA results from set-up 2 showed that hydrogen diffused into the ZDDP only (OBCaSul 0%) and OBCaSul 5.6% oils (Table 4-5 and Figure 4-10). TDA was not conducted on the OBCaSul 1.4% and 2.8% oils due to time considerations and so trends cannot be examined, further TDA on these oils should be conducted

so that a comparative assessment can be made. The reason why differences in measured hydrogen concentrations between roller and raceway may be due to,

(i) The differing dynamics experienced between roller and race, for example, number of contact cycles experienced and 'regeneration times' as mentioned above in 4.5.1.1. However, regeneration times are slightly longer for the rollers than the raceways, where longer times are said to lead to longer WEC lives, only the raceways failing during FAG-FE8 testing [95]. This was said to be due to the higher asperity energy accumulation experienced by the raceways. This is contradictory to results found by the authors of this manuscript, where only the rollers contained WECs [153] (Chapter 2).
(ii) It may be due to differences in steel cleanliness, the raceway being shown to be far 'cleaner' than the rollers [153] (Chapter 2), thus a lack of trapping sites for hydrogen being available.
(iii) Differences in respective tribofilms formed on the roller and raceway (see 4.5.4 for further discussion).

Finally, differences in the water content measured between the tested oils (see Table 4-1) may play a role in the amount of diffusible hydrogen measured. Results show a correlation between increase in water content (ppm) measured in the oils pre-RCF testing, and an increase in diffusible hydrogen concentration measured in the rollers (see Figure 4-9). The hygroscopic character of ZDDP, Na, Mg and Ca alkyl sulfonate additives may be a reflection on the increase in water content measured for the respective oils, where it is proposed that water dissociation and subsequent hydrogen generation due to high friction films formed by these additive components can occur [83]. Although water contents are low, small amounts of water as little as ~ 100 ppm have been shown to have a detrimental effect on fatigue life [216]. It has been said that water desorption spectra should be taken into account when measuring the total amount of diffusible hydrogen in steels, where thermal desorption and XPS analysis showed that the permeation of hydrogen is strongly influenced by the formation of oxide and/or hydroxide film when water is present [116]. It is noted, however, that when water is present hydrogen is mainly sourced from the oil opposed to water [117].

The trapping behaviour of hydrogen is discussed in Figure 4-16 below.

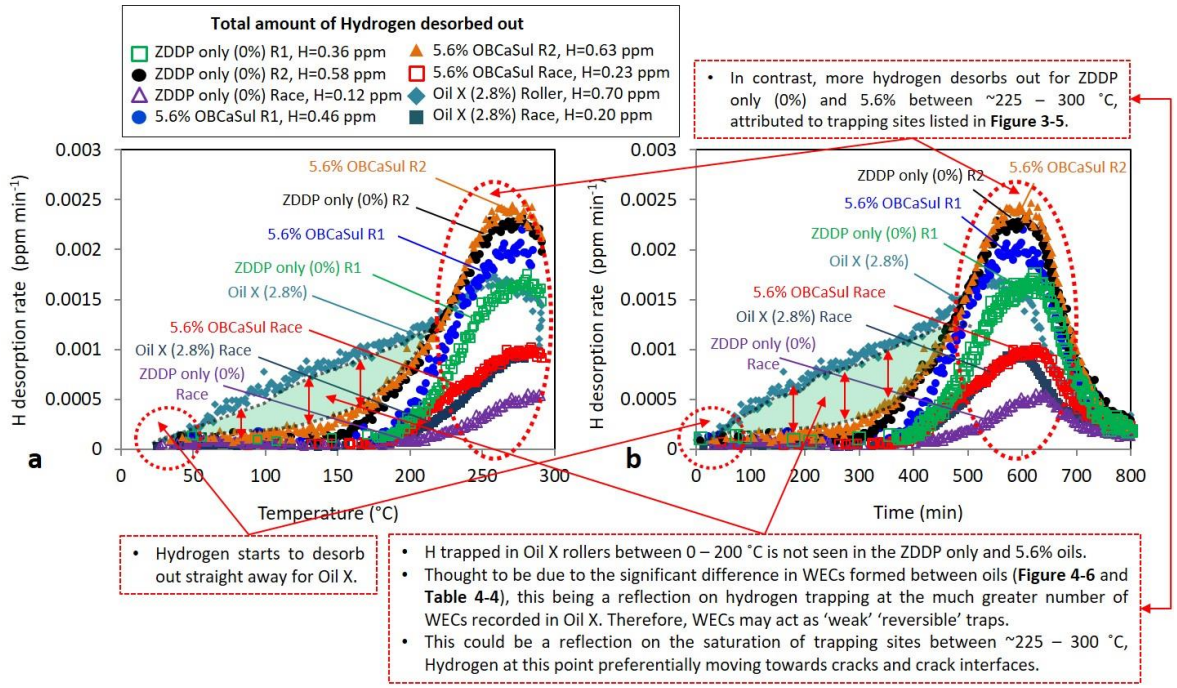

Figure 4-16: Trapping behaviour of hydrogen in FAG-FE8 tested rollers and raceways analysed through TDA set-up 2.

4.5.3 Hydrogen diffusion and its relation to WEC formations

Discussions are again focused on FE8 testing only.

While the diffusible hydrogen concentrations are comparable in the tests lubricated by the Oil X and OBCaSul oils, the number of WECs recorded in the rollers are significantly different, i.e. the concentration of diffusible hydrogen found in rollers lubricated by different oils may not have had the same effect on WEC formation. Comparing for example TDA results for Oil X at 12 hours and OBCaSul 1.4% at 18 hours (Figure 4-9). Although the average hydrogen concentrations are similar, no WECs were recorded in 1.4% OBCaSul rollers while a number of WECs were found to have formed in the Oil X 12 hour rollers (see [153] (Chapter 2) for Oil X 12 hour WEC details). Again, if we compare diffusible hydrogen concentrations between Oil X and OBCaSul 5.6% (at 18 hours), although their average hydrogen concentrations are similar, there is a vast difference in the number of WECs recorded (Table 4-4 and Figure 4-6). This supports the suggestion made in a previous study by the authors, that hydrogen may not be an initiator but an accelerator to WEC formation, and/or becomes instrumental in formation when in combination with other factors e.g. tribofilm formed. It is noted that, at this stage, it is not clear what the influence of local diffusible hydrogen, i.e. at crack tips or inclusions, may have due to the limitation of the TDA, which only measures diffusible hydrogen in the bulk of the specimens. It is also considered that differences in oil chemistries may affect the flux/rate of hydrogen diffusion and penetration, this

being directly related to the respective tribofilms formed (further discussion in 4.5.2). It could be that,

(i) Hydrogen diffused later towards the end of RCF operation, not allowing a sufficient amount of time for hydrogen to take effect. Further TDA to measure diffusible hydrogen at varying stages of RCF operation for the OBCaSul oils (test run to only 18 hrs for these oils) would be able to provide more detail on this.
(ii) Hydrogen penetration may be outside the zones of maximum subsurface shear stresses, or where critical inclusions are located in the depth of the steel.
(iii) Insufficient hydrogen diffusion in critical zones where greater propensity for WEC formations exists, the diffusion of hydrogen in these zones being governed by the presence of metal-containing additives in the film such as calcium sulfonates under high frictional energy accumulation [82].

A difference in hydrogen trapping behaviour is seen between Oil X, and the ZDDP only (OBCaSul 0%) and OBCaSul 5.6% oils (Figure 4-16). This may be a result of the greater number of WECs formed in the Oil X lubricated rollers in comparison, where it is suggested that crack interfaces have acted as 'weak' 'reversible' hydrogen traps.

Based on the TDA and serial sectioning analysis on the rollers tested on FAG-FE8, a positive correlation is shown between the OBCaSul concentration and the amount of diffusible hydrogen. In addition, a jump in diffusible hydrogen concentration is seen for a jump in WEC formations between OBCaSul 1.4% and 2.8%, further TDA and serial sectioning for OBCaSul wt% between 1.4% and 2.8% is recommended to explore this. An increase in hydrogen concentration is seen between OBCaSul 2.8% and 5.6%, however, no great difference in number of WECs was seen, although the length of WECs formations increased. TDA was not conducted on the MPR rollers due to time constraints and so it is not possible to derive this relationship for the MPR tests, further testing is thus required to make a comparative assessment. The vast majority of WECs recorded for the OBCaSul FE8 tested oils were contained entirely within the subsurface. This supports previous findings by the authors on FE8 Oil X testing [188] that the suggested mechanism of hydrogen entry into the steel during operation is at wear induced nascent surfaces or areas of heterogeneous tribofilm, hydrogen being generated by decomposition of lubricant through catalytic reactions and/or tribo-chemical reactions of water [115, 116].

4.5.4 Influence of oil chemistry on tribofilm formation

4.5.4.1 Tribofilm composition

Discussions below focus on SEM/EDX analysis of the tribofilm from FE8 tests only.

SEM/EDX has shown that the OBCaSul (1.4% - 5.6%) oils have formed thicker Ca dominated films across contact wear zones on the rollers in comparison to 'normal' Zn-S films that are shown to form for the ZDDP only (OBCaSul 0%) rollers and raceways, and the Oil X and OBCaSul (1.4% - 5.6%) raceways. For Oil X, an increase in RCF test duration has also resulted in thicker Ca films forming across wear zones on the rollers. ZDDP + OBCaSul combinations have shown that surfaces covering worn areas showed mainly Ca and O in the film [164], the Oil X and OBCaSul (1.4% - 5.6%) lubricated rollers in this study exhibiting this behaviour. AES has shown that by using neutral calcium sulfonate with ZDDP, films contained Ca but were otherwise similar to ZDDP, the OBCaSul showing Ca and O with no traces of ZDDP in the film and having a greater effect on the AW properties [164]. The dominance of Ca over Zn shown on the rollers, is suggested to be a reflection of OBCaSul additive being a 'strong' competitor to ZDDP in the oil. It is proposed that a replacement of Zn in the anti-wear tribofilm has resulted in thicker Ca films forming on the rollers. Ca replacement of Zn has been shown using multiple techniques on the analysis of automotive AW tribofilms on cam/tappet friction test specimens [180] and other engine parts [166].

As shown in Figure 4-11, for Oil X at 2 hours, the elements in the film are sporadically dispersed across the roller, while a well formed ZDDP tribofilm is shown to have developed on the raceway (indicated by the higher concentrations of Zn, S and P in the wear zones). In addition, the film thickness on the raceway is found to be thicker than that on the rollers at 2 hours (see Figure 4-12). Over time, while the film on the raceway does not change significantly, those on the rollers have developed and grow thicker, tribofilms on the raceway being on average thinner than the rollers. It is not clear why tribofilms form quicker on the raceway but it may be an explanation for why no WECs were found to have formed in them. It is suspected that the differing contact dynamics between roller and raceway may affect film formation. For example, the rollers experience slightly longer 'regeneration times' (the time between subsequent contact load cycles) than the raceways, where longer regeneration times are said to improve resistance to WEC formation [95]. This is, however, contradictory to the results found in studies by the authors on FE8 tests using Oil X, where rollers contained multiple WECs, the raceway sections not showing any [153] (Chapter 2). It is considered that longer regeneration times could influence film formation [95], which may be a reason as to why differences in tribofilm have been found in this study. It is also considered that the pre-roughening of the raceway before testing will affect the formation of the tribofilm, including the formation at the early stages of operation, greater

surface roughness increasing the amount of local 'hot spots' at asperity contact. This may also be a reason for the lack of diffusible hydrogen measured and WECs in the raceways in comparison to the rollers.

4.5.4.2 Tribofilm formation influence on H-diffusion and WEC formations

TDA showed a positive correlation between OBCaSul wt% and diffusible hydrogen concentration for the FE8 rollers (see Table 4-5 and Figure 4-9), where OBCaSul in oils containing ZDDP have formed thick Ca films. Therefore, it is suggested that the thick Ca films formed on the FE8 rollers have promoted hydrogen diffusion into the bearing steel. For Oil X an increase in RCF test duration also resulted in thicker Ca films forming, this being correlated with an increase in diffusible hydrogen concentration and WEC formations in the FE8 rollers. Based on TDA and serial sectioning analysis of the FE8 raceways, negligible hydrogen concentrations were detected and no evidence of WECs found, therefore, it is considered that the thinner Zn-S containing films formed on the raceways has demoted hydrogen diffusion and WEC formations.

Literature reports that an oil containing OBCaSul resulted in WEC detection (using ultrasound) in FE8 raceways, XPS/SNMS analysis showing increased film thickness (reaching 100 nm) over test duration and comprising of Ca-P on the raceway slip zones [92]. In contrast, removing OBCaSul resulted in no WEC detection, the developed film being thinner (20 nm) and comprising of Zn-S in the same regions. It must be noted that these tests used ceramic rollers to 'push' WEC failure to the raceways. ZDDPs are shown to reduce hydrogen permeation into steel, where it is suggested that these additives can form protective film preventing hydrogen permeation [186]. Studies in literature also propose that OBCaSul inhibit film formation and create 'weakened' heterogeneous ZDDP films [68, 157-162], OBCaSul being suggested to promote and prolong nascent metal exposure [163].

In literature, STEM analysis shows heterogeneous tribofilms containing Ca, S, Zn, P, Na and O with varying thickness (5 - 100 nm) to form on FE8 raceways that also showed WECs [62]. These elements were also observed on the roller films, where the study notes that the morphology and composition are different to the raceways, however, limited results are presented. It is worth mentioning that the rollers were not examined for damages since the majority of damage was found on the raceway surfaces, this contradicts what the authors of this study have seen on FE8 bearings using Oil X, where damage is only seen on the rollers [38, 153].

Finally, it has been shown that for higher water contents (ppm) measured in the tested oils pre-RCF testing, higher diffusible hydrogen concentrations were measured (see Figure 4-9). Water dissolved in the oil is said to influence the functionality of ZDDP AW additives and enhance wear

[217-220]. A feature of ZDDP, and Ca alkyl sulfonate is that they are hygroscopic, where these additives may carry water molecules to rubbing contact surfaces [83]. MTM-Slim studies have shown oils containing ZDDP, Na, Mg and Ca alkyl sulfonates form thick patchy tribofilm, which are proposed to cause high friction in an initial incubation period (~20 hrs for FE8) resulting in water dissociation at fresh nascent surfaces and subsequent generation of hydrogen that diffuses into the steel promoting WEC formations [83].

Mechanisms for why Ca tribofilms are thicker than the Zn tribofilms and why these films promote/demote hydrogen diffusion is still unclear based on the SEM/EDX analysis. Further tribofilm analysis using XPS and STEM has been conducted by the authors (to be published in a later study) and may be able to provide more information on the properties of the tribofilms and reveal mechanisms further. In addition, testing and analysis of oils containing OBCaSul *alone* is recommended to help deconvolute the competition between ZDDP and OBCaSul.

4.6 Conclusions

RCF testing has been conducted under non-hydrogen charged conditions on FAG-FE8 and MPR rigs using 100Cr6 steel samples lubricated with oils containing varying wt% of OBCaSul detergent additive. The effects that oils containing OBCaSul have on tribofilm formation, diffusion of hydrogen into the steel, and the formation of WECs has been investigated. The findings of this study are:

- Serial sectioning has shown that WECs can initiate and propagate entirely within the subsurface and are frequently found to interact with small/short non-metallic inclusions. This has confirmed and added further verification to the author's previous findings.
- The number of WECs formed in the FE8 rollers appears to be increasing with the increase of OBCaSul wt% from 1.4% at 0 WEC, to 2.8% and 5.6% at 17 and 12 WECs respectively, suggesting that OBCaSul has promoted WEC formation. However, in the MPR tested rollers, only the OBCaSul 1.4% lubricated roller showed WECs, higher OBCaSul wt% (2.8% and 5.6%) not creating any potentially due to their differences in contact dynamics.
- Similar to the results obtained by FAG-FE8 testing using the fully formulated 'bad' oil, TDA has also shown hydrogen to have diffused into the FE8 rollers and not the raceways during RCF operation for the OBCaSul containing and ZDDP only oils. TDA has shown a positive correlation between OBCaSul wt% and concentration of diffusible hydrogen. Further TDA should be conducted on the MPR rollers to confirm this relationship.
- Detailed tribofilm analysis has shown that oils containing OBCaSul additive form thicker Ca dominated tribofilms on the FE8 rollers as opposed to the normal Zn-S dominated

tribofilm. This may have promoted hydrogen diffusion and WEC formations in the FE8 rollers. Thinner Zn-S containing films have been found to form on the FE8 raceways however, and these may have demoted hydrogen diffusion and WEC formations.

Chapter 5 Conclusions and Future Work

This chapter overviews the work conducted, summarises the novelties and conclusions from this study. Towards the end of this chapter, potential future work has been recommended.

5.1 Overview

This PhD aimed at investigating White Structure Flaking/White Etching Crack (WEC) formation and propagation mechanisms in 100Cr6 bearing steels, commonly used in wind turbine gearbox bearings (WTGBs), focusing on the influence of diffusible hydrogen and over-based calcium sulfonates detergent additives in the oil on WECs. Following on from the PhD study conducted by Evans [26] at Southampton, this study has investigated WEC initiation and evolution mechanisms under non-hydrogen charged test conditions. Before commencing this PhD, the author of this thesis was experimentally involved in a study that analysed WECs formed in 100Cr6 cylindrical roller thrust bearings on an FAG-FE8 RCF test rig under *non*-hydrogen charged conditions [38] (see Appendix C). This study showed similar WEC initiation and formation mechanisms as that in RCF tested samples under pre-hydrogen charged conditions studied by Evans [26]. This initiated this PhD study, aiming to answer the following research questions as mentioned at the beginning of this thesis,

1. '*How do WECs initiate and evolve under non-hydrogen charged conditions?*'
2. '*What is the role of hydrogen diffusion in the WEC formation and propagation process?*'
3. '*How do specific additives, and in particular over-based calcium sulfonates (OBCaSul), in the lubricating oil affect WEC formations, hydrogen diffusion, and tribochemistry?*'

To answer these questions, extensive RCF testing, metallographic analysis, hydrogen diffusion analysis, and tribofilm examination have been conducted in this study.

To create WECs, RCF testing has been conducted on both FAG-FE8 and PCS-MPR test rigs under non-hydrogen charged conditions, lubricated with two types of oils: one was an 'off-the-shelf' fully formulated gear oil known to be 'bad' and promote WECs (also referred to as 'Oil X' in this work); and the second a purposely formulated oil containing ZDDP and OBCaSul detergent additive at various wt%. The first set of experiments on the FAG-FE8 aimed at capturing and investigating the evolution of WECs from initiation to final flaking, by testing the bearings for a series of durations and analysing WECs in the specimens using serial sectioning. Based on past literature, one of the hypotheses on the mechanism of WEC formation is that the OBCaSul in the 'bad' oil is the critical additive driving WEC formation. Hence, experiments were then conducted

on the FAG-FE8 and MPR rigs using purposely formulated lubricants containing only ZDDP and OBCaSul additives aimed at investigating the influence of OBCaSul detergent additives on the formation of WECs.

The second set of experiments on the FAG-FE8 and MPR rigs aimed to investigate the influence that OBCaSul detergent additives in the oil can have on the formation of WECs. The effect that different wt% of OBCaSul in the oil have on WEC formation propensity was examined, serial sectioning being used to quantify WEC damage formations.

In addition to the serial sectioning analysis, diffusion of hydrogen in the tested bearings from the FAG-FE8 testing was measured using Thermal Desorption Analysis (TDA) methods with two different setups to capture more details related to the diffusion of hydrogen. Combining TDA with the extensive serial sectioning analysis, the relationship between the number of WECs formed and the amount of diffusion hydrogen was investigated for both the 'off-the-shelf' fully formulated gear oil and OBCaSul oils.

To study the tribofilm formed during RCF operation SEM/EDX have been conducted, which enabled the exploration of relationships between tribofilm, hydrogen diffusion and WEC formation in this study and thus the influence of OBCaSul on WEC formation.

The main novelties of this study are that:

1. This study has investigated the initiation and evolution of WECs until final flaking under non-hydrogen charged conditions.
2. This study has conducted detailed diffusible hydrogen analysis on RCF tested bearings under non-hydrogen charged conditions using TDA that enabled the investigation of the influence of hydrogen on WEC formation.
3. This study has investigated the effect that OBCaSul detergent additives have on WEC formation by conducting RCF testing lubricated by oils containing various %wt of OBCaSul.
4. This study conducted detailed tribofilm analysis so the influence of OBCaSul on the tribofilm, and thus WEC formations via hydrogen diffusion are shown.

The main conclusions drawn from this study are summarised in the following section below.

5.1.1 Conclusions

The conclusions of this study are clustered in four parts relating to the characteristics of the WECs, quantification of hydrogen, effect of OBCaSul on WECs and its influence on tribofilm respectively.

5.1.1.1 The evolution of White Etching Cracks

Detailed serial sectioning analysis has been conducted on the WECs created in 100Cr6 steel samples on FAG-FE8 and MPR test rigs under non-hydrogen charged conditions lubricated with both the 'off-the-shelf' fully formulated gear oil known to promote WECs (Oil X) and the purposely formulated oils containing ZDDP and varying wt% (1.4% - 5.6%) of OBCaSul detergent additives. WECs were captured at very early stages of formation where the initiation processes were studied. In addition, the number of WECs formed under different conditions were tracked. The results have provided rich information on the WEC formation and evolution processes under non-hydrogen charged conditions. The conclusions are:

WEC Initiation:

- Under non-hydrogen charged conditions, WECs are found to be subsurface initiated from small/short non-metallic inclusions similar to what has been observed through serial sectioning under pre-hydrogen charged conditions [36, 37, 39]. Approximately 90% of all fully mapped WECs recorded (recorded from start to finish) were contained entirely within the subsurface and did not make connection to the surface, ruling out surface initiation of those WECs. Small/short inclusions (FE8: ~ 2 - 20 µm and MPR: ~ 2 – 13 µm) were found to frequently interact with WECs, inclusions being globular sulfides (D_{sulf}), globular duplex inclusions (globular manganese and/or calcium sulfide surrounding aluminate) (D_{Dup}), globular oxide inclusions (D) and manganese sulfide/sulfide duplex (A). For the FE8 tests, D_{Dup} and D type inclusions are found to interact with the WECs at the early infant stages of WEC formation, inclusions being either Al_2O_3 or MnS surrounding Al_2O_3. Inclusion types found to interact with large WEC networks found at the later stages of FE8 RCF duration (18 hrs) are consistent with those found at the early infant stages (4 and 6 hrs).
- Supporting evidence that WEA generation can occur due to crack face rubbing mechanism is shown. This is supported by detailed analysis and quantification of WEA microstructural change associated with WECs, where,
    i. The volume of WEA around the cracks increases with the increase of RCF test durations (longer duration = more time for crack rubbing).
    ii. WEA volumes were found to be greater within the planes of the WEC at an inclination angle to the contacting surface and little or no WEA was found in the plane of cracks perpendicular to the surface. Also the amount of WEA at the end 'tips' of the propagated WEC network is found to be minimal or non-existent.

iii. WEA volume decreases or 'disappears' at wider cracks, where less rubbing action would occur. The proposed mechanism for this is explained in Figure 2-19 and discussed in more detail in Chapter 2.

Conversely to this mechanism, numerous small very near-surface WEAs were also found without any visible crack in many FAG-FE8 bearing samples. This suggests that the formation of this type of microstructural change to WEA at near surface does not require the presence of a crack.

WEC evolution:

Again, the following conclusions on WEC evolution have been drawn from the FAG-FE8 tests with Oil X.

- The evolution of WECs from initiation to final flaking is proposed to occur as follows,
  i. WECs initiate at small/short non-metallic inclusions in the subsurface (see above).
  ii. At the early infant stages, WECs propagate into 'star-like' WECs with forking of the crack tips.
  iii. Cracks further propagate in the radial and over-rolling direction.
  iv. Cracks continue to propagate and the coalescence of independent WECs join to form larger WEC networks.
  v. Eventually final propagation of the crack to the surface results in flaking.

  This was achieved through mapping of WECs in FAG-FE8 RCF tests over a number of test durations under non-hydrogen charged conditions using serial sectioning methods for the first time. The proposed evolution is illustrated in Figure 2-17 and discussed in more detail in Chapter 2.

WEC formation:

- WECs were found to only form in the FE8 rollers and <u>not</u> the raceways for all tests. The propensity and size of WEC formations increases with test duration, a step increase in size and number of formations being seen at the later stages of RCF operation (between 12 – 18 hrs). The majority of the WECs recorded in the FE8 rollers were found in the outer roller edge in a relatively limited zone corresponding to regions of high-energy dissipation.
- The number of WEC formations in the FE8 rollers appears to increase for an increase in OBCaSul wt% from 1.4% OBCaSul at 0 WECs, to 2.8% and 5.6% at 17

and 12 WECs respectively, suggesting that OBCaSul has promoted WEC formations. In contrast in the MPR tested roller, only OBCaSul 1.4% lubricated rollers showed WECs, higher OBCaSul wt% (2.8% and 5.6%) not creating WECs. This converse effect on the MPR test rig may be due to the differences in dynamics of the contacts, which in turn affect the tribofilm and hydrogen diffusion. Further investigations are necessary to understand these differences.

5.1.1.2 Influence of Hydrogen diffusion on WEC formations

TDA through two independent set-ups/machines has been used to measure the concentration of diffusible hydrogen in standard 100Cr6 bearing steel tested on an FAG-FE8 test rig. This has been conducted for the first time under non-hydrogen charged conditions and over increasing RCF test durations. The conclusions from TDA are as follows:

- TDA showed that hydrogen diffused into the FE8 rollers and not the raceways during RCF operation, and the amount of diffusible hydrogen in the rollers increases with the test duration.
- The amount of diffusible hydrogen in the tested FE8 rollers has been found to be positively correlated with the number of WECs recorded in the rollers for the Oil X tested bearings.
- Diffusible hydrogen may not be an initiator, but rather an accelerator to WEC formation. This is because, although one single WEC was observed in the 4-hr test FE8 rollers, the diffusible hydrogen in this roller appears to be negligible. In addition, while the diffusible hydrogen concentrations are comparable in tests lubricated by the two types of oils (Oil X vs. OBCaSul oils), the numbers of WECs found in the FE8 rollers are significantly different, i.e. the concentration of diffusible hydrogen found in rollers lubricated by different oils may not have had the same effect on WEC formation. It is worth mentioning that, at this stage, it is not clear what the influence of local diffusible hydrogen at inclusions/cracks may have due to the limitation of the TDA, which only measures diffusible hydrogen in the bulk of the specimens.
- The mechanism of hydrogen entry into the steel is suggested to be diffusion at wear induced nascent surface or areas of heterogeneous tribofilm, hydrogen being generated by decomposition of lubricant through catalytic reactions and/or tribo-chemical reactions of water. As mentioned above, the vast majority of WECs recorded were contained entirely within the subsurface, where when a connection with the surface was made; these were small/short surface crack volume connections and are proposed to not allow sufficient lubricant penetration into the crack to aid WEC growth. Surface connections

were also found only for longer RCF test durations (18 hrs), where no surface connections were recorded for all WECs recorded below 18 hrs.

5.1.1.3 Effect of over-based calcium sulfonates (OBCaSul)

Based on literature, OBCaSul may be a critical additive in the 'bad oil' that promotes WECs. This study investigated the influence of OBCaSul detergent additives using purposely-formulated oils containing only ZDDP and OBCaSul additives. The conclusions from the investigations of oils containing a range of OBCaSul concentrations are summarised below.

- As mentioned above, increase of wt% of OBCaSul (from 1.4% to 2.8%) has shown a jump increase (from zero WECs to WECs being recorded respectively) in number of WEC formations found in the FE8 rollers. OBCaSul increase from 2.8% to 5.6% showed no huge difference in number of WECs recorded; though, length of WECs did increase. The influence of OBCaSul on WEC formations seems to be the opposite though in the MPR rollers, where only the 1.4% OBCaSul lubricated roller formed WECs, and no WECs were formed in those lubricated by the 2.8% and 5.6% OBCaSul oils. Hence, the influence of OBCaSul maybe affected by the differences in dynamics between the test rigs and thus the tribofilms (see below for more discussions).
- The ZDDP only (0% OBCaSul) oil behaved completely different on FAG-FE8 and on MPR, i.e. no WECs formed on the former while a number of WECs formed on the latter.
- Based on TDA on the FAG-FE8 tested rollers, a positive correlation is shown between the OBCaSul concentration and the amount of diffusible hydrogen. Due to time constraints, no TDA was conducted on the MPR rollers, so it is not possible to confirm this correlation for the MPR tests. Discussions have been made in Chapter 4 explaining the potential differences between the two rigs, which may have caused the differences in the relationship. Future work is thus required to investigate what has affected the MPR tests differently.

5.1.1.4 Role of the tribofilm

To investigate the mechanism and how OBCaSul has influenced WEC formation, detailed analysis of the tribofilms was conducted on the RCF tested FAG-FE8 samples using SEM/EDX.

The results clearly show that the OBCaSul containing oils have formed a thicker Calcium dominated film on the FAG-FE8 rollers comparing to the 'normal' Zn-S dominated tribofilm, which was found to have formed on the rollers lubricated by the ZDDP only (0% OBCaSul) oil and the raceways lubricated by Oil X and OBCaSul (1.4% - 5.6%) oils. This suggests that the OBCaSul additive was a strong competitor of the ZDDP in those oils. Replacement of Zn by Ca in the

tribofilm is proposed, although thicker, this film has promoted hydrogen diffusion into the bearing (TDA showing a positive correlation between OBCaSul wt% and diffusible hydrogen concentration in the FE8 rollers).

For the fully formulated 'off-the-shelf' gearbox oil (Oil X), the increase in RCF test duration has resulted in thicker Ca films formed on the FE8 rollers too, which is correlated with the increased diffusible hydrogen concentrations and WEC propensities observed in the rollers.

Overall, it is found that OBCaSul additive in the ZDDP containing oils can form a Ca dominated tribofilm on FE8 rollers, which are thicker, and may promote hydrogen diffusion into bearing steel and WEC formations. Thinner Zn-S films formed on the FE8 raceways on the other hand may demote hydrogen diffusion and WEC formations.

As mentioned above, hydrogen diffusion is proposed to occur at wear induced nascent surface or areas of heterogeneous tribofilm (due to the majority of WECs being contained entirely within the subsurface), the mechanism of hydrogen generation being lubricant decomposition through catalytic reactions and/or tribochemical reactions of water.

The reason why the Ca tribofilms are thicker than the Zn-S tribofilm and why it promotes hydrogen diffusion is still unclear based on the SEM/EDX analysis. Further tribofilm analysis has been conducted using XPS and STEM (to be published in a later study) that may be able to provide more details on the properties of the tribofilms and reveal the mechanisms further.

5.2 Future work

This thesis has presented a substantial amount of work in contribution to the understanding of the effect that oils containing over-based calcium sulfonate detergent additives have on hydrogen diffusion and WEC formations in bearing steel. In doing so a number of recommendations for future work have been made.

5.2.1 Tribofilm analysis

SEM/EDX has been used to examine the tribofilm formed during RCF operation in this PhD thesis. A number of interesting observations have been made regarding the effects that oil chemistries containing OBCaSul detergent additives have on the AW tribofilm formed, and how this can influence hydrogen diffusion, and thus WEC formations. If OBCaSul detergents do promote hydrogen diffusion, and thus WEC formations, then their synergism/antagonism with ZDDP AW additives could be a fundamental factor and this is still unclear based on SEM/EDX analysis.

To further analyse and elucidate this, the author has performed Focused Ion Beam (FIB) and Scanning Transmission Electron Microscopy (STEM) analysis. Cross-sectional imaging, chemical analysis of the tribofilm layers including EDX mapping, EDX line scans and diffraction analysis have been conducted. In addition, X-ray Photoelectron Spectroscopy (XPS) has been used to investigate the structure of the tribofilm. Full details are planned to be shown in a future publication.

5.2.2 Thermal desorption analysis (TDA) to measure diffusible hydrogen

This thesis has used TDA to measure the concentration of diffusible hydrogen using two experimental set-ups on FAG-FE8 RCF tested bearings. Both FAG-FE8 and MPR test rigs have been used in this study; however, TDA was only conducted on the FAG-FE8 bearings due to time considerations. Further TDA is recommended to measure the concentration of diffusible hydrogen in the MPR samples so that a comparative assessment can be made between the different test rigs. Multiple differences in dynamics between test rigs potentially having a significant effect on the diffusion of hydrogen, and thus WEC formations, where TDA can help to examine this.

Preferably, measuring diffusible hydrogen concentrations in actual WTGBs would be ideal, however, logistically and practically this would be near impossible to achieve, where bearings would have be ‘dumped’ in liquid nitrogen asap. Finally, in-situ measurements of diffusible hydrogen during RCF testing would provide more accuracy in determining the rate and concentration of diffusible hydrogen, however, again due to the difficulties in achieving this limited knowledge is available in the field, where in-situ RCF measurements of hydrogen have not been reported.

TDA has been conducted on FAG-FE8 bearings lubricated with varying weight percent of OBCaSul detergent in mix with ZDDP anti-wear additive; however, TDA was only conducted at a set RCF time for these oils (18 hrs on the FE8 rig). Therefore, further TDA to capture and measure diffusible hydrogen concentrations at multiple RCF durations (between 0 hour control and 18 hours) is recommended to make a comparative assessment between measurements and rates of diffusion.

5.2.3 OBCaSul oil testing

In this thesis, RCF testing has been conducted using oils with varying weight percent of OBCaSul detergents in mix with ZDDP anti-wear additive. To further analyse the effect of OBCaSul, RCF testing using oils containing OBCaSul detergents *alone* is recommended to pinpoint the explicit effects of OBCaSul. This is to help deconvolute the competition between OBCaSul and ZDDPs. Post

RCF testing, serial sectioning, TDA, and tribofilm analysis should be performed and a comparative study between OBCaSul oils *alone* and when in mix with ZDDP anti-wear additive made.

Results have shown that on the FE8 rig, the 1.4% OBCaSul oil showed no WECs to form, WECs only forming for higher concentrations (2.8% and 5.6%). Therefore, further testing of OBCaSul concentrations between 1.4% and 2.8% is recommended e.g. 1.8%, 2.2% etc. to see if any trends exist. For the MPR, the opposite was seen, higher OBCaSul concentrations (2.8% and 5.6%) showing no WECs to form, the lower concentration (1.4%) showing WECs. Again, concentrations between 2.8% and 1.4% should be examined, and in addition on the MPR, concentrations <1.4% should be tested to see if trends exist.

5.2.4 Steel cleanliness and inclusion analysis

5.2.4.1 Steel cleanliness

Steel cleanliness analysis is used to assess how 'clean' a steel is by taking into account factors such as type, number and size of inclusions under the ISO 4967-B standard [89]. Steels with different cleanliness levels have been assessed, where testing showed no difference in the time-to-spall, therefore it is suggested that inclusions do not participate in WEC initiation and formation [27, 53]. This argument is, however, contested where cleanliness standards used do not take into account small sized inclusions that are typically found to be associated with WEC-inclusion interactions, comparative differences of small inclusions between steels cannot be validated and the conclusions are void [36, 37, 39, 74]. It is proposed that cleanliness standards should focus on recording the density of small inclusions opposed to maximum inclusion lengths [36, 37, 39]. It is also suggested that standards should be able to differentiate between pure sulfides and sulfides in combination with oxide parts [36].

A number of studies have found extensive evidence for small/short sized inclusions interacting with WECs [26, 36-39, 75, 76, 85], this thesis adding further extension and clarification to this. It has been recognised by the author that the processes used to analyse steel cleanliness fails to capture extensive numbers of inclusions that fall out of the realms stated by the standards (taking into account the raw cleanliness data), in doing so vast numbers of potentially critical small inclusions are missed. By capturing inclusions that fall outside boundaries set by the standards, more accurate global cleanliness indexes (C_i) can be attained regards inclusion-WEC interactions, providing more accurate comparisons globally between samples. This thesis has shown that the C_i value can differ significantly when considering results obtained under the standards compared to those that also count inclusions outside of the set thresholds (raw cleanliness data). Significant differences in steel cleanliness between FAG-FE8 rollers and raceways have been found in this

study (see Chapter 2) when taking into account the raw cleanliness data, raceways being far 'cleaner', where no WECs were recorded in the raceways in comparison to the vast numbers of WECs recorded in the rollers.

Therefore, it is recommended to further investigate differences in steel cleanliness between multiple samples from multiple test rigs, including samples from actual WTGBs. In addition, the processes set out in the standards do not account for the location of inclusions, where for example inclusions located in critical regions throughout the steel (i.e. in the regions of maximum subsurface shear stresses) may be of greater importance than those embedded deep within the sample and outside of critical zones.

5.2.4.2 Inclusion analysis

Finally, where inclusions judged to be potential likely crack initiators are found in positions outside the maximum subsurface shear stress zones, it is recommended to investigate, in addition to type/orientation, the residual stress profiles around these WEC-inclusion interactions. Furthermore, it is also recommended to analyse and measure local hydrogen concentrations around inclusions/inclusion matrix interfaces for example using techniques such as SIMS (bulk diffusible hydrogen measurements being concentrated on in this study). In addition, analysing/modelling hydrogen diffusion rates and penetration depths in the steel is recommended, where hydrogen trapping at defects such as inclusions outside of the maximum subsurface shear stress zones may potentially lower the thresholds for crack initiation.

5.2.5 Effect of surface roughness

In this study, pre-roughening of the FAG-FE8 raceway surfaces was performed to induce boundary lubricating conditions in the re-creation of WECs. This study has shown significant differences in regards to the number of WECs and the concentration of diffusible hydrogen measured between the FE8 raceways and rollers, where no WECs and negligible (similar to a 0 hour control) diffusible hydrogen was measured in the raceways in comparison to numerous WECs and increased diffusible hydrogen concentrations in the rollers. A number of factors have been considered in this study to explain this, however, further analysis is recommended to help answer this. It is considered that pre-roughening of the raceway can affect tribofilm formation, including early tribofilm formation, where roughening has the effect of increasing local 'hot spots' at asperity contact. By investigating the effect of different pre-surface roughness on the FE8 raceways, coupled with tribofilm analysis through SEM/EDX, this effect can be explored.

Appendix A

A.1 Minimum oil film thickness and lambda ratio calculation

The minimum oil film thickness (hmin) between the rolling elements and raceway washer was calculated using Hamrock-Dowson equation [197, 198], see Eq. (A.1).

(A.1.1) $h_{min} = 3.63U0^{.68}G^{0.49}W^{-0.073}(1 - e^{-0.68k})$

where,

h_{min}: minimum film thickness [m]

U: dimensionless speed parameter, $u\eta_0/(E'R)$

G: dimensionless material parameter, $\alpha E'$

W: dimensionless load parameter, $N/(E'R^2)$

u: mean lubricant entrainment speed, [m/s]

$\eta 0$: viscosity at atmospheric pressure of lubricant, [Pa s]

E': effective elastic modulus [Pa]

R: reduced radius of curvature, [m]

α: pressure–viscosity coefficient, [Pa^{-1}]

N: normal load, [N]

k: ellipticity parameter defined as: k = a/b, where 'a' is the semiaxis of the contact ellipse in the transverse direction [m] and 'b' is the semiaxis in the direction of motion [m]. For line contact, k = ∞.

The initial lambda ratio (λ) was then calculated using Eq. (A.2), where Rq,1 and Rq,2 are the rms roughness values of the two contact surfaces.

(A.1.2) $\lambda = hmin / (Rq,1^2 + Rq,2^2)^{1/}$

A.2 Inclusion ranking system

Below is details on the inclusion ranking system used in this thesis developed by Evans [26].

Appendix A

Rank 1: Strong evidence for butterfly initiated WECs.

(i) Orientation of wings (+ ve or – ve) being consistent with the wings of independent butterflies found in the serial sectioning analysis (not in the WEC network). + ve or – ve wing orientation is determined by the over–rolling direction, a second pair of wings being formed upon reversal of the over-rolling direction after a certain period [221].

(ii) The crack/wing angle, this being mainly ~ 45˚ with a range of 0 - 60˚ for typical butterfly formations [12, 26].

(iii) If the microstructural change morphology associated with the crack/wing is of a typical 'classic wing-like pattern'.

Rank 2: Possible butterfly initiation or strong likelihood of WEC initiation independent of butterfly.

(i) This is the case when crack initiation features are observed however, the characteristics of butterfly formation as stated in Rank 1 type damage features are not observed.

Rank 3: Crack has passed through the inclusion during crack propagation; inclusion can therefore potentially aid in the propagation however, the inclusion is not involved in the initiation process of a crack.

(i) Orientation of the crack when passing through the inclusion was in a radial or near radial direction.

(ii) The inclusion interaction location is somewhere along one of the radial (depth direction) cracks of the WEC. In addition, microstructural change may not be observed around the crack.

(iii) The inclusion interaction depth is in an area of low subsurface shear stress.

(iv) The inclusion is small and is located inside a zone of considerable microstructural change with no crack visibly connecting to the inclusion.

Appendix B

Table B-1: Average normalised atomic % for FAG-FE8 Oil X analysed film by SEM/EDX.

	Norm. O%		Norm. Na%		Norm. S%		Norm. Zn%		Norm. Ca%		Norm. P%		Avg. Tribofilm thickness (nm)	
Test duration	**Roller**	**Race**	**Roller**	**Race**	**Roller**	**Race**	**Roller**	**Race**	**Roller**	**Race**	**Roller**	**Race**	**Roller**	**Race**
2 hrs	71.07	73.7	1.42	2.25	6.57	4.53	3.83	5.21	13.15	11.53	4.00	2.79	15	57
6 hrs	59.42	49.18	3.80	1.76	4.92	14.5	6.64	18.51	16.10	8.46	9.12	6.20	162	135
18 hrs	55.56	47.01	3.81	2.32	5.81	15.48	8.11	21.73	18.89	7.27	6.82	4.64	157	95

Table B-2: Normalised atomic % for EDX mapping of FAG-FE8 Oil X roller and raceway films.

Roller	**Phase**	**Norm. O%**	**Norm. Na%**	**Norm. P%**	**Norm. S%**	**Norm. Ca%**	**Norm. Zn%**
2 Hours	Tribofilm	66.97	0.00	4.68	7.54	15.47	5.20
	Roller Edges	94.07	1.40	2.85	0.00	0.00	1.57
6 Hours	Thick Tribofilm	54.60	4.38	12.13	3.86	17.46	7.57
	Medium Tribofilm	56.77	3.95	8.41	4.72	20.68	5.47
	Thin Tribofilm	64.35	0.00	3.68	8.63	16.23	7.11
	Roller Edges	79.75	3.27	3.71	3.68	0.00	4.41
18 Hours	Thick Tribofilm	54.26	3.93	8.23	4.70	22.47	6.39
	Thin Tribofilm	51.40	3.48	4.14	9.73	18.18	13.11
	Roller Edges	78.90	3.74	3.02	3.28	3.83	7.19
Race	**Phase**	**Norm. O%**	**Norm. Na%**	**Norm. P%**	**Norm. S%**	**Norm. Ca%**	**Norm. Zn%**
2 Hour	Steel/Tribofilm	20.46	0.81	1.03	1.50	4.04	1.50
	Embedded Silica?	23.84	0.87	1.00	1.44	3.92	2.11
	Marker	53.96	0.59	0.00	0.00	0.00	0.00
6 Hour	Thickest Tribofilm	31.29	0.00	6.74	25.33	2.44	28.08
	Thicker Tribofilm	32.66	0.00	4.73	15.49	2.59	18.85
	Thinner Tribofilm	26.82	1.20	3.61	6.87	5.74	9.21
	Thinnest Tribofilm	18.23	0.00	1.18	3.99	2.46	4.87
	Embedded Silica?	33.02	0.61	1.73	5.15	2.36	6.56
	Raceway Inner Edge	34.58	0.00	0.00	4.55	0.00	5.95
	Marker	51.39	0.00	1.50	4.83	0.00	6.75
18 Hour	Thickest Tribofilm	33.56	0.00	4.22	19.77	0.00	24.00
	Thicker Tribofilm	27.20	0.00	2.83	13.26	1.80	17.07
	Thinner Tribofilm	19.17	0.82	2.08	6.12	3.71	8.81
	Thinnest Tribofilm	11.81	0.00	0.42	2.26	0.00	3.33
18 Hour	Embedded Silica?	21.80	0.80	1.75	5.15	4.31	7.40

Table B-3: Average normalised atomic % for the FAG-FE8 OBCaSul oil films analysed by SEM/EDX.

	Norm. O%		Norm. S%		Norm. Zn%		Norm. Ca%		Norm. P%		Average tribofilm thickness (nm)	
Test Oil	**Roller**	**Race**	**Roller**	**Race**	**Roller**	**Race**	**Roller**	**Race**	**Roller**	**Race**	**Roller**	**Race**
Base oil mix (grp III) + ZDDP + OBCaSul 0%	61.47	59.21	7.10	11.16	19.11	17.21	0	1.06	12.31	11.34	137.2	167.7

Appendix B

Base oil mix (grp III) + ZDDP + OBCaSul 1.4%	57.36	45.85	5.46	16.47	9.72	21.45	16.87	10.4	10.59	5.83	225.9	129.7
Base oil mix (grp III) + ZDDP + OBCaSul 2.8%	57.75	44.02	6.00	17.94	7.60	21.94	21.59	10.76	7.07	5.33	200.1	127
Base oil mix (grp III) + ZDDP + OBCaSul 5.6%	60.59	46.49	6.12	18.87	5.87	16.89	19.53	11.56	7.89	6.19	218.8	134

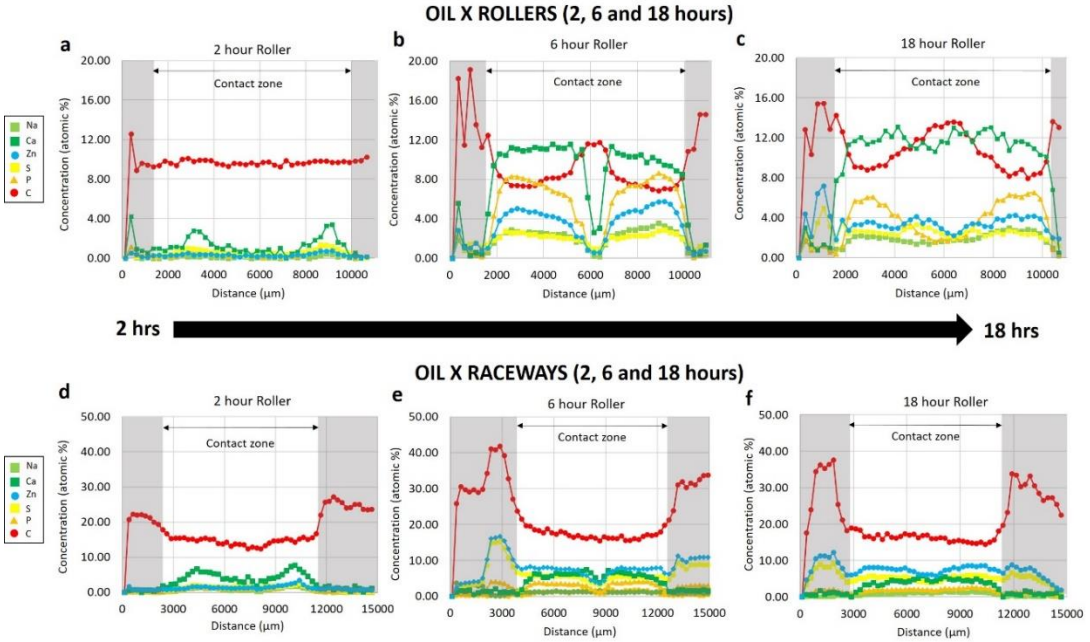

Figure B-1: Raw elemental data from EDX analysis of the RCF tested Oil X tribofilms formed across 2, 6 and 18-hours. (a-c) rollers and (d-f) raceways.

Table B-4: Raw elemental atomic % for FAG-FE8 Oil X analysed by SEM/EDX.

	O%		C%		Na%		S%		Zn%		Ca%		P%	
Test duration	**Roller**	**Race**	**Roller**	**Race**	**Roller**	**Race**	**Roller**	**Race**	**Roller**	**Race**	**Roller**	**Race**	**Roller**	**Race**
2 hrs	6.25	16.1	9.79	17.9	0.13	0.6	0.54	1.12	0.32	1.2	1.21	2.99	0.38	0.76
6 hrs	26.29	20.2	9.84	25.1	1.93	0.76	1.96	6.24	3.25	7.96	7.86	3.66	4.93	2.72
18 hrs	25.49	15.7	11.15	22.1	1.81	0.55	2.49	5.15	3.44	7.24	9.75	2.6	3.47	1.6

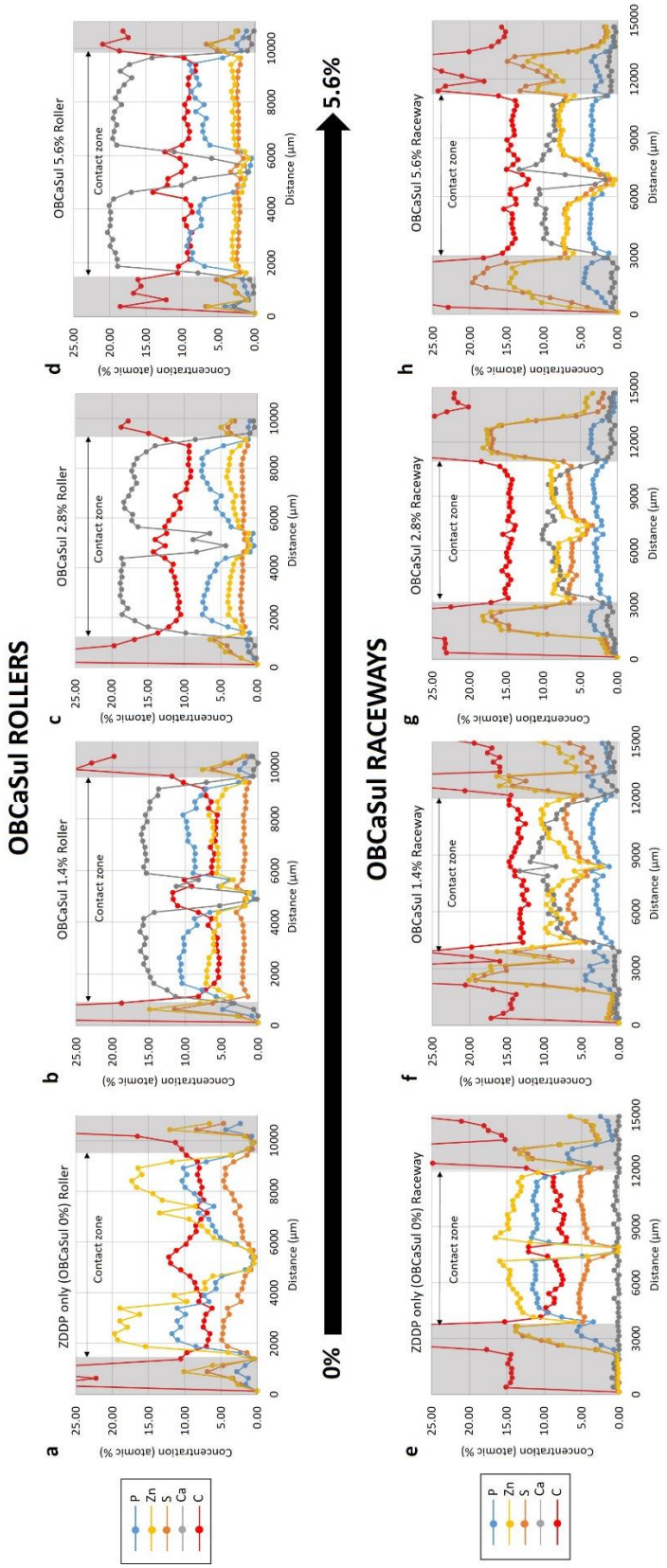

Figure B-2: Raw elemental data from EDX analysis of tribofilms formed for RCF tested ZDDP only (OBCaSul 0%) and OBCaSul (1.4% - 5.6%) oils. (a) ZDDP only (OBCaSul 0%) roller. (b - d) OBCaSul 1.4% - 5.6% rollers. (e) ZDDP only (OBCaSul 0%) raceways. (f – g) OBCaSul 1.4% - 5.6% raceways.

Appendix B

Table B-5: Raw elemental atomic % for FAG-FE8 OBCaSul oil films analysed by SEM/EDX.

	O%		C%		S%		Zn%		Ca%		P%	
Test Oil	**Roller**	**Race**	**Roller**	**Race**	**Roller**	**Race**	**Roller**	**Race**	**Roller**	**Race**	**Roller**	**Race**
ZDDP only (OBCaSul 0%)	23.06	25.56	11.97	16.17	2.88	5.11	9.01	9.37	0	0.25	5.51	6.37
OBCaSul 1.4%	33.08	17.22	11.28	18.55	2.44	6.86	5.34	8.86	11.05	4.8	6.86	2.48
OBCaSul 2.8%	31.09	16.29	14.23	21.4	2.28	7.66	3.27	9.13	12.63	4.61	4.31	2.32
OBCaSul 5.6%	33.9	18.19	11.53	19.11	2.66	8.01	2.81	7.20	12.7	5.16	5.14	2.73

Appendix C

Confirming subsurface initiation at non-metallic inclusions as one mechanism for white etching crack (WEC) formation

M.-H. Evans[a], A.D. Richardson[a], L. Wang[a], R.J.K. Wood[a], W.B. Anderson[b]

[a] National Centre for Advanced Tribology at Southampton (nCATS), University of Southampton, SO17 1BJ, UK

[b] Afton Chemical Corporation, Richmond, VA 23219, US

C.1 Abstract

White etching crack (WEC) formation beneath the contact surface in steel rolling element bearings causes a premature wear failure mode called white structure flaking (WSF). The drivers and initiation mechanisms are contested. Extensive work previously conducted by the authors showed strong evidence for one mechanism of WEC initiation being subsurface at inclusions. This paper conducts further work for final verification. Rolling contact fatigue testing of bearings on a FAG-FE8 test rig was conducted. Serial sectioning was used to map WECs in their entirety that formed under non-hydrogen charged conditions for the first time. Evidence from this paper and previous works by the authors confirms that subsurface initiation of WECs at non-metallic inclusions is at least *one* mechanism of WEC formation.

C.2 Introduction

White Structure Flaking (WSF) as a premature wear failure mode in steel rolling element bearings has occurred in a number of applications including bearings for automotive components and wind turbine gearboxes [12, 101]. WSF typically occurs in 1 – 20% of a bearing's L_{10} life [12, 14, 101]. Microstructural alterations in bearing steels called *white etching area* (WEA) and *white etching cracks* (WECs) that form in the ~1 mm zone beneath the contact surface cause WSF [12]. The white appearance of the altered microstructure after being etched in Nital (~2% Nitric acid in ethanol) and viewed under reflected light gives WEA its name. WEA is nano-crystalline with ferrite grains varying in size from ~10 – 300 nm and spherical carbides have been observed to dissolve as part of the WEA formation process [41, 47, 222-224].

WSF formation drivers are proposed as being either i) hydrogen release and diffusion into bearing steel (sourced from the lubricating oil or water contamination) [12, 101] or ii) transient operating

conditions [12, 14] such as transient loading events in wind turbines caused by wind gusts, braking, load reversals and generator-grid engagements and disengagements [25]. Computer simulations have shown that for spherical roller bearings in an intermediate shaft location of a wind turbine gearbox, moderate sliding (3–10% slide to roll ratio) at roller–raceway contacts in the unloaded zone occurs continuously [199] due to a phenomenon named Heathcote slip [14]. In addition estimation of slip in wind turbine gearbox spherical roller bearings during acceleration transients has been calculated by Kang, et al [199]. Slide to roll ratio's ranging between 30–110% were calculated to have been experienced at various points in the acceleration transient depending on the load applied to the bearing. Previous techniques for enabling WEC formation in laboratory involve either chemical acceleration by introduction of hydrogen into steel or mechanical acceleration by transient conditions [12].

During rolling contact, hydrogen entering the steel could occur by two mechanisms: 1) through surface cracks where water contamination or lubricant enters surface cracks allowing local release of hydrogen ions by tribochemical reactions at crack tip nascent surfaces [64]; 2) through wear induced nascent surfaces where hydrogen is generated by decomposition of lubricants through catalytic reactions [115] and tribochemical reactions of water. The wear in the latter mechanism could be attributed to the slip experienced in wind turbine gearbox bearings.

Limited metallographic analysis has been used in many previous WSF investigations which has led to incomplete conclusions on initiation and propagation mechanisms [12]. WEC initiation mechanisms are suggested as surface initiation at cracks [64], subsurface initiation by inclusions [86], impact events [77] and damage accumulation followed by rupture causing microstructural change to release energy [69]. The relation of the initiation process with so-called hairline axial cracks sometimes seen on wind turbine gearbox bearing raceways [11, 19, 64, 77] is also contested. Significant evidence for one mechanism of WEC formation being subsurface has been provided by the authors [26, 75] through the application of serial sectioning to map subsurface wear volumes of bearings from service and large scale test rigs [36] and test specimens from laboratory under hydrogen charged conditions [37, 39]. In the aim of finally confirming this, in this paper the serial sectioning process has been used to map WECs in their entirety that form under *non*-hydrogen charged conditions for the first time.

C.3 Techniques, experimental methods and materials

C.3.1 Rolling contact test rig and test conditions

A RCF test was carried out to investigate WSF under non-hydrogen charged conditions. The test was performed on an FAG-FE8 test rig (Figure C-1). Two cylindrical roller thrust bearings were tested simultaneously. Two plate springs provided the application of load. The bearings have 15 steel rolling elements mounted in a brass cage between two steel washer raceways (Figure C-1). The rolling elements and washer raceway are martensitically hardened 100Cr6 steel variants (see Table C-1 for properties). Roughness measurements were conducted using a contact profilometer and six measurements were taken to gain an average for each case.

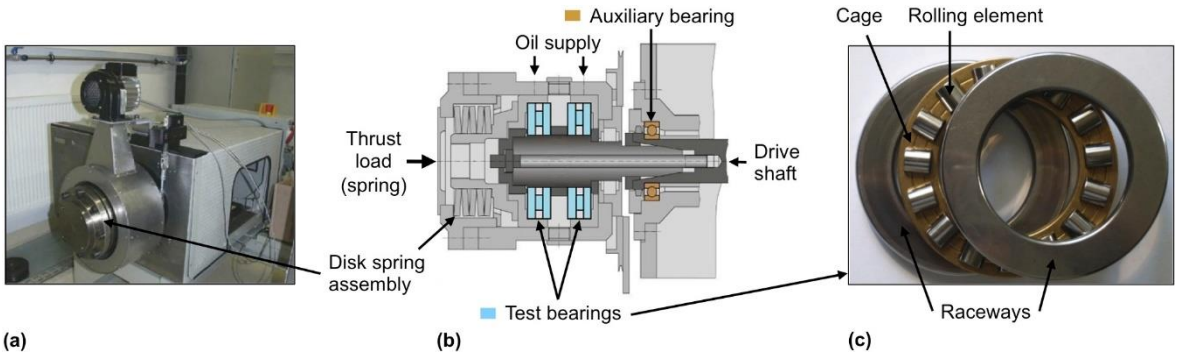

Figure C-1: (a) Photograph of the FAG-FE8 test rig, (b) Schematic of the test set-up, (c) Optical image of the cylindrical roller thrust bearings used in the WSF test.

Appendix C

Table C-1: FAG-FE8 WSF test conditions.

Test system	
Test rig	FAG-FE8
Test sample	Cylindrical roller thrust bearings
Bearing type	F-562831-01 / 81212
Oil properties	
Oil type	Automotive gear oil, fully formulated PAO (ISO VG64)
Viscosity	64 cSt (40°C), 9.5 cSt (100°C)
Pressure viscosity coefficient (α)	6.6 GPa^{-1}
Dynamic viscosity η_0 (100°C)	0.0046 Pas
Oil additives	Barium, sodium and calcium anti-corrosion sulfonates, ZDDP antiwear additives and molybdenum friction modifiers
Bearing material properties	
Washer / roller / cage material	Martensitic 100Cr6 steel / Martensitic 100Cr6 steel / Brass
Hardness	765 HV (rolling element), 590 HV (washer raceway)
Surface roughness (R_q)	0.09 µm (rolling element), 0.70 µm (washer raceway)
Test conditions	
Rotational shaft speed	750 rpm
Axial load	60 kN
Max contact pressure	~ 1.5 – 1.9 GPa (depending on contact length used between 7 and 9 mm)
Bearing/oil temperature	100 ˚C
Minimum film thickness (h_{min})	0.053 µm
Lambda ratio	0.1
Duration of test	18.5 hours
Number of shaft revolutions	~0.85 x 10^6 revolutions
Number of stress cycles	6 x 10^6 stress cycles (on any individual rolling element), 12.5 x 10^6 stress cycles (on any one point of the washer raceway)
Subsurface shear stresses	
Max orthogonal shear stress ($\tau_{o,max}$)	~ 375-475 MPa (acting @ a depth below contact surface of ~ 92 µm)
Max unidirectional shear stress (τ_{max})	~456-578 MPa (acting @ a depth below contact surface of ~ 145 µm)

A pure rolling condition exists at the centre of the rolling elements contact zone with a rising slippage up to 12.5% zone present in a direction towards the rolling element ends (Figure C-2) [225, 226]. Upon the absence of a fully separating lubricant film, sliding wear arises in the areas of slippage. The test conditions are shown in Table C-1. The initial minimum oil film thickness (h_{min}) between a rolling element and the washer raceway in the thrust washer bearing has been calculated using the Hamrock and Dowson equation [197, 198], see A.1 Eq. (A.1.1). The initial lambda ratio at the start of RCF has also been calculated based on the roughness values given in Table C-1; see A.1 Eq. (A.1.2). Based on the calculated values it is clear that the bearing was running in boundary lubrication for the entirety of the test. The RCF test was suspended at 18.5 hours due to a vibration threshold being exceeded. Flaking damage was observed on many of the rolling elements upon visual inspection, which has caused the vibration cut off. The magnitude and depths of the shear stresses in the steel during RCF are calculated for a maximum contact pressure of 1.5 – 1.9 GPa using the equations in references [33, 227, 228] for pure rolling conditions (see Table C-1). These values are indicative only as traction present in the contact can also affect the shear stresses and depths, e.g. the higher the traction the higher the magnitudes of the subsurface shear stresses and proximity to the contact surface.

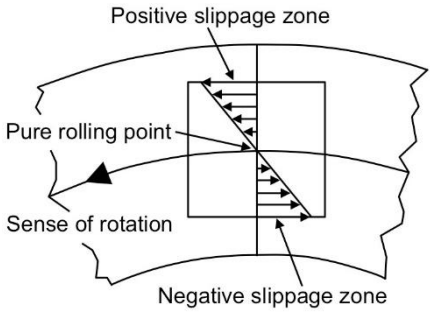

Figure C-2: Slippage condition in axial cylindrical roller thrust bearings.

C.3.2 Subsurface examination - standard

Standard metallographic analysis was conducted on sections of the washer raceway and the rolling elements.

Washer raceway: three segments covering approximately one third of its surface were cut and mounted in Bakelite mounts. These segments were mounted such that the actual contact surface would be prepared by metallography. The three segments were ground and polished using diamond products to depth intervals below the contact surface of approximately 10, 20, 50, 100 and 250 µm to determine the presence of WEC formations. Other depth intervals were also occasionally analysed for verification purposes.

Rolling elements: three rolling elements were analysed by metallography. One of these rolling elements was reserved for a detailed serial sectioning analysis which is described in the next section (C.3.3). The two remaining rolling elements were cut and mounted such that a plane parallel to the rolling direction (circumferential section) would be prepared by metallography. Approximately twenty sections were made across the length of both of these rolling elements to check for presence of WECs and any possible anomalies in the formation distribution of damage features.

C.3.3 Subsurface examination - serial sectioning

A serial sectioning process was conducted to investigate the formation of WECs in a test rolling element and map these subsurface damage features in 3-D. The process involves fine grinding and polishing of cross-sections of the rolling element at ~3.8 µm material removal intervals in the circumferential direction (see Figure C-3). All polished cross-sections were etched with Nital 2% before being examined with optical microscopy and selected ones with interesting features were further examined by SEM/EDX.

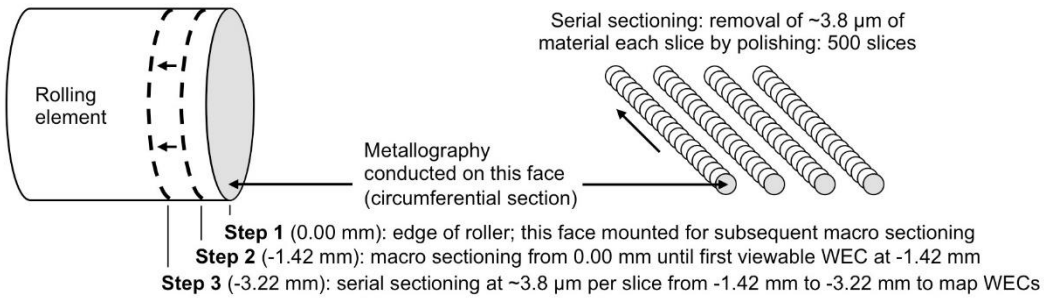

Figure C-3: Schematic illustrating the macro sectioning and serial sectioning metallographic processes conducted on the roller.

After the RCF test one of the rolling elements was chosen for detailed serial sectioning analysis due to its contact surface having small white structure flaking areas. This rolling element was hot mounted in a 30 mm diameter Bakelite resin mount, in an orientation where the rolling elements edge could be subject to metallography in a plane parallel to the direction of travel (see Figure C-3). Macro sectioning at ~50 µm material removal intervals was begun from the rolling elements edge (designated 0.00 mm) to find the first viewable WECs outer most edge. As soon as the first WEC was viewed (at -1.42 mm), the serial sectioning process at ~3.8 µm material removal intervals was begun to track the WECs orientation and location through the volume of the steel. The next four WECs that appeared were also fully mapped in the same way so that by the end of the analysis (end at -3.22 mm), five WECs were fully mapped (WEC 1, WEC 2-*S*, WEC 3, WEC 4-*S*, WEC 5-*S*). The '*S*' in some of the WECs refers to if the crack made a connection to the contact surface. Any other WECs that appeared during this process were also recorded, however optical images were not taken at each slice interval as a time saving consideration. In total thirteen WECs were recorded. Serial sectioning was conducted over 500 slices.

Vickers indentation on the exposed face of the cross section was used during the serial sectioning to enable accurate assessment of material removal rates and provide reference markers to track the WECs over multiple slices. Optically imaging at set magnifications of 100x or 200x with tracking markers allowed for subsequent image alignment.

C.3.4 WEC tomography

For three of the five WECs fully mapped (WEC 1, WEC 2-*S* and WEC 3), the optical microscopy images of the WECs at 200x magnification were aligned using layering tools in Photoshop CS3 to form a stack of aligned images. These images were subsequently used to make videos showing orthoslice sweeps of the three WECs at each slice demonstrating the morphology of the WECs in 3-dimensions.

C.4 Results

C.4.1 Surface inspection

Both the washer raceway surfaces and the rolling elements surfaces were examined. Upon inspection of the bearing washer raceway and rolling element surfaces, flaking had occurred at numerous locations on many of the rolling elements, however only very few small flaking were evident on the washer raceway. An example image of the washer raceway surface is shown in Figure C-4.

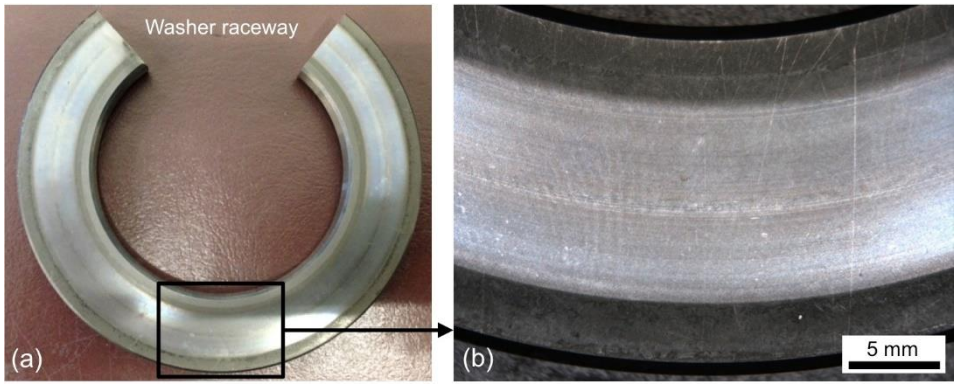

Figure C-4: Optical images of the washer raceway surface.

Optical images of the rolling element surface were taken around the rolling element at 45-degree intervals (octants) and are presented as eight zones (A – H) in Figure C-5. Distinctive wear zones on either side of the centre of the rolling element are evident and can be explained by the slip zones illustrated in Figure C-3. It can be observed that the locations of flaking on the rolling elements surface are always offset from either side of the centre of the rolling element corresponding to these wear zones. Upon close inspection of the rolling element surfaces under optical macroscopy, no evidence of axial hairline cracks were found which are sometimes observed in wind turbine gearbox bearings exhibiting the WSF failure mode.

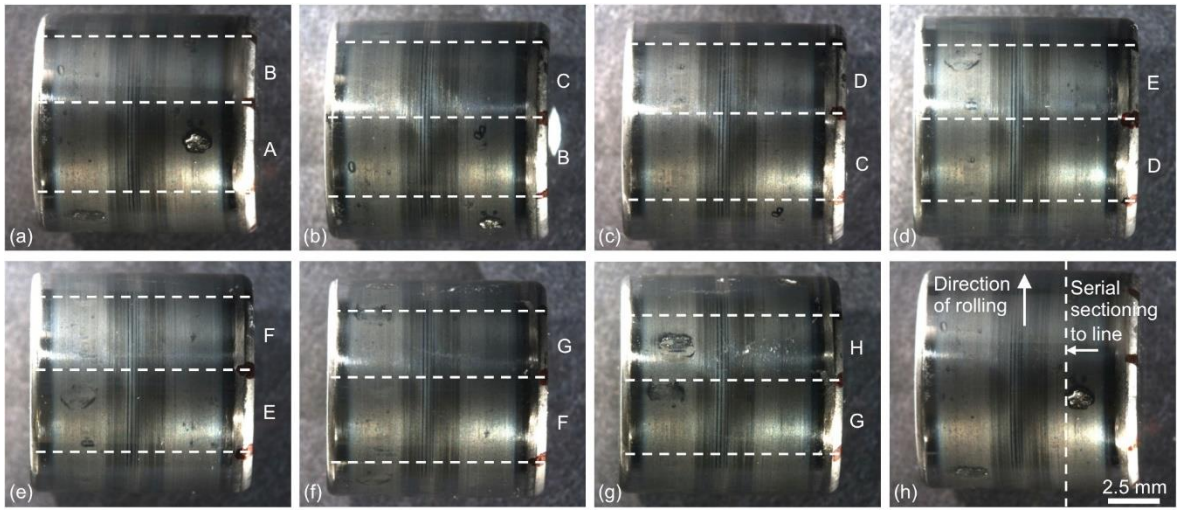

Figure C-5: Images of the single rolling element chosen for serial sectioning analysis. (a) – (g) eight zones (A – H) at 45-degree intervals (octants) were designated on the rolling elements surface and optical macro images taken of these zones. (h) same image as (a) showing rolling direction and zone of serial sectioning.

C.4.2 Subsurface examination

Washer raceway: upon examination of the washer raceway segments, although a few butterflies and very fine white etching 'lines' were observed, no extensive WECs were found. However, analysis on future test specimens is recommended to explore this further.

Rolling elements: examination of the three rolling elements showed extensive presence of WECs. Optical images of the typical WECs found in the rolling elements are shown in Figure C-6 and Figure C-7. WECs were found to form in all locations of the rolling elements and no particular formation distributions were observed. No formation of dark etching region (DER) was found in the subsurface of the rolling elements or raceway washer.

Figure C-6: Optical image of a typical WEC in the etched condition. Circumferential section, over-rolling direction right to left.

Serial sectioning of a rolling element: from the serial sectioning analysis conducted on one of the rolling elements, in total thirteen independent WECs were mapped and these varied in size, shape, orientation and location. Five of these WECs had optical images at every slice recorded; these images showing the cracks relative location with accompanying Vickers indent markers. Table C-2 summarises the features of these five WECs and the zones (see Figure C-5) in which they formed.

Table C-2: Matrix showing information of the five WECs that were recorded at each slice during serial sectioning. Data entries refer to inclusion-WEC interactions and their corresponding location.

Sectioning zone (µm)	**WEC 1** Zone B	**WEC 2-*S*** Zone C	**WEC 3** Zone C/D	**WEC 4-*S*** Zone E	**WEC 5-*S*** Zone E/F
0 - 75					
75 - 150					
150 - 225					
225 - 300					
300 - 375					
375 - 450					$D^{2\_80(2.5)}$, $D^{1\_59(2)*}$
450 - 525				$D_{sulf}^{1\_99(1.5)}$	$D_{sulf}^{1\_75(1.5)}$, $D_{sulf}^{2\_78(1.5)}$, $Ti(C,N)^{2\_175(1.5)}$
525 - 600		$D_{sulf}^{2\_103(1)}$		$A^{1\_105(C:6, A:\sim34)}$	$D_{Dup}^{2\_89(4)*}$, $D_{Dup}^{1\_90(1)*}$, $D_{Dup}^{2\_90(1)*}$, $D_{Dup}^{2\_80(C:4, A:\sim11)*}$, $D^{2\_85(2)}$ $D_{Dup}^{2\_92(C:2, A:\sim11)}$, $X^{1\_56(2)*}$, $D^{3\_241(3)}$, $D_{sulf}^{1\_81(1)*}$, $D^{2\_123(1.5)*}$
600 - 675		$D/D_{Dup}^{2\_52(2)*}$, $D_{sulf}^{3\_250(2)*}$, $D_{sulf}^{3\_80(1.5)}$		$D^{1\_111(4.5)}$, $D_{sulf}^{2\_132(4)}$	$D_{Dup}^{2\_239(1.5)}$, $D^{2\_94(2)*}$, $D_{DupTi(C,N)}^{2\_72(C:8, A:\sim11)}$
675 - 750					$D^{2\_86(6)}$
750 - 825	$D^{1\_154(C:8, A:\sim15)}$	$D_{Dup}^{2\_150(2)}$	$D^{3\_339(3)*}$		$D_{Dup}^{2\_133(5)}$, $D^{1\_290(9)}$, $D^{2\_132(5)}$
825 - 900		$D_{Dup}^{3\_238(2)}$	$D^{3\_266(2)*}$		$D^{2\_159(2.5)}$, $D^{1\_113(1)*}$
900 - 975		$D^{3\_187(3)*}$	$D_{sulf}^{1\_147(2.5)}$, $D_{Dup}^{2\_122(7)*}$		$D_{Dup}^{2\_78(2)}$
975 - 1050		$D_{DupTi(C,N)}^{1\_135(8)}$			$D_{Dup}^{2\_159(2.5)*}$
1050 - 1125			$X^{1\_141(2)}$		
1125 - 1200			$D^{1\_278(C:7.5, A:\sim15)}$		
1200 – 1275			$D_{Dup}^{2\_177(2)}$, $X^{2\_279(3)}$		
1275 - 1350			$D_{Dup}^{2\_201(5)}$		
1350 - 1425			$D^{3\_190(2)*}$		
1425 - 1500					
1500 - 1575					
1575 - 1650					
1650 - 1725					
1725 - 1800					
NMI Total (type)	1^1	1^1, 3^2, 4^3	3^1, 4^2, 3^3	3^1, 1^2	7^1, 18^2, 1^3
NMI Total	1	8	10	4	26

- See Figure C-8 for KEY to table data entries.

- The information of WEC length in the axial direction can be viewed under each WEC-# as shaded cells, indicating the first view and end view of the WEC during the serial sectioning process.

Inclusion type:

A: manganese sulfide or sulfide duplex, C: silicate, D: globular oxide, D_{sulf}: globular sulfide, D_{Dup}: globular duplex inclusion (e.g. globular manganese and/or calcium sulfide surrounding aluminate), $D_{DupTi(C,N)}$: globular sulfide with Ti(C,N), X: hole (assumed inclusion pull-out during polishing), Ti(C,N): titanium carbonitride, *: Assumed inclusion composition based on appearance in optical microscopy.

Appendix C

Only four of the thirteen WECs made a connection with the surface, the remaining nine WECs being entirely contained within the subsurface. Concerning the five WECs that were imaged at every slice, the WECs that connected with the contact surface had their connections over the following slices: WEC 2-*S* (slice 189 – 197), WEC 4-*S* (slice 28 – 119) and WEC 5-*S* (slice 42 – 57 (main connection) and 72 – 116 (secondary connection)). Figure C-7 shows example images of the contact surface connections.

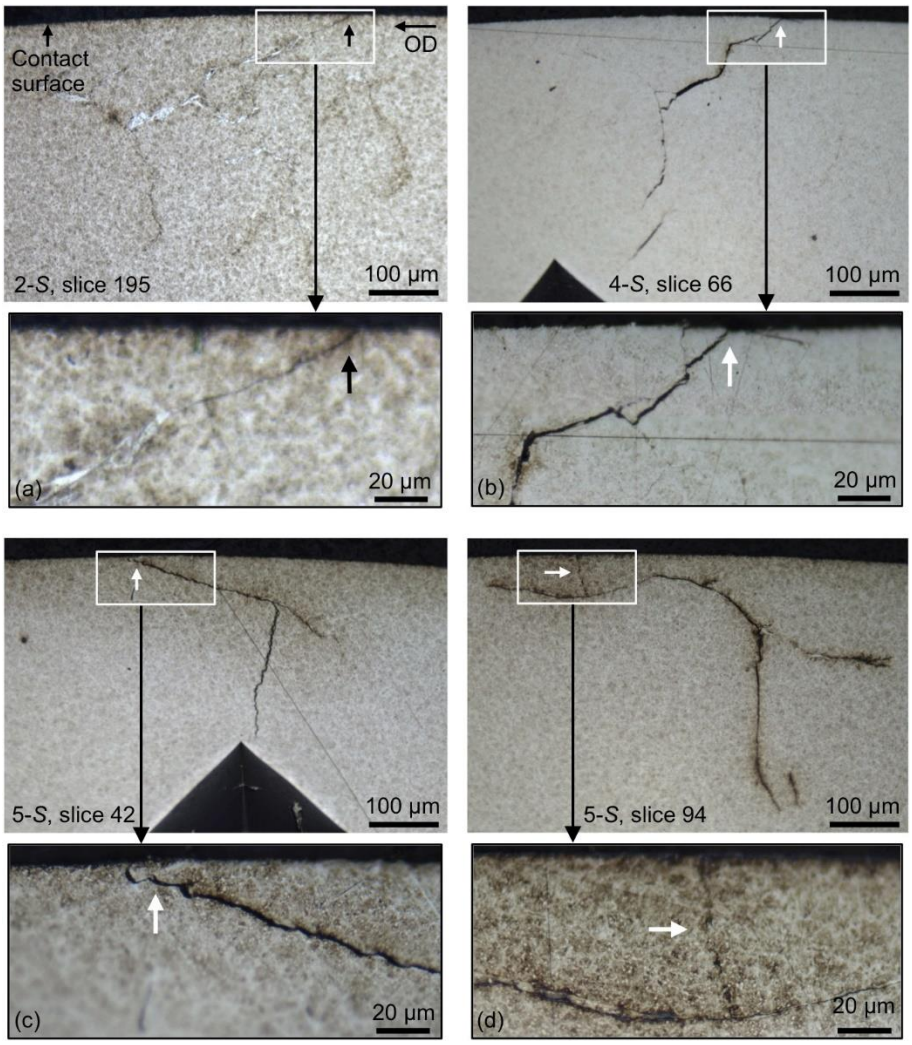

Figure C-7: Optical images of WEC contact surface interactions from Table 2. (a) WEC 2-*S* connects to the surface from slice 189 – 197 (see Video C.3 for a video showing all slices). (b) WEC 4-*S* connects to the surface from slice 28 – 119. (c) WEC 5-*S* contact surface connection (main) from slice 42 – 57. (d) WEC 5-*S* contact surface connection (secondary) from slice 72 – 116. Circumferential sections, over-rolling direction (OD) right to left.

Three WECs from Table C-1 (WEC 1, WEC 2-*S* and WEC 3) are shown to their full extent in this paper. The images obtained at each slice have been aligned into stacks of images and videos have been made to show orthoslice sweeps of the WECs and give a detailed view of the 3-dimensional nature of the cracks. See Video C.1 (WEC 1), Video C.2 (WEC 2-*S*) and Video C.3 (WEC 3). Note that

towards the end of Video C.1 (WEC 1) another separate WEC appears, however this is not connected to WEC 1.

From these five WECs, forty-nine inclusions in total were found to make interactions with the WECs. The data is summarised in Table C-1, including the inclusion type, location in the rolling element/WEC and likelihood of its initiation of the WECs (the later as a ranking from 1 to 3). A rank of 1 or 2 has been used for those inclusions that appear to have been involved in the initiation of the WEC, whereas a rank of 3 has been used when this did not appear to be the case. For a crack with the typical butterfly crack/wing orientation it is suggested that butterflies propagated to form WECs (rank 1), and if this relationship was not observed then it is suggested that the inclusions initiated cracks that propagated to become WECs (rank 2) (see the key above Figure C-8 and refer to C.5.4 and A.2 for more details on the ranking system). Small sized (~2 – 15 µm) sulfides (D_{sulf}), globular sulfide-oxides (D_{Dup} and $D_{DupTi(C,N)}$) and globular oxide inclusions (D) were the inclusions that were found to interact frequently with the WECs. Examples of inclusions interacting with the thirteen WECs can be viewed in Figure C-8(e) – Figure C-8(a-j) and Figure C-9. Figure C-8(a) – (h) show examples of the location of inclusions that interacted with a specific WEC (WEC 5-*S*, see Table C-1). Figure C-9 shows the same large oxide inclusion as that in Figure C-8(o) and shows the morphology and crack continuity over multiple slices. The spatial distribution and depth of inclusion–WEC interactions from the five WECs listed in Table C-1 that were judged to have a high likelihood of crack initiation (rank 1 & 2) are shown in Figure C-10.

Appendix C

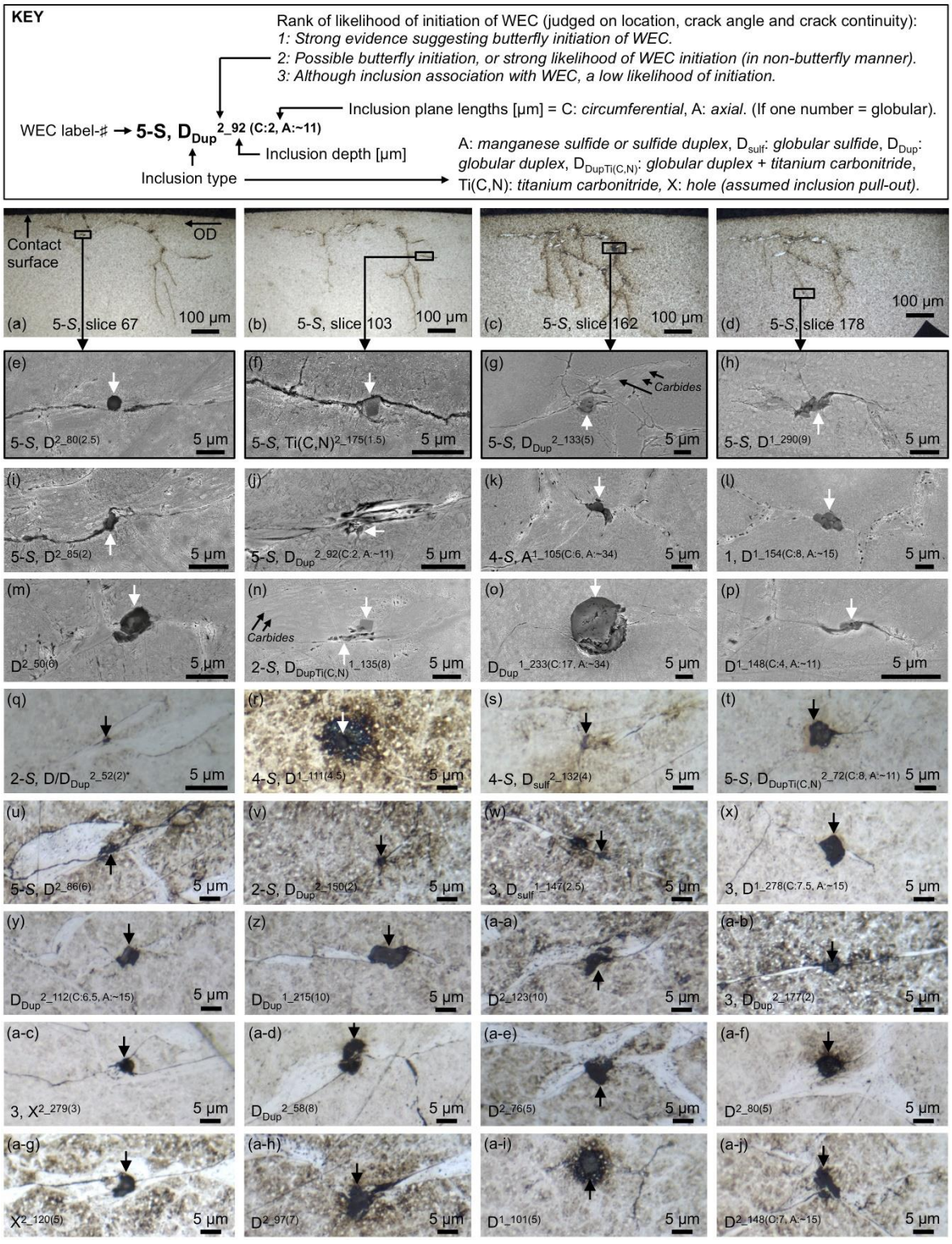

Figure C-8: Examples of inclusion-WEC interactions observed during serial sectioning. Images (a) – (d) show the location of the inclusions (e) – (h) respectively in WEC 5-*S*. Images (e) – (p) are SEM images and (q) – (a-j) are optical images. Small arrows highlight the inclusion in each case. A key above the image indicates how to interpret the information about each inclusion-WEC interaction. Images (g) and (n) show deformation of carbides inside the WEA. Circumferential sections, over-rolling direction (OD) right to left.

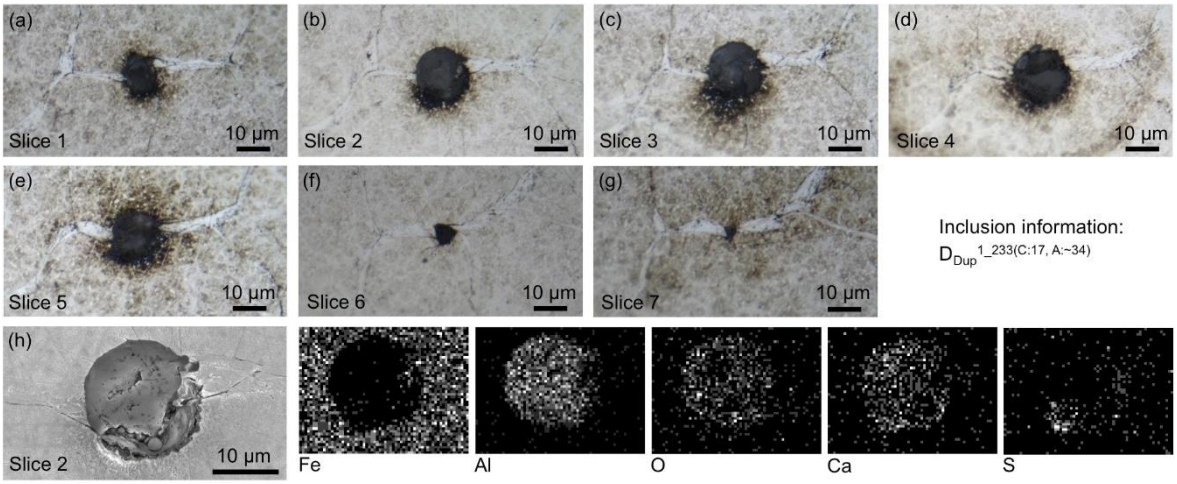

Figure C-9: Example of the large globular duplex inclusion shown in Figure C-8(o) showing the morphology and crack continuity over multiple slices. Images (a) – (g) are optical images and image (h) is a SEM image which corresponding EDX chemical maps.

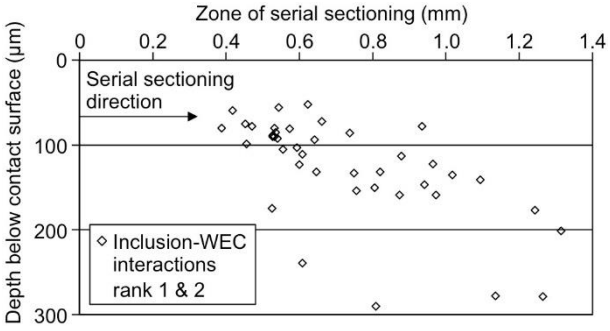

Figure C-10: Spatial distribution and depth of inclusion–WEC interactions that were judged to have a high likelihood of crack initiation (rank 1 & 2). Data from the five WECs in Table C-1.

White etching area (WEA) or small WECs were often found to be present in a zone less than 25 µm beneath the rolling elements surface and these features tend to span only a few slices, see examples given in Figure C-11.

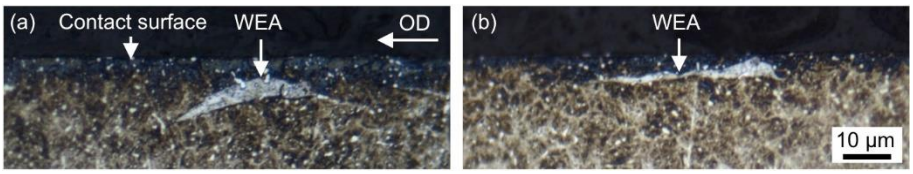

Figure C-11: Very near surface WEA/WECs in the rolling element.

C.5 Discussion

C.5.1 RCF test

Wind turbine gearbox bearings experience maximum contact pressures of ~1 – 2 GPa during service. In this study, WSF was created under very low contact pressures (P_{max}1.5 – 1.9 GPa) on bearings on the FAG-FE8 test rig, which is in contrast to many previous investigations that have used relatively high maximum contact pressures between 3 – 5.6 GPa in WSF RCF tests [60, 99, 104, 121, 187, 229-232]. This is important to consider, as use of unrealistically high contact pressures could lead to damage by different mechanisms. It must be noted that the dynamics of the FAG-FE8 test are different than those that would be experienced in wind turbine gearbox bearings.

It must be noted that the dynamics of the FAG-FE8 test in terms of the drill-like motion of the rolling elements under thrust loading are different than those that would be experienced in wind turbine gearbox bearings. However, some similarities exist. For example the FAG-FE8 test has a high amount of slip in conjunction with rolling contact (up to ± 12.5%, see Figure C-2). This compares to some wind turbine gearbox bearings, especially those of spherical type, which experience continuous moderate slip between 3 – 10% due to a geometrical constraint [199] and the possibility of high slip of ~30 - 110% during acceleration transients [199] (see introduction C.2). This is potentially important, as the amount of hydrogen penetrating into steel has been previously found to be proportional to the wear (nascent surface generation) on the steel during sliding wear tests [115] (see next section on oil influence, C.5.2). Another similarity between the FAG-FE8 test dynamics and another type of wind turbine gearbox bearing that suffers from WSF also exists, namely that of planet bearings that typically experience very low lambda ratios and boundary/mixed lubrication due to their low rpm. Contact of steel surfaces during boundary/mixed regimes could cause metal-to-metal contact, wear and tribo-chemical reactions that may cause hydrogen to be released and diffuse into the bearing steel.

Regarding the formation of WECs in the raceway washer, during the subsurface examination, although extensive sectioning and analysis were conducted, little evidence of WECs was found. It is not clear why this was the case, i.e. few extensive WECs formed (especially when a large number of WECs were formed in the rolling elements). Further investigation is thus recommended.

C.5.2 Influence of the oil

A 'special' lubricant, which was known to severely promote the occurrence of WSF, was purposely used in this study to aid the WECs formation.

Since the majority of WECs in this study did not make any connection to the contact surface, hydrogen diffusion is proposed to occur through wear induced nascent surfaces where hydrogen is generated by decomposition of lubricants through catalytic reactions [115]. Thermal desorption analysis (TDA) experiments are yet to be performed to confirm the level of diffusible hydrogen in the bearing components during RCF in this study. However, this proposition is supported by the observation that WECs would not have normally formed under the test conditions and environment used in this study, also that WECs and even the final flaking failure occurred extremely quickly in the test under a very low contact pressure (P_{max} 1.5 – 1.9 GPa) in very short time frame (18.5 hours, equating to a number of rolling cycles until flaking of 5.8 x 10^6 cycles on the rolling elements).

This mechanism of hydrogen entry is supported by a number of researchers who found that hydrogen diffused into steel during RCF tests [101, 104, 115, 121, 229] to concentrations between 0.1 – 4.2 ppm [101, 104, 115] and the amount of hydrogen that penetrated into steel was found to be proportional to the wear (nascent surface generation) on the steel [115]. It has also been shown in numerous studies that the lubricant and especially additives used can strongly control whether WSF occurs and how quickly [12, 53]. Various lubrication additives such as anti-corrosion sulfonates (sulphur acting to inhibit the recombination of molecular hydrogen to H_2 gas therefore allowing more hydrogen ions to enter the steel) have been shown to rapidly accelerate the formation of WSF, whereas other surface protecting additives or base oils containing no hydrogen radicals have been shown to offer degrees of prevention to WSF [53, 101, 120, 182]. These influences should be noted considering that the oil used in the FAG-FE8 cylindrical roller thrust bearing testing (non-hydrogen charged) was highly additised and known to promote WSF.

On the other hand, as some WECs made connection with the contact surface, for these particular WECs this could provide a route for hydrogen entry via the lubricant to accelerate the formation of these cracks. However, from the analyses conducted in this paper, features that were observed that count against this hypothesis are that; 1) some of the connections to the contact surface had small crack volumes, such as WEC 2-*S* and WEC 5-*S*, and (2) the angle the crack makes with the contact surface in relation to the over-rolling direction does not always match that suggested by other authors [64] who propose the surface crack initiation mechanism.

C.5.3 WEC characteristics

The inspection of WEA using serial sectioning observed in many cases that spherical carbide deformation or dissolution in the WEA was occurring (see Figure C-8(g) & Figure C-8(n)). This is due to the severe plastic deformation, dislocation interactions and grain refinement occurring in the local region. Detailed studies of carbide dissolution can be found in [41, 223].

No formation of dark etching region (DER) due to slip motions occurring was observed in either the washer raceway segments or the rolling elements analysed. This is expected due to the relatively low maximum contact pressure of 1200 MPa.

The presence of small sized very near surface WEA/WECs observed in the rolling elements (Figure C-11) has not often been reported in literature. However, the authors also found these to form in two-roller specimens under hydrogen charged testing conditions [37] and in analysis of actual wind turbine gearbox bearings from service. It has been found that these rarely connect with the surface and sometimes interact with inclusions [37].

C.5.4 Initiation and propagation of WECs

It is proposed that many of the WECs in this study were created from a network of cracks initiated from inclusions. As nine of the thirteen WECs mapped did *not* make any interaction with the contact surface, this makes surface crack initiation infeasible for these particular WECs. The four WECs that were connected to the surface could have initiated from cracking at the surface, however each of these WECs also interacted with multiple inclusions and some of the connections to the surface only had small crack volumes over few slices (WEC 2-*S* and WEC 5-*S*, see Figure C-7 and Video C.2). For those WECs with few inclusion interactions found (e.g. WEC 1 with only one) it should be remembered that some inclusion interactions may have been missed during the serial sectioning process that had ~3.8 µm material removal intervals. This is because the slice thickness is of the same order of magnitude as small globular inclusions that often interact with the WECs.

In the following more information is given concerning the ranking system for the likelihood of crack initiation at inclusions. The following characteristics of inclusion-WEC interactions were analysed to make an assumption on whether it is probable that a butterfly formation was involved (rank 1). i) The wing orientation (-ve or +ve) being consistent with those of independent butterflies. Butterfly crack/wing orientations are controlled by the direction of over-rolling, forming in either –ve or +ve orientations, where is has been shown that reversing rolling direction after a period of over-rolling forms a second pair of wings in the symmetric orientation [221]. During metallographic analysis of the rolling element, butterflies that did not interact with any WECs were identified and their wing orientation was noted (the butterflies showed a crack/wing

that was raised higher on the left side of the inclusion with respects to the right side when viewing the cross section). ii) The angle of the crack/wing (predominately ~45° with a range of 0 – 60° being consistent with typical butterfly formations [12, 26]), iii) The morphology of the microstructural change in respects to whether a 'classic wing-like pattern' with associated crack was present. See Figure C-8 (h, k, l, o) and Figure C-9 for examples. If features consistent with crack initiation were observed, but characteristics matching those of butterfly formations were not found, then it was suggested that the inclusions initiated cracks that propagated to become WECs (rank 2), see any superscript '2' in Figure C-8 for examples. It was judged that a crack passed through an inclusion and therefore the inclusion was not involved in the initiation of WECs (rank 3) when the following occurred. i) The cracks orientation interacting with the inclusion was in a radial or near radial direction as cracking initiated at inclusions due to RCF do not typically exhibit this relationship. ii) The location of the inclusion was somewhere along one of the radial (depth direction) forks of the WEC (e.g. see Figure C-6 and Figure C-8 (a-d) for examples of radial forks) and no microstructural change was observed around the crack. iii) The depth of the inclusion-WEC interaction was in a zone where the acting subsurface shear stress was low. iv) The inclusion was very small and was located inside an area of extensive microstructural change but no visible cracks connecting to the inclusion were observed.

Forty-one out of the forty-nine non-metallic inclusions that interacted with the five WECs shown in Table C-2 were ranked with a high likelihood for crack initiation (rank 1 or 2). The location below the contact surface of the majority of inclusion-WEC interactions is at 50 – 200 µm depth (see Figure C-10). Therefore the depth of the inclusion-crack interactions below the contact surface are consistent with the location of high subsurface shear stressing from rolling contact ($\tau_{o,max}$: 111 µm, τ_{max}: 175 µm) further supporting WEC initiation at inclusions. Small sized (~2 – 15 µm) sulfides (D_{sulf}), globular sulfide-oxides (D_{Dup} and $D_{DupTi(C,N)}$) and globular oxide inclusions (D) were the inclusions types found to interact most frequently with the WECs. Inclusions with oxide parts were found to be the type of inclusions that interacted the most with the WECs and appeared to be WEC initiators. This is expected due to the hardness mismatch with the tempered martensite matrix, poor coherence/debonding between the oxide part and matrix and the induced tensile residual stresses due to differing coefficient of thermal expansion compared to the matrix [12, 42, 86, 87].

The evidence gathered from this study under non-hydrogen charged testing conditions therefore confirm the proposition from references [36, 37, 39] that WECs can initiate and propagate entirely in the subsurface under RCF. Complete evidence from this paper through serial sectioning and from other studies [36, 37, 39] confirms that initiation of WECs by non-metallic inclusions is *one*

mechanism of WEC formation. It is important to consider that small sized inclusions (~2 – 20 µm) predominate as crack initiators in all the studies.

Referring to Figure C-7(d) a thin vertical crack can be observed to branch from the main WEC to the contact surface. It is proposed by the authors that this is a secondary crack that branched off from the main WEC due to the residual tensile stresses in the near surface of the martensitic steel. This could be an example of how subsurface propagated WECs eventually connect to the contact surface to cause flaking. In addition actual wind turbine gearbox bearings sometimes show hairline axial cracks on bearing raceways [77]. Figure C-7(d) from WEC 5-*S* could provide evidence of how hairline axial cracks form; i.e. propagated secondary to a subsurface WEC, rather than initiation of the hairline crack from the surface. Further work is required to verify this hypothesis.

C.6 Conclusions

WSF has been successfully reproduced in 100Cr6 steel cylindrical roller thrust bearings on an FAG-FE8 test rig. WSF was formed under RCF at low contact pressures (P_{max} 1.5 – 1.9 GPa) and *non*-hydrogen charged conditions. The application of serial sectioning has been used to map entire independent WECs formed under *non*-hydrogen charged conditions for the first time to confirm mechanisms of WEC formation. It was found that:

1. In total, nine of the thirteen WECs mapped did *not* make any interaction with the contact surface. This makes surface crack initiation infeasible for these particular WECs.
2. Strong evidence was found that WECs could be initiated by non-metallic inclusions. Regarding the five WECs focused on in this study, forty-nine non-metallic inclusions were found to make interaction and forty-one of these inclusions were ranked with a high likelihood for crack initiation.
3. Small sized (~2 – 15 µm) sulfides (type D_{sulf}), globular sulfide-oxides (type D_{Dup} and type $D_{DupTi(C,N)}$) and globular oxide inclusions (type D) predominated as crack initiators.
4. This study confirms that subsurface crack initiation and propagation of WECs is at least *one* of the mechanisms of WSF in bearing steels.

List of References and Permissions

1. Goch, G., W. Knapp, and F. Härtig, *Precision engineering for wind energy systems.* CIRP Annals, 2012. **61**(2): p. 611-634.

2. IRENA. *Renewable power generation*. 2017 [cited 2018 16 April]; Available from: https://www.irena.org/-/media/Files/IRENA/.../IRENA_2017_Power_Costs_2018.pdf.

3. WindEurope. *Wind in power 2017, Annual combined onshore and offshore wind energy statistics*. 2017 [cited 2018 16 April]; Available from: https://windeurope.org/wp-content/uploads/files/about-wind/statistics/WindEurope-Annual-Statistics-2017.pdf.

4. GEWEC, G.W.E.C. *Global Wind Statistics*. 2017 [cited 2018 16 April]; Available from: http://gwec.net/wp-content/uploads/vip/GWEC_PRstats2017_EN-003_FINAL.pdf.

5. REN21. *Renewables 2017, Global status report*. 2017 [cited 2018 16 April]; Available from: http://www.ren21.net/wp-content/uploads/2017/06/17-8399_GSR_2017_Full_Report_0621_Opt.pdf.

6. *European Commission (2010) Wind Energy Roadmap Implementation Plan, Developed by the European Wind Energy Technology Platform (TPWIND)- Secretariat, Published as Part of the Strategic Energy Technology Plan (SETPlan).*

7. *International Eletrotechnical Comission. IEC 61400-1 Wind Turbines - Part 1: Design requirements; 2005.*

8. Van Rensselar, J., *The elephant in the wind turbine.* Tribology & Lubrication Technology, 2010. **66**(6): p. 38.

9. Sheng, S., *Report on Wind Turbine Subsystem Reliability-A Survey of Various Databases (Presentation)*. 2013, National Renewable Energy Lab.(NREL), Golden, CO (United States).

10. Energiforsk. *Wind Turbine Gearboxes*. 2016 [cited 2018 18 April]; Available from: https://energiforskmedia.blob.core.windows.net/media/21270/wind-turbine-gearboxes-energiforskrapport-2016-279.pdf.

11. Greco, A., et al., *Material wear and fatigue in wind turbine systems.* Wear, 2013. **302**(1): p. 1583-1591.

12. Evans, M.H., *White structure flaking (WSF) in wind turbine gearbox bearings: effects of 'butterflies' and white etching cracks (WECs).* Materials Science and Technology, 2012. **28**(1): p. 3-22.

13. Yagi, S. and N. NINOYU, *Technical trends in wind turbine bearings.* TECHNICAL REVIEW, 2008.

14. Kotzalas, M.N. and G.L. Doll, *Tribological advancements for reliable wind turbine performance.* Philosophical Transactions of the Royal Society of London A: Mathematical, Physical and Engineering Sciences, 2010. **368**(1929): p. 4829-4850.

15. Terrell, E.J., W.M. Needelman, and J.P. Kyle, *Wind turbine tribology*, in *Green Tribology*. 2012, Springer. p. 483-530.

16. Hatch, C., A. Weiss, and M. Kalb, *Cracked bearing race detection in wind turbine gearboxes.* Orbit, 2010. **30**(1).

17. Sheng, S., M. McDade, and R. Errichello, *Wind Turbine Gearbox Failure Modes-A Brief (Presentation)*. 2011, National Renewable Energy Laboratory (NREL), Golden, CO.

18. (NREL), U.S.D.o.E.a.N.R.E.L. *Statistics Show Bearing Problems Cause the Majority of Wind Turbine Gearbox Failures*. 2015 [cited 2018 20 April]; Available from: https://www.energy.gov/eere/wind/articles/statistics-show-bearing-problems-cause-majority-wind-turbine-gearbox-failures.

19. Errichello, R., R. Budny, and R. Eckert, *Investigations of bearing failures associated with white etching areas (WEAs) in wind turbine gearboxes.* Tribology Transactions, 2013. **56**(6): p. 1069-1076.

20. Stadler, K. and A. Studenrauch, *Premature bearing failures in wind gearboxes and white etching cracks (WEC).* SKF Evol., March, 2013.

21. Rasmussen, F., K. Thomsen, and T.J. Larsen, *The gearbox problem revisited.* Risø Fact-Sheet AED-RB-17 (en), Risø National Laboratory, Roskilde, DenmarK, 2004.

22. Ragheb, A. and M. Ragheb. *Wind turbine gearbox technologies*. in *Nuclear & Renewable Energy Conference (INREC), 2010 1st International*. 2010. IEEE.

23. Vries, E.d. *Wind turbine gearboxes and the effort to improve their reliability*. 2010 [cited 2018 23 April]; Available from: https://www.windpowermonthly.com/article/1010395/wind-turbine-gearboxes-effort-improve-reliability.

24. Burton, T., D. Sharpe, and N. Jenkins, *Handbook of wind energy*. 2001: John Wiley & Sons.

25. Rosinski, J. and D. Smurthwaite, *Troubleshooting wind gearbox problems.* Gear Solutions, 2010. **8**: p. 22-33.

26. Evans, M.-H., *White structure flaking failure in bearings under rolling contact fatigue*. 2013, University of Southampton.

27. Du Crehu, A.R., *Tribological analysis of White Etching Crack (WEC) failures in rolling element bearings*. 2014, INSA de Lyon.

28. Hau, E. and H. von Renouard, *Wind turbines: fundamentals, technologies, application, economics*. 2003: Springer.

29. Tallian, T., *Failure atlas for rolling bearings in wind turbines*. 2006, National Renewable Energy Laboratory (NREL), Golden, CO.

30. Whittle, M., J. Trevelyan, and P. Tavner, *Bearing currents in wind turbine generators.* Journal of Renewable and Sustainable Energy, 2013. **5**(5): p. 053128.

31. Vance, J.M., A.B. Palazzolo, and F.Y. Zeidan. *Electric Shaft Currents In Turbomachinery*. in *Proceedings of the 16th Turbomachinery Symposium*. 1987. Texas A&M University. Turbomachinery Laboratories.

32. Prashad, H., *Tribology in electrical environments*. Vol. 49. 2005: Elsevier.

33. Lundberg, G., *Dynamic Capacity of Rolling Bearings, Acta Polytechnica.* Mechnical Engineering Series, 1947.

34. Umeda, A., T. Shiga, and K. Ihata, *Rolling bearing incorporated in auxiliary device for internal combustion engine*. 2009, Google Patents.

35. Bearings, N. *Modular system for planetary bearings in wind turbine gearboxes (Germany)*. [cited 2018 20 April]; Available from: http://www.nke.at/en/bearings-applications/special-bearings/modular-bearing-system-for-planetary-wind-turbine-gearboxes/.

36. Evans, M.-H., et al., *Serial sectioning investigation of butterfly and white etching crack (WEC) formation in wind turbine gearbox bearings.* Wear, 2013. **302**(1-2): p. 1573-1582.

37. Evans, M.-H., et al., *Effect of hydrogen on butterfly and white etching crack (WEC) formation under rolling contact fatigue (RCF).* Wear, 2013. **306**(1-2): p. 226-241.

38. Evans, M.-H., et al., *Confirming subsurface initiation at non-metallic inclusions as one mechanism for white etching crack (WEC) formation.* Tribology International, 2014. **75**: p. 87-97.

39. Evans, M.-H., et al., *White etching crack (WEC) investigation by serial sectioning, focused ion beam and 3-D crack modelling.* Tribology International, 2013. **65**: p. 146-160.

40. Becker, P., *Microstructural changes around non-metallic inclusions caused by rolling-contact fatigue of ball-bearing steels.* Metals Technology, 1981. **8**(1): p. 234-243.

41. Evans, M.-H., et al., *A FIB/TEM study of butterfly crack formation and white etching area (WEA) microstructural changes under rolling contact fatigue in 100Cr6 bearing steel.* Materials Science and Engineering: A, 2013. **570**: p. 127-134.

42. Grabulov, A., R. Petrov, and H. Zandbergen, *EBSD investigation of the crack initiation and TEM/FIB analyses of the microstructural changes around the cracks formed under rolling contact fatigue (RCF).* International Journal of Fatigue, 2010. **32**(3): p. 576-583.

43. Österlund, R., et al., *Butterflies in fatigued ball bearings-formation mechanism and structure.* Scand. J. Metall, 1982. **11**(23): p. e32.

44. Solano-Alvarez, W. and H. Bhadeshia, *White-etching matter in bearing steel. Part II: distinguishing cause and effect in bearing steel failure.* Metallurgical and Materials Transactions A, 2014. **45**(11): p. 4916-4931.

45. West, O., et al., *Application of complementary techniques for advanced characterization of white etching cracks.* Practical Metallography, 2013. **50**(6): p. 410-431.

46. Grabulov, A., U. Ziese, and H. Zandbergen, *TEM/SEM investigation of microstructural changes within the white etching area under rolling contact fatigue and 3-D crack reconstruction by focused ion beam.* Scripta Materialia, 2007. **57**(7): p. 635-638.

47. Harada, H., et al., *Microstructural changes and crack initiation with white etching area formation under rolling/sliding contact in bearing steel.* ISIJ international, 2005. **45**(12): p. 1897-1902.

48. Kadin, Y. and M.Y. Sherif, *Energy dissipation at rubbing crack faces in rolling contact fatigue as the mechanism of white etching area formation.* International Journal of Fatigue, 2017. **96**: p. 114-126.

49. Li, S.-X., et al., *Microstructural evolution in bearing steel under rolling contact fatigue.* Wear, 2017. **380**: p. 146-153.

50. Grabulov, A., *Fundamentals of rolling contact fatigue.* 2010.

51. Diederichs, A., et al. *Observation of deformation induced redistribution of chromium and carbon in bearing steel*. in *Microscopy conference*. 2015.

52. Diederichs, A.M., et al., *Electron microscopy analysis of structural changes within white etching areas.* Materials Science and Technology, 2016. **32**(16): p. 1683-1693.

53. Holweger, W., *Progresses in solving White etching crack phenoma.* NREL-Gearbox Reliability Collaborative, Golden, Colorado, 2014: p. 45.

54. Holweger, W., et al., *White Etching Crack Root Cause Investigations.* Tribology Transactions, 2015. **58**(1): p. 59-69.

55. Ščepanskis, M., et al., *The numerical model of electrothermal deformations of carbides in bearing steel as the possible cause of white etching cracks initiation.* Tribology Letters, 2015. **59**(2): p. 37.

56. Šmeļova, V., et al., *Microstructural changes in White Etching Cracks (WECs) and their relationship with those in Dark Etching Region (DER) and White Etching Bands (WEBs) due to Rolling Contact Fatigue (RCF).* International Journal of Fatigue, 2017. **100**: p. 148-158.

57. Šmeļova, V., et al., *Electron microscopy investigations of microstructural alterations due to classical Rolling Contact Fatigue (RCF) in martensitic AISI 52100 bearing steel.* International Journal of Fatigue, 2017. **98**: p. 142-154.

58. Rumpf, V., *A Study on the Microstructural Alterations in WEC, DER, LAB, and HAB in rolling contacts*. 2018, University of Southampton.

59. Bhadeshia, H. and W. Solano-Alvarez, *Critical assessment 13: elimination of white etching matter in bearing steels.* Materials Science and Technology, 2015. **31**(9): p. 1011-1015.

60. Vegter, R. and J. Slycke, *The role of hydrogen on rolling contact fatigue response of rolling element bearings.* Journal of ASTM international, 2009. **7**(2): p. 1-12.

61. Gould, B. and A. Greco, *The influence of sliding and contact severity on the generation of white etching cracks.* Tribology Letters, 2015. **60**(2): p. 29.

62. Paladugu, M., D.R. Lucas, and R. Scott Hyde, *Effect of lubricants on bearing damage in rolling-sliding conditions: Evolution of white etching cracks.* Wear, 2018. **398-399**: p. 165-177.

63. Diederichs, A.M., et al., *Study of subsurface initiation mechanism for white etching crack formation.* Materials Science and Technology, 2016. **32**(11): p. 1170-1178.

64. Gegner, J.r., *Tribological aspects of rolling bearing failures*, in *Tribology-lubricants and lubrication*. 2011, InTech.

65. Danielsen, H.K., et al., *Multiscale characterization of White Etching Cracks (WEC) in a 100Cr6 bearing from a thrust bearing test rig.* Wear, 2017. **370**: p. 73-82.

66. Gould, B., et al., *Using advanced tomography techniques to investigate the development of White Etching Cracks in a prematurely failed field bearing.* Tribology International, 2017. **116**: p. 362-370.

67. Gould, B., et al., *An analysis of premature cracking associated with microstructural alterations in an AISI 52100 failed wind turbine bearing using X-ray tomography.* Materials & Design, 2017. **117**: p. 417-429.

68. Gegner, J. and W. Nierlich. *The bearing axial cracks root cause hypothesis of frictional surface crack initiation and corrosion fatigue driven crack growth*. in *NREL wind turbine tribology seminar*. 2011.

69. Holweger, W. *Influence on bearing life by new material phenomena*. in *NREL-Wind Turbine Tribology Seminar, November*. 2011.

70. Gegner, J. and W. Nierlich. *Service loading analysis of wind turbine gearbox rolling bearings based on X-ray diffraction residual stress measurements*. in *Materials Science Forum*. 2014. Trans Tech Publ.

71. Hyde, R. *White etching areas: importance of microstructural characterization and modeling*. in *Gearbox reliability collaborative all members meeting, NREL Golden, CO*. 2014.

72. Grujicic, M., et al., *Wind-turbine gear-box roller-bearing premature-failure caused by grain-boundary hydrogen embrittlement: A multi-physics computational investigation.* Journal of materials engineering and performance, 2014. **23**(11): p. 3984-4001.

73. Grujicic, M., et al., *Multiphysics computational analysis of white-etch cracking failure mode in wind turbine gearbox bearings.* Proceedings of the Institution of Mechanical Engineers, Part L: Journal of Materials: Design and Applications, 2016. **230**(1): p. 43-63.

74. Evans, M.-H., *An updated review: white etching cracks (WECs) and axial cracks in wind turbine gearbox bearings.* Materials Science and Technology, 2016. **32**(11): p. 1133-1169.

75. Evans, M., L. Wang, and R. Wood, *Formation mechanisms of white etching cracks and white etching area under rolling contact fatigue.* Proceedings of the Institution of Mechanical Engineers, Part J: Journal of Engineering Tribology, 2014. **228**(10): p. 1047-1062.

76. Bruce, T., et al., *Characterisation of white etching crack damage in wind turbine gearbox bearings.* Wear, 2015. **338**: p. 164-177.

77. Luyckx, J. *Hammering wear impact fatigue hypothesis WEC/irWEA failure mode on roller bearings*. in *NREL Workshop*. 2011.

78. Luyckx, J., *White etching crack failure mode in roller bearings: from observation via analysis to understanding and an industrial solution*, in *Rolling element bearings*. 2012, ASTM International.

79. Stadler, K., J. Lai, and R. Vegter, *A review: the dilemma with premature white etching crack (WEC) bearing failures*, in *Bearing Steel Technologies: 10th Volume, Advances in Steel Technologies for Rolling Bearings*. 2015, ASTM International.

80. Uyama, H. and H. Yamada, *White structure flaking in rolling bearings for wind turbine gearboxes.* AGMA Technical Paper, 13FTM15, 2013.

81. Gould, B. and A. Greco, *Investigating the process of white etching crack initiation in bearing steel.* Tribology Letters, 2016. **62**(2): p. 26.

82. Franke, J., et al., *White Etching Cracking—Simulation in Bearing Rig and Bench Tests.* Tribology Transactions, 2017: p. 1-11.

83. Haque, T., et al., *Lubricant Effects on White Etching Cracking Failures in Thrust Bearing Rig Tests.* Tribology Transactions, 2018: p. 1-33.

84. Bruce, T., H. Long, and R.S. Dwyer-Joyce, *Threshold Maps for Inclusion-Initiated Micro-Cracks and White Etching Areas in Bearing Steel: The Role of Impact Loading and Surface Sliding.* Tribology Letters, 2018. **66**(3): p. 111.

85. Al-Tameemi, H.A., H. Long, and R.S. Dwyer-Joyce, *Initiation of sub-surface micro-cracks and white etching areas from debonding at non-metallic inclusions in wind turbine gearbox bearing.* Wear, 2018. **406-407**: p. 22-32.

86. Lund, T.B., *Sub-surface initiated rolling contact fatigue—influence of non-metallic inclusions, processing history, and operating conditions.* Journal of ASTM International, 2010. **7**(5): p. 1-12.

87. Vincent, A., et al., *From white etching areas formed around inclusions to crack nucleation in bearing steels under rolling contact fatigue*, in *Bearing steels: into the 21st century*. 1998, ASTM International.

88. Ruellan, A., et al., *Understanding white etching cracks in rolling element bearings: The effect of hydrogen charging on the formation mechanisms.* Proceedings of the Institution of Mechanical Engineers, Part J: Journal of Engineering Tribology, 2014. **228**(11): p. 1252-1265.

89. ISO, *Steel – determination of content of nonmetallic inclusions – micrographic method using standard diagrams*. ISO 4967, ISO, Geneve, Switzerland, 2013.

90. Murakami, Y. and S. Beretta, *Small defects and inhomogeneities in fatigue strength: experiments, models and statistical implications.* Extremes, 1999. **2**(2): p. 123-147.

91. Cerullo, M. and V. Tvergaard, *Micromechanical study of the effect of inclusions on fatigue failure in a roller bearing.* International Journal of Structural Integrity, 2015. **6**(1): p. 124-141.

92. Franke, J., et al. *Influence of tribolayer on rolling bearing fatigue performed on a FE8 test rig*. in *TAE 19th international colloquium tribology*. 2014.

93. Gutiérrez Guzmán, F., et al., *Reproduction of white etching cracks under rolling contact loading on thrust bearing and two-disc test rigs.* Wear, 2017. **390**(Supplement C): p. 23-32.

94. Gutiérrez Guzmán, F., et al., *Influence of Slip and Lubrication Regime on the Formation of White Etching Cracks on a Two-Disc Test Rig.* Lubricants, 2018. **6**(1): p. 8.

95. Kruhöffer, W. and J. Loos, *WEC formation in rolling bearings under mixed friction: influences and "friction energy accumulation" as indicator.* Tribology Transactions, 2017. **60**(3): p. 516-529.

96. Fujita, S., N. Mitamura, and Y. Murakami. *Research of new factors affecting rolling contact fatigue life*. in *World tribology congress III*. 2005. American Society of Mechanical Engineers.

97. Tanaka, S., N. Mitamura, and Y. Murakami, *Influence of sliding and chromium content in the steel on the white structural change under rolling contact.* Proc. Global Powertrain Cong., Dearborn, MI, USA, 2004: p. 6-13.

98. Uyama, H. *The mechanism of white structure flaking in rolling bearings*. in *National renewable energy laboratory wind turbine tribology seminar*. 2011.

99. Hiraoka, K., et al., *Generation process observation of micro-structural change in rolling contact fatigue by hydrogen-charged specimens.* Journal of Japanese Society of Tribologists, 2007. **52**(12): p. 888-895.

100. Loos, J., et al., *Influences on generation of white etching crack networks in rolling bearings.* J. Mech. Eng. Autom, 2016. **6**: p. 85-94.

101. Tamada, K. and H. Tanaka, *Occurrence of brittle flaking on bearings used for automotive electrical instruments and auxiliary devices.* Wear, 1996. **199**(2): p. 245-252.

102. Hamada, H. and Y. Matsubara, *The influence of hydrogen on tension-compression and rolling contact fatigue properties of bearing steel.* NTN Technical Review, 2006. **74**: p. 54-61.

103. Janakiraman, S., et al., *Observations of the effect of varying Hoop stress on fatigue failure and the formation of white etching areas in hydrogen infused 100Cr6 steel rings.* International Journal of Fatigue, 2015. **77**: p. 128-140.

104. Kino, N. and K. Otani, *The influence of hydrogen on rolling contact fatigue life and its improvement.* JSAE review, 2003. **24**(3): p. 289-294.

105. Newlands, C., A. Olver, and N. Brandon, *Gaseous evolution of hydrogen from hydrocarbon oil and grease lubricated contacts.* Tribology Series, 2003. **41**: p. 719-726.

106. Szost, B. and P. Rivera-Diaz-del-Castillo, *Unveiling the nature of hydrogen embrittlement in bearing steels employing a new technique.* Scripta Materialia, 2013. **68**(7): p. 467-470.

107. Ooi, S.W., et al., *Evolution of white-etching cracks and associated microstructural alterations during bearing tests.* Materials Science and Technology, 2017. **33**(14): p. 1657-1666.

108. Sreeraj, K. and P. Ramkumar, *Replication of white etching area evolution using novel modified dynamic load pin-on-disc tribometer on bearing steel.* Tribology International, 2018. **126**: p. 336-343.

109. Birnbaum, H.K. and P. Sofronis, *Hydrogen-enhanced localized plasticity—a mechanism for hydrogen-related fracture.* Materials Science and Engineering: A, 1994. **176**(1-2): p. 191-202.

110. Oriani, R., *Whitney award lecture—1987: hydrogen—the versatile embrittler.* Corrosion, 1987. **43**(7): p. 390-397.

111. Nagumo, M., *Hydrogen related failure of steels–a new aspect.* Materials Science and Technology, 2004. **20**(8): p. 940-950.

112. Fujita, S., et al., *Effect of hydrogen on Mode II fatigue crack behavior of tempered bearing steel and microstructural changes.* International Journal of Fatigue, 2010. **32**(6): p. 943-951.

113. Murakami, Y., et al., *Hydrogen Embrittlement Mechanism in Fatigue of Austenitic Stainless Steels.* Metallurgical and Materials Transactions A, 2008. **39**(6): p. 1327.

114. Lewis, M. and B. Tomkins, *A fracture mechanics interpretation of rolling bearing fatigue.* Proceedings of the Institution of Mechanical Engineers, Part J: Journal of Engineering Tribology, 2012. **226**(5): p. 389-405.

115. Kohara, M., T. Kawamura, and M. Egami, *Study on mechanism of hydrogen generation from lubricants.* Tribology Transactions, 2006. **49**(1): p. 53-60.

116. Tanimoto, H., H. Tanaka, and J. Sugimura, *Observation of hydrogen permeation into fresh bearing steel surface by thermal desorption spectroscopy.* Tribology Online, 2011. **6**(7): p. 291-296.

117. Grunberg, L., D. Jamieson, and D. Scott, *Hydrogen penetration in water-accelerated fatigue of rolling surfaces.* Philosophical Magazine, 1963. **8**(93): p. 1553-1568.

118. Matsubara, Y. and H. Hamada, *A novel method to evaluate the influence of hydrogen on fatigue properties of high strength steels.* Journal of ASTM International, 2005. **3**(2): p. 1-13.

119. Nagumo, M., M. Nakamura, and K. Takai, *Hydrogen thermal desorption relevant to delayed-fracture susceptibility of high-strength steels.* Metallurgical and Materials Transactions A, 2001. **32**(2): p. 339-347.

120. Mikami, H. and T. Kawamura, *Influence of electrical current on bearing flaking life*. 2007, SAE Technical Paper.

121. Iso, K., A. Yokouchi, and H. Takemura, *Research work for clarifying the mechanism of white structure flaking and extending the life of bearings*. 2005, SAE Technical Paper.

122. Kadin, Y., *Modeling of hydrogen transport in static and rolling contact.* Tribology Transactions, 2015. **58**(2): p. 260-273.

123. Winzer, N. and I. Khader, *Hydrogen diffusion and trapping in bodies undergoing rolling contact.* Wear, 2013. **303**(1): p. 451-458.

124. Konstantarakis, C., *Hydrogen degradation of high strength steel weldments*. 1993, Massachusetts Institute of Technology.

125. Solano-Alvarez, W., et al., *Cracks in martensite plates as hydrogen traps in a bearing steel.* Metallurgical and Materials Transactions A, 2015. **46**(2): p. 665-673.

126. *ISO 3690:2012, Welding and allied processes - Determination of hydrogen content in arc weld metal.*

127. Enomoto, M., D. Hirakami, and T. Tarui, *Thermal desorption analysis of hydrogen in high strength martensitic steels.* Metallurgical and Materials Transactions A, 2012. **43**(2): p. 572-581.

128. Szost, B., R. Vegter, and P. Rivera-Díaz-del-Castillo, *Developing bearing steels combining hydrogen resistance and improved hardness.* Materials & Design, 2013. **43**: p. 499-506.

129. Murakami, Y. and H. Matsunaga, *The effect of hydrogen on fatigue properties of steels used for fuel cell system.* International Journal of Fatigue, 2006. **28**(11): p. 1509-1520.

130. Takai, K., et al., *Lattice defects dominating hydrogen-related failure of metals.* Acta Materialia, 2008. **56**(18): p. 5158-5167.

131. Ciruna, J. and H. Szieleit, *The effect of hydrogen on the rolling contact fatigue life of AISI 52100 and 440C steel balls.* Wear, 1973. **24**(1): p. 107-118.

132. Hirth, J.P., *Effects of hydrogen on the properties of iron and steel.* Metallurgical Transactions A, 1980. **11**(6): p. 861-890.

133. Lee, J. and J.Y. Lee, *Hydrogen trapping in AISI 4340 steel.* Metal science, 2013.

134. Nagumo, M., K. Takai, and N. Okuda, *Nature of hydrogen trapping sites in steels induced by plastic deformation.* Journal of alloys and compounds, 1999. **293**: p. 310-316.

135. Otsuka, T., et al., *Observation of hydrogen distribution around non-metallic inclusions in steels with tritium microautoradiography.* Fusion science and technology, 2005. **48**(1): p. 708-711.

136. Park, Y., et al., *Retained austenite as a hydrogen trap in steel welds.* Welding Journal-New York-, 2002. **81**(2): p. 27-S.

137. Ray, D., et al., *Hydrogen embrittlement of a stainless ball bearing steel.* Wear, 1980. **65**(1): p. 103-111.

138. Solheim, K.G., et al., *The role of retained austenite in hydrogen embrittlement of supermartensitic stainless steel.* Engineering Failure Analysis, 2013. **34**: p. 140-149.

139. Walton, H. *Ubiquitous hydrogen*. in *19 th ASM Heat Treating Society Conference and Exposition including Steel Heat Treating in the New Millenium: An International Symposium in Honor of Professor George Krauss*. 1999.

140. Michler, T. and M.P. Balogh, *Hydrogen environment embrittlement of an ODS RAF steel–Role of irreversible hydrogen trap sites.* international journal of hydrogen energy, 2010. **35**(18): p. 9746-9754.

141. Pressouyre, G., *A classification of hydrogen traps in steel.* Metallurgical Transactions A, 1979. **10**(10): p. 1571-1573.

142. Tanaka, S. and Y. Murakami, *Rolling bearing*. 2008, Google Patents.

143. Hsu, S.M. and R.S. Gates, *Effect of materials on tribochemical reactions between hydrocarbons and surfaces.* Journal of Physics D: Applied Physics, 2006. **39**(15): p. 3128.

144. Sakamoto, T., et al., *The reaction layer formed on steel by additives based on sulphur and phosphorus compounds under conditions of boundary lubrication.* Wear, 1982. **77**(2): p. 139-157.

145. L'Hostis, B., et al., *Influence of lubricant formulation on rolling contact fatigue of gears – interaction of lubricant additives with fatigue cracks.* Wear, 2017. **382-383**: p. 113-122.

146. Meheux, M., et al., *Effect of lubricant additives in rolling contact fatigue.* Proceedings of the Institution of Mechanical Engineers, Part J: Journal of Engineering Tribology, 2010. **224**(9): p. 947-955.

147. Wan, G.T.Y., et al., *The Effect of Extreme Pressure (EP) Lubricants on the Life of Rolling Element Bearings.* Proceedings of the Institution of Mechanical Engineers, Part J: Journal of Engineering Tribology, 1994. **208**(4): p. 247-252.

148. Thompson, A.W. and I. Bernstein, *The role of metallurgical variables in hydrogen-assisted environmental fracture*, in *Advances in corrosion science and technology*. 1980, Springer. p. 53-175.

149. Han, B., J. Binns, and I. Nedelcu, *In situ detection of hydrogen uptake from lubricated rubbing contacts.* Tribology Online, 2016. **11**(2): p. 450-454.

150. Taylor, L. and H. Spikes, *Friction-enhancing properties of ZDDP antiwear additive: part I—friction and morphology of ZDDP reaction films.* Tribology Transactions, 2003. **46**(3): p. 303-309.

151. Lainé, E., et al., *The Effect of a Friction Modifier Additive on Micropitting.* Tribology Transactions, 2009. **52**(4): p. 526-533.

152. Ščepanskis, M., B. Gould, and A. Greco, *Empirical Investigation of Electricity Self-Generation in a Lubricated Sliding–Rolling Contact.* Tribology Letters, 2017. **65**(3): p. 109.

153. Richardson, A.D., et al., *The Evolution of White Etching Cracks (WECs) in Rolling Contact Fatigue-Tested 100Cr6 Steel.* Tribology Letters, 2017. **66**(1): p. 6.

154. Wright, J. *The Role of Extreme Pressure Additives in Gear Oil*. [cited 2018 27/02/2018]; Available from: http://www.machinerylubrication.com/read/28470/role-of-extreme-pressure-additives-in-gear-oil-?utm_content=67416001&utm_medium=social&utm_source=linkedin.

155. Rounds, F.G., *Additive Interactions and Their Effect on the Performance of a Zinc Dialkyl Dithiophosphate.* ASLE Transactions, 1978. **21**(2): p. 91-101.

156. Costello, M.T., R.A. Urrego, and M. Kasrai, *Study of surface films of crystalline and amorphous overbased sulfonates and sulfurized olefins by X-ray absorption near edge structure (XANES) spectroscopy.* Tribology Letters, 2007. **26**(2): p. 173-180.

157. Inoue, K. and H. Watanabe, *Interactions of Engine Oil Additives.* A S L E Transactions, 1983. **26**(2): p. 189-199.

158. Zhang, J., E. Yamaguchi, and H. Spikes, *The antagonism between succinimide dispersants and a secondary zinc dialkyl dithiophosphate.* Tribology Transactions, 2014. **57**(1): p. 57-65.

159. Fujita, H. and H.A. Spikes, *Study of Zinc Dialkyldithiophosphate Antiwear Film Formation and Removal Processes, Part II: Kinetic Model.* Tribology Transactions, 2005. **48**(4): p. 567-575.

160. Matsui, Y., S. Aoki, and M. Masuko, *Influence of coexisting functionalized polyalkylmethacrylates on the formation of ZnDTP-derived tribofilm.* Tribology International, 2016. **100**: p. 152-161.

161. Topolovec-Miklozic, K., T.R. Forbus, and H. Spikes, *Film Forming and Friction Properties of Overbased Calcium Sulphonate Detergents.* Tribology Letters, 2008. **29**(1): p. 33-44.

162. Yamaguchi, E.S., et al., *Boundary Film Formation by ZnDTPs and Detergents Using ECR.* Tribology Transactions, 1998. **41**(2): p. 262-272.

163. Liston, T.V., *Engine lubricant additives what they are and how they function.* Lubrication engineering, 1992. **48**(5): p. 389-397.

164. Kapsa, P., et al., *Antiwear Mechanism of ZDDP in the Presence of Calcium Sulfonate Detergent.* Journal of Lubrication Technology, 1981. **103**(4): p. 486-494.

165. Wan, Y., et al., *Effects of detergent on the chemistry of tribofilms from ZDDP: studied by X-ray absorption spectroscopy and XPS*, in *Tribology Series*, D. Dowson, et al., Editors. 2002, Elsevier. p. 155-166.

166. Smith, G.C. and J.C. Bell, *Multi-technique surface analytical studies of automotive anti-wear films.* Applied Surface Science, 1999. **144-145**: p. 222-227.

167. Willermet, P.A., et al., *The composition of lubricant-derived surface layers formed in a lubricated cam/tappet contact II. Effects of adding overbased detergent and dispersant to a simple ZDTP solution.* Tribology International, 1995. **28**(3): p. 163-175.

168. Kasrai, M., et al., *Study of the effects of Ca sulfonate on antiwear film formation by X-ray absorption spectroscopy using synchrotron radiation.* Journal of synchrotron radiation, 1999. **6**(3): p. 719-721.

169. *S. Shirahama and M. Hirata Proc. 5th Int. Colloq. on Additives for Lubricants and Operational Fluids. Esslingen, 1986.*

170. Rounds, F., *Effect of detergents on ZDP antiwear performance as measured in four-ball wear tests.* Lubrication engineering, 1989. **45**(12): p. 761-769.

171. Ramakumar, S.S.V., A.M. Rao, and S.P. Srivastava, *Studies on additive-additive interactions: Formulation of crankcase oils towards rationalization.* Wear, 1992. **156**(1): p. 101-120.

172. Chinas-Castillo, F. and H.A. Spikes, *Film Formation by Colloidal Overbased Detergents in Lubricated Contacts.* Tribology Transactions, 2000. **43**(3): p. 357-366.

173. Cizaire, L., et al., *Tribochemistry of Overbased Calcium Detergents Studied by ToF-SIMS and Other Surface Analyses.* Tribology Letters, 2004. **17**(4): p. 715-721.

174. Kubo, T., et al., *TOF-SIMS analysis of boundary films derived from calcium sulfonates.* Tribology Letters, 2006. **23**(2): p. 171-176.

175. Evans, R.D., et al., *Influence of steel type on the propensity for tribochemical wear in boundary lubrication with a wind turbine gear oil.* Tribology letters, 2010. **38**(1): p. 25-32.

176. Taylor, L., A. Dratva, and H.A. Spikes, *Friction and Wear Behavior of Zinc Dialkyldithiophosphate Additive.* Tribology Transactions, 2000. **43**(3): p. 469-479.

177. McGeehan, J., E. Yamaguchi, and J. Adams, *Some effects of zinc dithiophosphates and detergents on controlling engine wear*. 1985, SAE Technical Paper.

178. Yin, Z., et al., *Application of soft X-ray absorption spectroscopy in chemical characterization of antiwear films generated by ZDDP Part II: the effect of detergents and dispersants.* Wear, 1997. **202**(2): p. 192-201.

179. Willermet, P., R. Carter Iii, and E. Boulos, *Lubricant-derived tribochemical films—an infra-red spectroscopic study.* Tribology international, 1992. **25**(6): p. 371-380.

180. Willermet, P., et al., *The composition of surface layers formed in a lubricated cam/tappet contact.* Journal of Tribology, 1991. **113**(1): p. 38-47.

181. Gryenge, E., et al., *Hydrogen evolution inhibiting additives for zinc electrowinning*. 2005, Google Patents.

182. Iso, K., et al., *Rolling bearing, rolling bearing for fuel cell, compressor for fuel cell system and fuel cell system*. 2007, Google Patents.

183. Schatzberg, P., *Inhibition of water-accelerated rolling-contact fatigue.* Journal of Lubrication Technology, 1971. **93**(2): p. 231-233.

184. Kumar, P.G. and K. Yu-ichi, *Diffusible hydrogen in steel weldments.* Trans JWRI, 2013. **42**: p. 39-62.

185. Niste, V.B., et al., *WS 2 nanoadditized lubricant for applications affected by hydrogen embrittlement.* RSC Advances, 2015. **5**(51): p. 40678-40687.

186. Tanaka, H., et al., *The Effect of Lubricant Additives on Hydrogen Permeation Under Rolling Contact.* Tribology Letters, 2017. **65**(3): p. 94.

187. Endo, T., et al., *Study on rolling contact fatigue in hydrogen atmosphere-improvement of rolling contact fatigue life by formation of surface film*, in *Tribology and Interface Engineering Series*. 2005, Elsevier. p. 343-350.

188. Richardson, A.D., et al., *Thermal Desorption Analysis of Hydrogen in Non-hydrogen-Charged Rolling Contact Fatigue-Tested 100Cr6 Steel.* Tribology Letters, 2017. **66**(1): p. 4.

189. Gegner, J. and W. Nierlich. *Frictional surface crack initiation and corrosion fatigue driven crack growth*. in *NREL Workshop, Broomfield*. 2011.

190. Lai, J. and K. Stadler, *Investigation on the mechanisms of white etching crack (WEC) formation in rolling contact fatigue and identification of a root cause for bearing premature failure.* Wear, 2016. **364**: p. 244-256.

191. Danielsen, H.K., et al., *Multiscale characterization of White Etching Cracks (WEC) in a 100Cr6 bearing from a thrust bearing test rig.* Wear, 2017. **370**: p. 73-82.

192. Singh, H., et al., *Investigation of Microstructural Alterations in Low- and High-Speed Intermediate-Stage Wind Turbine Gearbox Bearings.* Tribology Letters, 2017. **65**(3): p. 81.

193. Paladugu, M. and R. Scott Hyde, *White etching matter promoted by intergranular embrittlement.* Scripta Materialia, 2017. **130**: p. 219-222.

194. Richardson, A.D., Wang, L., Wood, R. J. K., Evans, M.-H., Anderson, W. B., and Ingram, M., *Investigation of the Role of Hydrogen in White Structure Flaking (WSF) of Wind Turbine Gearbox Bearings.* STLE Annual Meeting, 17–21 May, Dallas, TX., 2015.

195. Richardson, A.D., Wang, L., Wood, R. J. K., Evans, M.-H., Anderson, W. B., and Ingram, M., *A combined TDA and metallographic study to investigate hydrogens role in white etching crack (WEC) formation.* STLE Annual Meeting, 15-19 May, Las Vegas, NV, 2016.

196. Kuhn, M., P. Gold, and J. Loos, *Wear protection and low friction in roller bearings by different PVD-coating systems.* Tribology Series, 2003. **43**: p. 459-465.

197. Hamrock, B.J. and D. Dowson, *Minimum film thickness in elliptical contacts for different regimes of fluid-film lubrication.* 1978.

198. Hamrock, B.J. and D. Dowson, *Ball bearing lubrication: the elastohydrodynamics of elliptical contacts.* 1981.

199. Kang, Y.S., R.D. Evans, and G.L. Doll. *Roller-raceway slip simulations of wind turbine gearbox bearings using dynamic bearing model*. in *STLE/ASME 2010 International Joint Tribology Conference*. 2010. American Society of Mechanical Engineers.

200. Holweger, W., et al., *Non-destructive subsurface damage monitoring in bearings failure mode using fractal dimension analysis.* Industrial Lubrication and Tribology, 2012. **64**(3): p. 132-137.

201. Anderson, P., N. Fleck, and K. Johnson, *Localization of plastic deformation in shear due to microcracks.* Journal of the Mechanics and Physics of Solids, 1990. **38**(5): p. 681-699.

202. Schlicht, H., *About adiabatic shear bands and the generation of "high-angle white bands" in roller bearingsAbout adiabatic shear bands and the generation of "high-angle white bands" in roller bearings.* Materialwissenschaft und Werkstofftechnik, 2008. **39**(3): p. 217-226.

203. Solano-Alvarez, W., et al., *Elucidating white-etching matter through high-strain rate tensile testing.* Materials Science and Technology, 2017. **33**(3): p. 307-310.

204. Pressouyre, G., *A classification of hydrogen traps in steel.* Metallurgical and Materials Transactions A, 1979. **10**(10): p. 1571-1573.

205. TAKAGI, S., et al., *A new evaluation method of hydrogen embrittlement fracture for high strength steel by local approach.* ISIJ international, 2005. **45**(2): p. 263-271.

206. Karsch, T., et al., *Influence of hydrogen content and microstructure on the fatigue behaviour of steel SAE 52100 in the VHCF regime.* International Journal of Fatigue, 2014. **60**: p. 74-89.

207. Murakami, Y. and N.N. Yokoyama, *Influence of hydrogen trapped by inclusions on fatigue strength of bearing steel*, in *Bearing Steel Technology*. 2002, ASTM International.

208. Jenkins, N., P. Hart, and D. Parker, *An evaluation of rapid methods for diffusible weld hydrogen.* Welding Journal-Including Welding Research Supplement, 1997. **76**(1): p. 1-6.

209. Kotecki, D. and R. LaFave, *AWS A5 Committee studies of weld metal diffusible hydrogen.* Welding Journal, 1985. **64**(3): p. 31-37.

210. Niste, V., *WS2 nanoparticles as lubricant additives*. 2015, University of Southampton.

211. Nolan, D. and M. Pitrun, *Diffusible hydrogen testing in Australia.* Welding in the World, 2004. **48**(1-2): p. 14-20.

212. Evans, M.H., *Tomographic Serial Sectioning Investigations of Butterfly and White Etching Crack (WEC) Formation for Wind Turbine Gearbox Bearing Applications.* STLE Annual Meeting, Detroit, Michigan, 2013.

213. Ćwiek, J., *Hydrogen degradation of high-strength steels.* Journal of Achievements in Materials and Manufacturing Engineering, 2009. **37**(2): p. 193-212.

214. Barnoush, A., *Hydrogen embrittlement.* Saarland University, 2011.

215. Wan, G., et al., *The effect of extreme pressure (EP) lubricants on the life of rolling element bearings.* Proceedings of the Institution of Mechanical Engineers, Part J: Journal of Engineering Tribology, 1994. **208**(4): p. 247-252.

216. Schatzberg, P. and I.M. Felsen, *Effects of water and oxygen during rolling contact lubrication.* Wear, 1968. **12**(5): p. 331-342.

217. Brizmer, V., H.R. Pasaribu, and G.E. Morales-Espejel, *Micropitting Performance of Oil Additives in Lubricated Rolling Contacts.* Tribology Transactions, 2013. **56**(5): p. 739-748.

218. Cen, H., et al., *Effect of water on ZDDP anti-wear performance and related tribochemistry in lubricated steel/steel pure sliding contacts.* Tribology International, 2012. **56**: p. 47-57.

219. Parsaeian, P., et al., *Study of the interfacial mechanism of ZDDP tribofilm in humid environment and its effect on tribochemical wear; Part I: Experimental.* Tribology International, 2017. **107**: p. 135-143.

220. Soltanahmadi, S., et al., *Tribochemical study of micropitting in tribocorrosive lubricated contacts: The influence of water and relative humidity.* Tribology International, 2017. **107**: p. 184-198.

221. Tricot, R., J. Monnot, and M. Lluansi, *How microstructural alterations affect fatigue properties of 52100 steel.* Met Eng Q, 1972. **12**(2): p. 39-47.

222. Buchwald, J. and R. Heckel, *An analysis of microstructural changes in 52100 steel bearings during cyclic stressing(Microstructural changes in 52100 steel bearing inner rings during cyclic stressing, obtaining thickening rate data on white-etching regions and lenticular carbides).* ASM Transactions Quarterly, 1968. **61**: p. 750-756.

223. Kang, J.-H., et al., *Solute redistribution in the nanocrystalline structure formed in bearing steels.* Scripta Materialia, 2013. **69**(8): p. 630-633.

224. O'Brien, J.L. and A.H. King, *Electron microscopy of stress-induced structural alterations near inclusions in bearing steels.* Journal of Basic Engineering, 1966. **88**(3): p. 568-571.

225. Kuhn, M., P. Gold, and J. Loos. *Wear protection and low friction in roller bearings by different PVD-coating systems*. in *Transient Processes in Tribology: Proceedings of the 30th Leeds-Lyon Symposium on Tribiology*. 2004. Elsevier.

226. Reichelt, M., et al., *Nanoindentation, TEM and ToF-SIMS studies of the tribological layer system of cylindrical roller thrust bearings lubricated with different oil additive formulations.* Wear, 2010. **268**(11-12): p. 1205-1213.

227. *Stachowiak GW, Batchelor AW. Engineering Tribology. 3rd ed. ed. Oxford, UK: Elsevier Butterworth-Heinemann; 2006.*

228. Johnson, K., *Contact Mechanics Cambridge Univ.* Press, Cambridge, 1985.

229. *NSK. Long life bearings for engine accessories. Motion & Control: NSK; 2004. p. 1-10.*

230. Hiraoka, K., M. Nagao, and T. Isomoto, *Study on flaking process in bearings by white etching area generation.* Journal of ASTM International, 2006. **3**(5): p. 1-7.

231. Imai, Y., et al., *Study on rolling contact fatigue in hydrogen environment at a contact pressure below basic static load capacity.* Tribology Transactions, 2010. **53**(5): p. 764-770.

232. Uyama, H., et al., *The effects of hydrogen on microstructural change and surface originated flaking in rolling contact fatigue.* Tribology Online, 2011. **6**(2): p. 123-132.

Permissions

[1.1] Reprinted from Wear, Vol 398-399, Paladugu, M., D.R. Lucas, and R. Scott Hyde, Effect of lubricants on bearing damage in rolling-sliding conditions: Evolution of white etching cracks, pages 165-177, Copyright (2018), with permission from Elsevier.

[1.2] Reprinted and adapted by permission from Springer Nature: Springer, Tribology Letters, Influence of Steel Type on the Propensity for Tribochemical Wear in Boundary Lubrication with a Wind Turbine Gear Oil, R. D. Evans, G. L. Doll, C. H. Hager et al, Copyright (2010).

[1.3] Reprinted from Applied Surface Science, Vol 144-145, Smith G.C and J.C Bell, Multi-technique surface analytical studies of automotive anti-wear films, pages 222-227, Copyright (1999), with permission from Elsevier.

[4.1] Reprinted and adapted by permission from Springer Nature: Springer, Tribology Letters, The Influence of sliding and contact severity on the generation of white etching cracks, Gould, B. and A. Greco, Copyright (2015).